VOLUME 22 (1961) No. 4

NUCLEAR PHYSICS

JOURNAL DEVOTED TO THE EXPERIMENTAL AND THEORETICAL STUDY OF THE FUNDAMENTAL CONSTITUENTS OF MATTER AND THEIR INTERACTIONS

EDITOR: L. ROSENFELD · COPENHAGEN

LAST NUMBER OF THIS VOLUME

SVEN A. E. JOHANSSON, Nuclear octupole deformation and the mechanism of fission 529

N. BRENE, L. EGARDT and B. QVIST, On the $K_{\mu 3}$ and K_{e3} decay modes 553

S. L. GLASHOW, Partial-symmetries of weak interactions 579

M. BEINER and K. BLEULER, Geometrical representation of nuclear properties 589

J. E. CLINE and R. L. HEATH, Levels in Gd^{156} fed by the decay of 15-day Eu^{156} 598

G. T. EWAN, R. L. GRAHAM and J. S. GEIGER, Negative parity levels in the even-even nucleus Dy^{160} 610

V. B. BERESTETSKY and I. Ya. POMERANCHUK, On the asymptotic behaviour of cross sections at high energies 629

P. H. BOWEN, J. P. SCANLON, G. H. STAFFORD, J. J. THRESHER and P. E. HODGSON, Neutron total cross-sections in the energy range 15 to 120 MeV 640

P. S. ISAEV and M. SEWERYNSKI, Approximate equations for partial π—K scattering amplitudes 663

A. DE-SHALIT, Effective moments in K^{39} and K^{40}. 677

E. P. GRIGORIEV and A. V. ZOLOTAVIN, Concerning the decay of Se^{74} 689

I. ŠLAUS, P. TOMAŠ and N. STIPČIĆ, Angular distribution of the $V^{51}(n, d)Ti^{50}$ ground state deuterons 692

News item 698

Report on Kingston Conference. 698

Erratum 699

Author index 700

Subject index 705

February 1961

NORTH-HOLLAND PUBLISHING COMPANY - AMSTERDAM

EDITORIAL BOARD

AUSTRALIA & NEW ZEALAND:	H. Messel (Sydney), M. L. Oliphant (Canberra)
AUSTRIA:	B. Karlik (Vienna), H. Thirring (Vienna)
BELGIUM:	M. de Hemptinne (Louvain), J. Verhaeghe (Ghent)
CANADA:	G. Volkoff (Vancouver)
DENMARK:	C. Møller (Copenhagen), S. Rozental (Copenhagen), G. E. Brown (Copenhagen)
FINLAND:	L. Simons (Helsinki)
FRANCE:	A. Berthelot (Saclay), S. Gorodetzky (Strasbourg)
GERMANY (DEM. REP.):	G. Hertz (Leipzig)
GERMANY (FED. REP.):	W. Gentner (Freiburg i. B.), J. H. D. Jensen (Heidelberg)
GREAT BRITAIN:	W. E. Burcham (Birmingham), T. H. R. Skyrme (Harwell)
HUNGARY:	L. Janossy (Budapest)
INDIA:	H. Bhabha (Bombay), R. Ramanna (Trombay)
IRISH REPUBLIC:	J. McConnell (Maynooth)
ISRAEL:	G. Racah (Jerusalem)
ITALY:	E. Amaldi (Rome)
JAPAN:	S. Kikuchi (Tokay), S. Tomonaga (Tokyo)
MEXICO:	M. Moshinsky (Mexico)
NETHERLANDS:	H. Brinkman (Groningen), S. R. de Groot (Leiden)
NORWAY:	E. Hylleraas (Oslo), A. Lundby (Oslo), H. Wergeland (Trondheim)
POLAND:	L. Infeld (Warsaw), J. Werle (Warsaw)
PORTUGAL:	J. M. Araújo (Porto), J. R. de Almeida Santos (Coimbra)
SOUTH AMERICA:	G. Beck (Saõ Paulo), J. Leite Lopes (Rio de Janeiro)
SPAIN:	J. M. Otero (Madrid), C. Sanchez del Rio (Madrid)
SWEDEN:	O. Klein (Stockholm), K. Siegbahn (Uppsala), I. Waller (Uppsala)
SWITZERLAND:	P. Huber (Basel), P. Scherrer (Zürich)
U.A.R. & ARAB COUNTRIES:	F. El Bedewi (Cairo), M. G. Nooh (Cairo)
U.S.A.:	H. H. Barschall (Madison, Wisconsin), S. Devons (New York), V. F. Weisskopf (Cambridge, Mass.)
U.S.S.R.:	M. A. Markov (Moscow), I. S. Shapiro (Moscow), D. V. Skobeltzyn (Moscow)
YUGOSLAVIA:	I. Supek (Zagreb)

CONTRIBUTIONS may be sent to the Editor, Professor L. Rosenfeld, NORDITA, Blegdamsvej 17, Copenhagen Ø, either directly, or preferably through the intermediary of one of the members of the Editorial Board of the country or region in which the author is working. They may be written in English, French or German.

NUCLEAR PHYSICS is published in fortnightly issues. The subscription price per volume of 700 pages is fl 57.00; 114s; $ 15.00. Post-free.

SUBSCRIPTIONS should be sent to the publishers, NORTH-HOLLAND PUBLISHING COMPANY P.O. Box 103, Amsterdam or to any subscription-agent.

BOOKS FOR REVIEW should be sent to Professor Rosenfeld.

No part of this issue may be reproduced in any form, by print, photoprint, microfilm or any other means without permission from the publisher.

Printed in the Netherlands

NUCLEAR PHYSICS

EDITORIAL BOARD

AUSTRALIA & NEW ZEALAND:	H. Messel (Sydney), M. L. Oliphant (Canberra)
AUSTRIA:	B. Karlik (Vienna), H. Thirring (Vienna)
BELGIUM:	M. de Hemptinne (Louvain), J. Verhaeghe (Ghent)
CANADA:	G. Volkoff (Vancouver)
DENMARK:	C. Møller (Copenhagen), S. Rozental (Copenhagen), G. E. Brown (Copenhagen)
FINLAND:	L. Simons (Helsinki)
FRANCE:	A. Berthelot (Saclay), S. Gorodetzky (Strasbourg)
GERMANY (DEM. REP.):	G. Hertz (Leipzig)
GERMANY (FED. REP.):	W. Gentner (Freiburg i. B.), J. H. D. Jensen (Heidelberg)
GREAT BRITAIN:	W. E. Burcham (Birmingham), T. H. R. Skyrme (Harwell)
HUNGARY:	L. Janossy (Budapest)
INDIA:	H. Bhabha (Bombay), R. Ramanna (Trombay)
IRISH REPUBLIC:	J. McConnell (Maynooth)
ISRAEL:	G. Racah (Jerusalem)
ITALY:	E. Amaldi (Rome)
JAPAN:	S. Kikuchi (Tokai), S. Tomonaga (Tokyo)
MEXICO:	M. Moshinsky (Mexico)
NETHERLANDS:	H. Brinkman (Groningen), S. R. de Groot (Leiden)
NORWAY:	E. Hylleraas (Oslo), A. Lundby (Oslo), H. Wergeland (Trondheim)
POLAND:	L. Infeld (Warsaw), J. Werle (Warsaw)
PORTUGAL:	J. M. Araújo (Porto), J. R. de Almeida Santos (Coimbra)
SOUTH AMERICA:	G. Beck (Saõ Paulo), J. Leite Lopes (Rio de Janeiro)
SPAIN:	J. M. Otero (Madrid), C. Sanchez del Rio (Madrid)
SWEDEN:	O. Klein (Stockholm), K. Siegbahn (Uppsala), I. Waller (Uppsala)
SWITZERLAND:	P. Huber (Basel), P. Scherrer (Zürich)
U.A.R. & ARAB COUNTRIES:	F. El Bedewi (Cairo), M. G. Nooh (Cairo)
U.S.A.:	H. H. Barschall (Madison, Wisconsin), S. Devons (New York), V. F. Weisskopf (Cambridge, Mass.)
U.S.S.R.:	M. A. Markov (Moscow), I. S. Shapiro (Moscow), D. V. Skobeltzyn (Moscow)
YUGOSLAVIA:	I. Supek (Zagreb)

NUCLEAR PHYSICS

JOURNAL DEVOTED TO THE EXPERIMENTAL AND THEORETICAL STUDY OF THE FUNDAMENTAL CONSTITUENTS OF MATTER AND THEIR INTERACTIONS

EDITOR: L. ROSENFELD - COPENHAGEN

VOLUME XXII

JANUARY 1961 — FEBRUARY 1961

NORTH-HOLLAND PUBLISHING COMPANY - AMSTERDAM

PRINTED IN THE NETHERLANDS

2.J

Nuclear Physics **22** (1961) 529—552; ©*North-Holland Publishing Co., Amsterdam*

Not to be reproduced by photoprint or microfilm without written permission from the publisher

NUCLEAR OCTUPOLE DEFORMATION AND THE MECHANISM OF FISSION

SVEN A. E. JOHANSSON

Department of Physics, University of Lund, Lund, Sweden

Received 20 October 1960

Abstract: The stability of nuclei against an octupole deformation has been calculated. It is found that the interaction of levels of opposite parity makes the nuclei in certain regions very soft to octupole deformation. The negative parity collective states in heavy nuclei and in the rare earth region can be interpreted as octupole vibrations. The predicted A-dependence of the energy of these states agrees well with experimental data.

For very elongated shapes, which are of interest in fission, it is found that stable octupole deformation occurs. The potential surface of the fission barrier will therefore possess two asymmetric valleys. There is a linear relationship between the mass ratio of the fission fragments and the degree of octupole deformation at the saddle point. The occurrence of symmetric fission in the lighter elements is explained. The influence of the octupole deformation on the fission barrier also provides a basis for understanding the variation in fission threshold. The experimental data agree with the calculated values. The peak to valley ratio in the mass distribution is calculated, with the assumption of statistical equilibrium at the saddle point. Good agreement is found for excitation energies below 10 MeV. For higher energies a symmetric component appears which rises with increasing energy.

1. Introduction

Nuclear deformation of the octupole type is of interest in several ways. It was suggested by Christy [1]) that the low-energy negative parity states in heavy nuclei could be explained as octupole vibrations. Strutinsky [2]) pointed out that the coupling between a filled and an unfilled level of opposite parity gives a tendency towards octupole deformation. This problem was investigated more in detail by Lee and Inglis [3]). Using perturbation theory and assuming a spheroidal harmonic-oscillator potential, they calculated the strength of the deforming force. They concluded that the decrease in energy due to this effect is not quite enough to overcome the increase arising from the requirement of volume conservation. Because of the simple potential used the right level order is not reproduced and it is not possible to compare the results of this calculation with the situation in any real nuclei. Furthermore, the neglect of the spin-orbit coupling will have a decisive influence on the calculations. The spin-orbit coupling will bring the interacting levels closer together and hence increase the deforming force.

Suekane [4]), Araujo [5]), and Lane and Pendlebury [6]) have treated octupole vibrations of spherical nuclei but this case is of less interest in connection with the problems discussed in the present paper.

Octupole deformation is also of interest in connection with the fission process, especially the mass asymmetry of the fission fragments. It is natural to assume that the mass asymmetry can be explained in terms of an octupole deformation of the fissioning nucleus. This problem has been treated on the basis of the liquid-drop model by Businaro and Gallone [7]), Nossoff [8]), and Swiatecki [9]).

In the present work we will investigate the octupole deformation in a manner similar to that of Lee and Inglis. The spin-orbit coupling will be included by using the asymptotic approximation of Nilsson [10]). Furthermore, we will investigate how the octupole deformation varies with the quadrupole deformation. Various problems of fission will be discussed using the results of this calculation.

2. Calculations

The Hamiltonian of the unperturbed system is

$$H = T+\tfrac{1}{2}K\left[\frac{x^2+y^2}{b^2}+\frac{z^2}{a^2}\right]+C\mathbf{l}\cdot\mathbf{s}+D\mathbf{l}^2. \tag{1}$$

A small perturbation term

$$H'_1 = \tfrac{1}{2}K\left[\frac{3(x^2+y^2)}{b^2}-\frac{2z^2}{a^2}\right]\frac{z}{a}\frac{\alpha_3}{R} \tag{2}$$

is added.

The pear-shaped potential, which represents the average interaction of one nucleon with all the others, has then the form

$$V = \tfrac{1}{2}K\left[\frac{x^2+y^2}{b^2}\left(1+3\alpha_3\frac{z}{aR}\right)+\frac{z^2}{a^2}\left(1-2\alpha_3\frac{z}{aR}\right)\right]. \tag{3}$$

The α_3-term is proportional to Y_{30} in terms of the angles associated with the coordinates x/b, y/b and z/a.

It is easy to show that the centre of mass of the potential remains fixed to the first order in α_3.

The perturbation term H'_1 gives rise to a repulsion of levels of opposite parity when certain selection rules are obeyed. When two filled levels are considered, one is pushed up and the other one down by the same amount and there is no net change in energy. If we consider one filled and one unfilled level, the former will be depressed and the energy of the system will be lowered. Since there are no diagonal elements, the total change in energy is given by the expression

$$E_1 = \sum_{n_x n_y n_z} \sum_{n'_x n'_y n'_z} \frac{\langle n_x n_y n_z | H'_1 | n'_x n'_y n'_z \rangle^2}{E_{n_x n_y n_z} - E_{n'_x n'_y n'_z}}. \tag{4}$$

The first summation extends over all levels obeying the selection rules and the second summation over all filled levels.

In evaluating the matrix elements we make the substitutions

$$\xi = x \sqrt{\frac{m\omega_x}{\hbar}}, \quad \text{etc.}, \quad \xi^2 + \eta^2 = \rho^2.$$

We need the matrix elements

$$\langle n_\zeta n_\perp \Lambda\Sigma | \zeta^3 | n'_\zeta n'_\perp \Lambda' \Sigma' \rangle = \delta_{n_\perp n'_\perp} \delta_{\Lambda\Lambda'} \delta_{\Sigma\Sigma'} \langle n_\zeta | \zeta^3 | n'_\zeta \rangle, \tag{5}$$

$$\langle n_\zeta n_\perp \Lambda\Sigma | \zeta\rho^2 | n'_\zeta n'_\perp \Lambda' \Sigma' \rangle = \delta_{\Lambda\Lambda'} \delta_{\Sigma\Sigma'} \langle n_\zeta | \zeta | n'_\zeta \rangle \langle n_\perp \Lambda | \rho^2 | n'_\perp \Lambda \rangle. \tag{6}$$

The matrix elements containing ζ are easily calculated by use of the recursion formula for the Hermite polynomials. The element containing ρ^2 is calculated by the method described by Mottelson and Nilsson [11]).

The following selection rules are obtained:

$$\text{for } \langle|\zeta^3|\rangle: \quad n'_\zeta = n_\zeta \pm 1 \quad \text{or} \quad n_\zeta + 3, \quad n'_\perp = n_\perp, \quad \Lambda' = \Lambda, \quad \Sigma' = \Sigma; \tag{7}$$

$$\text{for } \langle|\rho^2\zeta|\rangle: \quad n'_\zeta = n_\zeta \pm 1, \quad n'_\perp = n_\perp \quad \text{or} \quad n_\perp \pm 2, \quad \Lambda' = \Lambda, \quad \Sigma' = \Sigma. \tag{8}$$

The corresponding matrix elements have the form

$$\begin{aligned} &\langle n_\zeta | \zeta | n_\zeta + 1 \rangle = \sqrt{\frac{n_\zeta + 1}{2}}, \quad \langle n_\zeta | \zeta^3 | n_\zeta + 1 \rangle = 3 \left(\frac{n_\zeta + 1}{2} \right)^{\frac{3}{2}}, \\ &\langle n_\zeta | \zeta^3 | n_\zeta + 3 \rangle = \sqrt{\frac{(n_\zeta + 1)(n_\zeta + 2)(n_\zeta + 3)}{8}}, \quad \langle n_\perp \Lambda | \rho^2 | n_\perp \Lambda \rangle = n_\perp + 1, \\ &\langle n_\perp \Lambda | \rho^2 | n_\perp + 2, \Lambda \rangle = \tfrac{1}{2} \sqrt{(n_\perp + 2)^2 - \Lambda^2}. \end{aligned} \tag{9}$$

The energy eigenvalue of a state characterized by the quantum numbers n_z, $n_\perp$, Λ and Σ is given in the asymptotic approximation by the expression

$$\begin{aligned} E(n_z n_\perp \Lambda\Sigma) = {} & (n_\perp + 1)\hbar\omega_\perp \\ & + (n_z + \tfrac{1}{2})\hbar\omega_z - \kappa\hbar\omega_0 [2\Lambda\Sigma + \mu(2n_z n_\perp + 2n_z + n_\perp + \Lambda^2)]. \end{aligned} \tag{10}$$

The energy denominators in (4) now have the following values in the four cases permitted by the selection rules

$$\begin{aligned} E(n_z+1, n_\perp \Lambda\Sigma) - E(n_z n_\perp \Lambda\Sigma) &= [1 - \tfrac{2}{3}\varepsilon - 2\kappa\mu(n_\perp + 1)]\hbar\omega_0, && \text{(I)} \\ E(n_z+3, n_\perp \Lambda\Sigma) - E(n_z n_\perp \Lambda\Sigma) &= [3 - 2\varepsilon - 6\kappa\mu(n_\perp + 1)]\hbar\omega_0, && \text{(II)} \\ E(n_z-1, n_\perp+2, \Lambda\Sigma) - E(n_z n_\perp \Lambda\Sigma) &= [1 + \tfrac{4}{3}\varepsilon - 2\kappa\mu(2n_z - n_\perp - 2)]\hbar\omega_0, && \text{(III)} \\ E(n_z+1, n_\perp+2, \Lambda\Sigma) - E(n_z n_\perp \Lambda\Sigma) &= [3 - 2\kappa\mu(2n_z + n_\perp + 4)]\hbar\omega_0. && \text{(IV)} \end{aligned} \tag{11}$$

It is evident that the smallest values for the energy difference are obtained in case (I). With increasing ε the two levels will come closer together and eventually they will cross. Since the matrix elements are of the same order of magnitude, the predominant contribution to E_1 will come from levels connected by the selection rules in case (I).

The deforming force is opposed by the cohesiveness of nuclear matter, which has a tendency to keep the volume constant. It turns out that with increasing octupole deformation the contraction in some directions is not quite compensated by relaxation in other directions. Hence there is a net effect which raises the energy of the single-particle levels. This can be accounted for by a readjustment of the constant K in (3). The result is that we get a second perturbation term in the Hamiltonian of the system. Lee and Inglis [3]) have shown that it has the form

$$H'_2 = \tfrac{1}{2}K'\left[\frac{x^2+y^2}{b^2}+\frac{z^2}{a^2}\right]^2\frac{\alpha_3^2}{R^2}. \tag{12}$$

The increase in energy will be

$$E_2 = \sum \langle n_x n_\perp \Lambda\Sigma|H'_2|n_x n_\perp \Lambda\Sigma\rangle.$$

The matrix elements needed in this case are calculated in the same way as described above. The result is

$$\begin{aligned}
&\langle n_\zeta n_\perp \Lambda\Sigma|\rho^4|n_\zeta n_\perp \Lambda\Sigma\rangle = \langle n_\perp \Lambda|\rho^4|n_\perp \Lambda\rangle = \tfrac{3}{2}n_\perp{}^2+3n_\perp+2-\tfrac{1}{2}\Lambda^2,\\
&\langle n_\zeta n_\perp \Lambda\Sigma|\rho^2\zeta^2|n_\zeta n_\perp \Lambda\Sigma\rangle = \langle n_\perp \Lambda|\rho^2|n_\perp \Lambda\rangle\langle n_\zeta|\zeta^2|n_\zeta\rangle = (n_\perp+1)(n_\zeta+\tfrac{1}{2}),\\
&\langle n_\zeta n_\perp \Lambda\Sigma|\zeta^4|n_\zeta n_\perp \Lambda\Sigma\rangle = \langle n_\zeta|\zeta^4|n_\zeta\rangle = \tfrac{3}{2}(n_\zeta{}^2+n_\zeta+\tfrac{1}{2}).
\end{aligned} \tag{13}$$

In addition to the single-particle forces there are other types of interaction affecting the deformation. It is obviously necessary to include the Coulomb energy. The surface energy might also be included. In the liquid-drop model, the surface energy and the Coulomb energy are assumed to give the only contributions to the deformation energy. As will be shown below, the single-particle contribution is the predominant one. Hence any calculation based only on the liquid drop model is necessarily incomplete and cannot be expected to give reasonable results. On the other hand if we make a more complete calculation including the single-particle effects, it is difficult to say whether it is permissible to neglect the surface energy. In the expression for the energy in the single-particle model there appear terms which can be interpreted as a surface energy. They do not represent more than a fraction of the empirical surface energy, however. We have therefore included the drop model surface energy in the present calculation but it must be emphasized that this is an oversimplification which will give rise to some overestimation of the restoring force. Since we will not try to calculate the deformation energy absolutely but will normalize to experimental values, this uncertainty will not seriously affect the conclusions of the present work.

The surface and Coulomb energies are well known from the calculations based on the liquid-drop model. We have used the calculations of Businaro and Gallone [7]). They use curvilinear coordinates and expand the surface around an ellipsoid. The deformation energy ΔE is given by

$$\frac{\Delta E}{E_s} = [(0.714-0.408x)+(1.829-1.339x)\alpha-(0.404+0.657x)\alpha^2]\alpha_3^2, \qquad (14)$$

where E_s is the surface energy of the undeformed nucleus. α is a parameter describing the eccentricity of the basic ellipsoid and is defined by $(a^2-b^2)/3a^2$.

For small distance between two interacting levels and for large values of α_3, it is no longer possible to use perturbation theory. The two levels mix and the energy values of the system are in the first approximation

$$E = \tfrac{1}{2}(E_a+E_b)\pm\tfrac{1}{2}[(E_a-E_b)^2+4M_{ab}^2\alpha_3^2]^{\frac{1}{2}}. \qquad (15)$$

E_a and E_b are the energies of the two unperturbed levels and M_{ab} is the matrix element of the interaction. Strutinsky [2]) has discussed this problem in the case of two crossing levels. In the present case we have many interacting levels but the situation is similar in the two cases.

The total potential energy is given by

$$E = C\alpha_3^2-\sum\tfrac{1}{2}[(E_a-E_b)^2+4M_{ab}^2\alpha_3^2]^{\frac{1}{2}}. \qquad (16)$$

The constant C determines the net restoring force and includes the surface and Coulomb energies and the volume conservation energy E_2 (12). For small values of α_3 (16) is reduced to the familiar second order perturbation expression

$$E = C\alpha_3^2-\sum\frac{M_{ab}}{E_a-E_b}\alpha_3^2. \qquad (17)$$

If $\sum M_{ab}^2/(E_a-E_b) > C$, the energy will decrease with increasing α_3. Hence the nucleus will tend to assume a pear-shape. For large values of α_3 the energy will increase and there will thus be a value α'_3 where the energy has a minimum and where the nucleus is in stable equilibrium. In order to calculate α'_3 approximately, we note that the matrix elements M_{ab} can be divided into two classes. Some of the matrix elements are quite small. Their influence on the deformation can be calculated by perturbation theory and their contribution to the deformation energy will be included in the constant C. The other matrix elements which give the main contribution to the deforming force are found to be all about the same size. We therefore assume that in the summation in (16) we have n equal elements $\bar{M}_{ab}$. The following simple expression for α'_3 is then obtained:

$$\alpha'_3 = \tfrac{1}{2}\left[\left(\frac{\bar{M}_{ab}n}{C}\right)^2-\left(\frac{E_a-E_b}{\bar{M}_{ab}}\right)^2\right]^{\frac{1}{2}}. \qquad (18)$$

A discussion of this formula will be postponed until after the presentation of the results of the more exact calculation based on (16).

When the elongation of a nucleus is relatively small, its shape can probably be approximated by an ellipsoid. Kjällquist [12]) calculated the amount of Y_{40} deformation for heavy nuclei. The deformation parameter β_4 was found to be small, about 0.03. For the elongations which are of interest in fission, however, it is necessary to include deformations up to at least the fourth order. Hence we will assume the potential to be ellipsoidal with a small Y_{40} deformation superimposed. It is then necessary to investigate how our calculation of the octupole deformation is influenced by the Y_{40} deformation. The predominant effect is that the position of the levels will change slightly. It was shown above that the octupole deformation is determined by the interaction of nearby levels of opposite parity and that the interaction is inversely proportional to the distance between the levels. This distance is of the order 2—3 MeV. Hence even a relatively small change in the position of the levels will change this distance considerably.

In order to calculate the influence of the Y_{40} deformation, we use perturbation theory. The perturbation term in the Hamiltonian is assumed to have the following form:

$$H'_3 = \tfrac{1}{2}K\left[\frac{z^4}{a^4} - 3\,\frac{(x^2+y^2)z^2}{a^2b^2} + \tfrac{3}{8}\,\frac{(x^2+y^2)^2}{b^4}\right]\frac{\alpha_4}{R^2}. \tag{19}$$

In the spherical case this corresponds to adding a deformation of the form Y_{40}.

The matrix elements needed are the same as those already calculated (13). For the present purpose it is sufficient to take into account only the diagonal elements; it can be shown that the non-diagonal elements give a negligible contribution. The change in energy due to the Y_{40}-deformation is then given by

$$\Delta E = \frac{\hbar^2}{Ma^2R^2}\left[\tfrac{3}{2}(n_z^2+n_z+\tfrac{1}{2}) - \tfrac{3}{2}r(n_\perp+1)(2n_z+1) + \tfrac{3}{16}r^2(3n_\perp^2+6n_\perp-\Lambda^2+4)\right]\alpha_4. \tag{30}$$

This change is of importance only for levels which are close together, i.e., levels connected by the selection rule $n'_z = n_z+1$. The change in the energy difference between two such levels is

$$\Delta(E_{n_z+1}-E_{n_z}) = \frac{3\hbar^2}{Ma^2R^2}\left[(n_z+1)-r(n_\perp+1)\right]\alpha_4. \tag{21}$$

3. Results

The results of the preceding section are used to calculate the deformation energy in some heavy nucleides. Table 1 shows the calculated values.

According to these results, the parameter of the deformation energy is small

but positive. Hence these nuclei do not have a stable octupole deformation but are only very soft to octupole vibrations. It is obvious, however, that no definite conclusion can be drawn. The present calculation is certainly not accurate enough to decide the question of the stability against an octupole deformation. It only shows that these nuclei are close to the point where the transition to a stable octupole deformation occurs.

TABLE 1

The deformation energy is given by $\Delta E = (C_{\text{restoring}} + C_{\text{surface}} - C_{\text{deforming}} - C_{\text{coulomb}})\alpha_3^2 = C_t\alpha_3^2$. The table lists the constants C (in MeV) for a number of nucleides

Nucleide	$C_{\text{restoring}}$	$C_{\text{deforming}}$	$C_{\text{surface}} - C_{\text{coulomb}}$	C_t
Th^{228}	363	393	40	10
U^{234}	375	402	40	13
Pu^{240}	389	415	40	14
Cm^{246}	402	420	40	22
Cf^{250}	412	424	40	28

It appears rather unlikely that it will be possible to improve the calculations so that they can give an unambiguous answer to the question of stability. Hence in the present work we will normalize the calculated values so that they are consistent with the experimental energy values of the collective, negative parity states in heavy nuclei. It will then be possible to draw some important conclusions; for example, concerning the A-dependence of the energy of the negative parity states and, especially, the situation for large elongations which are of interest in fission.

4. Negative Parity Collective States

Negative parity states of low energy occur in heavy nuclei. It seems very likely that they are collective states in some way connected with an octupole deformation. Two different explanations are possible.

According to the first one, the nucleus does not possess a stable octupole deformation. It is only soft to octupole deformations and hence the energy of the collective vibrations is very low. There will be a series of vibrational states, $0+$, $1-$, $2+$ etc. Based on the first vibrational state, there is a rotational band, $1-$, $3-$, $5-$ etc.

A second possibility is that the nucleus has a stable octupole deformation. The lowest levels are those belonging to the rotational band, $0+$, $1-$, $2+$, $3-$, $4+$ etc., based on the ground state. The negative parity levels are not in their normal position between the even parity levels, however, but are displaced upward. The displacement is proportional to the frequency of the tunneling motion through the barrier which separates the two points of stable equilibrium.

In order to discriminate between these two alternatives we have calculated the barrier height which gives the experimental value for the displacement in the second alternative. We have also estimated the variation of the displacement with A in the region from thorium to plutonium. It turns out that this explanation meets with great difficulties. One cannot in this way obtain a consistent explanation. It is possible, however, that this explanation works for some particular nucleides, perhaps some radium isotopes, where the energy of the negative parity states is very low. In the following, we will assume, however, that the first alternative is the right one, that is, that the nucleus is very soft to octupole deformation.

There does not seem to exist any detailed treatment of the problem of the octupole vibrations in deformed nuclei. In order to get a crude estimate, we will use the hydrodynamical expression for the vibrational energy:

$$E = \hbar \sqrt{\frac{C_t}{B}} = \hbar \sqrt{\frac{4\pi C_t}{AMR^2}}, \tag{22}$$

where B is the mass parameter and C_t is the parameter of the total deformation energy.

C_t has been calculated for a number of nucleides (Table 1). Insertion of these values gives the energy values of the 1− states.

The calculated values are now normalized so that they give the experimental energy value for one particular nucleide. The states in the radium isotopes, which have a very low energy, are not suitable for this purpose. The reason is that radium is located in the transition region between the spherical and deformed nuclei. The asymptotic approximation is not too good in this region. Instead we have used the nucleide Th^{228}. Similar results are obtained with other nucleides having a collective 1− state, for example U^{234} and Pu^{240}. The result is that in order to get agreement with the experimental energy value, the volume conservation energy calculated above (12) has to be multiplied by a factor 0.98. The fact that the normalization constant is so close to 1, which would indicate that the calculation is quite accurate, is fortuitous.

It is now of interest to see what predictions the present calculation makes about the variation with A in the energy of the 1− states. The value of C_t is calculated for a number of heavy nucleides and inserted in (22). The resulting energy values are shown in fig. 1, connected by a line. The circles indicate the experimental values. The calculated values seem to reproduce quite well the trend in the experimental values. In view of the uncertainties in the calculation any detailed comparison would have no meaning.

An attempt will also be made to extend this calculation to the rare earth region. The procedure is exactly the same as for the heavy nuclei. The same normalization constant is used. The result is shown to the left in fig. 1. Even here the calculated values follow reasonably well the experimental ones. It

must be kept in mind that the energy of these states is determined by a small difference between two large numbers. It is then rather surprising that this long extrapolation gives such a good agreement. One explanation might be that the nuclei slightly heavier than samarium have a configuration which is very similar to that of the nuclei in the uranium region. The difference between calculated and experimental values at both ends of the rare earth region is probably due to the fact that the mass parameter cannot be approximated by the hydrodynamic expression over the whole region.

It is necessary to point out that it is not known with certainty that the 1− states in the rare earth region correspond to collective octupole vibrations. They could also be due to nucleonic excitation. An examination of the available single

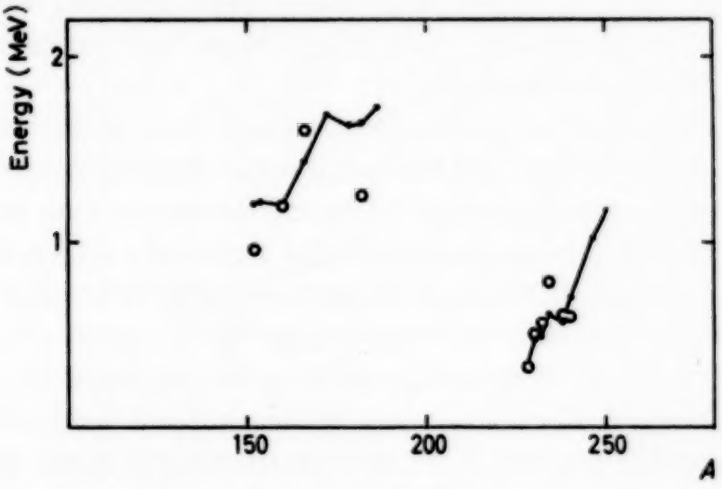

Fig. 1. Energy of the 1− states. Dots: calculated values for the following nucleides: Sm^{152}, Gd^{154}, Dy^{160}, Er^{166}, Yb^{172}, Hf^{178}, W^{182}, Os^{186}, Th^{228}, Th^{230}, U^{232}, U^{234}, Pu^{238}, Pu^{240}, Cm^{246} and Cf^{250}. Experimental values are marked with circles. References can be found in Strominger, Hollander and Seaborg, Revs. Mod. Phys. **30** (1958) 585 and in Nuclear Data Sheets, National Research Council, Washington, D. C. Additional references: Th^{230}, U^{230}: ref. [36]); U^{234}: ref. [37]).

particle levels shows, however, that it is difficult to explain all of them in this way. The systematic occurrence of these states and the rough agreement with the calculated values lend some support to the assumption about the collective nature of these states.

The main purpose of this discussion about the energy of the negative parity states has been to show that there is no serious disagreement between calculated and experimental energy values. It also provides a normalization of the calculation which will be used in the subsequent discussion on fission. In order to obtain detailed predictions it is necessary to derive a more exact formula for the energy of the octupole vibrations. The present results might still be of some interest in nuclear spectroscopy since they can predict at least in what energy range one should search for the 1− state.

5. Fission

Having discussed the conditions at the equilibrium deformation, we will now investigate the octupole deformation for the more elongated shapes which are of interest in fission. In doing so it is necessary to know the shape of the nucleus during the fission process. Practically the only available information comes from calculations based on the liquid-drop model. The work of Swiatecki [9]) will be used here. We approximate the calculated shapes by an ellipsoid with a superimposed Y_{40} deformation. It is possible to get a rather good fit to the drop-model shapes in this way. A more satisfactory estimate of the Y_{40} deformation has been obtained by Kjällquist [12]). Unfortunately, however, her calculation is limited to the equilibiium deformation. It is interesting to note that the results of Kjällquist are about the same as those obtained from the liquid-drop model for this deformation. One might hope that this agreement will continue up to larger deformations.

Another important problem in this connection is that of the level crossings. When the deformation is increased there will occur many crossings in the level diagram. The question now is whether the nucleons stay in their original orbits or if the nucleus adjusts its configuration so that the energy always is minimized. The probability of jumps in the level diagram depends on several factors, e.g. the speed of the deformation, the relative slope of the levels etc. We will be interested mainly in the nuclear configuration at the saddle point and in rather low excitation energies. There is experimental evidence suggesting that the passage over the saddle point is slow and that the nuclear modes are in equilibrium there (see, for example, ref. [13]) for a discussion of this problem). It is then reasonable to assume that the nuclear configuration at the saddle point is adjusted so that the energy is minimized. This means that the nucleons are transferred from levels of the type [500], [600], etc., which rise steeply with increasing deformation, to levels of the type [770], [761] etc., which fall steeply with increasing deformation (the level diagram is to be found in ref. [11])). In determining the nuclear configuration from the level diagram it is also necessary to take into account the fact that the position of the levels is slightly affected by the Y_{40} deformation. For deformations corresponding to the saddle point of nuclei in the uranium region, the neutrons transfer from the levels [501], [503], [501], and [606] to the levels [761], [880], [871], and [750]. For the protons the situation is similar. For even larger deformations the neutron levels [505], [615] and [503] will be emptied and the proton levels will behave correspondingly.

It should be emphasized in this connection that the present calculation is rather insensitive to the exact configuration. The predominant contribution to the deforming force comes from about thirty matrix elements, which are of about equal size. Altogether there are about 250 matrix elements involved in

the calculation. Hence if there is some uncertainty in the choice of the highest occupied level or levels, this will not change qualitatively the results reported below.

In the following discussion we will determine the octupole deformation at the saddle point. Hence it is necessary to know the elongation of the nucleus at this point. The liquid-drop model results [9]) have been used with a slight modification [14]) in order to account for the equilibrium quadrupole deformation.

Fig. 2 shows the calculated values of the potential energy as a function of α_3 for different values of $r = a/b$. The curves are calculated for the nucleide Cf^{250}

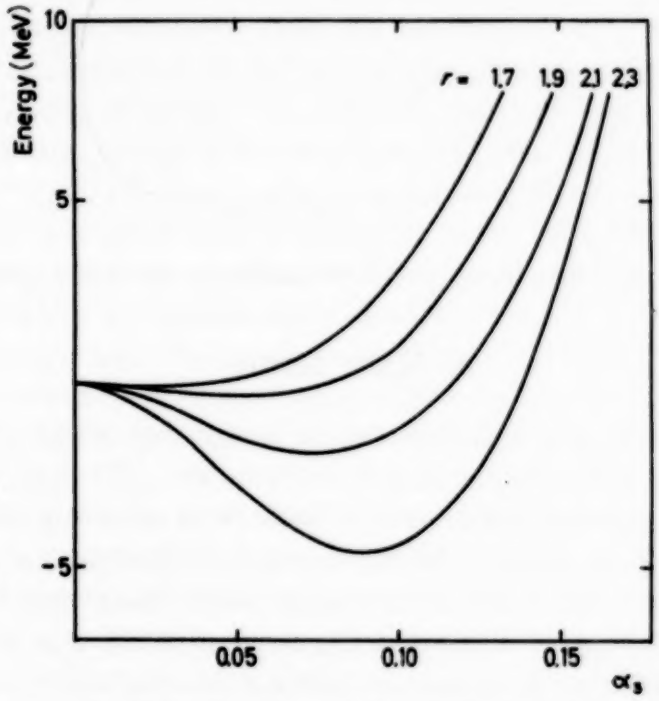

Fig. 2. The potential energy of a Cf^{250} nucleus as a function of the octupole deformation parameter for different values of $r = a/b$.

but similar curves are obtained for other nucleides in this region. Obviously the potential surface has two valleys corresponding to an asymmetric deformation. The degree of asymmetry increases with the elongation at the saddle point. Hence it increases with decreasing values of the parameter Z^2/A. The variation with Z and A for a given r is less rapid than the variation with r.

When r approaches the value 2.5, the situation changes radically for the following reason: The main contribution to the deforming force comes from levels of the type [400], [500] etc. which have small n_z and large $n_\perp$. They slope steeply upward in the diagram. Hence when the deformation increases they are replaced with other levels which slope downward. The large matrix elements disappear and are replaced by small ones. This process starts even for smaller deformations but at about $r = 2.5$ it reaches a point where the restoring forces

in the nucleus become predominant. For r-values increasing beyond $r = 2.5$ the deforming force will continue to decrease. Hence for nuclei with low Z^2/A having saddle point shapes with $r > 2.5$ the potential surface has only one valley, corresponding to symmetric fission.

The results of the present calculation make it possible to calculate the nuclear shape during the fission process. As an illustration, Fig. 3 shows the shape at the saddle point for U^{238}. The pear-shape is quite evident.

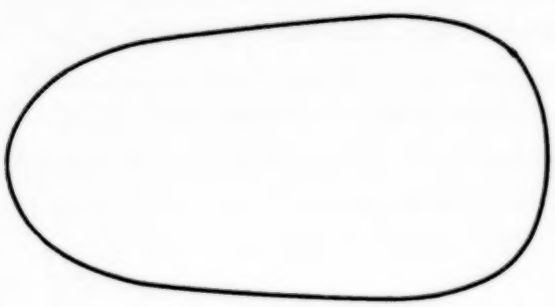

Fig. 3. Calculated shape of a U^{238} nucleus at the saddle point.

6. Mass Ratio

The problem of the mass distribution in fission has always received much attention, particularly the fact that it is asymmetric. Although many explanations have been suggested, none seem to have been generally accepted.

One of the important points in fission theory is to determine at which stage in the fission process the mass distribution is decided. One assumption is that the motion from the top of the barrier to the point of scission is slow. Statistical equilibrium is assumed to be maintained during this stage. The available energy is shared among the various degrees of freedom. The kinetic energy of the fissioning nucleus will be half the temperature or about 0.5 MeV. The mass distribution is determined by the statistical weights at the point of scission [15, 16, 17]). There does not seem to exist any definite experimental evidence for this point of view, however. One indication that it might be wrong is the fact that the excitation energy of the fragments does not have a maximum at the most probable mode of division, in contrast to what is expected from a statistical theory.

Some other information comes from a study of the fragment energy as a function of the excitation energy. It is well known that the fragment kinetic energy is almost independent of the excitation. This is the main evidence for assuming statistical equilibrium at the saddle point. There are, however, some indications that a small part of the excitation energy goes into the kinetic energy of the fragments (see ref. [13]) for a discussion of this problem). Also it has recently been shown that the kinetic energy is considerably greater for fission induced

by 14 MeV neutrons than in thermal fission [18]). Hence it would not seem impossible that part of the 10—20 MeV which are available in the motion from the top of the barrier to scission goes into the kinetic energy of the fissioning nucleus. Then the kinetic energy could be considerably greater than the 0.5 MeV allowed by the assumption of statistical equilibrium.

In this connection it is instructive to discuss the time required for the fragments to separate relative to the nucleonic period. Fig. 3 shows the calculated shape of a uranium nucleus at the saddle point. It is immediately obvious that two touching spherical fragments can be formed practically without further elongation of the nucleus. The size of the kinetic energy of the fragments after the separation shows, however, that the two fragments, regarded as spheres, start to separate at a distance 20 % further apart than if they were just touching. These considerations show that the distance travelled by the centre of mass of the fragments from the top of the barrier to the point of scission is quite small (about 1×10^{-13} cm). The time needed for this motion turns out to be the same as the nucleonic period even if the kinetic energy is as low as 0.5 MeV. As discussed above, it is quite possible that the kinetic energy is greater and this time could therefore be considerably shorter than the nucleonic period.

Hence the motion from the saddle point to the point of scission might not be a process in statistical equilibrium but rather a rapid disruption of the nucleus. The asymmetry of the fissioning nucleus will not have time to change very much during this process. Therefore the mass ratio will already be determined during the passage over the saddle point. This hypothesis is admittedly rather extreme, yet not more extreme than the assumption of statistical equilibrium at the scission point. It is in any case worth while to examine the consequences of this hypothesis and compare them with experimental data.

It is, of course, difficult to define exactly the point at which the mass asymmetry is determined. For the sake of simplicity we have assumed it to be at the top of the barrier. It is more likely that it comes slightly later, at the falling side of the barrier, but the exact location is not too important for the following discussion.

It is unfortunately very difficult to calculate the mass distribution from the nuclear shape at the saddle point. Instead one can see if there is any correlation between the experimentally determined mass ratio and the calculated values of the octupole deformation parameter at the saddle point, α'_3. Fig. 4 shows the result (it should be borne in mind that there is a considerable experimental uncertainty in the mass ratios, of the order of 0.03—0.05). It will be noted that there is a strong correlation between the two quantities. The mass ratio appears to be roughly proportional to α'_3.

As discussed above, the asymmetric saddle points disappear at a deformation of $r = 2.5$, corresponding to the saddle point shape for a nucleus having $Z^2/A = 34.3$. Experimentally it is known that fission is asymmetric for

$Z^2/A > 34.7$ and symmetric for $Z^2/A < 33.3$. Between these two limits is a transition region where both symmetric and asymmetric fission occur. Hence without any further assumptions we get a quantitatively correct explanation of the sudden change in mass distribution. The various theories which have been put forward to explain the mass asymmetry are quite general and do not seem to allow for any sudden transition to symmetric fission.

There is apparently a very close relationship between the shape of the fissioning nucleus at the saddle point and the character of the mass distribution. The mass ratio is proportional to the octupole deformation parameter. When the saddle point shape becomes symmetric, the asymmetry in the mass distri-

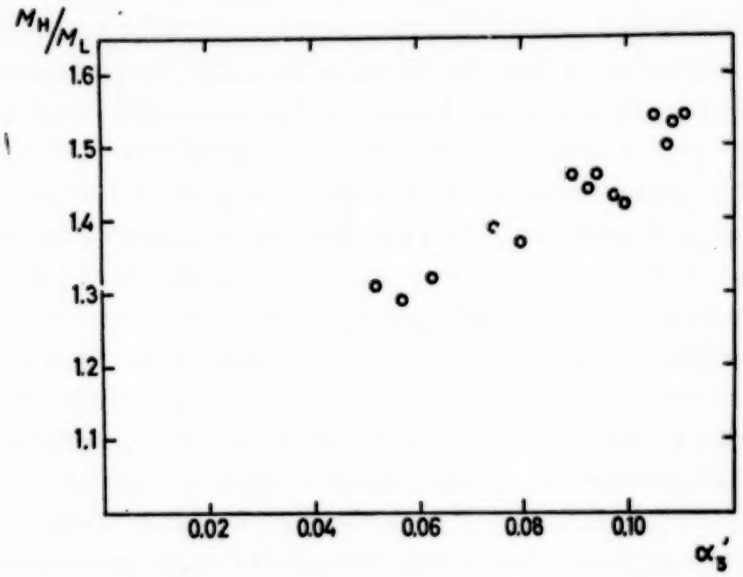

Fig. 4. The experimentally determined most probable mass ratios as a function of α'_3 (the value of the octupole deformation parameter α_3 at the saddle point). Values for the following nucleides are shown (from left to right): Cf^{252} (refs. [38, 39, 29]), Cm^{242} (ref. [38]), Cm^{244} (ref. [38]), Pu^{240} (refs. [38, 40, 41]), Pu^{242} (ref. [38]), U^{234} (refs. [40, 41]), U^{235} (ref. [42]), U^{236} (refs. [40, 42, 43]), U^{238} (refs. [42, 44, 45]), U^{239} (ref. [41]), Th^{230} (ref. [19]), Th^{232} (refs. [42, 46]), Th^{233} (ref. [41]), and Ac^{227} (ref. [35]).

bution disappears. These facts lend strong support to the hypothesis that the mass distribution is determined at the saddle point. It is, of course, still possible that there are other effects, for example dynamic effects, which to some extent affect the mass distribution during the later part of the fission process.

An interesting problem is the character of the mass distribution for the elements lighter than bismuth. Experimentally it has been shown that fission in these elements in general is symmetric. The peak becomes broader with decreasing mass number, however [19]). For α-induced fission in rhenium it has even been reported that the mass distribution is asymmetric at an excitation of 30 MeV [20]). These facts indicate that for elements lighter than bismuth there is a tendency towards mass asymmetry which increases with decreasing mass number. It is difficult to make any detailed calculation for these elements on

the basis of the present work. Since the value of Z^2/A is low, the shapes at the saddle point are very elongated. The single particle level diagram becomes increasingly uncertain for large deformations. The same is true for the calculation of the nuclear shape at the saddle point. The uncertainty in these respects makes any detailed calculation rather meaningless. Qualitatively an inspection of the level diagram shows that the tendency for asymmetric fission should be greatest for Z-values around 72. It is not at all impossible that the asymmetric fission of rhenium ($Z = 75$) can have a natural explanation in this way. As has been shown above the asymmetric mass distribution is correlated with the occurrence of special levels in the level diagram. These levels show a periodic shell effect and the mass asymmetry might also show this shell effect.

A related problem is high energy fission. It has been shown that there is a tendency towards mass asymmetry when the bombarding energy of the particles is increased above about 100 MeV. The mass distributions are symmetric but there is a broadening which can be attributed to an asymmetric component. The interpretation of these data is made very difficult by the fact that the excitation energy of the fissioning nucleus is not known with any certainty. Only part of the energy of the incoming particle is transferred to excitation energy of the nucleus. Furthermore the excitation energy is decreased by nucleon emission before fission. As a matter of fact there seems to be strong evidence that most of the emitted particles precede fission and that the remaining excitation energy is quite low. This will evidently lead to some amount of asymmetry. Another effect is that the neutron emission will increase the value of Z^2/A of the fissioning nucleus. This has the effect that the nuclear shape at the saddle point will be less elongated than in low energy fission of the same nucleide. From the discussion above it follows that this effect in some cases, for example, high energy fission of bismuth, will increase the probability of asymmetric fission. A systematic study of these effects will probably give valuable information which could be used to check the present calculations.

7. Fission Thresholds

It has been known for a long time that the fission thresholds do not agree with the predictions of the liquid-drop model. The experimental values are roughly constant in contrast to the rather strong dependence on Z^2/A expected from the drop model. However, it must be kept in mind that the drop-model prediction refers to symmetric fission whereas the fission is actually asymmetric. The present work gives the energy difference between the symmetric and asymmetric thresholds. It is therefore possible to get the symmetric threshold from the experimental values plus the results of the present calculation.

In fig. 5 the dots represent the experimental threshold values taken from a compilation of Halpern [13]). The circles represent the result of adding the

calculated differences between the symmetric and asymmetric thresholds. The experimental values unfortunately cover only a limited range of the parameter Z^2/A. We have therefore extended the figure to heavier nuclei by a point for Cf^{246}. The threshold value, represented by a dot, has been estimated from the competition between fission and spallation in the α-particle bombardment of Cm^{244}. It turns out that this competition is determined essentially by the difference between the thresholds for neutron emission and fission. The necessary data are taken from the compilation of Vandenbosch and Huizenga[21]) where the principles of the calculation are also discussed. The circle at Cf^{246} represents the symmetric threshold. For the lighter elements also no experi-

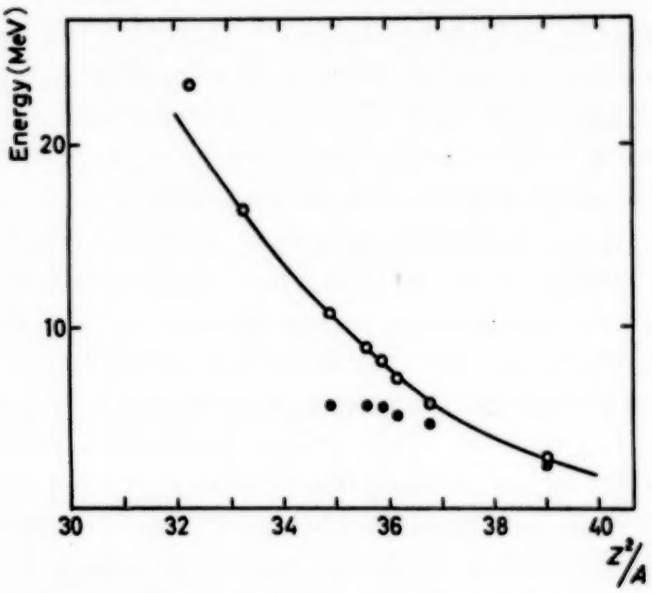

Fig. 5. Symmetric and asymmetric thresholds as a function of Z^2/A. Dots: experimental threshold values for Th^{232}, U^{234}, U^{236}, U^{238}, Pu^{240} and Cf^{246}. The corresponding circles denote the symmetric thresholds for these nuclei. The two circles to the left denote the thresholds for Hg and Po^{212}. The curve is fitted to the symmetric thresholds.

mental determination of fission thresholds exists. Here too, they can be calculated from the competition between neutron emission and fission. Halpern [13]) gives some estimates of fission thresholds using the measurements of Neuzil and Fairhall [22]). We have slightly refined this calculation but get essentially the same results. The two circles to the left in fig. 5 refer to α-particle bombardment of Pb^{208} and Os, which give the compound nuclei Po^{212} and Hg, respectively. These values give directly the symmetric thresholds, since fission is known to be symmetric for these nuclei.

It will be noted that the symmetric threshold values fall on a smooth curve. A good fit is obtained by a curve of the form

$$B_f = 0.0078 \left(46 - \frac{Z^2}{A}\right)^3 \text{MeV}. \qquad (23)$$

It is interesting to note that an expression of this form is predicted by the liquid-drop model. Swiatecki [23]) showed by general arguments based essentially on the properties of Taylor series expansions that the thresholds should be given by the expression $(1-x)^3$, where $x = (Z^2/A)/(Z^2/A)_{\text{lim}}$. This derivation is only valid for small values on x. He showed later, however, by more detailed calculations [9]) that this expression is valid also for such x values as are of interest in fission.

The fact that the experimental threshold values corrected for the difference between symmetric and asymmetric thresholds are in such good agreement with the prediction of the liquid-drop model indicates that this model works fairly well for symmetric deformations. As was shown earlier [14]) the influence of the single particle levels tends to change threshold values but the changes are small compared to the height of the fission barrier. This is a consequence of the fact that the level spacings are relatively small and that the level crossings tend to smooth out the fluctuations in spacing. The present calculations show, however, that in the case of octupole deformation the coupling between single particle states of different parity gives a large effect. This is completely different than the drop model results.

The present discussion has been limited to even nuclei. This is because the thresholds of odd-mass and odd nuclei are strongly influenced by the character of the single particle levels. The odd nucleon is expected to stay in its original orbit when the deformation increases [24, 25]). This leads in general to a higher barrier but there are great fluctuations between different nuclei, depending on the slope of the level filled by the odd nucleon [14]). Hence by limiting the discussion to even nuclei these fluctuations are eliminated and the effect of interest is seen more clearly.

It is interesting to note that the threshold values for symmetric and asymmetric fission obtained in the present work agree well with the semiempirical formula of Swiatecki [26]). This formula, however, contains a quantity δM, which is the difference between the experimental ground state mass and the value predicted by the semiempirical mass formula. Furthermore two of the constants in the threshold expression are adjusted empirically to give agreement with experimental data. It is therefore difficult to see the relation between Swiatecki's formula and the results of the present work.

The variations in fission threshold are apparently well explained. The almost constant threshold in the elements heavier than thorium is a consequence of the fact that the rise of the symmetric barrier is compensated by the increase of the energy difference between the symmetric and asymmetric barriers. When fission becomes symmetric for the lighter elements, there is a sudden increase of threshold to the symmetric barrier height. The threshold for these elements is above 20 MeV, as can be seen from their steep excitation curves. There is a transition region around radium where the barrier height changes rapidly with Z^2/A. An

interesting example is the neutron-induced fission of Ra^{226}. The excitation curve is irregular and fairly steep [17]). At lower excitation the mass distribution is asymmetric. As was shown above, the difference between the symmetric and asymmetric barriers is smaller than for uranium and thorium. The asymmetric barrier might therefore have a height of about 10 MeV. The exponential rise of the first part of the excitation curve is thus explained. The further rise might have something to do with the occurrence of the symmetric component which will be discussed in the next section. A further complication is the possibility of neutron emission of the compound nucleus leading to Ra^{226}. Since it is possible that neighbouring nucleides in this region have a considerably different threshold, the analysis of the excitation curve is difficult.

8. Peak to Valley Ratio

On the basis of the results in the previous section it is possible to get some further information about the mass distribution. In this section we will discuss the peak to valley ratio, i.e., the ratio of the fission yields at the two asymmetric peaks to that in the valley in between.

For fission close to threshold it is mainly a problem of barrier penetration. The yield of asymmetric fission is determined by the number of available channels. The symmetric fission should correspond to penetration through the barrier, which normally is higher for symmetric fission. For nucleides around uranium the extra height of the barrier is of the order of 2—3 MeV. It is easy to see, using penetration values from spontaneous fission, that the yield of symmetric fission in such a case would be extremely small, which is in disagreement with the experimental values. Hence we seem to have a discrepancy. We are forced to assume that in symmetric fission the nucleus passes over the barrier in the asymmetric valley and that the shape becomes symmetric later in the fission process. It is interesting to note that a similar conclusion has been reached from quite a different point of view. Fraser and Milton [28]) and Whetstone [29]) found that the neutron emission in near symmetric fission is asymmetric, more neutrons being emitted from the lighter fragment than from the heavier one. Vladimirski [30]) pointed out that symmetric fission in this particular case cannot be a real symmetric process.

Hence the mass distribution is not entirely determined at the saddle point. There must be some tendency towards symmetric fission when the nucleus passes from the top of the barrier to the point of scission. A possible explanation can be found in the shape of the potential surface. As was described above the asymmetric valleys disappear at an elongation corresponding to $r = 2.5$. If the internal motion of the nucleus is not fast enough, the mass division could be somewhat shifted to smaller mass ratios during the later part of the fission process. It is conceivable that even pure symmetric fission can be produced in this way.

Bohr [31]) has suggested that the yield of symmetric fission should depend on the properties of the particular channel through which the nucleus passes over the barrier. Experimentally some dependence on the excitation energy has been found but the results are to some extent contradictory. In any case the variations seem to be rather small. From the point of view of the present work no radical difference between different channels can be expected. There is no obvious connection between the properties of the channels at the saddle point and the behaviour of the fissioning nucleus during the later part of the fission process.

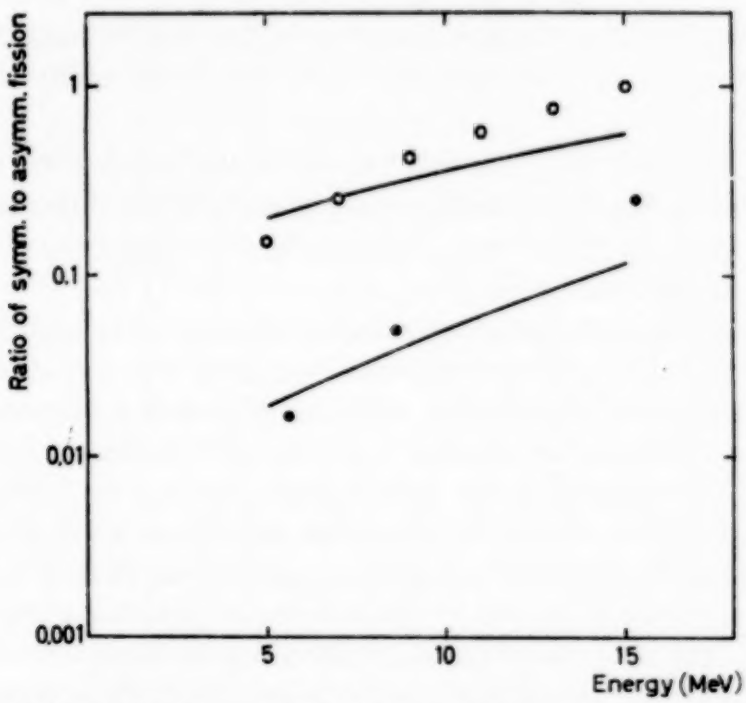

Fig. 6. The ratio of the yields of symmetric and asymmetric fission as a function of the excitation energy above the asymmetric saddle point. Dots: experimental values for U^{236}, circles: experimental values for Am^{240}. The two curves show calculated values.

For fission well above the threshold it is reasonable to try to determine the mass distribution from statistical considerations. We assume that the yield of a particular mass ratio can be set proportional to the number of available fission channels. Hence the peak to valley ratio will be determined by the level densities at the excitation energies corresponding to asymmetric and symmetric fission, respectively. Level densities are taken from the work of Ericson [32]). Since they are calculated for deformed nuclei, they should be applicable to the present problem.

Fig. 6 shows the yield of symmetric fission relative to asymmetric fission as a function of the excitation energy above the asymmetric saddle point. Two nucleides have been selected for this study, U^{236} and Am^{240}. The experimental data are taken from the neutron induced fission of U^{235} (ref. [33])) and the proton

induced fission of Pu^{239} (ref.[34])). The interpretation of the experimental data is complicated by the fact that, for higher excitation energies, fission can be preceded by neutron evaporation. Part of the fission processes therefore correspond to a lower excitation energy. It is necessary to correct for this effect. The necessary data on the competition between fission and neutron emission have been taken from a compilation by Vandenbosch and Huizenga [21]).

As can be seen from fig. 6 there is a reasonably good agreement between the experimental points and the theoretical values given by the two lines. The agreement is best for low excitation and there is a clear tendency for the yield of symmetric fission to rise above the theoretical value with increasing excitation energy. Part of the symmetric fission at higher energy seems to come from an energy dependent term which is not accounted for by statistical considerations.

The energy difference between the symmetric and asymmetric saddle points depends on Z^2/A, as has been shown above. It is therefore of interest to see how the predicted peak to valley ratios agree with the experimental distributions for nucleides of different Z^2/A.

Several difficulties arise in the evaluation of the experimental material for such a comparison. In most cases the ratio is known only for a limited number of energy values of the bombarding particle. It is then necessary to make an interpolation or extrapolation in order to get the ratio for the excitation energies chosen here. This involves some uncertainty. Another difficulty is that the fission threshold is not known for all nuclei considered here. It can be fairly well estimated but the possibility of error cannot be excluded. It is also necessary to make a correction for the neutron emission preceding fission.

Fig. 7 shows the available experimental values for excitation energies of 5 and 10 MeV above the asymmetric saddle point. Theoretical values are shown by the two lines. They are intended to give only a qualitative picture of the variation of the peak to valley ratio as a function of Z^2/A. Actually this ratio is not a simple function of Z^2/A but depends on the nucleonic configuration. In view of the uncertainties of the experimental values, a comparison with a more detailed theoretical prediction is hardly warranted.

It can be seen that for an excitation energy of 5 MeV the agreement between theory and experiment is satisfactory. At 10 MeV excitation, however, there is a systematic deviation, the experimental values being above the theoretical values. It is interesting to note that the excess over the theoretical values is constant. The deviations are therefore relatively more important for nucleides with a low Z^2/A.

The most natural explanation of these deviations seems to be that there is an energy dependent symmetric component which is rather independent of Z^2/A. It might indicate that the assumption of statistical equilibrium at the saddle point is not fulfilled at higher energies. If the passage over the fission

barrier is fast enough, the nucleus will not be affected by the asymmetry of the barrier but will remain symmetric during the whole fission process. This effect seems to be small at 5 MeV but at 10 MeV it begins to give an appreciable contribution to the symmetric fission. At higher energies it dominates. That there cannot be statistical equilibrium at higher energies is evident from the fact that the valley of the mass distribution eventually rises above the two asymmetric peaks.

There is some experimental evidence which point in the same direction as the peak to valley ratios discussed here. It has recently been shown [18]) that the

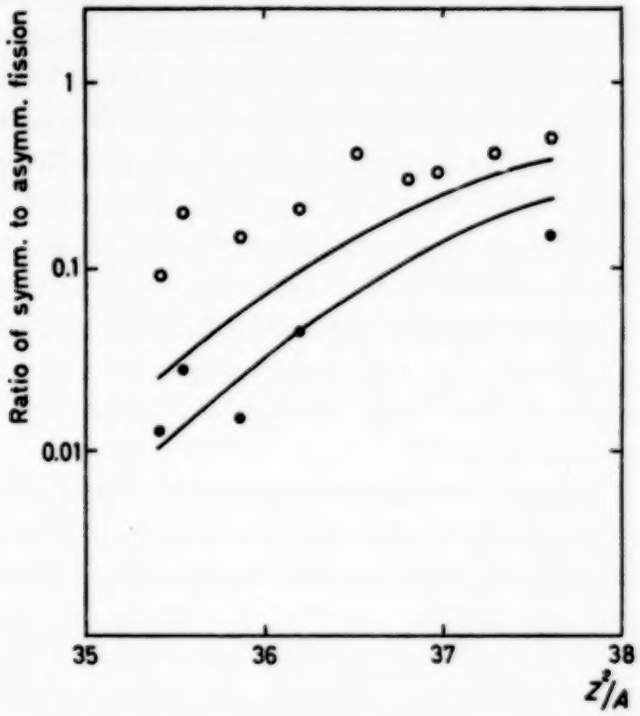

Fig. 7. The ratio of the yields of symmetric and asymmetric fission as a function of Z^2/A. Dots: experimental values for an excitation energy of 5 MeV above the asymmetric saddle point, circles: experimental values for an excitation energy of 10 MeV. The two curves show calculated values. The following nucleides have been included (from left to right): U^{239} (ref. [33])), Pa^{233} (ref. [34])), U^{236} (refs. [33, 47])), Np^{239} (ref. [34])), Pu^{242} (ref. [48])), Np^{235} (ref. [48])), Pu^{239} (refs. [48, 49])), Pu^{237} (ref. [48])), and Am^{240} (ref. [34])).

kinetic energy of the fragments is greater for fission induced by 14 MeV neutrons than in thermal fission. This clearly shows that at higher energies there are deviations from the statistical equilibrium at the saddle point.

Another piece of evidence comes from the work of Nobles and Leachman [27]) on the neutron induced fission of radium. They found that an increase of the neutron energy from 4 MeV to 15 MeV changed the mass distribution from asymmetric to symmetric. That the increase of the symmetric component is so pronounced in this case might have something to do with the fact that radium is located in the transition region where the barrier changes from asymmetric to

symmetric. The energy difference between the symmetric and asymmetric saddle points is small, which would be favourable for the increase of the symmetric component.

It has been suggested [35]) that symmetric and asymmetric fission are two independent modes of fission. Symmetric fission is assumed to be common to all elements and to increase regularly with energy and atomic number. In the lighter fissionable elements it gives a single peak and in the heavier ones it appears as a filling in of the valley between the asymmetric peaks. The present work gives a different picture. The mechanism of symmetric fission is different for different nucleides. The symmetric fission in the lighter elements, like bismuth, is due to the fact that the saddle is symmetric. In thorium and heavier elements at low excitation the fissioning nucleus passes over the asymmetric saddle point but later in the fission process, there is a tendency towards a symmetric shape which gives a certain amount of symmetric fission. At higher excitation energies in these elements, the ratio of symmetric to asymmetric fission is determined by a statistical equilibrium at the saddle point and depends on the difference in excitation energy for the two types of mass division. At even higher excitation energies (above 10 MeV) there appears a symmetric component which appears to be relatively independent of the nuclear species. It might be interpreted as a "fast" component caused by lack of statistical equilibrium at the saddle point.

The fact that the peak to valley ratio can be calculated from statistical factors at the saddle point, if the excitation energy is not too high, gives additional support to the assumption that the mass distribution is determined at the passage over the saddle.

9. Discussion

It is interesting to investigate how sensitive the results are to the details of the calculation. One can show that, for example, small changes in the nuclear configuration or in the level diagram do not change the results considerably. As a matter of fact it turns out, as we will now show, that some of the main results can be derived from rather general arguments.

Experimentally we know that the $1-$ states have a very low energy in some elements, especially radium and thorium. This requires that the deforming and restoring forces are about equal. In order to find the A-dependence of the $1-$ states, we note that the main contribution to the deformation energy E_1 which tends to make the nucleus pear-shaped comes from the matrix elements corresponding to the selection rules $n'_z = n_z+1$, $n'_\perp = n_\perp$, $\Lambda' = \Lambda$. It is immediately seen that this matrix element has a large value for levels having n_z large and $n_\perp$ small or vice versa. The levels which are filled when we go from radium and thorium to the heavier elements have n_z and $n_\perp$ about equal and

give only a small contribution to E_1. The volume conservation energy E_2, which opposes the tendency to pear-shape, does not depend so strongly on the character of the levels and hence increases rather regularly as the mass number increases. The result will thus be that above thorium the nuclei will become less soft to the octupole deformation and the energy of the 1— state will increase. In the rare earth region we expect a similar situation, since these nucleides have a configuration which is rather similar to that of the heavy ones.

When the elongation of the nucleus is increased, (18) makes possible a crude estimate of the equilibrium octupole deformation. The deformation energy parameter C and the matrix elements M_{ab} do not very much with the deformation and for the present purpose they can be considered as constant. C can easily be estimated as well as n, the number of matrix elements which are great enough to give an appreciable contribution to the deforming force. The distance between the interacting levels ΔE is given by (11). At the equilibrium elongation we can set $\alpha'_3 = 0$ since the nucleus is here very soft to octupole deformation and this implies $C = n\bar{M}_{ab}/\Delta E_{eq}$, where ΔE_{eq} is the level distance at the equilibrium elongation. Hence we get directly $\bar{M}_{ab}$. If this value is inserted in (18) we get the following approximate expression:

$$\alpha'_3 = \left(\frac{n}{2C}\right)^{\frac{1}{2}} \left(\frac{\Delta E_{eq}^2 - \Delta E^2}{\Delta E_{eq}}\right)^{\frac{1}{2}}. \tag{24}$$

We see immediately that α'_3 increases when the elongation is increased, since ΔE decreases. It will be noted that α'_3 does not depend strongly on C or n. The values calculated according to (24) agree reasonably well with the result of the more exact calculation.

As was discussed above n will decrease for large deformations due to the transfer of nucleons to other levels. As can be seen from (18), α'_3 will decrease and eventually become imaginary, corresponding to a symmetric saddle point. Also in this case a crude estimate shows good agreement with the detailed calculation.

This discussion shows that the main results can be derived from the general properties of the level diagram and the matrix elements. They are not critical in regard to the details of the level diagram or the assumed nuclear configuration.

The present calculations are necessarily simplified in several respects, but still they seem to be able to reproduce the experimental facts quite well. When more experimental data become available an even better comparison between theory and experiment can be made. Several interesting experiments are suggested by these calculations. It would, for example, be of great value to know more about the various fission parameters in the transition region around radium. A systematic study of fission in the rare earth region would also be of interest.

The author would like to thank Professor T. Gustafson, Professor B. R. Mottelson and Dr. S. G. Nilsson for helpful discussions.

References

1) R. F. Christy, private communication quoted in Alaga *et al.*, Revs. Mod. Phys. **28** (1956) 432
2) W. M. Strutinsky, J. Nucl. Energy **4** (1957) 523
3) K. Lee and D. R. Inglis, Phys. Rev. **108** (1957) 774
4) S. Suekane, Progr. Theor. Phys. **21** (1959) 74
5) J. M. Araujo, Nuclear Physics **13** (1959) 360
6) A. M. Lane and E. D. Pendlebury, Nuclear Physics **15** (1960) 39
7) U. L. Businaro and S. Gallone, Nuovo Cimento **1** (1955) 629
8) V. G. Nossoff, Proc. First Conf. Peaceful Uses Atomic Energy, Paper P/653 (Geneva 1955)
9) W. J. Swiatecki, Phys. Rev. **104** (1956) 993
10) S. G. Nilsson, Mat. Fys. Medd. Dan. Vid. Selsk. **29**, Nr. 16 (1955)
11) B. R. Mottelson and S. G. Nilsson, Nuclear Physics **13** (1959) 281
12) K. Kjällquist, Nuclear Physics **9** (1958) 168
13) I. Halpern, Ann. Rev. Nucl. Science **9** (1959) 245
14) S. A. E. Johansson, Nuclear Physics **12** (1959) 449
15) P. Fong, Phys. Rev. **89** (1953) 434
16) T. D. Newton, Chalk River Report CRP-642-A
17) A. G. W. Cameron, Proc. Second Conf. Peaceful Uses Atomic Energy, Paper P/198 (Geneva 1958)
18) P. C. Stevenson, H. G. Hicks, J. C. Armstrong and S. R. Gunn, Phys. Rev. **117** (1960) 186
19) R. C. Jensen and A. W. Fairhall, Phys. Rev. **118** (1960) 771
20) R. D. Griffioen and J. W. Cobble, Phys. Rev. (to be published)
21) R. Vandenbosch and J. R. Huizenga, Proc. Second Conf. Peaceful Uses Atomic Energy, Paper P/688 (Geneva 1958)
22) A. W. Fairhall and E. F. Neuzil, Univ. of Washington Progress Report (1959)
23) W. J. Swiatecki, Phys. Rev. **101** (1956) 651
24) J. O. Newton, Progress in Nuclear Physics **4** (1955) 234
25) J. A. Wheeler, in: Niels Bohr and the Development of Physics (Pergamon Press, London 1955)
26) W. J. Swiatecki, Phys. Rev. **101** (1956) 97
27) R. A. Nobles and R. B. Leachman, Nuclear Physics **5** (1958) 211
28) J. S. Fraser and J. C. D. Milton, Phys. Rev. **93** (1954) 818
29) S. L. Whetstone, Phys. Rev. **114** (1959) 581
30) V. V. Vladimirsky, JETP (USSR) **32** (1957) 822
31) A. Bohr, Proc. First Conf. Peaceful Uses Atomic Energy, Paper P/911 (Geneva 1955)
32) T. Ericson, Nuclear Physics **6** (1958) 62
33) R. B. Leachman, Proc. Second Conf. Peaceful Uses Atomic Energy, Paper P/2467 (Geneva 1958)
34) J. P. Butler, B. J. Bowles and F. Brown, Proc. Second Conf. Peaceful Uses Atomic Energy, Paper P/6 (Geneva 1958)
35) A. W. Fairhall, R. C. Jensen, and E. F. Neuzil, Proc. Second Conf. Peaceful Uses Atomic Energy, Paper P/677 (Geneva 1958)
36) O. B. Nielsen, private communication
37) G. J. Gallagher and T. D. Thomas, Nuclear Physics **14** (1959) 1
38) A. Smith, P. Fields, A. Friedman, S. Cox and R. Sjoblom, Proc. Second Conf. Peaceful Uses Atomic Energy, Paper P/690 (Geneva 1958)
39) J. S. Fraser and J. C. D. Milton, Proc. Second Conf. Peaceful Uses Atomic Energy, Paper P/199 (Geneva 1958)
40) W. E. Stein, Phys. Rev. **108** (1957) 94
41) S. Katcoff, Nucleonics **16** nr. 4 (1958) 78
42) R. B. Duffield, Proc. Second Conf. Peaceful Uses Atomic Energy, Paper P/678 (Geneva 1958)
43) L. E. Glendenin, E. P. Steinberg, M. G. Inghram and D. C. Hess, Phys. Rev. **84** (1951) 860
44) H. G. Richter and C. D. Coryell, Phys. Rev. **95** (1954) 1550
45) L. Katz, T. M. Kavanagh, A. G. W. Cameron, E. C. Bailey and J. W. T. Spinks, Phys. Rev. **99** (1955) 98
46) D. M. Hiller and D. S. Martin, Phys. Rev. **90** (1953) 581
47) B. M. Foreman, W. M. Gibson, R. A. Glass and G. T. Seaborg, Phys. Rev. **116** (1959) 382
48) R. Vandenbosch, T. D. Thomas, S. E. Vandenbosch, R. A. Glass and G. T. Seaborg, Phys. Rev. **111** (1958) 1358
49) R. Gunnink and J. W. Cobble, Phys. Rev. **115** (1959) 1247

8.B

Nuclear Physics **22** (1961) 553—578; ©*North-Holland Publishing Co., Amsterdam*

Not to be reproduced by photoprint or microfilm without written permission from the publisher

ON THE $K_{\mu 3}$ AND K_{e3} DECAY MODES

N. BRENE, L. EGARDT and B. QVIST

NORDITA, Nordisk Institut for Teoretisk Atomfysik, Copenhagen

Received 6 October 1960

Abstract: On the basis of the usual local current-current coupling between the lepton fields and the boson fields some general expressions are obtained for the muon (electron) and pion spectra and the muon polarization in an arbitrary direction taken as a function of the muon energy. The derivation of the muon spectrum and polarization involves a phase space integration over the pion momenta, on which, however, the two unknown form factors $f_{\pm}(p_\pi p_K)$ describing the effect of strong interactions are dependent. By means of a covariant integration technique originally due to Berman † the phase space integral is recast into a sum of products of factors depending on the muon and kaon momenta alone and very simple integrals over the form factors. These integrals depend on the muon and kaon momenta only through their upper and lower limits. In the CMS of the decaying kaon the factors depend solely on E_1, the muon or electron energy. The general expressions are applied to two special examples, viz. constant form factors and form factors derived by MacDowell by means of a dispersion technique. The results for these cases are very much alike.

1. Introduction

The leptonic 3-body decay modes

$$K \to \mu + \nu + \pi, \tag{1.1}$$

$$K \to e + \nu + \pi, \tag{1.2}$$

have been considered by numerous authors [1–9]), who — under various assumptions about the couplings and character of the particles — give expressions for the total decay rate, the energy spectrum of the emitted particles, muons (electrons) and pions, and the degree of polarization of muons (electrons) in certain directions.

For the study of the 3-body decay modes (1.1) and (1.2) the neutral K-mesons offer the advantage over the charged ones that the difference in lifetime between K_{01} and K_{02} helps us to obtain the 3-body decay modes without contamination from 2-body decay modes. On the other hand, difficulties arise because:

1) the decay always takes place in flight;

2) if the properties of the leptons are examined far from the decay point, also the effect of the leptons secondary to the pions must be taken into account.

† We are much indebted to Dr. S. Berman for discussion of this point.

The numerical results given here refer to the decay of neutral K-mesons (K_{02}), but apply — with appropriate changes of masses — equally well to that of charged K-mesons. It should be noted, however, that if K^+ and K^0 (K^- and $\bar{K}^0$) do not form an isospin doublet [10, 11]), one must be careful in applying results from K^+-decay to K^0-decay and vice versa. Some of the expressions for spectra and polarization are given both for decay at rest and for decay in flight. In the latter situation the polarization is most conveniently referred to the direction of motion of the K-meson. One step further is the consideration of decaying K-mesons with different velocities, which completes the adaptation of the results to an actual experimental situation in which a beam of K-mesons, produced with a certain energy distribution, decays. This step is performed in the approximation of constant form factors (appendix 3).

2. The Decay Matrix Element

We shall here consider in particular the decay mode

$$K^0 \to l^+ + (\nu)_L + \pi^- \tag{2.1}$$

(l standing for muon or electron) and assume [12, 13]) that the effective decay interaction is the product of a V—A leptonic current and a strangeness non-conserving current due to strongly interacting particles, vector or axial vector depending on the relative parity of these particles.

Thus the invariant matrix element will be of the form

$$M \propto \langle \pi | J_\lambda | K \rangle \bar{u}(p_\nu)\gamma_\lambda(1+\gamma_5)v(p_l). \tag{2.2}$$

In the approximation that the muon (electron) and the neutrino have a common origin (when electromagnetic effects are neglected), only the sum of their momenta will be present in the matrix element, i.e. $\langle \pi | J_\lambda | K \rangle$ depends only on p_K and p_π:

$$\langle \pi | J_\lambda | K \rangle = \tfrac{1}{2} f_+ (p_K + p_\pi)_\lambda + \tfrac{1}{2} f_- (p_K - p_\pi)_\lambda, \tag{2.3}$$

where the form factors f_+ and f_- are scalar functions of $p_K p_\pi$, i.e. of $(p_K - p_\pi)^2$. Time-reversal invariance requires that f_+ and f_- are real (have the same phase).

Thus the full matrix element is

$$M = \{\tfrac{1}{2} f_+ (p_K + p_\pi) + \tfrac{1}{2} f_- (p_K - p_\pi)\}_\lambda \bar{u}(p_\nu)\gamma_\lambda(1+\gamma_5)v(p_l). \tag{2.4}$$

It may be rewritten in the forms

$$M = \tfrac{1}{2} f_+ (p_K + p_\pi)_\lambda \bar{u}(p_\nu)\gamma_\lambda(1+\gamma_5)v(p_l) - \tfrac{1}{2} i f_- m_l \bar{u}(p_\nu)(1-\gamma_5)v(p_l), \tag{2.4'}$$

$$M = f_+ (p_K)_\lambda \bar{u}(p_\nu)\gamma_\lambda(1+\gamma_5)v(p_l) + \tfrac{1}{2} i (f_+ - f_-) m_l \bar{u}(p_\nu)(1-\gamma_5)v(p_l). \tag{2.4''}$$

It is an important feature of universal weak interaction that the matrix elements for the processes (1.1) and (1.2) are identical except for the mass values.

3. General Expressions

3.1. THE MUON (ELECTRON) ENERGY SPECTRUM

Evaluation of the square of the matrix element (2.4) and integration over the possible final states by the technique of appendix 1 lead to the following expression for the total decay probability in an arbitrary Lorentz frame (from here on we use the metric $g^{00} = -g^{11} = -g^{22} = -g^{33} = +1$):

$$\begin{aligned}
\Gamma_t &= \tfrac{1}{2}\pi C \int \frac{\mathrm{d}^3 p_1}{2E_1} \{(Gp_K)^2 - M_K{}^2 G^2\}^{-\frac{1}{2}} [g_0{}^{++} I_0{}^{++} \\
&\qquad + g_0{}^{--} I_0{}^{--} + g_0{}^{+-} I_0{}^{+-} + g_1{}^{++} I_1{}^{++} + g_1{}^{--} I_1{}^{--} + g_1{}^{+-} I_1{}^{+-}], \\
C &= \frac{4(2\pi)^{-5}}{2E_K}, \quad G_\lambda = (p_K - p_1)_\lambda, \\
I_0{}^{++} &= \int_\alpha^\beta (f_+(u))^2 \mathrm{d}u, \quad I_0{}^{--} = \int_\alpha^\beta (f_-(u))^2 \mathrm{d}u, \quad I_0{}^{+-} = \int_\alpha^\beta 2 f_+(u) f_-(u) \mathrm{d}u, \\
I_1{}^{++} &= \int_\alpha^\beta (f_+(u))^2 u \mathrm{d}u, \quad I_1{}^{--} = \int_\alpha^\beta (f_-(u))^2 u \mathrm{d}u, \quad I_1{}^{+-} = \int_\alpha^\beta 2 f_+(u) f_-(u) u \mathrm{d}u, \\
g_0{}^{++} &= -G^2(G^2 - m_1{}^2) - M_K{}^2 m_\pi{}^2 + \frac{m_1{}^2}{4}(M_K{}^2 + m_\pi{}^2 - m_1{}^2), \qquad (3.1) \\
g_0{}^{--} &= \tfrac{1}{4} m_1{}^2 (M_K{}^2 + m_\pi{}^2 - m_1{}^2), \quad g_0{}^{+-} = \tfrac{1}{4} m_1{}^2 (2G^2 + M_K{}^2 - m_\pi{}^2 - m_1{}^2), \\
g_1{}^{++} &= 2G^2 - \tfrac{1}{2} m_1{}^2, \quad g_1{}^{--} = g_1{}^{+-} = -\tfrac{1}{2} m_1{}^2,
\end{aligned}$$

with α and β given in (A.1.4) (appendix 1). Note that all the functions g^{--} and g^{+-} contain the factor $m_1{}^2$. They are generally small compared with the g^{++}-terms.

For decay at rest the angular integrations can be performed, and we obtain for the differential muon energy spectrum

$$\mathrm{d}\Gamma_t(E_1) = \frac{(2\pi)^{-3}}{2M_K{}^2} \sum g I \mathrm{d}E_1, \qquad (3.2)$$

where the functions g and the integration limits α and β in the I's are now expressed in CMS variables ($G^2 = M_K{}^2 + m_1{}^2 - 2M_K E_1$) and the sum is taken over the six integrals in (3.1).

For decay in flight we obtain for the total number of muons (electrons) with energy E_1 in the laboratory system, without any reference to the direction of emission (appendix 2),

$$\mathrm{d}\Gamma_t(E_1) = \frac{(2\pi)^{-3}}{4M_K{}^2} \frac{1}{\gamma^2 v_K} \left(\int_{\varepsilon_{\min}}^{\varepsilon_{\max}} (\varepsilon^2 - m_1{}^2)^{-\frac{1}{2}} \sum g I \mathrm{d}\varepsilon \right) \mathrm{d}E_1 \qquad (3.3)$$

with

$$\gamma = (1 - v_K{}^2)^{-\frac{1}{2}},$$

where the functions g and the integration limits α and β in the integrals $I_0^{++},\ldots,$ are expressed in terms of the variable $\varepsilon(G^2 = M_K^2+m_l^2-2M_K\varepsilon)$. The limits of ε are

$$\begin{aligned}\varepsilon_{\min} &= \gamma(E_l - v_K(E_l^2-m_l^2)^{\frac{1}{2}}) \\ &\approx \tfrac{1}{2}\left(m_l^2\frac{\gamma}{E_l}+\frac{E_l}{\gamma}\right) \quad \text{for} \quad \gamma \gg 1,\ E_l \gg m_l, \\ \varepsilon_{\max} &= \min\,[E_0,\ \gamma(E_l+v_K(E_l^2-m_l^2)^{\frac{1}{2}})],\end{aligned} \tag{3.4}$$

with

$$E_0 = \frac{1}{2M_K}(M_K^2+m_l^2-m_\pi^2).$$

E_0 is the maximum energy of the muon (electron) in the kaon CMS. For $\gamma > E_0/m_l$, the upper limit $\varepsilon_{\max}$ is always equal to E_0.

3.2. THE MUON (ELECTRON) POLARIZATION

To obtain the degree of polarization in an arbitrary direction it is advantageous to employ invariant spin-projection operators of the type [14])

$$\tfrac{1}{2}(1\pm i\gamma_5\gamma_\sigma t_\sigma), \tag{3.5}$$

selecting states with spins pointing in the directions $\mathbf{t}$ and $-\mathbf{t}$ (space components of t_σ) respectively. Here t_σ are the components of a four-vector satisfying

$$t^2 = -1 \text{ (space-like) and } t_\sigma(p_l)_\sigma = 0. \tag{3.6}$$

Using these spin-projection operators and the covariant integration technique, one obtains for the excess of decays with muon (electron) spin parallel to $\mathbf{t}$ over those with spin antiparallel to $\mathbf{t}$

$$\begin{aligned}\Gamma_s &= 2m_l C\tfrac{1}{2}\pi\int\frac{d^3p_l}{2E_l}\{(Gp_K)^2-M_K^2G^2\}^{-\frac{1}{2}}[h_0^{++}I_0^{++}+h_0^{--}I_0^{--} \\ &\qquad +h_0^{+-}I_0^{+-}+h_l^{++}I_l^{++}+h_l^{--}I_l^{--}+h_l^{+-}I_l^{+-}](t\cdot G), \\ h_0^{++} &= \tfrac{1}{4}\{G^2(G^2-m_l^2)^2-(G^2+m_l^2)(G^2-m_\pi^2)M_K^2-M_K^4m_\pi^2\} \\ &\qquad +\frac{m_l^2}{16}\{G^2m_\pi^2+(G^2-m_\pi^2)(M_K^2+m_l^2)-(M_K^2-m_l^2)^2\}, \\ h_0^{--} &= \frac{m_l^2}{16}\{G^2(M_K^2+m_\pi^2+m_l^2)-(M_K^2-m_l^2)^2-m_\pi^2(M_K^2+m_l^2)\}, \\ h_0^{+-} &= \frac{m_l^2}{16}\{-2G^4-G^2(M_K^2+m_\pi^2-3m_l^2)-m_\pi^2(3M_K^2-m_l^2)-(M_K^2-m_l^2)^2\}, \\ h_l^{++} &= \tfrac{1}{2}G^2(-G^2+M_K^2+m_l^2)+\tfrac{1}{8}m_l^2(-G^2+M_K^2-m_l^2), \\ h_l^{--} &= \tfrac{1}{8}m_l^2(-G^2+m_K^2-m_l^2), \quad h_l^{+-} = \tfrac{1}{8}m_l^2(3G^2+M_K^2-m_l^2).\end{aligned} \tag{3.7}$$

For decay at rest this leads to the differential expression

$$\mathrm{d}\Gamma_s(E_1) = \frac{(2\pi)^{-3}}{2M_K{}^2}\, 2m_1 \frac{(t\cdot G)}{(M_K \mathbf{p}_1)^2} \sum hI \mathrm{d}E_1, \tag{3.8}$$

where, as before, the functions h and the integration limits α and β in the I's are expressed in CMS variables and the sum is taken over the six I's.

From eqs. (3.2) and (3.8) we obtain the degree of polarization in the direction $\mathbf{t}$ †:

$$P(E_1) = \frac{\mathrm{d}\Gamma_s(E_1)}{\mathrm{d}\Gamma_t(E_1)} = 2m_1 \frac{(t\cdot G)}{(M_K \mathbf{p}_1)^2} \frac{\sum hI}{\sum gI}. \tag{3.9}$$

For decay in flight we obtain the differential expression (see appendix 2)

$$\mathrm{d}\Gamma_s(E_1) = 2m_1 \frac{(2\pi)^{-3}}{4M_K{}^2} \frac{1}{M_K{}^2} \frac{1}{\gamma^2 v_K} \left\{ \int_{\varepsilon_{\min}}^{\varepsilon_{\max}} \mathrm{d}\varepsilon (\varepsilon^2 - m_1{}^2)^{-\frac{1}{2}} (t\cdot G) \sum hI \right\} \mathrm{d}E_1, \tag{3.10}$$

where the functions h and the integration limits α and β in the I's are expressed in terms of the variable ε. Finally we obtain the degree of polarization in an arbitrary direction $\mathbf{t}$ ††:

$$P(E_1) = \frac{2m_1}{M_K{}^2} \frac{\int_{\varepsilon_{\min}}^{\varepsilon_{\max}} \mathrm{d}\varepsilon (\varepsilon^2 - m_1{}^2)^{-\frac{1}{2}} (t\cdot G) \sum hI}{\int_{\varepsilon_{\min}}^{\varepsilon_{\max}} \mathrm{d}\varepsilon (\varepsilon^2 - m_1{}^2)^{-\frac{1}{2}} \sum gI}. \tag{3.11}$$

3.3. THE PION ENERGY SPECTRUM

In the calculation of the pion spectrum the integration over final states is an integration over neutrino and muon momenta, $p_K p_\pi$ and consequently also f_+ and f_- being kept constant. By means of a technique similar to that of appendix 1 the total decay rate in an arbitrary Lorentz frame may be written

$$\Gamma_t{}^{(\pi)} = (\Gamma_t{}^{(1)}) = \tfrac{1}{2}\pi C \int \frac{\mathrm{d}^3 p_\pi}{2E_\pi} \frac{(J^2 - m_1{}^2)^2}{3J^4} \{ f_+{}^2 k^{++} + 2 f_+ f_- k^{+-} + f_-{}^2 k^{--} \}, \tag{3.12}$$

with

$$C = \frac{4(2\pi)^{-5}}{2E_K}, \quad J_\lambda = (p_K - p_\pi)_\lambda,$$

$$k^{++} = 2\{(Jp_\pi)^2 - J^2 m_\pi{}^2\} + \tfrac{1}{4} \frac{m_1{}^2}{J^2} \{16((J\cdot p_\pi)^2 - J^2 m_\pi{}^2) - 3J^2(J^2 - 2M_K{}^2 - 2m_\pi{}^2)\},$$

$$k^{--} = \tfrac{3}{4} J^2 m_1{}^2; \quad k^{+-} = \tfrac{3}{4} m_1{}^2 (M_K{}^2 - m_\pi{}^2), \tag{3.12}$$

where

$$\{(J\cdot p_\pi)^2 - J^2 m_\pi{}^2\}^{\frac{1}{2}}_{\mathrm{CMS}} = M_K |\mathbf{p}_\pi|.$$

† A reasonable choice of the direction $\mathbf{t}$ in the CMS of the K-meson would be along the muon (electron), the neutrino, or perhaps the pion momentum.

†† Here also the choice of $\mathbf{t}$ parallel to $\mathbf{p}_K$ might be relevant.

For decay at rest we thus obtain the differential energy spectrum

$$\mathrm{d}\Gamma_t(E_\pi)=\frac{(2\pi)^{-3}}{2M_K}(E_\pi^2-m_\pi^2)^{\frac{1}{2}}\frac{(J^2-m_l^2)^2}{3J^4}\{f_+^2k^{++}+2f_+f_-k^{+-}+f_-^2k^{--}\}\mathrm{d}E_\pi, \tag{3.13}$$

where the functions J^2, k^{++}, k^{+-}, k^{--} and the form factors f are all expressed in CMS variables ($J^2=M_K^2+m_\pi^2-2M_KE_\pi$).

For decay in flight the number of pions of energy E_π is

$$\mathrm{d}\Gamma_t(E_\pi)=\frac{(2\pi)^{-3}}{4M_K}\frac{1}{\gamma^2v_K}\left\{\int_{\delta_{min}}^{\delta_{max}}\mathrm{d}\delta\,\frac{(J^2-m_l^2)^2}{3J^4}(f_+^2k^{++}+2f_+f_-k^{+-}+f_-^2k^{--})\right\}\mathrm{d}E_\pi, \tag{3.14}$$

where all functions in the integral are expressed in terms of δ, ($J^2=M_K^2+$ $+m_\pi^2-2M_K\delta$), and δ varies between the limits

$$\delta_{min}=\gamma(E_\pi-v_K(E_\pi^2-m_\pi^2)^{\frac{1}{2}})\approx\tfrac{1}{2}\left(m_\pi^2\frac{\gamma}{E_\pi}+\frac{E_\pi}{\gamma}\right)\quad\text{for}\quad\gamma\gg1,\quad E_\pi\gg m_\pi,$$

$$\delta_{max}=\min\,[E'_0,\gamma(E_\pi+v_K(E_\pi^2-m_\pi^2)^{\frac{1}{2}})], \tag{3.15}$$

with

$$E'_0=\frac{1}{2M_K}(M_K^2+m_\pi^2-m_l^2).$$

E'_0 is the maximum pion energy in the kaon CMS. For $\gamma>E'_0/m_\pi$, the upper limit δ_{max} is always equal to E'_0.

At first sight the expressions of this section seem unnecessarily complicated. However, it must be remembered that no assumptions (apart from time-reversal invariance and common origin of the leptons) have been made about the form factors f_+ and f_- in which the effects of strong interactions are contained. Thus, if some detailed model of the decay mechanism predicts f_+ and f_-, the six integrals I_0^{++}, . . . can be evaluated, and the spectra and the polarization of the muon in a given direction can be obtained.

The numerical values of the functions $g(E_l)$, $h(E_l)$ and $k(E_l)$ and the integration limits $\alpha(E_l)$ and $\beta(E_l)$ are given for the $K^0_{\mu3}$ decay in tables 1 to 4, and for K^0_{e3}-decay in tables 5 to 8, where the following mass values have been employed (energy unit 100 MeV):

$$M_{K^0}=4.979,\quad m_\pi=1.396,\quad m_\mu=1.057,\quad m_e=0.005110.$$

In the next two sections we shall make two explicit assumptions about the form factors †:

1) they are both constant;
2) their variation follows from dispersion relations.

† In a recent publication by the Rochester group [15]) the consequences of the current conservation $\partial(\langle\pi|J_\lambda|K\rangle)/\partial x_\lambda=0$ have been examined.

TABLE 1

The coefficients g for $K^0_{\mu 3}$ decay as functions of E_μ in the CMS. Energy unit: 10^2 MeV.

E_μ	g_0^{++}	g_1^{++}	g_0^{--}	g_1^{--}	g_0^{+-}	g_1^{+-}
1.10	−248.07	29.35	7.155	−0.5585	14.42	−0.5585
1.20	−220.39	27.36			13.86	
1.30	−194.71	25.37			13.31	
1.40	−171.00	23.37			12.75	
1.50	−149.27	21.38			12.19	
1.60	−129.52	19.39			11.64	
1.70	−111.75	17.40			11.08	
1.80	−95.99	15.41			10.52	
1.90	−82.19	13.42			9.97	
2.00	−70.38	11.42			9.41	
2.10	−60.55	9.43			8.86	
2.20	−52.70	7.44			8.30	
2.30	−46.85	5.45			7.74	
2.40	−43.14	3.46			7.19	

TABLE 2

The coefficients h for $K^0_{\mu 3}$ decay as functions of E_μ in the CMS. Energy unit: 10^2 MeV.

E_μ	h_0^{++}	h_1^{++}	h_0^{--}	h_1^{--}	h_0^{+-}	h_1^{+-}
1.10	−892.56	83.12	−13.57	1.218	−104.73	9.569
1.20	−861.56	84.75	−15.51	1.356	−99.08	9.152
1.30	−823.15	85.40	−17.44	1.496	−93.72	8.735
1.40	−778.91	85.05	−19.38	1.635	−88.62	8.318
1.50	−730.28	83.71	−21.32	1.774	−83.81	7.900
1.60	−678.79	81.37	−23.25	1.913	−79.30	7.483
1.70	−625.77	78.04	−25.19	2.052	−75.01	7.066
1.80	−572.81	73.74	−27.13	2.191	−71.03	6.649
1.90	−521.38	68.43	−29.06	2.330	−67.32	6.232
2.00	−472.96	62.13	−31.00	2.469	−63.89	5.815
2.10	−429.08	54.84	−32.94	2.608	−60.73	5.398
2.20	−391.10	46.55	−34.87	2.747	−57.86	4.980
2.30	−360.58	37.29	−36.81	2.886	−55.26	4.564
2.40	−338.97	26.98	−38.75	3.025	−52.93	4.146

TABLE 3

The coefficients k for $K^0_{\mu 3}$ decay as functions of E_π in the CMS. Energy unit: 10^2 MeV.

E_π	k^{++}	k^{--}	k^{+-}
1.40	39.41	10.73	19.13
1.50	52.71	9.89	
1.60	72.36	9.06	
1.70	93.94	8.22	
1.80	117.73	7.39	
1.90	143.71	6.55	
2.00	174.21	5.72	
2.10	208.89	4.88	
2.20	250.61	4.05	
2.30	304.01	3.22	
2.40	380.45	2.38	
2.50	515.57	1.55	
2.55	644.93	1.13	

TABLE 4

The limits occurring in the integrals ($K^0_{\mu 3}$ decay) over the form factors, given as functions of E_μ in the CMS. Energy unit: 10^2 MeV.

E_μ	β	α
1.10	11.58	10.26
1.20	11.94	9.51
1.30	12.14	8.94
1.40	12.27	8.45
1.50	12.38	8.02
1.60	12.46	7.65
1.70	12.53	7.34
1.80	12.59	7.11
1.90	12.64	6.97
2.00	12.68	6.98
2.10	12.72	7.21
2.20	12.75	7.83
2.30	12.78	9.21
2.40	12.81	12.50

TABLE 5

The coefficients g for K^0_{e3} decay as functions of E_e in the CMS. Energy unit: 10^2 MeV.

E_l	g_0^{++}	g_1^{++}	g_0^{--} ($\times 10^4$)	g_1^{--} ($\times 10^5$)	g_0^{+-} ($\times 10^4$)	g_1^{+-} ($\times 10^5$)
0.10	−614.48	47.59	1.745	−1.306	4.597	−1.306
0.20	−568.08	45.60			4.468	
0.30	−523.66	43.60			4.337	
0.40	−481.26	41.61			4.208	
0.50	−440.81	39.62			4.078	
0.60	−402.33	37.63			3.948	
0.70	−365.24	35.64			3.818	
0.80	−331.38	33.65			3.687	
0.90	−298.86	31.66			3.558	
1.00	−268.32	29.66			3.428	
1.10	−239.77	27.67			3.298	
1.20	−213.22	25.68			3.167	
1.30	−188.63	23.69			3.038	
1.40	−166.03	21.70			2.907	
1.50	−145.41	19.71			2.777	
1.60	−126.78	17.71			2.647	
1.70	−110.14	15.72			2.517	
1.80	−95.47	13.73			2.387	
1.90	−82.79	11.74			2.257	
2.00	−72.09	9.748			2.127	
2.10	−63.37	7.756			1.997	
2.20	−56.64	5.764			1.867	
2.25	−54.01	4.768			1.801	

TABLE 6

The coefficients h for K^0_{e3} decay as functions of E_e in the CMS. Energy unit: 10^2 MeV.

E_e	h_0^{++}	h_1^{++}	h_0^{--} ($\times 10^4$)	h_1^{--} ($\times 10^6$)	h_0^{+-} ($\times 10^3$)	h_1^{+-} ($\times 10^4$)
0.10	−152.96	11.85	−0.435	3.251	−4.126	3.139
0.20	−282.83	22.71	−0.869	6.501	−3.931	3.041
0.30	−391.10	32.57	−1.304	9.752	−3.743	2.944
0.40	−479.21	41.44	−1.738	13.000	−3.561	2.846
0.50	−548.61	49.32	−2.175	16.250	−3.385	2.749
0.60	−600.95	56.21	−2.607	19.500	−3.216	2.651
0.70	−637.53	62.10	−3.042	22.748	−3.054	2.554
0.80	−659.90	67.01	−3.477	25.998	−2.898	2.456
0.90	−669.55	70.93	−3.911	29.250	−2.748	2.359
1.00	−667.92	73.85	−4.346	32.500	−2.605	2.261
1.10	−656.57	75.78	−4.781	35.751	−2.469	2.164
1.20	−636.93	76.72	−5.214	38.998	−2.338	2.066
1.30	−610.47	76.67	−5.649	42.250	−2.215	1.969
1.40	−578.65	75.63	−6.083	45.500	−2.098	1.871
1.50	−543.00	73.59	−6.518	48.750	−1.986	1.774
1.60	−504.92	70.57	−6.952	52.000	−1.882	1.676
1.70	−466.11	66.54	−7.387	55.250	−1.785	1.579
1.80	−427.80	61.53	−7.822	58.500	−1.694	1.481
1.90	−391.57	55.53	−8.256	61.750	−1.610	1.384
2.00	−358.91	48.54	−8.691	65.000	−1.530	1.286
2.10	−331.29	40.55	−9.126	68.251	−1.458	1.189
2.20	−310.19	31.57	−9.550	71.501	−1.393	1.091
2.25	−302.56	26.71	−9.767	73.128	−1.363	1.043

TABLE 7

The coefficients k for K^0_{e3} decay as functions of E_π in the CMS. Energy unit: 10^2 MeV.

E_π	k^{++}	k^{--} ($\times 10^6$)	k^{+-} ($\times 10^4$)
1.40	0.51	250.6	4.473
1.50	14.87	231.1	
1.60	30.25	211.6	
1.70	46.60	192.1	
1.80	63.98	172.6	
1.90	82.25	153.1	
2.00	101.67	133.6	
2.10	121.90	114.1	
2.20	143.28	94.60	
2.30	165.69	75.12	
2.40	188.90	55.61	
2.50	213.25	36.11	
2.60	238.45	16.61	
2.65	251.46	6.85	

TABLE 8

The limits occurring in the integrals (K^0_{e3} decay) over the form factors, given as functions of E_e in the CMS. Energy unit: 10^3 MeV.

E_e	β	α
0.10	13.37	12.91
0.20		12.46
0.30		12.01
0.40		11.57
0.50		11.13
0.60		10.69
0.70		10.27
0.80		9.85
0.90		9.44
1.00		9.05
1.10		8.67
1.20		8.30
1.30		7.96
1.40		7.65
1.50		7.38
1.60		7.16
1.70		7.01
1.80		6.95
1.90		7.05
2.00		7.40
2.10		8.17
2.20		9.83
2.25		11.33

4. Constant Form Factors

The assumption that f_+ and f_- are constants might very well turn out to be a good approximation; therefore we shall consider it here in some detail.

The integrals I of section 3 are easily evaluated:

$$I_0 = (2)ff\frac{G^2-m_\pi^2}{G^2}\left((Gp_K)^2-G^2M_K^2\right)^{\frac{1}{2}}, \tag{4.1}$$

$$I_1 = (2)ff\frac{G^2-m_\pi^2}{2G^2}\left((Gp_K)^2-G^2M_K^2\right)^{\frac{1}{2}}\frac{G^2+m_\pi^2}{G^2}(Gp_K), \tag{4.2}$$

where the factor (2) is present in the f_+f_- integrals and absent from the f_+f_+ and f_-f_- integrals (cf. eq. (3.1)).

4.1. THE MUON SPECTRUM

The muon spectrum (3.2) for decay at rest is thus reduced to

$$d\Gamma_t(E_l) = C'(E_l^2-m_l^2)^{\frac{1}{2}}\{H_1(E_l)\}dE_l \tag{4.3a}$$

with

$$C' = \frac{(2\pi)^{-3}}{2M_K}, \quad E_1 = E_\mu, \quad m_1 = m_\mu, \quad p_1 = p_\mu,$$

and

$$H_1(E_\mu) = \frac{(\Delta - m_\pi^2 - 2M_K E_\mu)^2}{(\Delta - 2M_K E_\mu)} \left\{ f_+^2 \left(M_K E_\mu + \tfrac{1}{4} m_\mu^2 \frac{M_K E_\mu - m_\mu^2}{\Delta - 2M_K E_\mu} \right) + f_-^2 \tfrac{1}{4} m_\mu^2 \frac{M_K E_\mu - m_\mu^2}{\Delta - 2M_K E_\mu} + 2 f_+ f_- \tfrac{1}{4} \frac{2M_K^2 + m_\mu^2 - 3M_K E_\mu}{\Delta - 2M_K E_\mu} \right\}, \tag{4.3b}$$

with

$$\Delta = M_K^2 + m_\mu^2.$$

The spectrum is shown in figs. 1 and 2 for some particular choices of $\xi = f_-/f_+$. For ξ near zero the spectrum has its maximum at about 165 MeV. For large

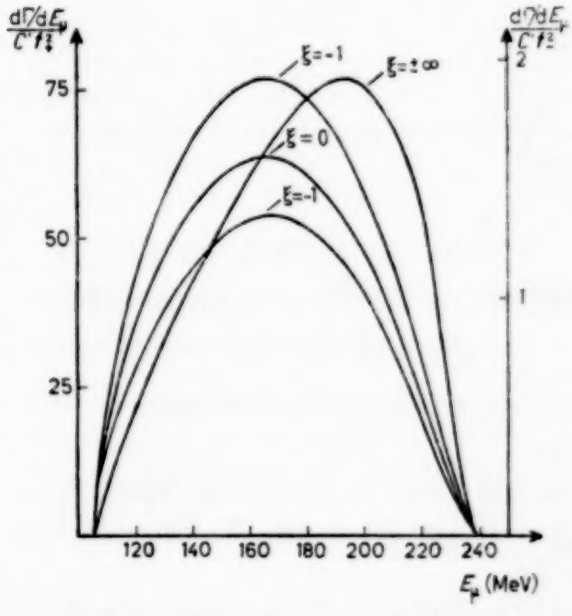

Fig. 1. Muon spectrum in the CMS for constant form factors. Left scale for $\xi = f_-/f_+ = -1, 0, +1$, right scale for $\xi = \pm\infty$.

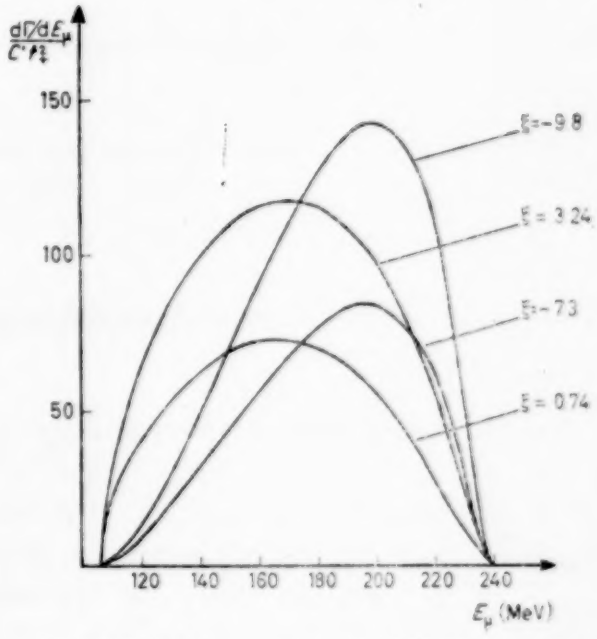

Fig. 2. Muon spectrum in the CMS for constant form factors.

values of $|\xi|$, when f_+ is relatively almost absent, the maximum moves to about 195 MeV. The terms containing $f_+ f_-$ and f_-^2 will generally be small compared with the f_+^2-term.

The spectrum for decay in flight is

$$d\Gamma_t(E_\mu) = \frac{C'}{\gamma v_K} \left\{ \int_{\varepsilon_{min}}^{\varepsilon_{max}} d\varepsilon \, H_1(\varepsilon) \right\} dE_\mu. \tag{4.4}$$

This spectrum is shown in fig. 3 for $\xi = -1$. It is here rather insensitive to the value of ξ (except near the upper and lower ends of the energy range). One can

thus show that for $\gamma > E_0/m_\mu$ all curves will have their maxima at $E_\mu = \gamma m_\mu$ ($c = 1$) independently of ξ: the integrand in eq. (4.4) is essentially the CMS spectrum (apart from a factor $|\mathbf{p}_\mu|$) and is thus positive. As the upper limit of

Fig. 3. Muon spectrum for decay in flight ($\gamma = (1-v_K^2)^{-\frac{1}{2}}$); constant form factors, $\xi = -1$.

the integrand is constant, E_0, the integral will have its maximum when the lower limit has its minimum, i.e. for $\varepsilon_{\min} = m_\mu$ or $E_\mu = \gamma m_\mu$ †. For $\gamma \gg 1$, $E_\mu \gg m_\mu$, one can make the approximation

$$d\Gamma_1(E_\mu) \approx \frac{C'}{\gamma^2} \int_{\frac{1}{2}\left(m_\mu^2 \frac{\gamma}{E_\mu} + \frac{E_\mu}{\gamma}\right)}^{E_0} d\varepsilon H_1(\varepsilon) dE_\mu = \frac{1}{\gamma^2} G\left(\frac{\gamma}{E_\mu}\right) dE_\mu. \qquad (4.5)$$

Using this approximation, one is allowed to plot the spectrum (and polarization) for any large value of γ in a single set of curves with the abscissa $(E_\mu/\gamma) \cdot 40$ (the original calculations were carried out for $\gamma = 40$). For $\gamma = 10$ the error is of the order of 1 %.

4.2. THE ELECTRON SPECTRUM

Owing to the smallness of m_e the expression for the spectrum is considerably reduced. If f_- and f_+ are of the same order of magnitude, the f_--terms can be

† The statement about the position of the maximum actually holds true down to $\gamma = 1.28$ for $K_{\mu 3}$-decay.

neglected (the $\xi = 0$ curve, fig. 4). The possibility that $f_- \gg f_+$ (the $\xi = \pm\infty$ curve, fig. 4) is ruled out by the experimental ratio $\Gamma_{\mu 3}/\Gamma_{e3}$.

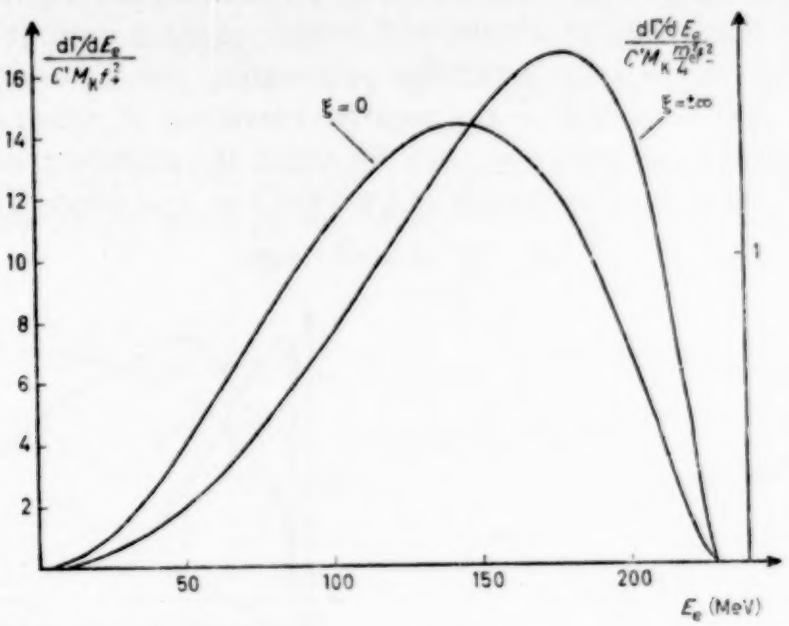

Fig. 4. Electron spectrum in the CMS for constant form factors. Left scale for $\xi = 0$, right scale for $\xi = \pm\infty$.

4.3. THE MUON POLARIZATION

For decay at rest we are mainly interested in the longitudinal polarization of the muon, and we shall use

$$t = \frac{1}{m_1}\left\{|\mathbf{p}_1|, \mathbf{p}_1 \frac{E_1}{|\mathbf{p}_1|}\right\}, \tag{4.6}$$

with

$$E_1 = E_\mu, \quad m_1 = m_\mu, \quad \not{p}_1 = \not{p}_\mu.$$

The expression (2.9) is then reduced to

$$P(E_\mu) = M_K(E_\mu^2 - m_\mu^2)^{\frac{1}{2}} \frac{H_2(E_\mu)}{H_1(E_\mu)},$$

$$H_2(E_\mu) = \frac{(\Delta - m_\pi^2 - 2M_K E_\mu)^2}{(\Delta - 2M_K E_\mu)}\left\{f_+^2\left(1 - \tfrac{1}{4}m_\mu^2 \frac{1}{\Delta - 2M_K E_\mu}\right)\right. \tag{4.7}$$

$$\left. - f_-^2 \tfrac{1}{4} m_\mu^2 \frac{1}{\Delta - 2M_K E_\mu} - 2f_+ f_- \tfrac{1}{4} m_\mu^2 \frac{1}{(\Delta - 2M_K E_\mu)}\right\}.$$

This quantity is plotted in figs. 5 and 6, labelled with the value of ξ. The variation of the curves with ξ is quite interesting. In the region $\xi = +\infty$ (pure f_-) to $\xi = 0$ (pure f_+) the curves change gradually from (high) negative

polarization (for high energy) to positive polarization. Letting ξ go to negative values, we soon obtain (for ξ slightly beyond -1)a curve with maximum polarization for full energy ($E_\mu = 240$ MeV). As ξ becomes more negative, the full polarization takes place at smaller and smaller energies until at $\xi = -3.48$ ($\xi = -(2M_K - m_\mu)/m_\mu$) the maximum polarization (for $E_\mu = m_\mu$) suddenly changes its sign. From now on the negative maximum of polarization occurs for increasing energies until $\xi = -70$, for which the maximum comes at full energy. This curve deviates very little from the $\xi = \pm\infty$ curve. The polarization for $\overset{0}{K}^- \to \mu^- + \bar{\nu} + \overset{+}{\pi}{}^0$ has the opposite sign.

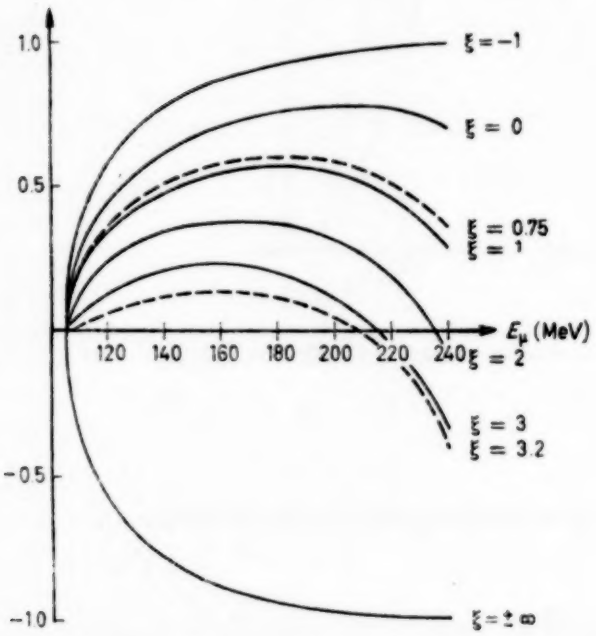

Fig. 5. Muon polarization in the CMS for constant form factors.

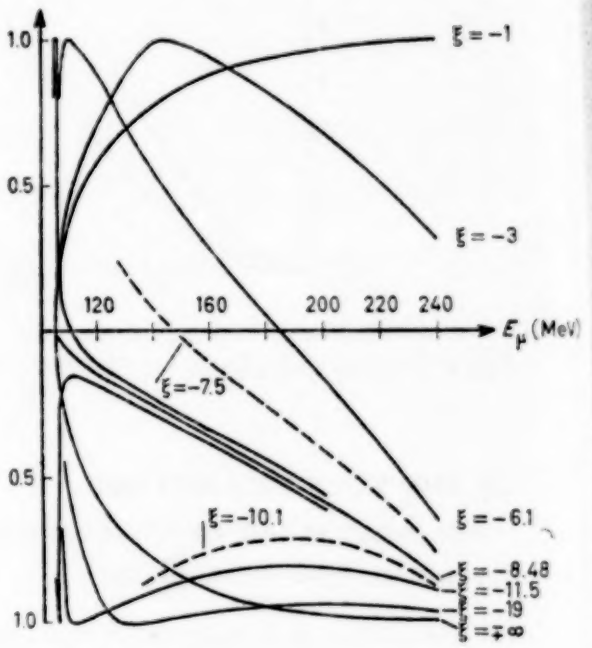

Fig. 6. Muon polarization in the CMS for constant form factors.

For decay in flight we have one more direction of reference, viz. the direction of motion of the decaying K-meson. If, in an experiment, the K-meson velocity is great, $\gamma \gg 1$, and the muon is brought to rest before its polarization is measured, the original direction of motion of the muon will in general be almost completely veiled by Coulomb scattering in the stopping medium. In such an experiment it is reasonable to refer the polarization to the direction of motion of the K-meson. Hence t is chosen as

$$t = (E_1^2 - (\mathbf{p}_1 \cdot \mathbf{e})^2)^{-\frac{1}{2}}\{(\mathbf{p}_1 \cdot \mathbf{e}), \mathbf{e}E_1\} \tag{4.8}$$

with

$$\mathbf{e} = \frac{\mathbf{p}_K}{|\mathbf{p}_K|}, \quad E_1 = E_\mu, \quad m_1 = m_\mu, \quad p_1 = p_\mu,$$

for which (3.11) is reduced to

$$P(E_\mu) = M_K m_\mu \frac{\int_{\varepsilon_{min}}^{\varepsilon_{max}} d\varepsilon \frac{E_\mu - \varepsilon\gamma}{(2\gamma\varepsilon E_\mu - E_\mu^2 - \varepsilon^2)^{\frac{1}{2}}} H_2(\varepsilon)}{\int_{\varepsilon_{min}}^{\varepsilon_{max}} d\varepsilon H_1(\varepsilon)}. \tag{4.9}$$

The polarization in the kaon direction is plotted in figs. 7 and 8. When E_μ is near its maximum (for given γ), the muons are emitted in a forward direction

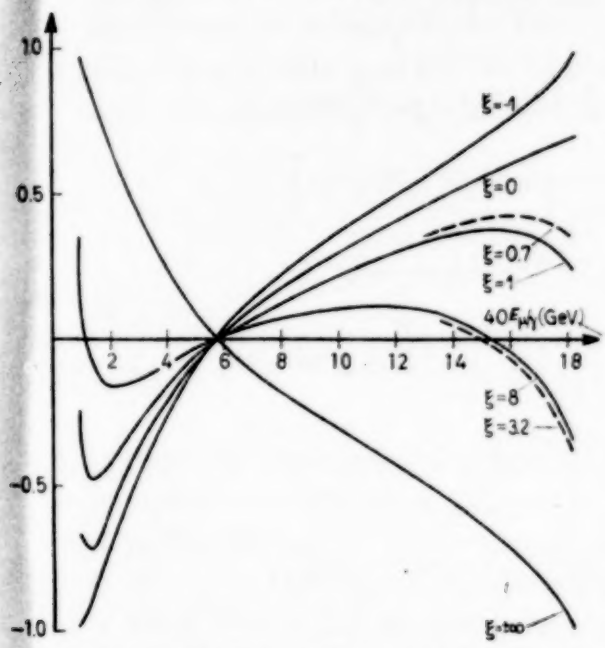

Fig. 7. Muon polarization in the K-direction for decay in flight; constant form factors.

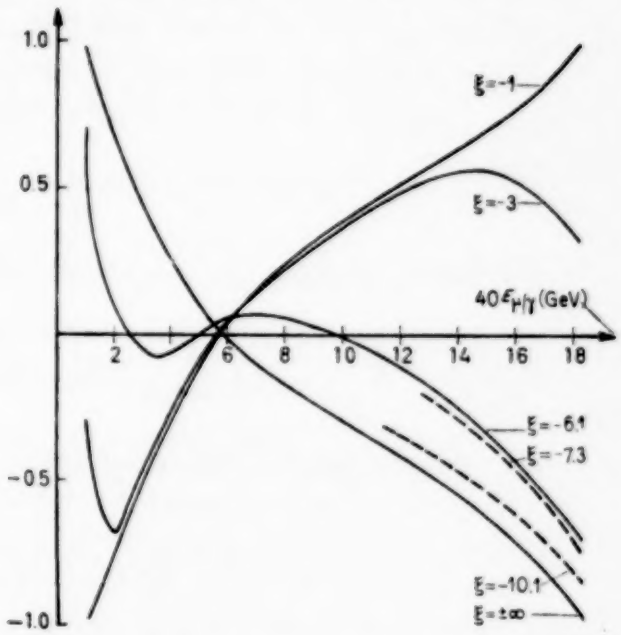

Fig. 8. Muon polarization in the K-direction for decay in flight; constant form factors.

in the kaon CMS; therefore the polarization for $E_\mu \to E_{\mu_{max}}$ tends to the same limit as in the CMS (figs. 4 and 5). The muons of low energy are emitted backwards in the CMS; their spins therefore point in the opposite direction and the low-energy-limit polarization has minus the value in the CMS. Apart from the sign shift at about $(\gamma/40) \cdot 6$ GeV the curves have the same character as in the CMS.

For large values $E_\mu \gg m_\mu$, $\gamma \gg 1$, the polarization may be approximated by a function of (E_μ/γ) only:

$$P(E_\mu, \gamma) = P(E_\mu/\gamma). \tag{4.10}$$

Cf. the remark below eq. (3.5).

4.4. THE ELECTRON POLARIZATION

The polarization in K_{e3}-decay behaves in principle like that in $K_{\mu 3}$-decay. However, on account of the smallness of m_e the f_- terms can be neglected

(except when $f_- \gg f_+$), and from the matrix element (2.4′) we immediately see that e^- is lefthanded, e^+ righthanded. if $f_- \gg f_+$, the polarization is reversed.

4.5. THE PION SPECTRUM

For decay at rest the energy spectrum (3.13) of the emitted π-meson becomes

$$\begin{aligned} d\Gamma(E_\pi) = \frac{C'}{3}(E_\pi^2 - m_\pi^2)^{\frac{1}{2}} \left(\frac{\Phi - m_l^2 - 2M_K E_\pi}{\Phi - 2M_K E_\pi}\right)^2 \Big\{ f_+^2 \Big(2M_K^2(E_\pi^2 - m_\pi^2) \\ + \tfrac{1}{4} m_l^2 \frac{4M_K^2(E_\pi^2 - m_\pi^2) + 3(M_K^2 - m_\pi^2)^2}{\Phi - 2M_K E_\pi} \Big) \\ + f_-^2 \tfrac{3}{4} m_l^2 (\Phi - 2M_K E_\pi) + 2 f_+ f_- \tfrac{3}{4} m_l^2 (M_K^2 - m_\pi^2) \Big\} dE_\pi \end{aligned} \tag{4.11}$$

with

$$\Phi = M_K^2 + m_\pi^2.$$

For decay in flight we obtain the corresponding expression

$$\begin{aligned} d\Gamma(E_\pi) = \tfrac{1}{3} \frac{C'}{\gamma(\gamma^2-1)^{\frac{1}{2}}} \Big[\int_{\delta_{min}}^{\delta_{max}} d\delta \left(\frac{\Phi - m_l^2 - 2M_K\delta}{\Phi - 2M_K\delta}\right)^2 \Big\{ f_+^2 \Big(2M_K^2(\delta^2 - m_\pi^2) \\ + \tfrac{1}{4} m_l^2 \frac{4M_K^2(\delta^2 - m_\pi^2) + 3(M_K^2 - m_\pi^2)^2}{\Phi - 2M_K\delta} \Big) \\ + f_-^2 \tfrac{3}{4} m_l^2 (\Phi - 2M_K\delta) + 2 f_+ f_- \tfrac{3}{4} m_l^2 (M_K^2 - m_\pi^2) \Big\} \Big] dE_\pi . \end{aligned} \tag{4.12}$$

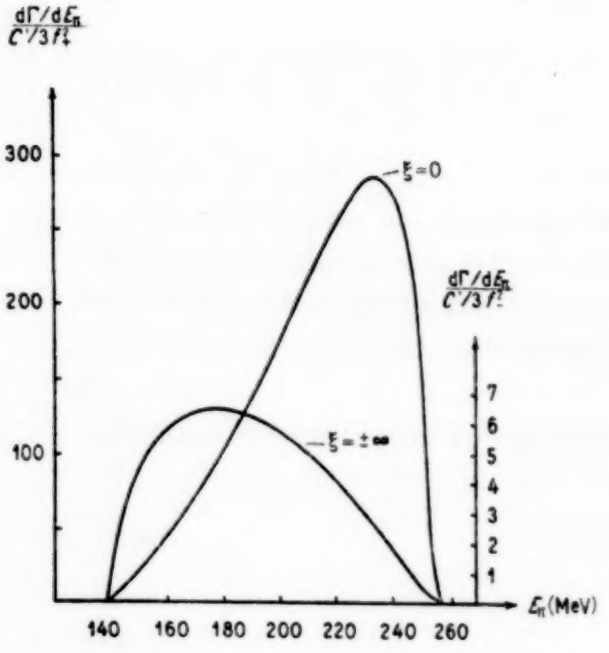

Fig. 9. Pion spectrum for $K_{\mu 3}$-decay at rest; constant form factors. Left scale for $\xi = 0$; right scale for $\xi = \pm\infty$.

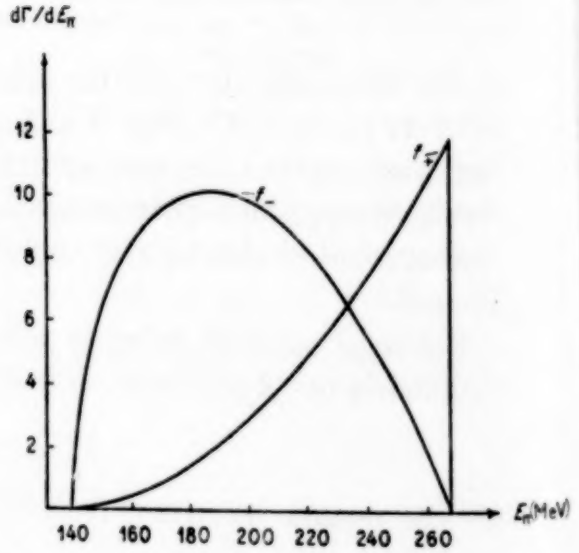

Fig. 10. Pion spectrum for K_{e3}-decay at rest; constant form factors. $d\Gamma/\frac{1}{3}C' M_K^2 f_+^2 dE_\pi$ is plotted for $\xi = 0$, $d\Gamma/\frac{1}{4}C' m_e^2 f_-^2 dE_\pi$ for $\xi = \pm\infty$.

The curves for $\xi = 0$ and $\xi = \pm\infty$ are shown in fig. 9 ($K_{\mu 3}$-decay) and fig. 10 (K_{e3}-decay).

4.6. DETERMINATION OF f_-/f_+ FROM THE $K_{\mu 3}/K_{e3}$ BRANCHING RATIO

The possibility of determining $f_-/f_+ = \xi$ by means of the experimental ratio between the $K_{\mu 3}$ and the K_{e3} decay rates has been pointed out by several authors [6, 9]) and rests on the assumption that the muon and the electron have identical couplings except for differences due to their different masses; this assumption is strongly supported by the experimental ratio between electrons and muons in π-decay [17, 18]). Thus f_+ (and f_-) is the same in the $K_{\mu 3}$ and the K_{e3} decay modes, and for the total decay rate (in the CMS) we obtain, in the approximation that m_e can be neglected,

$$\int \mathrm{d}\Gamma_\mu(E_\mu) = \text{const.} \cdot (4.78 f_+^2 + 0.92 f_+ f_- + 0.14 f_-^2), \tag{4.13}$$

$$\int \mathrm{d}\Gamma_e(E_e) = \text{const.} \cdot 7.4\, f_+^2, \tag{4.14}$$

or

$$\nu = \frac{\Gamma_\mu^{\text{tot}}}{\Gamma_e^{\text{tot}}} = 0.65 + 0.124\xi + 0.0190\xi^2 \geqq 0.46. \tag{4.15}$$

Now the experimental determination of the ratio ν for K^0-decay is very incomplete; we only know that ν is of the order of 1. However, for K^+-decay [19]) it is better known †, $\nu = 1 \pm 0.25$. Assuming ν for K^0-decay to lie in the interval $0.75 < \nu < 1.25$, we see that the value of ξ must lie in one of the intervals ††
$-9.8 < \xi < -7.3$ (a) and $0.74 < \xi < 3.24$ (b). The spectrum for ξ lying in interval (a) has its maximum near 195 MeV, while that for ξ in the interval (b) has its maximum near 165 MeV. The muon polarization curves in the CMS for ξ in interval (a) show full positive or negative polarization for low energies and large negative (≈ -0.8) polarization for high energies. The polarization for ξ in interval (b) is limited to lie between 10 % and 60 % for moderate energies and between -40 % and $+35$ % for high energies. For decay in flight the polarization behaves correspondingly. Thus a rough measurement of the muon spectrum for decay at rest (K^+) or of the muon polarization for decay at rest or in flight (K^+ or K^0) should make possible a distinction between the two possibilities (a) and (b). If ξ is in interval (a), the sign of the polarization at low energies further restricts the interval.

5. Form Factors Derived from Dispersion Relations

In a recent publication, MacDowell [16]) has derived expressions for f_+ and f_- by means of a dispersion technique neglecting all intermediate states except

† Cf., however, the remark in section 1 about the isospin multiplet structure of the K-mesons.
†† Cf. solutions 1 and 2 of refs. [6, 9]).

$|n\rangle = |K\pi\rangle$ and $|n\rangle = |N\bar{Y}\rangle$. In the derivation the form factors are related to the scattering of π-mesons on K-mesons, and on the assumption that this scattering proceeds mainly through S-states (scattering length a) the following results are obtained for a positive (repulsive scattering) and negative (attractive scattering) respectively:

$$(a > 0) \qquad f_+ \approx \text{const.}, \quad f_- = f_+ Q \frac{(2M_K m_\pi + 2p_K p_\pi)^{\frac{1}{2}} - (M_K + m_\pi)}{M_K^2 + m_\pi^2 - 2p_K p_\pi}, \tag{5.1}$$

where

$$Q = \frac{(M_K^2 - m_\pi^2)a}{1 + a(M_K + m_\pi)},$$

$(a < 0)$

$$f_+ \approx \text{const.}, \quad f_- = f_+ \frac{a(M_K^2 - m_\pi^2)\left((2M_K m_\pi + 2p_K p_\pi) - (M_K + m_\pi)\right)}{\left(1 - a(2M_K m_\pi + 2p_K p_\pi)^{\frac{1}{2}}\right)(M_K^2 + m_\pi^2 - 2p_K p_\pi)}. \tag{5.2}$$

The numerical calculations lead to the muon spectrum and muon polarization (longitudinal, in the CMS) shown in fig. 11 and fig. 12 for the values $a = +\infty$,

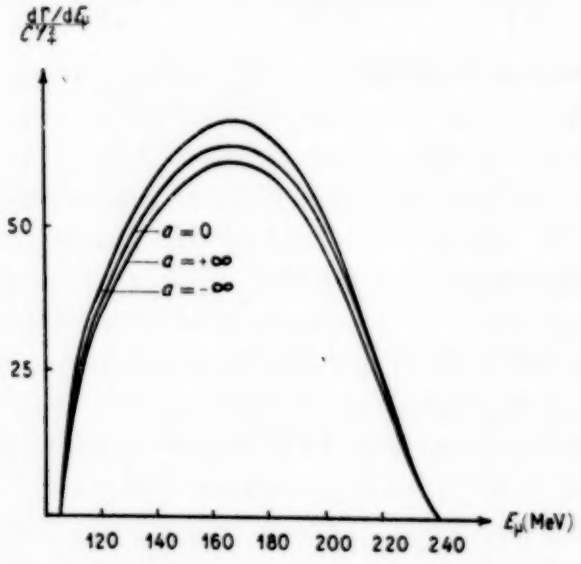

Fig. 11. Muon spectrum in the CMS for MacDowell's form factors.

$a = 0$, $a = -\infty$, and to the pion spectrum, fig. 13, for the same a-values. The rather small deviations from the $a = 0$ curves ($f_- = 0$) are not surprising in view of the relative smallness of f_- (f_- for $p_\pi p_K = M_K m_\pi$, lower end of the physical region, $M_K m_\pi < p_\pi p_K < \frac{1}{2}(M_K^2 + m_\pi^2 - m_\mu^2)$, lies between $-0.33\, f_+$ for $a = +\infty$ and $+0.41\, f_+$ for $a = -\infty$) and the slow variation over the physical region. For the same reason we expect the electron spectrum and polarization and the corresponding pion spectrum to be identical with those for $f_+ = \text{const.}$, $f_- = 0$ (figs. 4 and 10).

The branching ratio Γ_μ/Γ_e does not deviate much from that for $a = 0$ ($\Gamma_\mu/\Gamma_e(a = 0) = \Gamma_\mu/\Gamma_e(f_+) \approx 0.65$): the electron decay constant Γ_e depends negligibly on f_- and therefore also on a (factor m_e^2) so that

$$\Gamma_\mu(a)/\Gamma_e(a) = \Gamma_\mu(0)/\Gamma_e(0)\Gamma_\mu(a)/\Gamma_\mu(0), \tag{5.3}$$

and the value must lie between $0.61 (a = -\infty)$ and 0.68 $(a = +\infty)$.

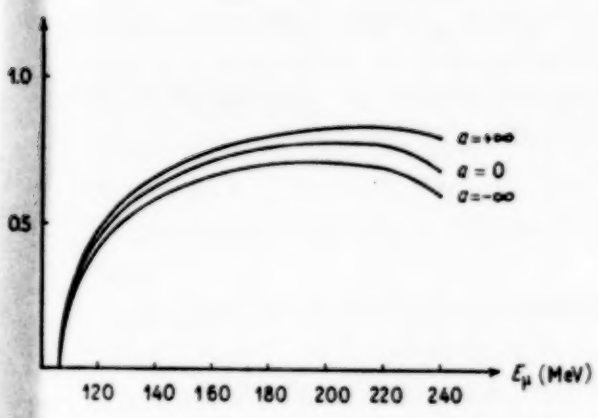

Fig. 12. Muon polarization in the CMS for MacDowell's form factors.

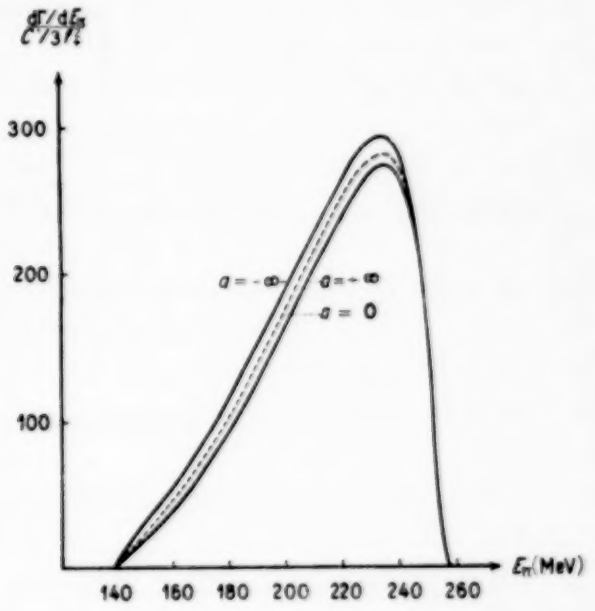

Fig. 13. Pion spectrum for $K_{\mu 3}$-decay at rest; MacDowell's form factors.

Thus MacDowell's expressions (5.1) and (5.2) (and consequently his assumptions) may be discarded if the muon energy spectrum does not have its maximum at 165—170 MeV, or if the longitudinal polarization or the branching ratio (5.3) deviate more than 5 % from those for $f_+ = \text{const.}, f_- = 0$. If, on the other hand, the expressions (5.1) and (5.2) are correct, the determination of the scattering length requires very accurate polarization or branching-ratio experiments.

6. Final Remarks

The form factors f_+ and f_- appear in rather different ways in the expression (3.12) for the pion spectrum and the expressions (3.1) and (3.7) for the muon (electron) spectrum and polarization. In the former, f_+ and f_- are just two variable factors, whereas in the latter the squares and product of f_+ and f_- are integrated between certain limits α and β (A.1.4) which are — in the CMS of the decaying particle — proportional to the minimum and the maximum pion energy for a given muon energy.

The situation is illustrated in figs. 14 (a, b) and 15, which show these limits (fig. 14(a) and fig. 15) and how the form factors (squared) might vary over the region of interest (fig. 14(b)).

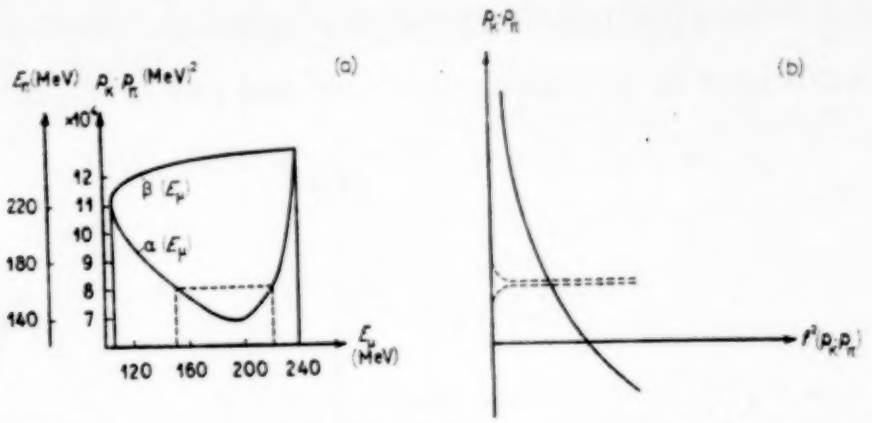

Fig. 14. The limits of integration $\alpha(E_\mu)$, $\beta(E_\mu)$ for $K_{\mu 3}$-decay at rest (a) and examples of the dependence of the form factors on the pion momentum (b).

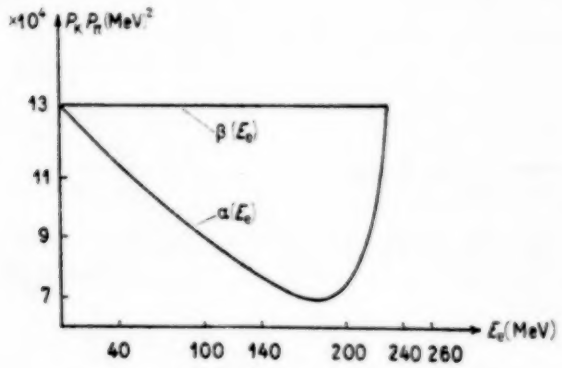

Fig. 15. The limits of integration $\alpha(E_e)$, $\beta(E_e)$ for K_{e3}-decay at rest.

As already mentioned, MacDowell's form factors show only a small variation over this region. However, in MacDowell's as well as in the present work a possible non-locality of the basic Fermi interaction has been neglected.

If the basic weak interaction proceeds via an intermediate (vector) boson of mass M_B, the form factors should be multiplied by the boson propagator so that the matrix element (2.4) is replaced by

$$M = \frac{G^2}{F}\{\tfrac{1}{2}f_+(p_K+p_\pi)+\tfrac{1}{2}f_-(p_K-p_\pi)\}_\kappa \frac{g_{\kappa\lambda}-M_B{}^{-2}(p_K-p_\pi)_\kappa(p_K-p_\pi)_\lambda}{M_B{}^2-(p_K-p_\pi)^2} \times \bar{u}(p_\nu)\gamma_\lambda(1-i\gamma_5)v(p_l) \tag{6.1}$$

(F is the Fermi coupling constant, G the corresponding intermediate coupling constant).

This can be brought back into the form (2.4) with the new effective form

factors

$$F_+ = \frac{G^2}{F} f_+ \frac{1}{M_B{}^2 - (p_K - p_\pi)^2},$$
$$F_- = \frac{G^2}{F} \frac{1}{M_B{}^2}\left[f_- - f_+ \frac{M_K{}^2 - m_\pi{}^2}{M_B{}^2 - (p_K - p_\pi)^2}\right] = \frac{1}{M_B{}^2}\left[\frac{G^2}{F} f_- - (M_K{}^2 - m_\pi{}^2) F_+\right]. \quad (6.2)$$

In the $K_{\mu 3}(K_{e3})$ decay mode the momentum transfer $[(p_K - p_\pi)^2]^{\frac{1}{2}}$ varies between m_μ and $M_K - m_\pi$ (m_e and $M_K - m_\pi$). Thus, for M_B not too much larger than M_K ($M_B > M_K$ prevents a rapid K decay into the B-particle) we expect a fairly great variation of F_+. To the extent that we believe in MacDowell's result, constancy of f_+, this variation is solely due to the existence of an intermediate particle. The K_{e3} decay mode for which the F_- terms can be neglected offers a possibility of testing the intermediate-boson hypothesis. If the boson has a large mass, or does not exist, the pion spectrum will be given by the $f_+{}^2$ term of eq. (4.11) (the $f_- = 0$ curve of fig. 8). For a mass $M_B = 1000$ MeV the upper end of the spectrum will have a correction factor 0.78 as compared with the lower end; for $M_B = 800$ MeV the factor is 0.70 and for $M_B = 600$ MeV it is 0.49.

It is interesting that f_+ occurs in F_- so that F_- might be different from zero even when $f_- = 0$ (scattering length $a = 0$ in K—π scattering). In this case F_+ and F_- have the same momentum dependence and the constant ratio $M_B{}^2/(M_K{}^2 - m_\pi{}^2)$. In the limit $M_B \to \infty$ ($G^2/M_B{}^2 \to F$) F_+ and F_- are f_+ and f_- respectively, and the results of section 5 are again valid.

As a mathematically extreme case we shall consider an apparent 3-body decay which is really two successive 2-body decays (M_K, M_B, m_π, m_1, m_ν now refer to the particles in question, not especially to those involved in K-meson decay). Here the intermediate particle is real, and the form factors (squares) contain a δ-function so that the integrals I are immediately calculated. From fig. 14 (modified according to the actual case) we see that the π-particle will be emitted monoenergetically whereas the l-particle spectrum is continuous between certain restricted limits. This corresponds to the spectrum in the laboratory system of the l-particle which in the CMS of the intermediate particle is emitted monoenergetically but with some angular distribution.

We wish to express our sincere gratitude to Professors A. Bohr and B. Peters and to Drs. S. Berman and D. Geffen for helpful discussions. The financial support of NORDITA is gratefully acknowledged.

Appendix

A.1. INTEGRATION OVER POSSIBLE FINAL STATES

Evaluation of the muon (electron) spectrum and polarization involves integrations of the following types:

$$\int \frac{\mathrm{d}^3 p_\pi}{2E_\pi} \frac{\mathrm{d}^3 p_\nu}{2E_\nu} \delta(p_\mathrm{K} - p_\pi - p_\mathrm{l} - p_\nu) f(p_\mathrm{K} \cdot p_\pi), \tag{A.1.1}$$

$$\int \frac{\mathrm{d}^3 p_\pi}{2E_\pi} \frac{\mathrm{d}^3 p_\nu}{2E_\nu} \delta(p_\mathrm{K} - p_\pi - p_\mathrm{l} - p_\nu) f(p_\mathrm{K} \cdot p_\pi)(p_\pi)_\lambda, \tag{A.1.2}$$

where $f(p_\mathrm{K} p_\pi)$ is one of the scalar (pseudoscalar) functions f_+^2, f_-^2, $f_+ f_-$, and $(p_\pi)_\lambda$ is a component of the pion 4-momentum.

These integrals may be evaluated by means of a covariant-integration technique. Eq. (A.1.1) can be rewritten (after integration over the neutrino momenta) in the form

$$\int \mathrm{d}^3 p_\pi \, \mathrm{d}E_\pi \delta(p_\pi^2 - m_\pi^2) \delta(G_0^2 + m_\pi^2 - 2G_0 (p_\pi)_0) f(p_\mathrm{K} \cdot p_\pi), \tag{A.1.3}$$

where $G_\lambda = (p_\mathrm{K} - p_\mathrm{l})_\lambda$ and we have chosen a coordinate system in which $\mathbf{G} = 0$. After integration over E_π and transition to polar coordinates we obtain

$$\begin{aligned} &\frac{2\pi}{2G_0} \int_{x=-1}^{+1} \mathrm{d}x \int_{\mathbf{p}_\pi=0}^{\infty} \mathrm{d}|\mathbf{p}_\pi| \frac{|\mathbf{p}_\pi|}{2} \delta\left(|\mathbf{p}_\pi| - \frac{G_0^2 - m_\pi^2}{2G_0}\right) \\ &\quad \times f\left(\frac{G_0^2 + m_\pi^2}{2G_0^2} (G_0 p_{\mathrm{K}0}) - |\mathbf{p}_\mathrm{K}||\mathbf{p}_\pi| x\right) \\ &= \tfrac{1}{2}\pi [(G p_\mathrm{K})^2 - G^2 M_\mathrm{K}^2]^{-\frac{1}{2}} \int_\alpha^\beta \mathrm{d}u f(u) = \tfrac{1}{2}\pi [(G p_\mathrm{K})^2 - G^2 M_\mathrm{K}^2]^{-\frac{1}{2}} I_0 \end{aligned} \tag{A.1.4}$$

with †

$$\begin{aligned} I_0 &= \int_\alpha^\beta \mathrm{d}u \, f(u) \\ \left.\begin{matrix}\beta \\ \alpha\end{matrix}\right| &= \frac{G^2 + m_\pi^2}{2G^2} (G p_\mathrm{K}) \pm \frac{G^2 - m_\pi^2}{2G^2} [(G p_\mathrm{K})^2 - G^2 M_\mathrm{K}^2]^{\frac{1}{2}}. \end{aligned}$$

The expression (A.1.2) is transformed under Lorentz transformations as a 4-vector and must therefore be of the form

$$A G_\lambda + B (p_\mathrm{K})_\lambda. \tag{A.1.5}$$

A and B are scalar functions. Scalar multiplication by G_λ and $(p_\mathrm{K})_\lambda$ gives us

† $\{(G p_\mathrm{K})^2 - G^2 M_\mathrm{K}^2\}^{\frac{1}{2}}_{\mathrm{CMS}} = M_\mathrm{K} |\mathbf{p}_\mathrm{l}|$. $\{(G p_\mathrm{K})^2 - G^2 M_\mathrm{K}^2\}^{\frac{1}{2}}_{\mathrm{lab}} = M_\mathrm{K}(\varepsilon^2 - m_\mathrm{l}^2)^{\frac{1}{2}}$, where $\varepsilon = \gamma(E_\mathrm{l} - v_\mathrm{K} p_{\mathrm{l}z})$, cf. appendix 2.

two equations for the determination of A and B. The solution is

$$\begin{aligned} B &= \tfrac{1}{2}\pi\{(Gp_K)^2-G^2M_K^2\}^{-\frac{1}{2}}\{\tfrac{1}{2}(G^2+m_\pi^2)(Gp_K)I_0-G^2I_1\}, \\ A &= \tfrac{1}{2}\pi\{(Gp_K)^2-G^2M_K^2\}^{-\frac{1}{2}}\{-\tfrac{1}{2}(G^2+m_\pi^2)M_K^2I_0+(Gp_K)I_1\}, \\ I_1 &= \int_\alpha^\beta \mathrm{d}u f(u)u. \end{aligned} \tag{A.1.6}$$

The limits of integration, α and β, are given numerically in tables 4 (for $K_{\mu 3}$-decay) and 8 (for K_{e3}-decay).

A.2. THE DIFFERENTIAL LEPTON SPECTRUM

The total decay probability may be written

$$\begin{aligned} \Gamma_i &= \tfrac{1}{2}\pi C\int\frac{\mathrm{d}^3p_1}{2E_1}\{(Gp_K)^2-G^2M_K^2\}^{-\frac{1}{2}}\sum_i g_i(G^2)I_i(G^2) \\ &= \int\frac{\mathrm{d}^3p_1}{2E_1}H(G^2), \end{aligned} \tag{A.2.1}$$

where i runs over the six combinations in (3.1) and the functions and integrals g_i and I_i can all be expressed in terms of G^2, G^2 depending on (p_{1x}, p_{1y}, p_{1z}). By a change of variables

$$(p_{1x}, p_{1y}, p_{1z}) \to (p_{1x}, E_1, \varphi)$$

the integral is transformed into

$$\tfrac{1}{2}\int \mathrm{d}E_1\mathrm{d}p_{1x}\mathrm{d}\varphi H(G^2) = \frac{2\pi}{2}\int \mathrm{d}E_1\mathrm{d}p_{1x}H(G^2). \tag{A.2.2}$$

We note that

$$G^2 = (p_K-p_1)^2 = M_K^2+m_1^2-2M_K\gamma(E_1-v_Kp_{1x})$$

(x-axis chosen parallel to the momentum $\mathbf{p}_K$) contains E_1 and p_{1x} in the combination

$$\varepsilon = \gamma(E_1-v_Kp_{1x}),$$

where ε is the energy in the CMS). Hence, on a new change of variables

$$(p_{1x}, E_1) \to (\varepsilon, E_1)$$

the integral is transformed into

$$-\frac{1}{\gamma v_K}\frac{2\pi}{2}\int_{\varepsilon_{max}}^{\varepsilon_{min}}\mathrm{d}E_1\mathrm{d}\varepsilon H(G^2(\varepsilon)), \tag{A.2.3}$$

where H does not depend on E_1.

The spectrum is therefore

$$dI_1(E_1) = \left(\frac{2\pi}{2}\frac{1}{\gamma\beta_K}\int_{\varepsilon_{min}}^{\varepsilon_{max}} d\varepsilon H(\varepsilon)\right) dE_1. \qquad (A.2.4)$$

i.e. we essentially perform the integration over the spectrum in the rest system.

A.3 DECAY IN FLIGHT OF A K-MESON BEAM OF ENERGY COMPOSITION $D(\gamma)$ (FORM FACTORS f_+ AND f_- CONSTANT)

If the decaying K-mesons have different energies ($\gamma = E_K/M_K$) but the same direction, the decay rate is obtained by integration over their energy distribution $D(\gamma)$; thus the total number of decays in a short time of flight Δt is by (4.4) and (4.5) for $\gamma \gg 1$, $E_1 \gg m_1$,

$$dI_1^D(E_1) = \Delta t C' \left(\int_{\gamma_{min}}^{\gamma_{max}} d\gamma \frac{D(\gamma)}{\gamma^2} \int_{\varepsilon_{min}}^{\varepsilon_{max}} d\varepsilon H_1(\varepsilon)\right) dE_1. \qquad (A.3.1)$$

with

$$\varepsilon_{min} \approx \tfrac{1}{2}\left(m_1^2 \frac{\gamma}{E_1} + \frac{E_1}{\gamma}\right); \quad \varepsilon_{max} = E_0. \qquad (A.3.2)$$
$$\gamma_{min} \approx E_1/(E_0+P_0), \quad \gamma_{max} \approx E_1/(E_0-P_0),$$

where

$$P_0 = (E_0^2 - m_1^2)^{\frac{1}{2}}.$$

A similar expression is obtained for the excess of decays with muon (electron) spin parallel to the K-momentum, and dividing this by (A.3.1) we find the polarization

$$P^D(E_1) = \frac{m_1 M_K \int_{\gamma_{min}}^{\gamma_{max}} d\gamma \frac{D(\gamma)}{\gamma^2} \int_{\varepsilon_{min}}^{\varepsilon_{max}} d\varepsilon \left(1-\varepsilon\frac{\gamma}{E_1}\right)\left(2\varepsilon\frac{\gamma}{E_1}-1\right)^{-\frac{1}{2}} H_2(\varepsilon)}{\int_{\gamma_{min}}^{\gamma_{max}} d\gamma \frac{D(\gamma)}{\gamma^2} \int_{\varepsilon_{min}}^{\varepsilon_{max}} d\varepsilon H_1(\varepsilon)}. \qquad (A.3.3)$$

The formulae (A.3.1) and (A.3.3) are immediately applicable if the K-production spectrum is known from other experiments. On the other hand, from the measured muon (electron) spectrum and polarization and (A.3.1) and (A.3.3) the K-spectrum can be deduced:

Let $D(\gamma)$ be expanded in an inverse power series

$$D(\gamma) = \sum_\nu \frac{A_\nu}{\gamma^\nu}, \qquad (A.3.4)$$

where the coefficients A_ν are to be determined. If this is inserted in (A.3.1), we

obtain the muon (electron) spectrum in the form

$$\mathrm{d}\Gamma_t^{D'}(E_1) = \delta t C' \sum_\nu \frac{A_\nu}{E_1^{\nu+1}} \int_{x_{\min}}^{x_{\max}} \frac{\mathrm{d}x}{x^{\nu+2}} \int_{\varepsilon_{\min}}^{E_0} \mathrm{d}\varepsilon H_1(\varepsilon)\mathrm{d}E_1, \qquad \text{(A.3.5)}$$

where

$$x = \gamma/E_1, \qquad x_{\min} = 1/(E_0+P_0) \quad (= 2.99\,\mathrm{GeV}^{-1} \text{ for } \mathrm{K}_{\mu 3}),$$
$$x_{\max} = 1(/E_0-P_0) \quad (= 40.82\,\mathrm{GeV}^{-1} \text{ for } \mathrm{K}_{\mu 3}).$$

The integrations can be performed, and we finally obtain

$$\mathrm{d}\Gamma_t^{D'}(E_1) = \sum_\nu \frac{A_\nu C_\nu(f_+, f_-)}{E_1^{\nu+1}}, \qquad \text{(A.3.6)}$$

where $C_\nu(f_+, f_-)$ are constants depending on (f_+, f_-). Thus, for a given set of values (f_+, f_-) the experimental muon spectrum determines the coefficients in the K-spectrum (in this determination it is important to choose the coefficients A_ν so that the K-spectrum is zero from the maximum value of γ present in the beam right up to the value corresponding to $x_{\max}$: $\gamma = x_{\max} E_\mu = 40.82 E_\mu$). To check the chosen values of (f_+, f_-) one could compare the experimental polarization of the muon with the expression obtained from (A.3.3):

$$P^{D'}(E_1) = \frac{m_1 M_K \sum_\nu \frac{A_\nu}{E_1^{\nu+1}} \int_{x_{\min}}^{x_{\max}} \frac{\mathrm{d}x}{x^{\nu+2}} \int_{\varepsilon_{\min}}^{\varepsilon_{\max}} \mathrm{d}\varepsilon (1-\varepsilon x)(2\varepsilon x - 1)^{-\frac{1}{2}} H_2(\varepsilon)}{\sum_\nu \frac{A_\nu}{E_1^{\nu+1}} \int_{x_{\min}}^{x_{\max}} \frac{\mathrm{d}x}{x^{\nu+2}} \int_{\varepsilon_{\min}}^{\varepsilon_{\max}} \mathrm{d}\varepsilon H_1(\varepsilon)}, \qquad \text{(A.3.7)}$$

where

$$E_1 = E_\mu, \; m_1 = m_\mu.$$

It would be reasonable to choose f_-/f_+ within one of the intervals (a) and (b) of section 4.

References

1) S. Furuichi, Nuovo Cim. **6** (1957) 1416
2) S. W. MacDowell, Nuovo Cim. **6** (1957) 1445
3) J. Werle, Nuclear Physics **4** (1957) 171
4) L. Okun, Nuclear Physics **5** (1958) 455
5) F. Zachariasen, Phys. Rev. **110** (1958) 1481
6) R. Gatto, Phys. Rev. **111** (1958) 1426
7) A. Fujii and Kawaguchi, Phys. Rev. **113** (1959) 1156
8) J. Nilsson, Nuclear Physics **14** (1960) 639
9) S. G. Matinyan and L. Okun, JETP **36** (1959) 933
10) A. Pais, Phys. Rev. **112** (1958) 624

11) N. Dallaporta, Nuovo Cim. **11** (1959) 142
12) R. P. Feynman and M. Gell-Mann, Phys. Rev. **109** (1958) **193**
13) R. E. Marshak and E. C. G. Sudarshan, Phys. Rev. **109** (1958) **1860**
14) See e.g. J. Hamilton, The theory of elementary particles (Oxford University Press 1959) p. **126**
15) S. Hatsukade *et al.*, Nuovo Cim. **16** (1960) **332**
16) S. W. MacDowell, Phys. Rev. **116** (1959) 1047
17) Fazzim *et al.*, Phys. Rev. Let. **1** (1958) 247
18) Impeduglia *et al.*, Phys. Rev. Let. **1** (1958) 249
19) K. H. Hansen, private communication

8.B

Nuclear Physics **22** (1961) 579—588; © *North-Holland Publishing Co., Amsterdam*

Not to be reproduced by photoprint or microfilm without written permission from the publisher

PARTIAL-SYMMETRIES OF WEAK INTERACTIONS

SHELDON L. GLASHOW †

Institute for Theoretical Physics, University of Copenhagen, Copenhagen, Denmark

Received 9 September 1960

Abstract: Weak and electromagnetic interactions of the leptons are examined under the hypothesis that the weak interactions are mediated by vector bosons. With only an isotopic triplet of leptons coupled to a triplet of vector bosons (two charged decay-intermediaries and the photon) the theory possesses no partial-symmetries. Such symmetries may be established if additional vector bosons or additional leptons are introduced. Since the latter possibility yields a theory disagreeing with experiment, the simplest partially-symmetric model reproducing the observed electromagnetic and weak interactions of leptons requires the existence of at least four vector-boson fields (including the photon). Corresponding partially-conserved quantities suggest leptonic analogues to the conserved quantities associated with strong interactions: strangeness and isobaric spin.

1. Introduction

At first sight there may be little or no similarity between electromagnetic effects and the phenomena associated with weak interactions. Yet certain remarkable parallels emerge with the supposition that the weak interactions are mediated by unstable bosons. Both interactions are universal, for only a single coupling constant suffices to describe a wide class of phenomena: both interactions are generated by vectorial Yukawa couplings of spin-one fields ††. Schwinger first suggested the existence of an "isotopic" triplet of vector fields whose universal couplings would generate both the weak interactions and electromagnetism — the two oppositely charged fields mediate weak interactions and the neutral field is light [2]). A certain ambiguity beclouds the self-interactions among the three vector bosons; these can equivalently be interpreted as weak or electromagnetic couplings. The more recent accumulation of experimental evidence supporting the $\Delta I = \frac{1}{2}$ rule characterizing the non-leptonic decay modes of strange particles indicates a need for at least one additional neutral intermediary [3]).

The mass of the charged intermediaries must be greater than the K-meson mass, but the photon mass is zero — surely this is the principal stumbling block in any pursuit of the analogy between hypothetical vector mesons and photons. It is a stumbling block we must overlook. To say that the decay intermediaries

† National Science Foundation Post-Doctoral Fellow. Present Address: Physics Department, California Institute of Technology, Pasadena.

†† A scalar intermediary is also conceivable. See ref. [1]).

together with the photon comprise a multiplet leads to no more than an excessively obscure notation unless a principle of symmetry is discovered which can relate the forms of weak and electromagnetic couplings. Because of the large mass splittings among the vector mesons, only a very limited symmetry among them may be anticipated. The purpose of this note is to seek such symmetries among the interactions of leptons in order to make less fanciful the unification of electromagnetism and weak interactions.

2. Partially-Symmetric Interactions

In the conventional Lagrangian formulation of quantum field theory the relation between symmetries of the Lagrange function and conservation laws is well known. We recently introduced the notion of "partial-symmetry" — invariance of only part of the Lagrange function under a group of infinitesimal transformations [4]). The part of the Lagrange function bilinear in the field variables which produces masses of the elementary particles need not be invariant under a partial-symmetry. Corresponding "partial-conservation laws" become conservation laws only with the neglect of appropriate masses or mass differences. This is the only sort of symmetry which could relate the massive decay intermediaries to the massless photon.

The most familiar example of a partial-symmetry is produced by an infinitesimal change of scale. If we change the coordinates, $x_\mu \to (1+\lambda)x_\mu$, and at the same time replace each field variable χ by $(1-\lambda)\chi$, that part of the integrated Lagrange function not involving dimensional parameters will be left unchanged. As long as all the interactions involve only dimensionless coupling constants the scale transformation will be a partial-symmetry. To require this partial-symmetry excludes such interactions as ps—pv meson theory and direct four-Fermion couplings.

Another kind of partial-symmetry has been recently examined by Gell-Mann and his collaborators [5]). They are led to a proportionality between the divergence of the axial-vector weak interaction current and the pion field. This they recognize as a partial-conservation law. (They must neglect both weak and electromagnetic interactions. We shall demand partial-symmetry of these interactions themselves.) It can result from the invariance of strong interactions under the infinitesimal unitary transformation,

$$\psi_N \to (1+ia\gamma_5\tau^\pm)\psi_N,$$

where ψ_N are the nucleon fields, together with appropriate accompanying transformations of meson and hyperon fields. Requiring this partial-symmetry in order to generate a partially-conserved axial-vector current provides them a powerful restriction on the acceptable form of the strong interactions. If we may invert historical sequence for the sake of pedagogy, in the same fashion

the assertion of Feynman and Gell-Mann [6]) that the vector weak-interaction current is conserved could have led to the discovery that the strong interactions are charge-independent.

A last prerequisite to our discussion is the possibility of constructing partially-symmetric interactions among a triplet of vector mesons, $Z_\mu{}^1$, $Z_\mu{}^2$ and $Z_\mu{}^3$. We shall assume that under the CP transformation, $Z_0{}^1 \to -Z_0{}^1$, $Z_0{}^2 \to +Z_0{}^2$, and $Z_0{}^3 \to +Z_0{}^3$. The most general self-interaction tri-linear in the fields and consistent with CP invariance † is

$$g_1 Z^1_{\mu\nu} Z_\mu{}^2 Z_\nu{}^3 + g_2 Z^2_{\mu\nu} Z_\mu{}^3 Z_\nu{}^1 + g_3 Z^3_{\mu\nu} Z_\mu{}^1 Z_\nu{}^2 + f_1 Z^1_{\mu\nu} Z^2_{\nu\lambda} Z^3_{\lambda\mu} + f_2 Z^2_{\mu\nu} Z^3_{\nu\lambda} Z^1_{\lambda\mu} + f_3 Z^3_{\mu\nu} Z^1_{\nu\lambda} Z^2_{\lambda\mu}.$$

To obtain a three-parameter group of partial-symmetries, we must choose $g_1 = g_2 = g_3$ and $f_1 = f_2 = f_3$. The resulting partial-conservation laws are

$$\partial_\mu (Z^1_{\mu\nu} Z_\nu{}^2 - Z^2_{\mu\nu} Z_\nu{}^1) = (M_1{}^2 - M_2{}^2) Z_\mu{}^1 Z_\mu{}^2,$$
$$\partial_\mu (Z^2_{\mu\nu} Z_\nu{}^3 - Z^3_{\mu\nu} Z_\nu{}^2) = (M_2{}^2 - M_3{}^2) Z_\mu{}^2 Z_\mu{}^3,$$
$$\partial_\mu (Z^3_{\mu\nu} Z_\nu{}^1 - Z^1_{\mu\nu} Z_\nu{}^3) = (M_3{}^2 - M_1{}^2) Z_\mu{}^3 Z_\mu{}^1,$$

corresponding to the infinitesimal transformations

$$\mathbf{Z} \to (1 + i\mathbf{a} \cdot \mathbf{t})\mathbf{Z},$$

where the $\mathbf{t}$ are the conventional anti-symmetric imaginary 3×3 matrices.

Without the quadrupole couplings (they involve implicit cubes of momenta), and with $M_1 = M_2$ and $M_3 = 0$, this partially-symmetric interaction describes the electrodynamics (with $Z_\mu{}^3$ the vector potential) of a charged pair of vector bosons, $Z^\pm = (Z^1 + iZ^2)/\sqrt{2}$, with gyromagnetic ratio of two and with no electric quadrupole coupling. Some properties of this version of spin-one electrodynamics we have discussed elsewhere [4]).

3. Interactions of Leptons

We consider the interactions of a multiplet of vector bosons with a triplet of real Majorana fields, $\psi_1 = (\psi^+ + \psi^-)/\sqrt{2}$, $\psi_2 = i(\psi^+ - \psi^-)/\sqrt{2}$ and ψ_3. The mass-producing term has the form $m\psi\beta t_3{}^2\psi$, so that we may regard $\psi^\pm$ as the positon and negaton and ψ_3 as that variety of neutrino produced in association with negatons and positons. To escape the $\mu \to e + \gamma$ difficulty [7]), we assume (with Schwinger [2])) that a quite distinct triplet of fields describes muons and those neutrinos produced with muons. No interaction shall be introduced that couples the one triplet to the other. The interactions between the Fermions and

† Our choice of the CP behaviour of the Z-meson triplet is such as to exclude the interactions $\varepsilon^{\mu\nu\lambda\sigma} Z^1_{\mu\nu} Z^2_\lambda Z^3_\sigma$ and $\varepsilon^{\mu\nu\lambda\sigma} Z^1_{\mu\nu} Z^2_{\lambda\beta} Z^3_{\beta\sigma}$.

the vector mesons should include both electromagnetism and such weak interactions as are necessary to produce observed decay phenomena.

The interaction Lagrangian,

$$g\mathbf{Z}_\mu \cdot \mathbf{J}_\mu = g\mathbf{Z}_\mu \cdot [(\mathbf{Z}_{\mu\nu} \times \mathbf{Z}_\nu) + i\psi\beta\gamma_\mu \mathbf{O}\psi], \tag{3.1}$$

includes both a symmetrical self-interaction of the Z-triplet and the Yukawa interaction of the bosons to the Fermions. The common coupling strength is in accord with the universality both of the electric charge and of the weak interaction coupling constant. For partial-symmetry, the three imaginary anti-symmetric matrices $\mathbf{O}$ must satisfy the commutation relations of an angular momentum,

$$\mathbf{O} \times \mathbf{O} = i\mathbf{O}. \tag{3.2}$$

In that case three partially-conserved currents

$$\mathbf{J}_\mu = \mathbf{Z}_{\mu\nu} \times \mathbf{Z}_\nu + \psi\beta\gamma_\mu \mathbf{O}\psi \tag{3.3}$$

result from the three infinitesimal transformations (i.e., partial-symmetries)

$$\psi \to (1 + i\mathbf{a} \cdot \mathbf{O})\psi, \quad \mathbf{Z} \to (1 + i\mathbf{a} \cdot \mathbf{t})\mathbf{Z}. \tag{3.4}$$

The $\mathbf{O}$ must commute with $\beta\gamma_\mu$ in order to leave invariant the kinematic terms of the Lagrange function. They must have the form $\mathbf{O} = \mathbf{A} + i\gamma_5\mathbf{S}$, where the $\mathbf{A}$ are anti-symmetric, the $\mathbf{S}$ are symmetric, and both are Hermitean 3×3 matrices acting between the ψ_i. Further restrictions upon the $\mathbf{O}$ arise if we demand CP invariance and limit the currents to neutral and singly charged. The simplest choice is evidently $\mathbf{O} = \mathbf{t}$. Certainly J_μ^3 is the total electrical current, so that Z_μ^3 may be interpreted as the electromagnetic vector potential. But the charged currents do not display symmetric parity violation, hence they cannot reproduce the observed weak interactions.

Other matrices satisfying (3.2) but violating parity conservation are obtained from the $\mathbf{t}$ by a unitary transformation,

$$U\mathbf{t}U^{-1} = e^{-(\gamma_5 t_3 \theta)}\, \mathbf{t}\, e^{+(\gamma_5 t_3 \theta)}.$$

Clearly U commutes with t_3 so that the leptons' electrical current j_μ^3 remains unchanged. To obtain symmetric parity violation in the charged currents we take $\theta = \frac{1}{4}\pi$, whereupon

$$'O_1 = (t_1 + i\gamma_5\{t_2, t_3\})/\sqrt{2}, \qquad 'O_2 = (t_2 - i\gamma_5\{t_1, t_3\})/\sqrt{2}, \tag{3.5}$$

where curly brackets signify anti-commutators. Unfortunately the charged currents $j_\mu^{1,2} = \psi\beta\gamma_\mu\, 'O_{1,2}\psi$ are not acceptable weak interaction currents. The parity-violating unitary transformation U is not invariant under the CP transformation so that, under CP,

$$'O_1 \to \tfrac{1}{2}(t_1 - i\gamma_5\{t_2, t_3\}).$$

In terms of charge eigenstates these currents involve the interaction of both negaton and positon to the same handed neutrino. The theory generated with '**O**, partially-symmetric and parity violating though it may be, is not a faithful model of the weak and electromagnetic interactions of leptons.

Recent experiments have determined the form of the charged leptonic currents. We shall choose O_1 and O_2 in accordance with these experiments. Negatons are produced in elementary-particle decays only in association with left-handed neutrinos whereas positons are accompanied by right-handed ones. The correct charged currents $j_\mu^{1,2} = \psi\beta\gamma_\mu O_{1,2}\psi$ are produced with [2])

$$O_1 = (t_1 + i\gamma_5\{t_1, t_3\})/\sqrt{8}, \qquad O_2 = (t_2 + i\gamma_5\{t_2, t_3\})/\sqrt{8}. \tag{3.6}$$

The decay interaction is partially-symmetric only when all three vector bosons participate, $g\mathbf{Z}_\mu \cdot \mathbf{j}_\mu$, where the neutral current is given by $j_\mu^3 = \psi\beta\gamma_\mu O_3\psi$ and

$$O_3 = -i[O_1, O_2] = \tfrac{1}{4}(t_3 + i\gamma_5(3t_3^2 - 2)). \tag{3.7}$$

It is readily seen that these three O_i satisfy (3.2). Since j_μ^3 is not the lepton electric current, Z_3 cannot be interpreted as the electromagnetic field. Thus the theory containing only the necessary weak interactions of two oppositely charged decay intermediaries together with the electromagnetic interactions of both the leptons and the bosons is not partially-symmetric.

4. Partially-Symmetric Synthesis

In order to achieve a partially-symmetric theory of weak and electromagnetic interactions, we must go beyond the hypothesis of only a triplet of vector bosons and introduce an additional neutral vector boson Z_S. It will have the same behaviour under CP as Z_3 and it is coupled to its own neutral lepton current $J_\mu^S = \psi\beta\gamma_\mu S\psi$. The three partial symmetries of section 3 are undisturbed by this new interaction provided that

$$[\mathbf{O}, S] = 0. \tag{4.1}$$

We use the **O** that yield correct weak interactions of charged currents, (3.6) and (3.7), and we define

$$S = \tfrac{3}{4}(t_3 - i\gamma_5(t_3^2 - \tfrac{2}{3})). \tag{4.2}$$

Note that (4.1) is satisfied, and moreover,

$$O_1^2 + O_2^2 + O_3^2 + S^2 = 1 \tag{4.3}$$

and

$$Q = t_3 = O_3 + S. \tag{4.4}$$

The last relation suggests the analogous expression relating strangeness and the

third component of isobaric spin to the electrical charge of strongly interacting particles. Far more transparent expressions for $\mathbf{O}$ and S and for the relations among them emerge in a notation wherein the handedness of leptons is diagonal †.

The interaction Lagrange function including the couplings of four vector bosons is

$$e \sec\theta \ \mathbf{Z}_\mu \cdot [(\mathbf{Z}_{\mu\nu} \times \mathbf{Z}_\nu) + \psi\beta\gamma_\mu \mathbf{O}\psi] + e \csc\theta \ Z_\mu^{\,S} \psi\beta\gamma_\mu S\psi. \tag{4.5}$$

The parameter θ appears in order to permit an arbitrary choice of the strengths of the triplet and singlet interactions. The three partial-symmetries (3.4) have been preserved and an additional partial-symmetry yielding a partial-conservation law for $J_\mu^{\,S}$ is obtained,

$$\psi \to (1+ibS)\psi, \qquad \mathbf{Z} \to \mathbf{Z}, \qquad Z^S \to Z^S. \tag{4.6}$$

The reader may wonder what has been gained by the introduction of another neutral vector meson. Neither Z_3 nor Z_S interacts with the electrical current so that neither interaction may be identified with electromagnetism. (To have chosen $J_\mu^{\,S}$ to be the electrical current would have violated (4.1) and lost partial-symmetry.) However, both the neutral fields have the same CP property so that linear combinations of the two fields may correspond to "particles." The most general form for the boson mass producing part of the Lagrange function is a positive-definite bilinear expression in $Z_\mu^{\,3}$ and $Z_\mu^{\,S}$ whose diagonalization identifies those linear combinations of the fields which display unique masses (i.e., the "particles"). Most generally we may have

$$L_M = \tfrac{1}{2} M_A^{\,2} (Z_\mu^{\,3} \cos\theta' + Z_\mu^{\,S} \sin\theta')^2 + \tfrac{1}{2} M_B^{\,2} (Z_\mu^{\,S} \cos\theta' - Z_\mu^{\,3} \sin\theta')^2,$$

in which the fields

$$A_\mu = Z_\mu^{\,3} \cos\theta' + Z_\mu^{\,S} \sin\theta', \qquad B_\mu = Z_\mu^{\,S} \cos\theta' - Z_\mu^{\,3} \sin\theta' \tag{4.7}$$

describe spin-one particles with masses M_A and M_B. In terms of these fields the interaction Lagrange function (4.5) becomes

$$\begin{aligned} &eA_\mu J_\mu^{\,Q} + eF_{\mu\nu} \mathbf{Z}_\mu t_3 \mathbf{Z}_\nu + e \sec\theta (Z_\mu^{\,1} j_\mu^{\,1} + Z_\mu^{\,2} j_\mu^{\,2}) \\ &\quad - e \tan\theta (B_{\mu\nu} \mathbf{Z}_\mu t_3 \mathbf{Z}_\nu + B_\mu \mathbf{Z}_{\mu\nu} t_3 \mathbf{Z}_\nu) + eB_\mu \psi\beta\gamma_\mu (S \cot\theta - O_3 \tan\theta)\psi, \end{aligned} \tag{4.8}$$

when θ' is put equal to θ. The total electrical current of leptons and bosons is denoted by $J_\mu^{\,Q}$,

$$J_\mu^{\,Q} = \mathbf{Z}_{\mu\nu} t_3 \mathbf{Z}_\nu + \psi\beta\gamma_\mu (S + O_3)\psi.$$

The interaction of A_μ is precisely the electrodynamic interaction of the charged

† We are indebted to Professor M. Gell-Mann for this observation, and for presenting part of our work, in his notation, at the 1960 Conference on High Energy Physics in Rochester, New York.

Fermions and of the charged vector mesons (with gyromagnetic ratio of two). We may identify A_μ with the electromagnetic field if we put $M_A = 0$. This isolation of the electromagnetic interaction has been possible only because of (4.4) and our apparently arbitrary choice of S is now justified. The interactions of Z_1 and Z_2 generate the correct parity-violating decay interactions with coupling constant $g_W = e \sec \theta$. Remaining terms in (4.8) comprise the interaction of B with a neutral partially-conserved current. They are the price we must pay for partial-symmetry. The symmetries of (4.5) under the four-parameter group of transformations (3.4 and 4.6) are unaffected by the re-definition of fields required by the mass-producing part of the Lagrange function. Expressed in terms of A and B one of these symmetries yields the conservation of electrical charge; the other three shuffle the photon with decay-intermediaries and lead only to partial-conservation laws for the three weak interaction currents. For no choice of θ is the interaction of the neutral current small compared with weak interactions involving charged currents. The masses of the charged intermediaries M_Z and of the neutral M_B are as yet arbitrary.

5. Discussion

It seems remarkable that both the requirement of partial-symmetry and quite independent experimental considerations indicate the existence of neutral weakly interacting currents. It would be gratifying if the introduction of only a single neutral vector-meson field B could secure both partial-symmetry and the $\Delta I = \frac{1}{2}$ rule. Whether this is possible depends upon the extension of our work to the interactions of the vector-meson multiplet with strongly interacting particles. But the roles of B and of $Z^{\pm}$ are far from symmetrical in the leptonic decays of strange particles. Indeed, the modes $K \to \pi + \nu_R + \nu_L$ and $K \to \pi + e^+ + e^-$ have never been seen. Since the coupling strengths of Z to charged leptonic currents and of B to its neutral current are limited by the requirement of partial-symmetry, the absence of neutral leptonic decay modes must be attributed to a mass splitting between $Z^{\pm}$ and B. The unobserved modes are then suppressed by the factor $(M_Z/M_B)^4$. Does not this mass splitting prevent the symmetrical participation of the three decay intermediaries prerequisite to a $\Delta I = \frac{1}{2}$ rule? While in a leptonic decay mode, the momentum of the decay intermediary is just the sum of the momenta of the emerging leptons, in non-leptonic modes one must integrate over all momenta of the intermediary. Thus the matrix element for non-leptonic modes is expected to be less sensitive a function of the vector-meson mass than the matrix element for non-leptonic modes. Vector meson theory is less well-behaved than quantum-electrodynamics or pseudoscalar meson theory, so that it is not unreasonable to suppose that the non-leptonic modes are dominated by contributions at virtual momenta far beyond M_B. If this is so the mass difference between

$Z^{\pm}$ and B would be without significant effect and a $\Delta I = \frac{1}{2}$ rule might be secured.

To assure the experimentally observed selection rules of strangeness as well as of isotopic spin, two neutral decay intermediaries are needed [3]). One of these has CP behaviour opposite to that of A and B. It is not discouraging that this particle has not yet appeared in the interactions of the vector-meson multiplet with leptons, since no such interaction exists consistent with CP invariance.

We have argued that any underlying symmetries relating weak interactions and electromagnetism are obscured by the masses of elementary particles. Without a theory of the origins of these masses, any study based upon the analogy between decay-intermediaries and photons may make use only of partial-symmetries. The simplest partially-symmetric system exhibiting all known interactions of the leptons, the weak and the electromagnetic, has been determined. Although we cannot say *why* the weak interactions violate parity conservation while electromagnetism does not, we have shown *how* this property can be embedded in a unified model of both interactions. Unfortunately our considerations seem without decisive experimental consequence. For this approach to be more than academic, a partially-symmetric system correctly describing all decay modes of all elementary particles should be sought.

Appendix

A.1. ANOTHER ALTERNATIVE

In section 4 we said it is necessary to go beyond the framework of a triplet of vector mesons and a triplet of leptons in order to obtain a partially-symmetric system including the known interactions. This is true, but it is not entirely obvious that the introduction of additional lepton fields rather than an additional boson would not also do the trick. Two triplets of real Fermion fields were needed to describe all the leptons — one triplet including the electrons and one the muons, each with its own neutrino. Let us keep our original triplet of vector mesons while introducing two new (i.e., unobserved) Fermion fields. They will correspond to a massive neutral muon and to its distinct antiparticle. Altogether there are now eight kinds of Fermions. Half of them are defined to be leptons: μ^+, μ^0, e^-, and ν; and their antiparticles are anti-leptons. Conservation of lepton number will assure the absence of unwanted modes of muon decay. Four by four matrices which describe isobaric spin $\frac{1}{2}$ are the most convenient to use †. The doublet (μ^+, μ^0) is characterized by $\zeta_3 = +1$, while (e^-, ν) has $\zeta_3 = -1$. Similarly, the doublet (μ^+, ν) has $\tau_3 = +1$, while (e^-, μ^0) has $\tau_3 = -1$. The electrical charge has the form $Q = \frac{1}{2}(\tau_3 + \zeta_3)$. We assume that the μ^0 is sufficiently massive so that the possibility of $\pi \to \mu^0 + e$ is avoided. The problem is again to find a set of **O** satisfying (3.2) which generates charged

† The notation of J. Schwinger is employed. See ref. [2]).

currents embodying symmetric parity violation yet conserving CP. Since we have introduced only a triplet of vector mesons, the neutral must be the photon and $O_3 = \frac{1}{2}(\tau_3+\zeta_3)$. Such a set of **O** is

$$O_1 = [\tau_1(1+i\gamma_5\zeta_3)+\zeta_1(1-i\gamma_5\tau_3)]/\sqrt{8},$$
$$O_2 = [\tau_2(1+i\gamma_5\zeta_3)+\zeta_2(1-i\gamma_5\tau_3)]/\sqrt{8}.$$

With these **O** we may construct a partially-symmetric theory including both weak and electromagnetic interactions of the leptons. Unfortunately it is the wrong theory. If the electron is associated with a left-handed neutrino, the μ^- will be associated with a right-handed one. (A change of sign produces a converse assignment.) But it cannot be arranged for both electron and μ^- to be coupled with the same handed neutrino. Experiments indicate that the handedness of the neutrino is determined solely by the lepton's charge. With this theory muons would decay according to the schemes: $\mu^+ \rightarrow e^+ + 2\nu_R$ and $\mu^- \rightarrow e^- + 2\nu_L$. The electron spectrum from muon decay would necessarily be of the $\rho = 0$ shape and is now probably excluded by experiment. A more acceptable set of just three **O** has not been found.

A.2. OTHER INTERACTIONS

One might conclude from existing experimental determinations of the electrical charge and of the weak interaction strength g_W^2/M_Z^2 that $M_Z > \approx 137$ nucleon masses. But whatever mechanism is responsible for the large mass of the intermediaries should also produce a large wave-function renormalization of the massive vector fields not shared by the photon. This results in a reduction of the weak coupling strength compared with the electric charge and consequently relaxes this lower limit to the Z-meson mass.

Both its mass and its charge renormalization would arise if there were strong interactions quadratic in the Z-field. Should these couplings involve strongly interacting particles they would generate effective six-Fermion interactions of comparable strength to the existing four-Fermion couplings responsible for decay phenomena. A possible experimental consequence of these interactions is the stimulated decay of a muon:

$$\mu^- + N = e^- + \nu_R + \nu_L + N,$$

in the presence of nuclear matter Observable effects upon the decay rate of negative muons bound to heavy nuclei might result, but at this time we cannot exclude the possible existence of strong interactions of the decay intermediaries. Of course these interactions could also be detected in a search for the real production of decay intermediaries.

A.3. ANOTHER SYMMETRY

If only for completeness, we exhibit one remaining symmetry of (4 5)

Defining $W = 1 - t_0^2 - i\gamma_5 t_0$, we discover $WO = OW = O$ and $WS = SW$. The infinitesimal transformation $\psi \to (1 + i\alpha\gamma_5 W)\psi$ is not merely a partial symmetry, but it is a complete symmetry providing the neutrino mass is zero. The corresponding conserved current,

$$J_\mu^{\,W} = \bar{\psi}\beta\gamma_\mu(t_0 - i\gamma_5(1 - t_0^2))\psi,$$

describes the "neutrinic" quantum number of Schwinger [2]. It is the leptons' electrical charge plus the number of left-handed neutrinos less the number of right-handed ones.

The author wishes to thank Professor Niels Bohr and Professor Aage Bohr for the hospitality extended to him at this Institute during the past two years. He is also very grateful to the CERN laboratories in Geneva for their hospitality while much of this work was done. Conservations with Professor M. Gell-Mann and with members of both Institutes are gratefully acknowledged.

References

1) C. Fronsdal and S. Glashow, Phys. Rev. Letters **3** (1959) 370
2) J. Schwinger, Ann. of Phys. **2** (1957) 407
3) M. Gell-Mann, private communication;
T. D. Lee and C. N. Yang, preprint
4) S. Glashow, Nuclear Physics **10** (1959) 107
5) M. Gell-Mann and M. Levy, Nuovo Cim. **16** (1960) 705;
J. Bernstein, M. Gell-Mann and L. Michel, Nuovo Cim. **16** (1960) 560
6) R. Feynman and M. Gell-Mann, Phys. Rev. **109** (1958) 193
7) e.g., G. Bernberg, Phys. Rev. **110** (1958) 1482

1.E.1

Nuclear Physics **22** (1961) 589—597; ©*North-Holland Publishing Co., Amsterdam*

Not to be reproduced by photoprint or microfilm without written permission from the publisher

GEOMETRICAL REPRESENTATION OF NUCLEAR PROPERTIES

M. BEINER and K. BLEULER

Department of Theoretical Nuclear Physics, University of Bonn, Bonn, Germany

Received 3 October 1960

Abstract: Experimental nuclear data are represented with the help of a geometrical method, which allows a comprehensive survey of nuclear properties and a more direct comparison with theoretical results. We first consider the separation energies (for protons and neutrons) defined in a suitable way (mean value according to formula (3)). These values (for all nuclei so far measured with sufficient accuracy) are then represented by two surfaces in 3-dimensional space, which are projected in a convenient manner (figs. 3 and 4). We immediately observe some striking features of the general behaviour of these surfaces: a) well pronounced shell structure effects in the middle part of the periodic table (energy steps after the closing of each shell), b) a typical discontinuity for $N = 90$ corresponding to the well known sudden deformation of nuclear shape, c) effects of complex structure for lighter elements. With the help of these diagrams we then give a method for the representation of single particle states of odd-mass nuclei (fig. 5). This work represents the continuation of two earlier publications (see refs. [16, 17])).

1. Introduction

For several reasons a comprehensive survey of experimental results on nuclear properties is quite useful; we think about a comparison between experimental data and nuclear models, the consistency of experimental values and proposals for new measurements. The purpose of our paper is to show that a large part of the experimental material so far known can be, if combined in a suitable way, represented with the help of geometrical constructions.

We begin with the discussion of nuclear masses as measured by a large number of authors. From these values we form experimental separation energies in a special way (so-called mean separation energy, see section 2). These new separation energies are seen to be very convenient for a geometrical representation with the help of 2-dim. surfaces in 3-dim. space (section 2, figs. 3 and 4) as well as for a physical interpretation on the basis of wellknown nuclear models. These surfaces give in fact a rather complete survey of experimental nuclear properties. At the same time, some characteristic features of nuclear models are seen directly: shell structure effects, e.g. energy steps connected with magic numbers; a striking break corresponding to the sudden deformation of nuclear shape; and the effects related to the formation of sub-structures if lighter elements are considered.

The reason for this is that the separation energy of nucleons has a very natural and simple significance in a general independent particle model

Defining $W = 1 - t_3^2 + i\gamma_5 t_3$, we discover $W\mathbf{O} = \mathbf{O}W = \mathbf{O}$ and $WS = SW$. The infinitesimal transformation $\psi \to (1 + ia\gamma_5 W)\psi$ is not merely a partial symmetry, but it is a complete symmetry providing the neutrino mass is zero. The corresponding conserved current,

$$J_\mu^{\mathrm{W}} = \psi\beta\gamma_\mu(t_3 - i\gamma_5(1 - t_3^2))\psi,$$

describes the "neutrinic" quantum number of Schwinger [2]). It is the leptons' electrical charge plus the number of left-handed neutrinos less the number of right-handed ones.

The author wishes to thank Professor Niels Bohr and Professor Aage Bohr for the hospitality extended to him at this Institute during the past two years. He is also very grateful to the CERN laboratories in Geneva for their hospitality while much of this work was done. Conservations with Professor M. Gell-Mann and with members of both Institutes are gratefully acknowledged.

References

1) C. Fronsdal and S. Glashow, Phys. Rev. Letters **3** (1959) 570
2) J. Schwinger, Ann. of Phys. **2** (1957) 407
3) M. Gell-Mann, private communication;
T. D. Lee and C. N. Yang, preprint
4) S. Glashow, Nuclear Physics **10** (1959) 107
5) M. Gell-Mann and M. Lévy, Nuovo Cim. **16** (1960) 705;
J. Bernstein, M. Gell-Mann and L. Michel, Nuovo Cim. **16** (1960) 560
6) R. Feynman and M. Gell-Mann, Phys. Rev. **109** (1958) 193
7) e. g., G. Feinberg, Phys. Rev. **110** (1958) 1482

1.E.1

Nuclear Physics **22** (1961) 589—597; ©*North-Holland Publishing Co., Amsterdam*

Not to be reproduced by photoprint or microfilm without written permission from the publisher

GEOMETRICAL REPRESENTATION OF NUCLEAR PROPERTIES

M. BEINER and K. BLEULER

Department of Theoretical Nuclear Physics, University of Bonn, Bonn, Germany

Received 3 October 1960

Abstract: Experimental nuclear data are represented with the help of a geometrical method, which allows a comprehensive survey of nuclear properties and a more direct comparison with theoretical results. We first consider the separation energies (for protons and neutrons) defined in a suitable way (mean value according to formula (3)). These values (for all nuclei so far measured with sufficient accuracy) are then represented by two surfaces in 3-dimensional space, which are projected in a convenient manner (figs. 3 and 4). We immediately observe some striking features of the general behaviour of these surfaces: a) well pronounced shell structure effects in the middle part of the periodic table (energy steps after the closing of each shell), b) a typical discontinuity for $N = 90$ corresponding to the well known sudden deformation of nuclear shape, c) effects of complex structure for lighter elements. With the help of these diagrams we then give a method for the representation of single particle states of odd-mass nuclei (fig. 5). This work represents the continuation of two earlier publications (see refs. [16, 17])).

1. Introduction

For several reasons a comprehensive survey of experimental results on nuclear properties is quite useful; we think about a comparison between experimental data and nuclear models, the consistency of experimental values and proposals for new measurements. The purpose of our paper is to show that a large part of the experimental material so far known can be, if combined in a suitable way, represented with the help of geometrical constructions.

We begin with the discussion of nuclear masses as measured by a large number of authors. From these values we form experimental separation energies in a special way (so-called mean separation energy, see section 2). These new separation energies are seen to be very convenient for a geometrical representation with the help of 2-dim. surfaces in 3-dim. space (section 2, figs. 3 and 4) as well as for a physical interpretation on the basis of wellknown nuclear models. These surfaces give in fact a rather complete survey of experimental nuclear properties. At the same time, some characteristic features of nuclear models are seen directly: shell structure effects, e.g. energy steps connected with magic numbers; a striking break corresponding to the sudden deformation of nuclear shape; and the effects related to the formation of sub-structures if lighter elements are considered.

The reason for this is that the separation energy of nucleons has a very natural and simple significance in a general independent particle model

(spherical and deformed shells): it is determined by the energy difference of the highest occupied level and the lowest free state (compare fig. 1) and therefore depends in a characteristic way on the parameters which determine the nuclear shape and on the occupation numbers of the single particle levels. Thus, energy steps connected with the magic numbers are very characteristic for this interpretation. They really show that the single particle levels do exhibit a band structure and even the heights of these steps can be compared with a calculated level structure (compare fig. 5 in our former publication, ref. [17]).

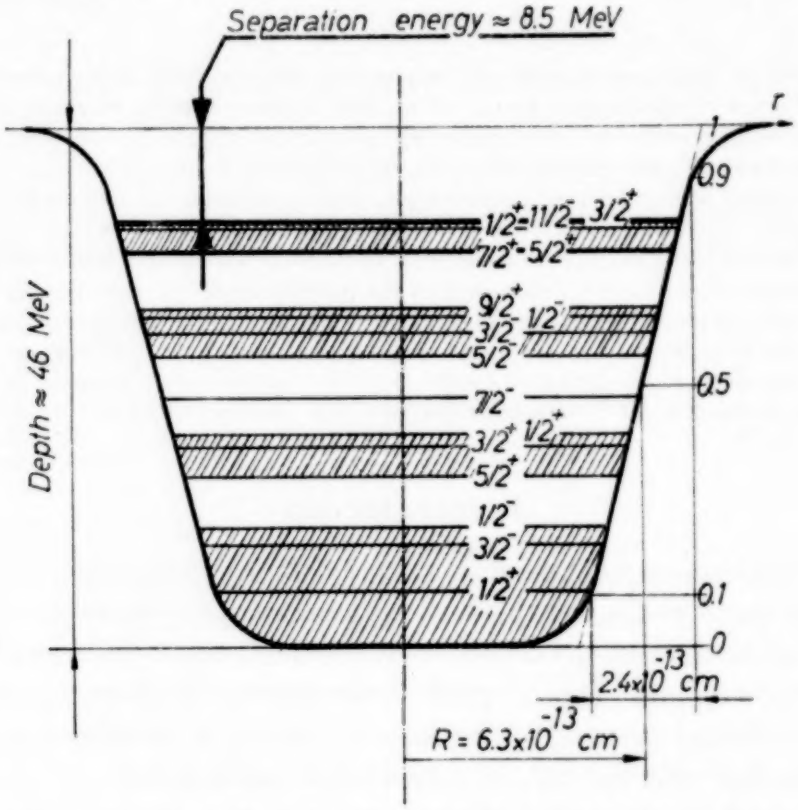

Fig. 1. Neutron potential well for $A = 125$ with occupied single particle levels.

In addition the smooth parts of our surfaces are directly related to the very regular variation of nuclear shape as a function of N and Z and to a certain mixing of single particle states within a shell. It is clear from the very beginning that a sudden change of the shape parameters will also be immediately felt in the behaviour of our separation energy. This effect is in fact well observed in the region of $N = 90$ in the neutron diagram representing there the transition from the spherical to the deformed shape (see section 4).

This simple interpretation is, of course, based on a very rough approximation: admixtures of single particle states will change the separation energy and they might have a rather large effect, but the overall behaviour (e.g. the relative variation of separation energies) still seems to keep many features of this lowest order independent particle approximation. It was therefore worthwhile to

extend our construction to the very lightest elements, where shell structure loses its significance more and more. We can now judge from the behaviour of our surfaces the amount of deviation from ordinary independent particle structure.

Finally, the construction of our separation energy surfaces forms a natural basis for a geometrical representation of the well known single particle levels of odd-mass nuclei. If the experimental excitation energy is combined (form. (4)) with the separation energy (defined in the usual way for this purpose), we reproduce, so to speak, the absolute energy of the single particle levels (compare fig. 1). We then should again obtain a smooth variation of this energy value as a function of N and Z, which can be checked from the behaviour of a corresponding surface. Here, we give just one example of such a single particle level surface (fig. 5), whereas a more complete analysis will be contained given in a further publication.

2. The Construction of the Surfaces representing the Separation Energies

We first consider the binding energies $B(Z,N)$ of all nuclei as a function of the number of neutrons N and the number of protons Z. We then introduce the usual definition of the separation energy for a neutron, denoted by B_n, and for a proton, denoted by B_p,

$$B_n = B(Z,N)-B(Z,N-1), \quad B_p = B(Z,N)-B(Z-1,N). \tag{1}$$

These values are in part directly determined from experimental data, but they are not convenient for our construction because they are, as well known, quite different for even, odd-mass and odd nuclei, because of the effect of pairing energies. It is therefore suitable to introduce a new kind of separation energy which has practically the same significance for all kinds of nuclei. In other words, we try to eliminate the pairing-energy effect and we thus define our mean separation energies $B_{\overline{2n}}$ and $B_{\overline{2p}}$ for neutrons and protons introducing a double step in the corresponding nucleon number when forming the differences of binding energies. Then compensating by a factor one half, we obtain

$$B_{\overline{2n}} = \tfrac{1}{2}\{B(Z,N)-B(Z,N-2)\}, \quad B_{\overline{2p}} = \tfrac{1}{2}\{B(Z,N)-B(Z-2,N)\}. \tag{2}$$

These new values are also directly related to the ordinary separation energies by the relations

$$B_{\overline{2n}} = \tfrac{1}{2}\{B_n(Z,N)+B_n(Z,N-1)\}, \quad B_{\overline{2p}} = \tfrac{1}{2}\{B_p(Z,N)+B_p(Z-1,N)\}, \tag{3}$$

which are quite suitable for practical purposes if the ordinary separation energies are measured directly.

Our new mean separation energies are now plotted in a 3-dimensional coor-

dinate system using the two axes of the horizontal plane for N and Z and the vertical axis for the separation energy ($B_{\overline{2n}}$ and $B_{\overline{2p}}$ respectively). For practical purposes we use Z and $N-Z$ instead of N and Z and we also draw the separation energy in the negative direction of the vertical axis corresponding to its single particle interpretation. This method is explained in fig. 2.

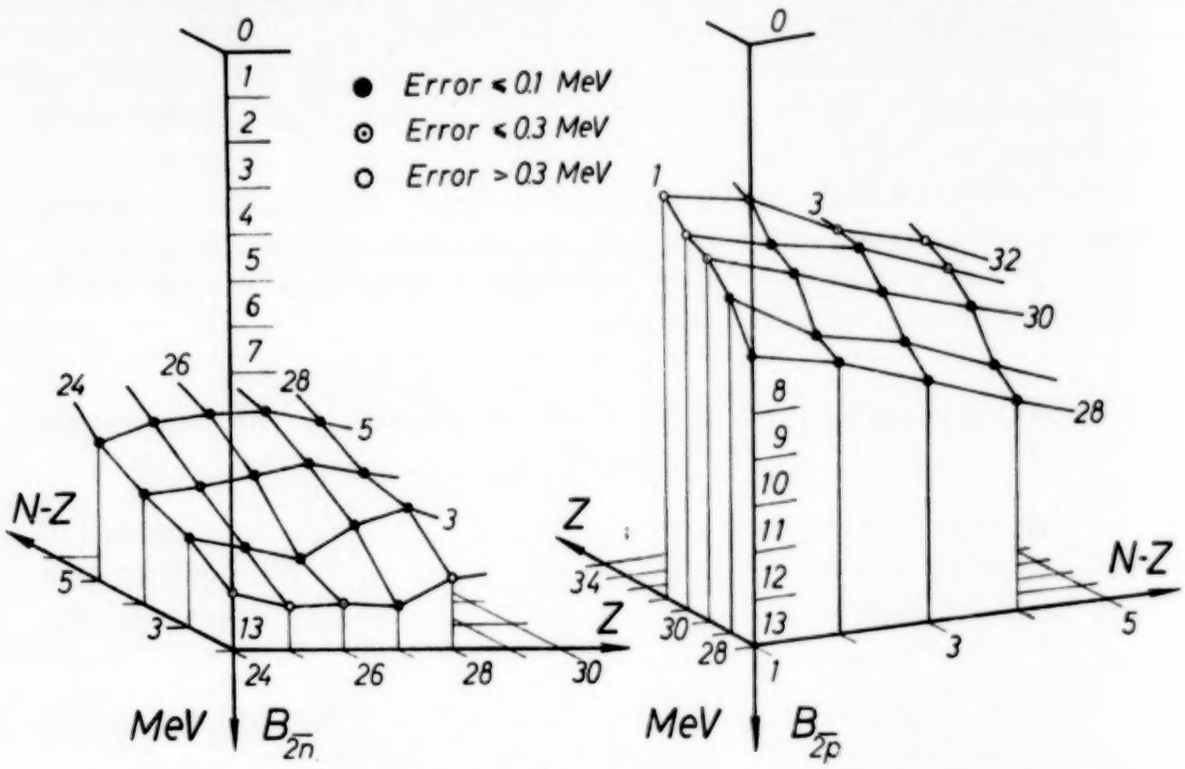

Fig. 2. Parts of the surfaces $B_{\overline{2n}}(Z, N)$ and $B_{\overline{2p}}(Z, N)$ showing their construction.

We thus obtain two separate surfaces (fig. 3 and 4) for the separation energies for neutrons and protons respectively. Each of these diagrams contains simultaneously all types of nuclei (even, odd-mass, odd) and it is seen that the corresponding points do fit in the same quasi-analytic surface which is thus defined by a rather large number of points representing all stable and unstable isotopes of the periodic table in their fundamental state. It was of course very suitable to have all nuclei of the periodic system on one single surface in order to obtain an overall survey of the behaviour of separation energies. It is indeed seen from the very beginning that these two surfaces exhibit quite characteristic features and give, so to speak, an intuitive survey of experimental values.

Eventually, we construct our surface representing the single particle levels in the following way (fig. 5): we collect states with the same assignment J^P (in our case $\frac{7}{2}^-$) in a certain region of the periodic table (Z from 8 to 28) and we define the single particle level energy $B_n{}^{J^P}$ for a neutron state (E^{J^P} represents the

● Error < 0.1 MeV

⊙ Error < 0.3 MeV

○ Error > 0.3 MeV

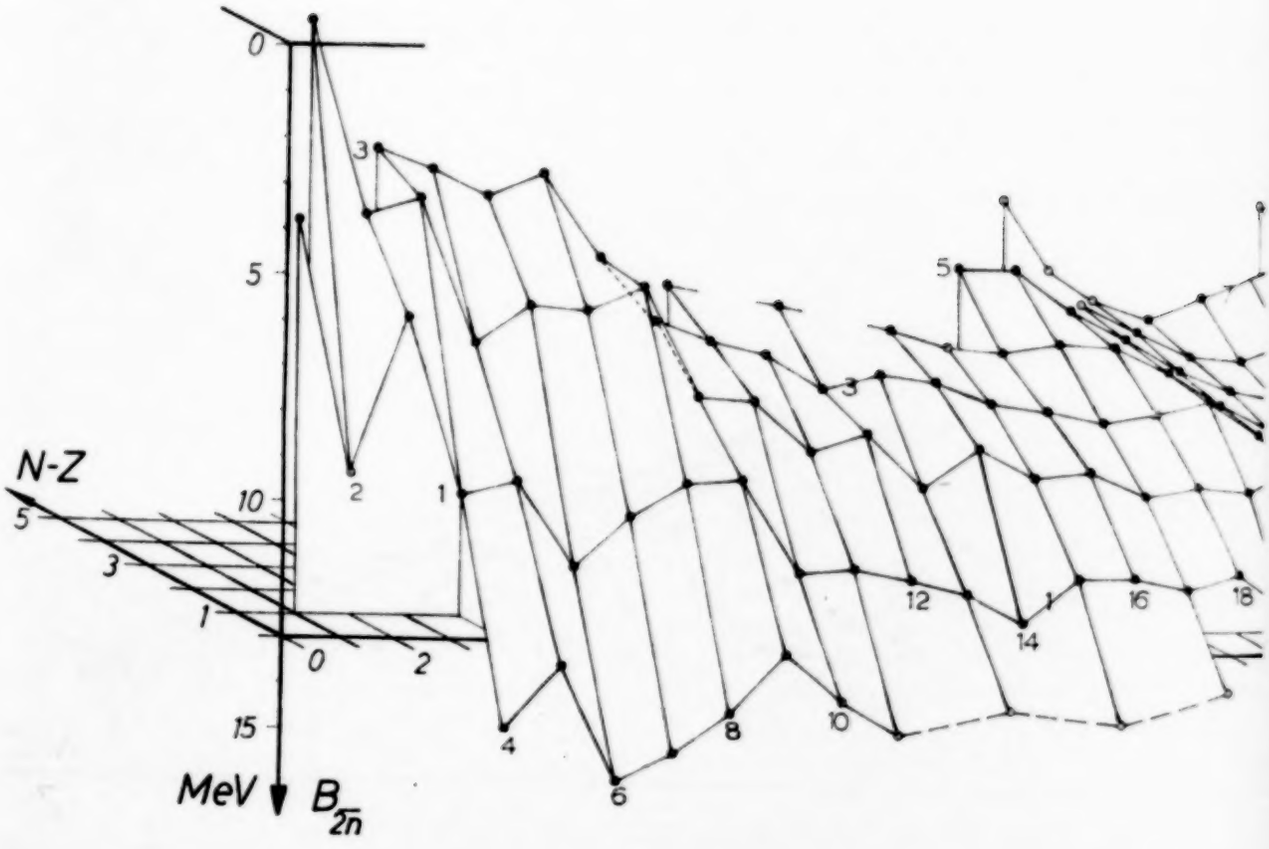

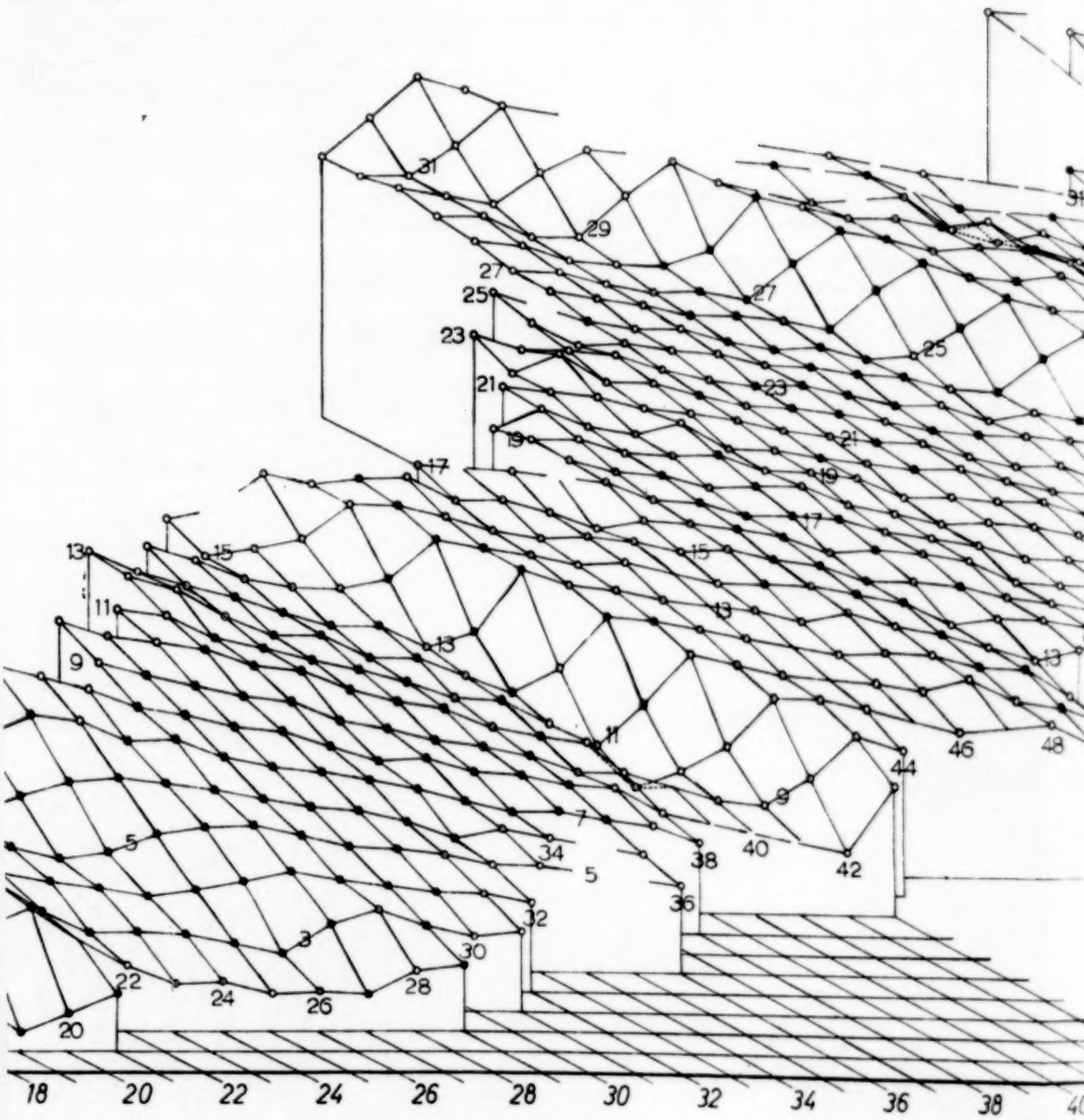

Fig. 3. Experimental mean separation energies for neutrons $B_{\overline{2n}}$ (eq. (2)).

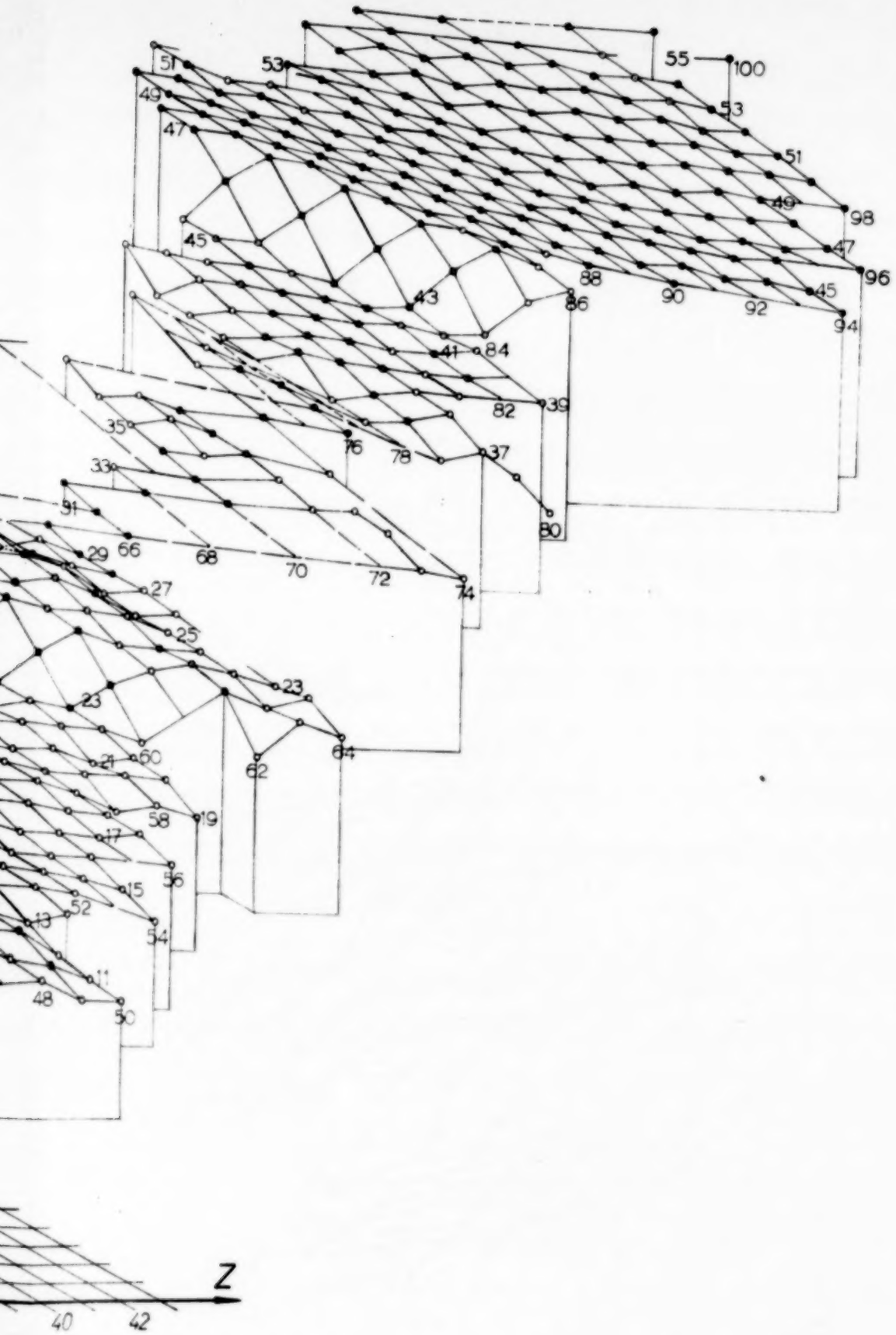
55
100
53
51
49
98
47
96
45
94
88
90
92
86
43
41
84
82
39
37
80
35
76
78
33
91
29
66
68
70
72
74
27
25
23
23
21
60
62
64
58
19
17
56
15
52
13
54
11
48
50
Z
40
42

● Error ≤ 0.1 MeV

⊙ Error ≤ 0.3 MeV

○ Error > 0.3 MeV

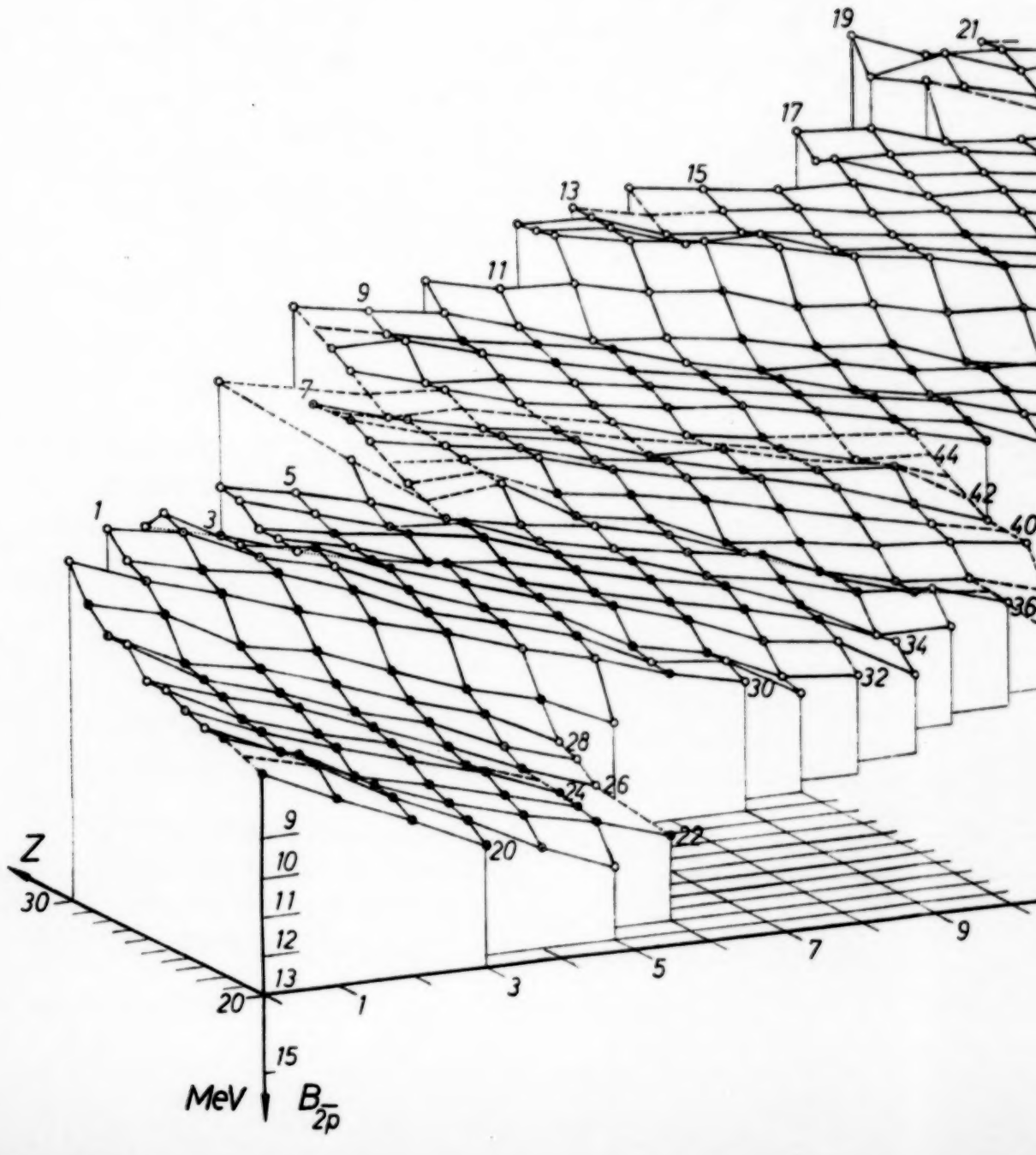

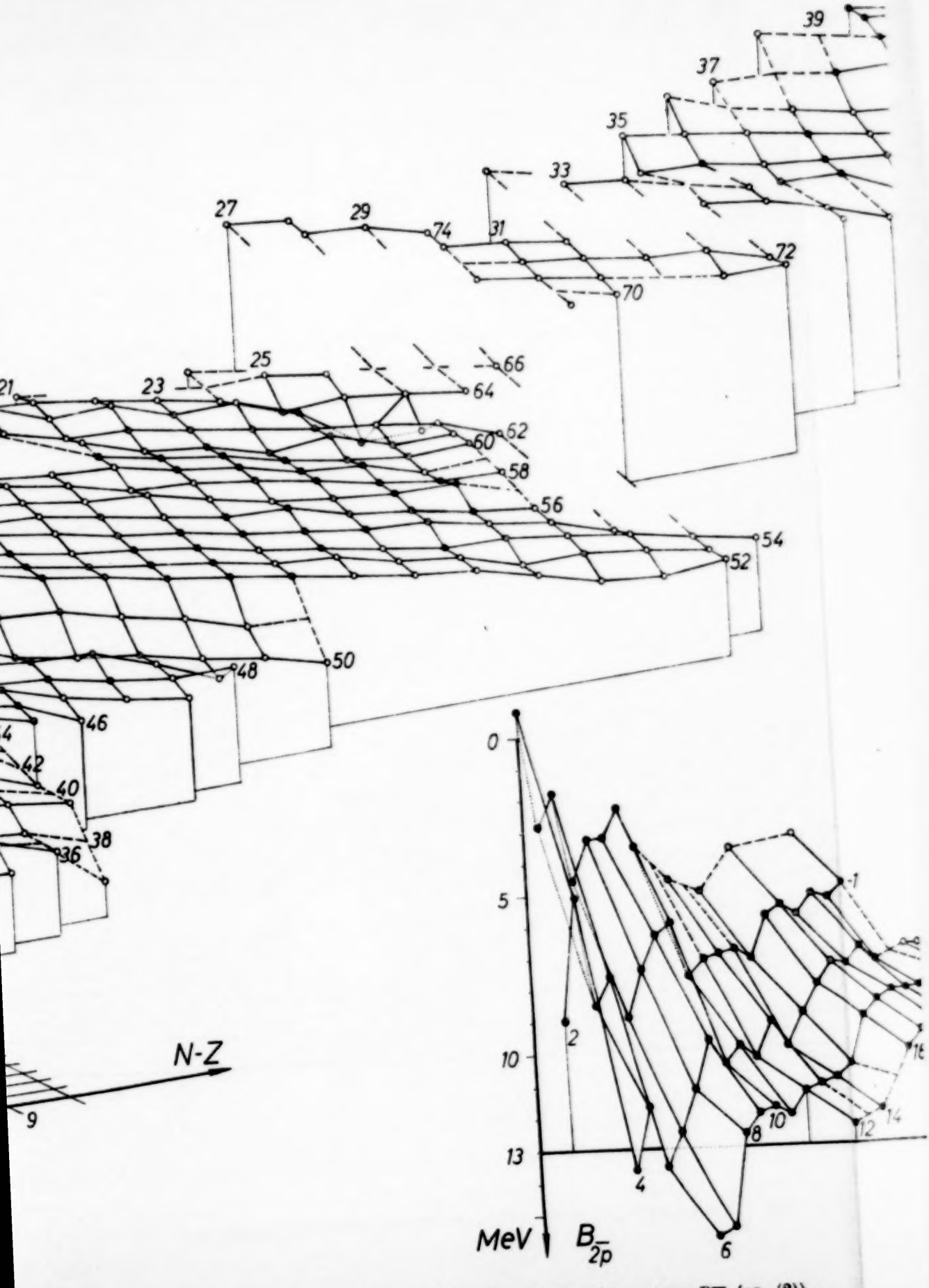

Fig. 4. Experimental mean separation energies for protons $B_{\overline{2p}}$ (eq. (2)).

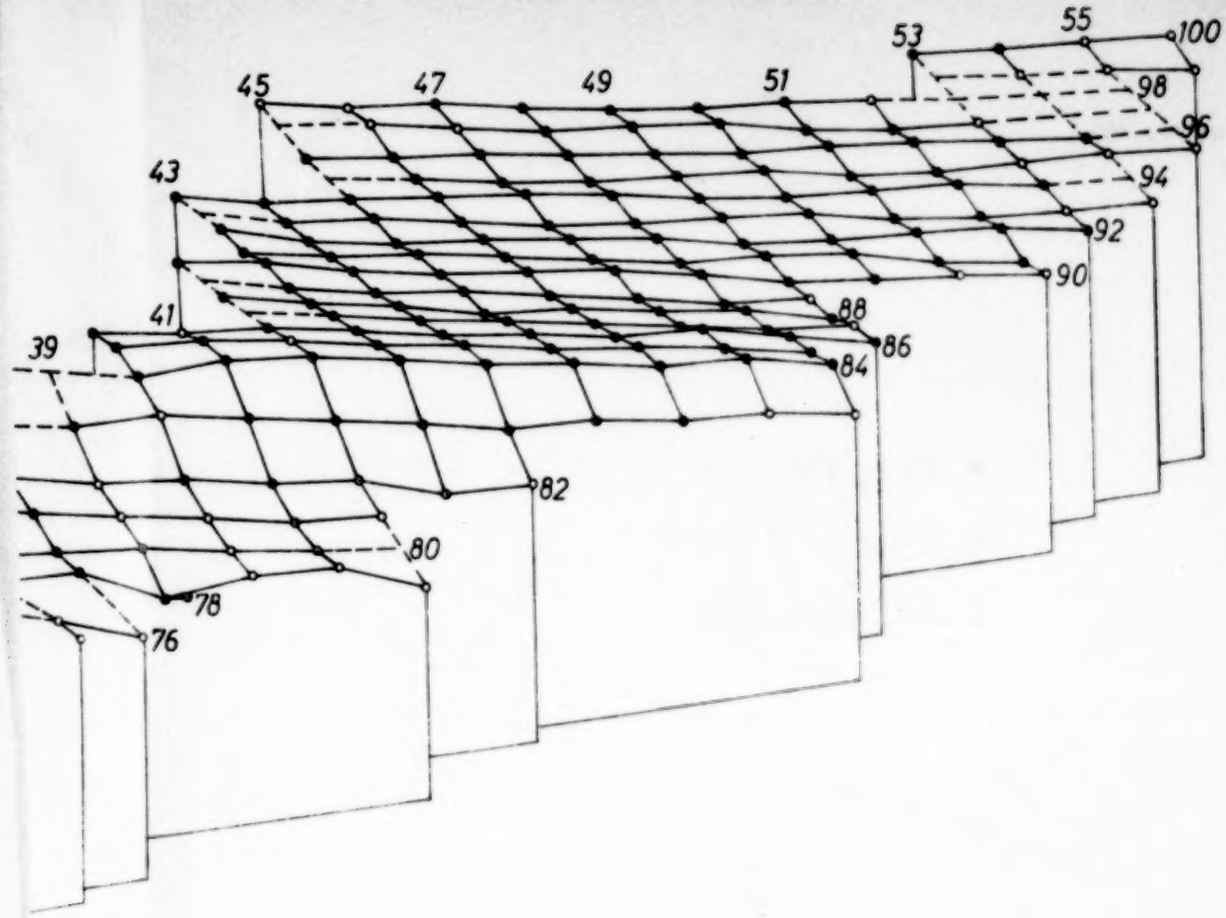
53
55
100
45
47
49
51
98
96
43
94
92
90
41
88
86
39
84
82
80
78
76

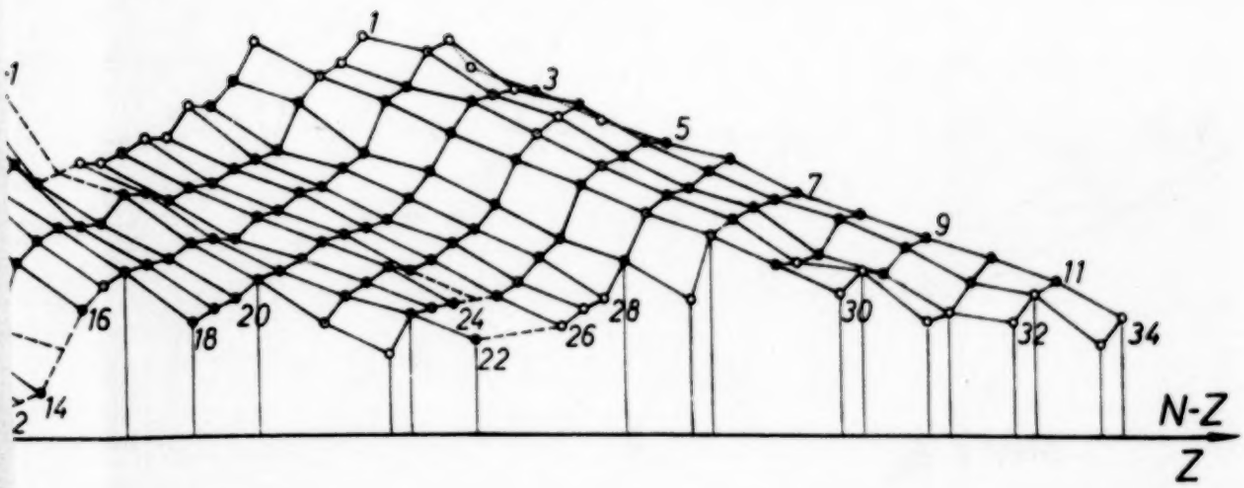
1
3
5
7
9
11
16
18
20
24
26
28
30
32
34
22
14
N-Z
Z

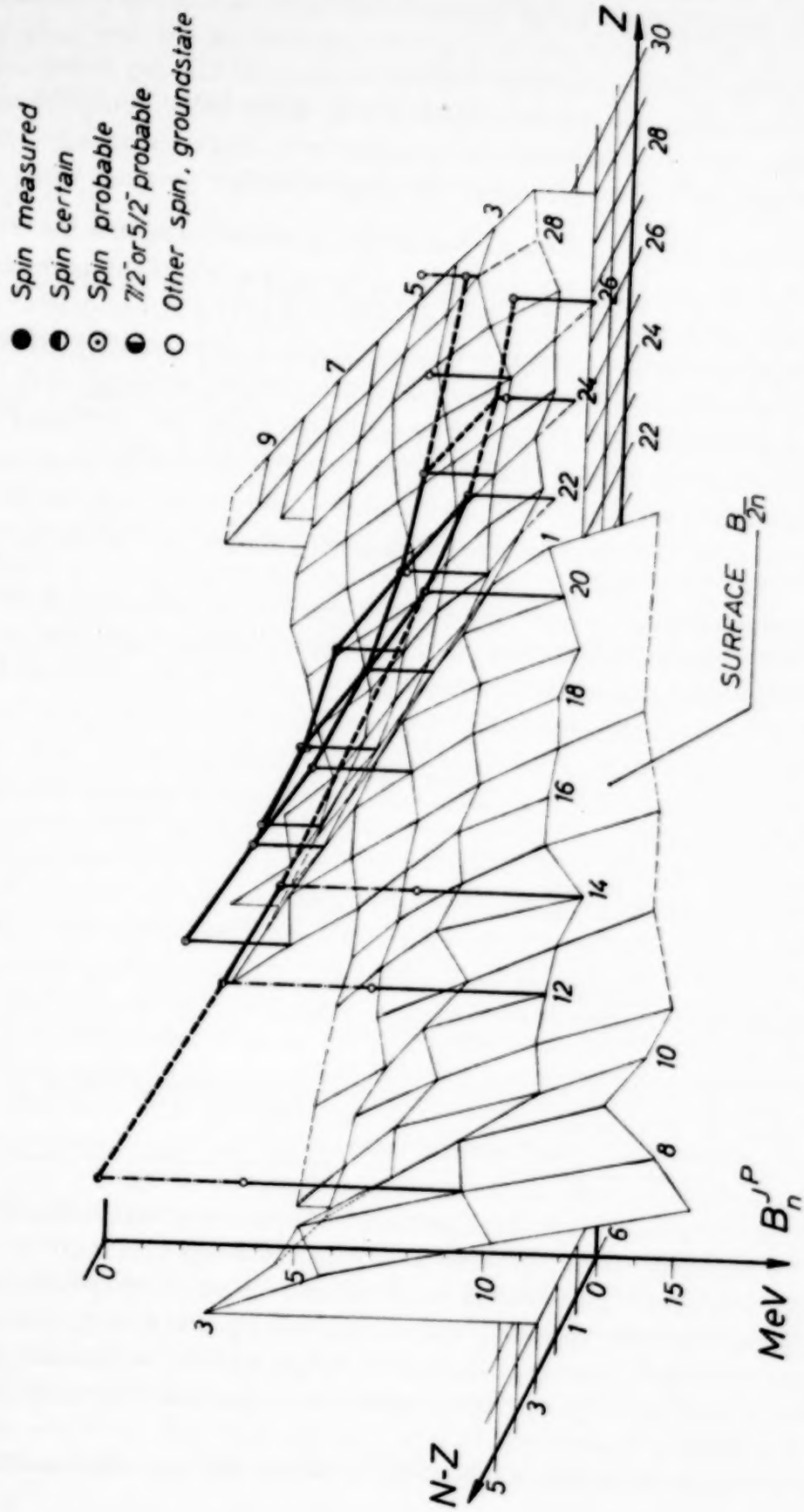

Fig. 5. The surface $B_n J^-$ (error < 0.1 MeV).

excitation energy of the level) by

$$B_n{}^{J^P} = \begin{cases} B_n - E^{J^P} & \text{for ordinary states,} \\ B_n & \text{for ground states which must have the same assignment,} \\ B_n + E^{J^P} & \text{for hole states (in simple cases).} \end{cases} \quad (4)$$

We then insert these values in our 3-dimensional system using now the vertical axis for $B_n{}^{J^P}$ in very much the same sense as in figs. 3 and 4. We thus obtain the diagram for the $\frac{7}{2}^-$ levels in the region of lighter nuclei (fig. 5, heavy lines (they are dotted if intermediate points are lacking)) which shows a rather surprising regularity. This surface is composed of 4 ordinary excited states ($Z = 8$, 12, 14 and 22; the corresponding ground states are indicated by open circles), several ground states of the same spin $\frac{7}{2}^-$ and one hole state ($Z = 28$).

3. The Experimental Values

For the construction of our two surfaces representing the mean separation energy for neutrons and protons we used a large number of publications and summaries according to the different domains of the periodic system. In table 1

TABLE 1
List of references

For Z from:	
1 to 10	Ajzenberg-Lauritsen [1])
10 to 14	Wapstra [2])
15 to 25	Giese-Benson [3]) (Wapstra [2]), NLS [4]))
26 to 30	Quisenberry-Scolman-Nier [5]) (NDS [6]), Wapstra [2]))
31 to 35	NDS [6]) (Wapstra, NLS)
36 to 39	NLS [4]) (NDS, Wapstra)
40 to 53	NDS [6]) (NLS, Wapstra)
54 to 63	NDS [6]), Johnson-Nier [7])
64 to 79	Johnson-Bhanot [8]), NDS [6])
80 to 82	NDS [6]) (Benson-Damerow-Ries [9]), Glass-Thompson-Seaborg [10]))
83 to 86	Heizenga [11]) (Glass-Thompson-Seaborg [10])
87 to 100	Glass-Thompson-Seaborg [10])

we mention the most important publications which we used in the different intervals indicated there. The references in parentheses were used in order to complete the values given in the main reference. Most of the papers indicate directly the ordinary separation energies B_n and B_p according to formula (1); we then determined our mean separation energy with the help of formula (3). In some cases (refs. [2, 11])) the mean separation energy was determined directly from the binding energies.

Unfortunately a recent publication [12]) and a private communication of

Mattauch, Wapstra *et al.* is not yet taken completely into account in our two large diagrams, but we have already checked that with the help of these new values certain parts of our surfaces will become even smoother, especially in the region of lighter nuclei and in the region of $N \approx 120$ where some irregularities seem to disappear. These new values will be considered in more detail in our next paper and they were already used successfully in the construction of our fig. 5.

4. Discussion of our Results

Our construction shows that the actual state of mass determination already permits a rather detailed comparison with theoretical considerations in large parts of the periodic table. Nevertheless, the accuracy of measurements should be increased in certain critical domains (beginning of deformation at $N = 90$ and returning to spherical shape before $N = 126$). In addition there is also a lack of experimental values in the region of $A = 100$ and in one of the most interesting parts of the periodic table, namely the realm of deformed nuclei between $N = 90$ and 120, which just coincides with the occurrence of the rare earths. Several inconsistencies in experimental values, which become apparent from this construction, will be discussed in a further more critical publication.

Comparing now the actual shape of our surfaces with the predictions of different models, we immediately observe some quite characteristic features. First of all, the typical properties of spherical shells are well pronounced in the middle part of the periodic table: between the magic numbers 28, 50, 82 (and just below and above $N = 126$ in the neutron diagram), we observe an extremely smooth behaviour of our surface. This perfectly corresponds to the fact that the single particle levels in these regions are relatively dense and that direct interactions produce a rather complete admixing between different configurations within these shells. On the other hand, the well defined energy steps just connected with the closing of spherical shells are extremely conspicuous and their shape perfectly corresponds to the existence of a gap in the single particle levels structure. It is interesting to compare these facts with the theoretical shell structure single particle levels which we have calculated in an earlier paper (ref. [17]), fig. 5) for the 'middle-line' of the flow of elements. In this connexion it is rather impressive that the heights of the steps are practically constant for the complete breadth of our surfaces and it might be worth checking the corresponding '3-dimensional property' of the theoretical levels.

We then observe that for the well known magic numbers 20 and 28, the steps are less pronounced than for the higher ones. Thus, a rather important perturbation of spherical shells seems to occur already for these relatively large nucleon numbers. For even lighter elements we see a more and more pronounced undulation of our surfaces. This seems to indicate the formation of

substructures which are well known to occur in light nuclei. Nevertheless, it is quite striking that there is no definite break in our surfaces if we proceed from the middle region of the periodic table down to the very lightest elements. This indicates that shell structure still has a certain meaning in these cases and that substructures might just be formed with the help of characteristic admixtures of a few higher excited states.

It is quite impressive to see that our separation energy surface for neutrons shows a typical break for the well known critical number $N = 90$. This break corresponds, as already mentioned, to a sudden deformation of nuclear shape which in turn is also seen from the level structure of the corresponding nuclei, the quadrupole moments and a characteristic isotopic shift of the electron states. It seems that there is no corresponding step in the domain of $N = 120$ where the structure becomes spherical again. An apparent small irregularity of our neutron surface in this region will be reduced if some new experimental results (compare refs. [12, 18])) are taken into account. This regularity is in accordance with the observed continuous behaviour of all other nuclear properties.

The construction of our single particle surface for the $\frac{7}{2}^-$ states represents a generalization and a certain improvement of the corresponding construction in our earlier publication [17]) in which only the mean values corresponding to the 'middle-line' were explicitly given. These former constructions (ref. [17]), figs. 4 and 5, upper part) were hampered by a somewhat arbitrary averaging process (the energy step connected with $N = 20$ is by far too high and the step with $N = 64$ is not real for this reason) and by the inaccuracy of the former experimental data. The construction of such single particle surfaces requires in fact an extremely precise mass determination which by now seems to be achievable.

The authors wish to thank Professor J. Mattauch for most interesting discussions and one of us expresses his thanks to the 'Fonds National Suisse pour la Recherche Scientifique' for his stipendium.

References

1) F. Ajzenberg-Selove and T. Lauritsen, Nuclear Physics **11** (1959)
2) A. H. Wapstra, Physica **21** (1955) 367
3) C. F. Giese and J. L. Benson, Phys. Rev. **110** (1958) 712
4) Nuclear Levels Schemes TID 5300, United States Atomic Energy Commission
5) K. S. Quisenberry, T. T. Scolman and A. O. Nier, Phys. Rev. **104** (1956) 461
6) Nuclear Data Sheets, National Research Counsil, Washington
7) W. H. Johnson and A. O. Nier, Phys. Rev. **105** (1957) 1014
8) W. H. Johnson and V. B. Bhanot, Phys. Rev. **107** (1957) 1669
9) J. L. Benson, R. A. Damerow and R. R. Ries, Phys. Rev. **113** (1959) 1105

10) R. A. Glass, S. G. Thompson and G. T. Seaborg, J. of Inorganic and Nuclear Chemistry **1** (1955) **3**
11) J. R. Huizenga, Physica **21** (1955) 410
12) Everling, König, Mattauch and Wapstra, Nuclear Physics **15** (1960) 342 and private communication
13) D. Strominger, J. M. Hollander and G. T. Seaborg, Rev. Mod. Phys. **30** (1958) 585
14) P. M. Endt and C. M. Braams, Rev. Mod. Phys. **29** (1957) 683
15) H. E. Duckworth, Canad. I. of Phys. **38** (1960) 819
16) K. Bleuler and Ch. Terreaux, HPA **28** (1955) 245
17) K. Bleuler and Ch. Terreaux, HPA **30** (1957) 183
18) Bhanot, Johnson and Nier, private communication (1960)

1.E.1:
3.A

Nuclear Physics **22** (1961) 598—609; © *North-Holland Publishing Co., Amsterdam*
Not to be reproduced by photoprint or microfilm without written permission from the publisher

LEVELS IN Gd^{156} FED BY THE DECAY OF 15-DAY Eu^{156}

J. E. CLINE and R. L. HEATH

Phillips Petroleum Co., National Reactor Testing Station, Idaho Falls, Idaho †

Received 6 October 1960

Abstract: Radiations following the decay of 15-day Eu^{156} have been studied using the techniques of coincidence scintillation spectrometry and 4π beta counting. Twenty-eight gamma rays were identified as transitions from excited levels in Gd^{156}. The energies of these gamma rays, along with their coincidence relationships, indicate that levels are present in the daughter nucleide at 89, 290, 520, 1150, 1240, 1250, 1320, 1360, 1960, 2030, 2180 and 2200 keV. Gamma-gamma directional correlation measurements have been made leading to spin assignments for the levels at 1320, 1960 and 2030 keV.

1. Introduction

The Bohr-Mottelson model of collective nuclear structure [1]) has achieved considerable success in explaining nuclear spectroscopic data. Applications of this model to nuclei which lie in the transition region between the spherically symmetric and non-spherical nuclei are of considerable theoretical interest, since in this region the nuclear parameters of neighboring nuclei are often radically different. The Gd^{156} nucleus, which has 92 neutrons, lies in such a transition region. This paper presents the results of a study of the levels in this nucleide excited in the decay of 15-day Eu^{156}.

Levels in Gd^{156} populated through electron capture in Tb^{156} have been studied at several laboratories [2–7]). Level schemes presented by Ofer [6]) and by Gregers Hansen *et al.* [7]) demonstrate the collective phenomena in nuclear structure predicted by the model.

The decay of Eu^{156} has, however, received relatively little study. Boehm and Hatch [8]) examined the gamma-ray spectrum and suggested that as many as 25 gamma rays might be present. Ewan *et al.* [9]) studied the isotope and suggested levels at 89, 298, 1940 and 2140 keV. Detailed analysis of their data was not possible due to the presence of Eu^{154} as a contaminant in the source material. More recently, the results of concurrent investigations at this laboratory [10]) and by Ewan *et al.* [11]) have revealed several additional energy levels in the Gd^{156} nucleus.

2. Experimental Techniques and Data

2.1. SOURCE PREPARATION

Sources of Eu^{156} were prepared by irradiation of Sm_2O_3, supplied by Oak Ridge National Laboratory with an enrichment of 99 % in Sm^{154}, in a high

† Work performed under the auspices of the U. S. Atomic Energy Commission.

flux region of the Materials Testing Reactor ($\approx 5\times 10^{14}$ neutrons per cm^2 per sec). The samples of Sm_2O_3 (about 0.1 mg) were placed in quartz vials and irradiated for 15 days. Eu^{156} was produced by double neutron capture with an intermediate beta decay. Following an 8-day" cooling-off" period, the Eu^{156} activity was two orders of magnitude higher than the highest contaminant activity (Eu^{155}). The irradiated material was dissolved in $8N$ HNO_3, taken to dryness and re-dissolved in $\frac{1}{100}$ N HNO_3. Sources 1 mm in diameter were

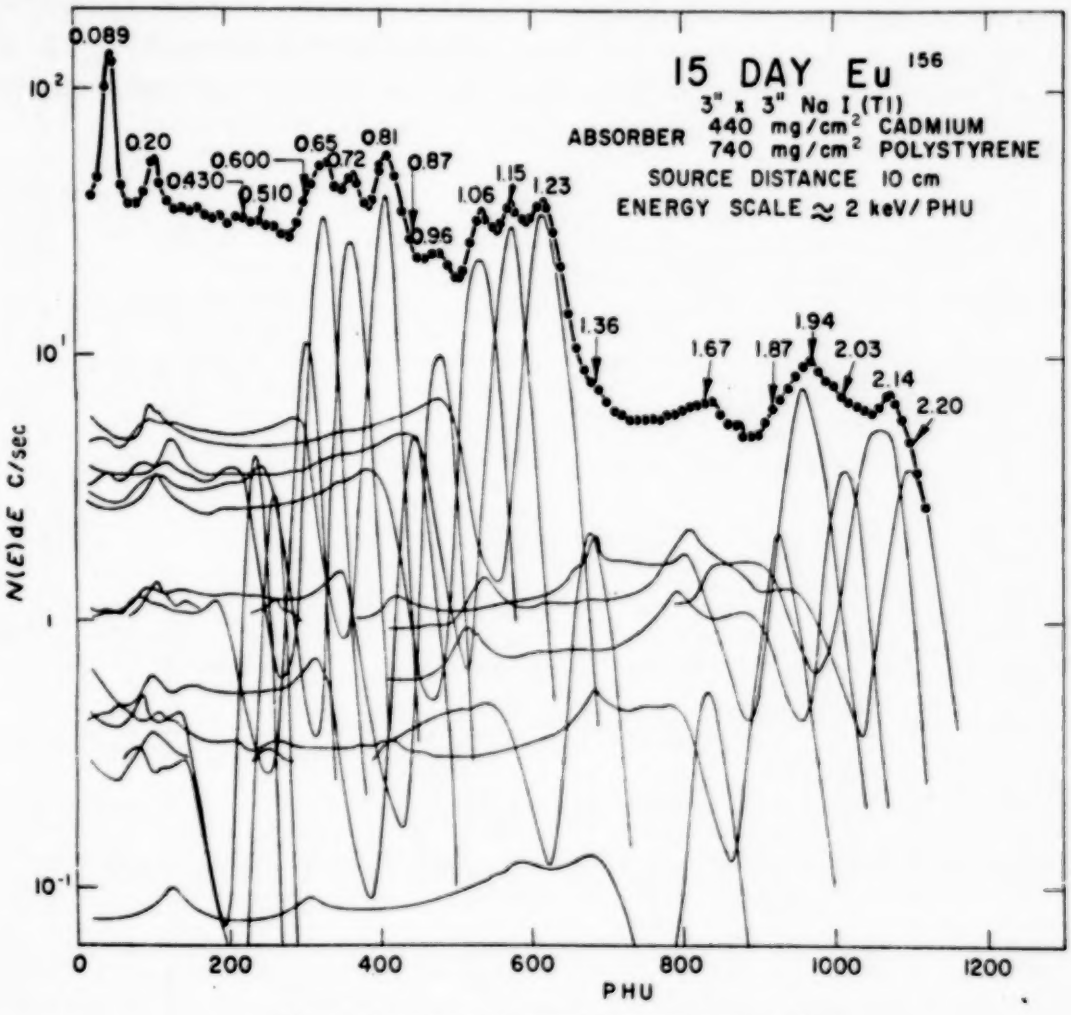

Fig. 1. Spectrum of gamma rays from Eu^{156}.

prepared for gamma-ray studies by evaporation of this solution on 10 mg/cm^2 plastic films. Liquid sources for gamma-gamma directional correlation studies were contained in thin-walled, 0.16 cm ID, lucite holders. Sources for absolute beta counting were prepared by evaporation of solution on 5 μg/cm^2 films of VYNS coated on both sides with 20 μg/cm^2 of gold.

2.2. GAMMA RAY MEASUREMENTS

The gamma radiation emitted in the decay of Eu^{156} was observed with 7.6 cm diameter by 7.6 cm cylindrical NAI(Tl) detectors. Sources were measured

in point geometry, at 10 cm along the vertical axis of the detector to reduce coincidence summing in the detectors. Polystyrene absorbers were interposed between the sources and detectors to remove the beta radiation. All measurements were made in a large cubical detector shield with inside dimensions of 80 cm to insure no complications resulting from scattered radiation. Energy calibration of the scintillation spectrometers was achieved by the method of internal comparison to reduce the effect of rate-dependent gain fluctuations in the photomultipliers and amplifiers.

A typical pulse-height spectrum obtained from Eu^{156} is shown in fig. 1. All gamma rays were observed to decay with a 15-day half-life. The spectrum was

TABLE 1

Gamma-ray energies and intensities

Gamma ray energies [a] (keV)	Gamma ray energies [b] (keV)	Relative intensity		Percentage of decays per β-decay	
89		2.39		44.8	
200		0.18		3.2	
430 ± 10		0.03		0.6	
600 ± 10		0.09		1.8	
630 ± 10		0.35		6.6	
	720	0.21		3.8	
720 ± 10			0.35		6.3
	720	0.14		2.5	
810 ± 10		0.50		9.3	
870 ± 10		0.09		1.7	
960 ± 10		0.18		3.2	
	1050	0.22		4.1	
1050 ± 10			0.51		9.6
	1060	0.29		5.5	
	1150	0.21		3.9	
1150			0.70		13.1
	1160	0.49		9.2	
	1230	0.70		13.2	
1240 ± 20			1.00		18.8
	1240	0.30		5.6	
1360 ± 20		0.09		1.8	
1670 ± 20		0.02		0.4	
1870 ± 20		0.10		1.9	
	1940	0.19		3.6	
1930 ± 20			0.38		7.2
	1960	0.19		3.6	
2030 ± 20		0.19		3.6	
	2100	0.20		3.7	
2140 ± 20			0.38		7.0
	2180	0.18		3.3	
2200 ± 20		0.12		2.2	

[a] Determined from singles spectra.

[b] Determined from level scheme and coincidence relations.

unfolded by means of the subtraction process using known spectrum shapes [12]); and relative intensities of the gamma rays were obtained. Branching ratios for the gamma rays were determined by comparison with absolute beta-decay rates, obtained using a 4π flow proportional counter. These data are presented in columns 1, 3 and 4 of table 1.

Gamma-gamma coincidence measurements were made on these gamma rays using NaI(Tl) detectors. Graded backscatter shields were used to reduce false coincidence effects due to the scattering of gamma rays between the detectors.

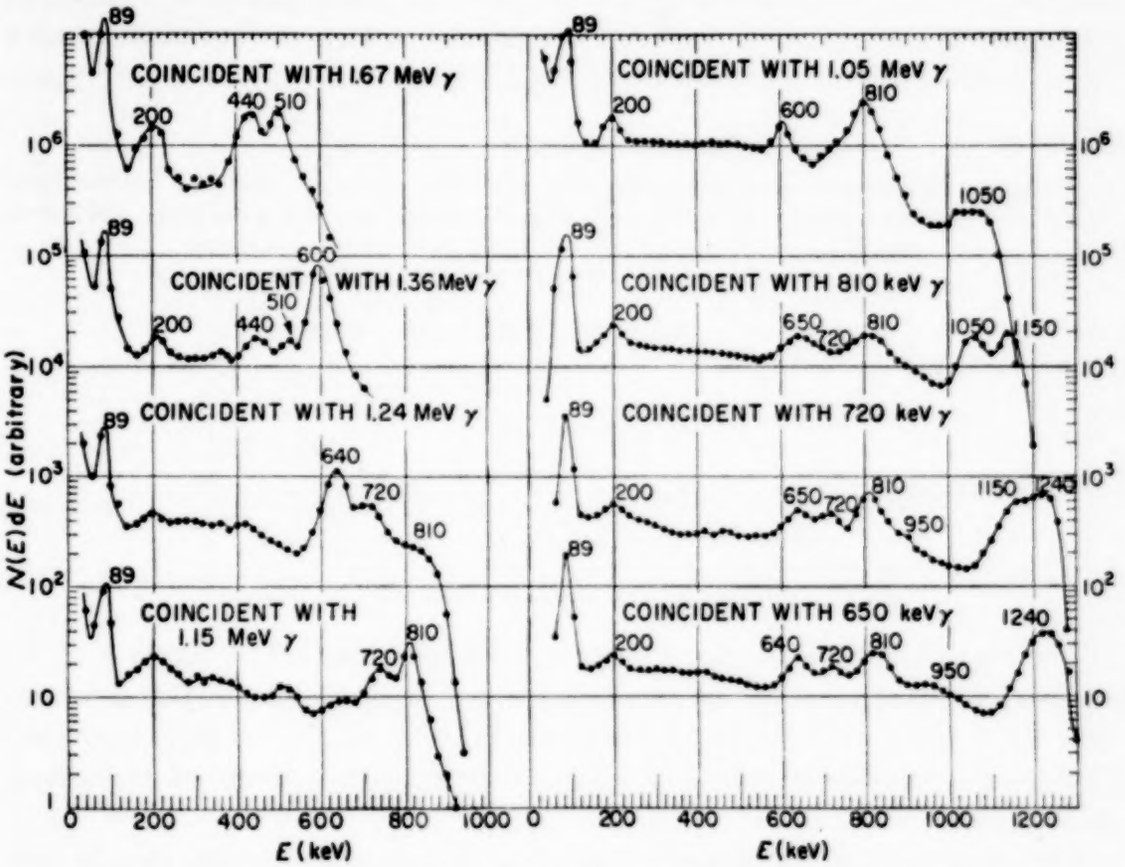
COINCIDENT WITH 1.67 MeV γ
COINCIDENT WITH 1.05 MeV γ
COINCIDENT WITH 1.36 MeV γ
COINCIDENT WITH 810 keV γ
COINCIDENT WITH 1.24 MeV γ
COINCIDENT WITH 720 keV γ
COINCIDENT WITH 1.15 MeV γ
COINCIDENT WITH 650 keV γ
N(E)dE (arbitrary)
E (keV)
E (keV)

Fig. 2. Typical Eu^{156} coincidence spectra from systematic coincidence scanning.

Coincidence circuitry used was of the fast-slow type with a fast resolution of 6×10^{-7} seconds. The coincidence spectrometry consisted of an automatic sliding-window, single-channel analyzer operated in coincidence with a fast 120-channel discriminator type analyzer. A 7.6 cm × 7.6 cm NaI(Tl) detector was used in conjunction with the multi-channel analyzer in all measurements. A 0.16 cm × 5.1 cm NaI(Tl) detector was used with the single-channel analyzer for settings at low energies to reduce the Compton effects from the high energy gamma rays. For high energies, a 7.6 cm × 7.6 cm detector was used for this channel.

Coincidence spectra were obtained for all settings of the single-channel analyzer from 60 keV to 2.24 MeV in 40 keV steps. This systematic scanning

permitted the observation of the behavior of a coincidence photopeak as the energy window of the single-channel analyzer was moved across a small region of the gamma-ray singles spectrum. Thus it was possible to determine if a gamma ray were truly in coincidence with a particular photopeak, or with the Compton distribution associated with higher energy gamma rays. Analysis of these data established coincidence relationships between the major resolved gamma rays. Typical spectra obtained from the systematic coincidence scanning are shown in fig. 2. Of particular interest were the coincidence relationships among the 650, 720, 810, 1050, 1150 and 1240 keV gamma rays. A quantitative analysis was made of the gamma-ray spectra in coincidence with each of these gamma rays. Table 2 shows the results of this analysis.

TABLE 2

Coincidence relationships between the 650, 720, 810, 1050, 1150, and 1240 keV gamma rays. The number in each square represents the percentage of the gamma ray in the horizontal row in coincidence with the gamma ray listed in the vertical column.

Gamma ray energy (keV)	650	720	810	1050	1150	1240
650						30
720					70	30
810				45	30	
1050			55	5		
1150		45	45			
1240	100	40				

The maximum β^- end-point energy of 2430 keV reported by Ewan *et al.* [11]) limits energy levels excited in this decay to less than 2300 keV. This information, when combined with the results shown in tables 1 and 2, strongly suggested that the photopeaks at 720, 1050, 1150 and 1240 keV are groups of unresolved gamma rays.

Fig. 3 shows the gamma-ray spectrum in coincidence with the 89-keV ground state transition. Also included in this figure is a gamma ray singles spectrum for comparison. The photopeak at 650 keV, corrected for the Compton contribution from higher energy gamma rays, served to normalize these spectra. This normalization was based on the 650-1240-89 keV cascade. It is noted in table 2 that the 650 keV transition is 100 % in coincidence with a 1240-keV gamma ray. Therefore, this 650-keV gamma ray must be either completely or not at all in coincidence with the 89-keV gamma ray. The coincidence spectrum of fig. 3 indicates a definite coincidence relationship between the 89 and the 650 keV transitions. The comparison of these two spectra permitted a determination of the fraction of each photopeak in coincidence with the 89-keV gamma ray. Results of this analysis are shown in table 3. The gamma ray at 1950 keV was shown from this measurement to contain two components,

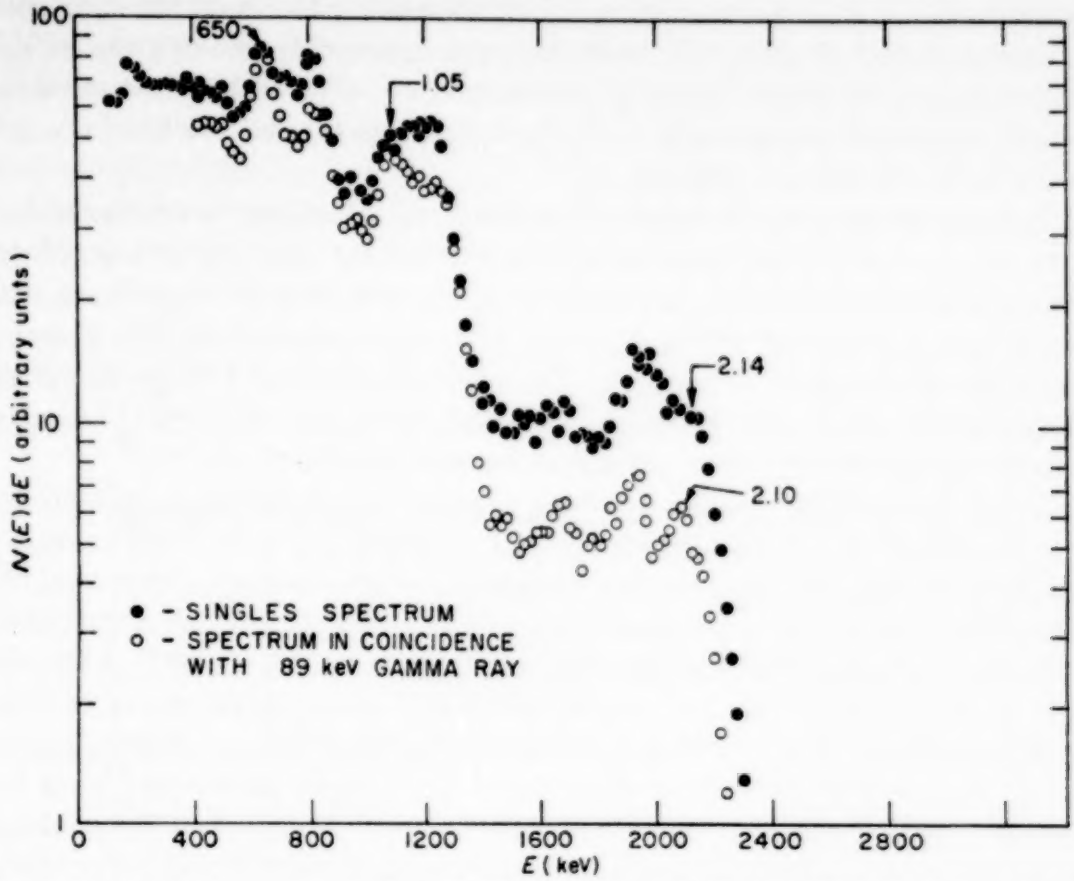

Fig. 3. Spectrum of gamma rays from Eu^{156} emitted in coincidence with 89 keV ground state transition.

TABLE 3

Fractions of photopeaks in coincidence with 89-keV ground state transition

Photopeak energies (keV)	Percentage in coincidence with 89 keV γ-ray
650	100
720	60±10
810	60±10
960	100
1050	100
1150	70±10
1230	70±10
1940	100
1950	
1960	0
2030	0
2100	100
2140	
2180	0
2200	0

unresolved in the singles spectrum, one of 1940 keV which was 100 % in coincidence and one of 1960 keV which was not in coincidence with the 89-keV ground state transition. Similarly, the gamma ray at 2140 keV was shown to be a composite of two gamma rays, one in coincidence and one not in coincidence with the 89-keV gamma ray.

Since the gamma ray at 2100 keV is 100 % in coincidence with the 89-keV transition and is the only gamma ray above 1950 keV which is in coincidence with any gamma transition, an analysis of the spectrum in coincidence with the energy region about 2100 keV served as a measurement of the K conversion coefficient of the 89-keV transition. The resultant value of 1.35 ± 0.20 for the K conversion coefficient compares favorably with the theoretical value of 1.42 for an E2 transition as calculated by Sliv and Band [13]).

Due to the extreme complexity of the gamma-ray spectrum, gamma-gamma directional correlation measurements could be made for only a few cascades. Attempts were made only for those cascades in which the gamma rays could be adequately resolved in the singles spectrum and where the coincidence relationships were simple. Data were obtained for the 810—1050, the 810—1150, the 650—1240, the 89—1940, and the 89—2100 keV cascades. Detectors used for these measurements were 7.6 cm $\times$ 7.6 cm NaI(Tl) scintillation counters located 10 cm from the source. Data were taken in 9-degree increments from 90° through 180°. At least three determinations were made of the coincidence counting rate and each angle, each determination containing about 1000 counts. The random coincidence rate was found to be about 3 % of the gross coincidence rate.

3. Results and Discussion

3.1. RESULTS

Fig. 4 presents a level scheme consistent with the data. The levels at 89, 290, 1150 and 1250 keV are also populated by the decay from Tb^{156}. The spin I, projection K of the nuclear spin on the axis of nuclear symmetry, and parity for each of these levels are well established, as are the intensity ratios for gamma rays depopulating the states. These ratios, used in conjunction with the coincidence data listed in tables 2 and 3 and with absolute intensities listed in column 4 of table 1, allow the splitting of the photopeaks at 720, 1050, 1150 and 1230 keV into pairs of gamma rays centered about the average energy of the unresolved gamma rays. The energies of these pairs, along with their relative and absolute intensities, are also listed in table 1. In many cases, although the gamma ray energies and coincidence relationships are certain, the chronological order of the transitions is in doubt. Where this is true, the energy levels are represented by dashed lines. Less certain transitions are also indicated by dashed lines.

It is apparent from the decay scheme that the multipolarities of the gamma

transitions are in all cases either 1 or 2. Since the population of the 4+ state at 290 keV is so small, it becomes apparent that the spins of the higher energy levels are also quite small, certainly no larger than 3. Multipolarities shown in the scheme were assigned by Ewan *et al.* [11]) on the basis of conversion coefficient measurements.

On the basis of the decay systematics, multipolarity assignments, and these arguments for low spins, probable spins and parities have been assigned to the

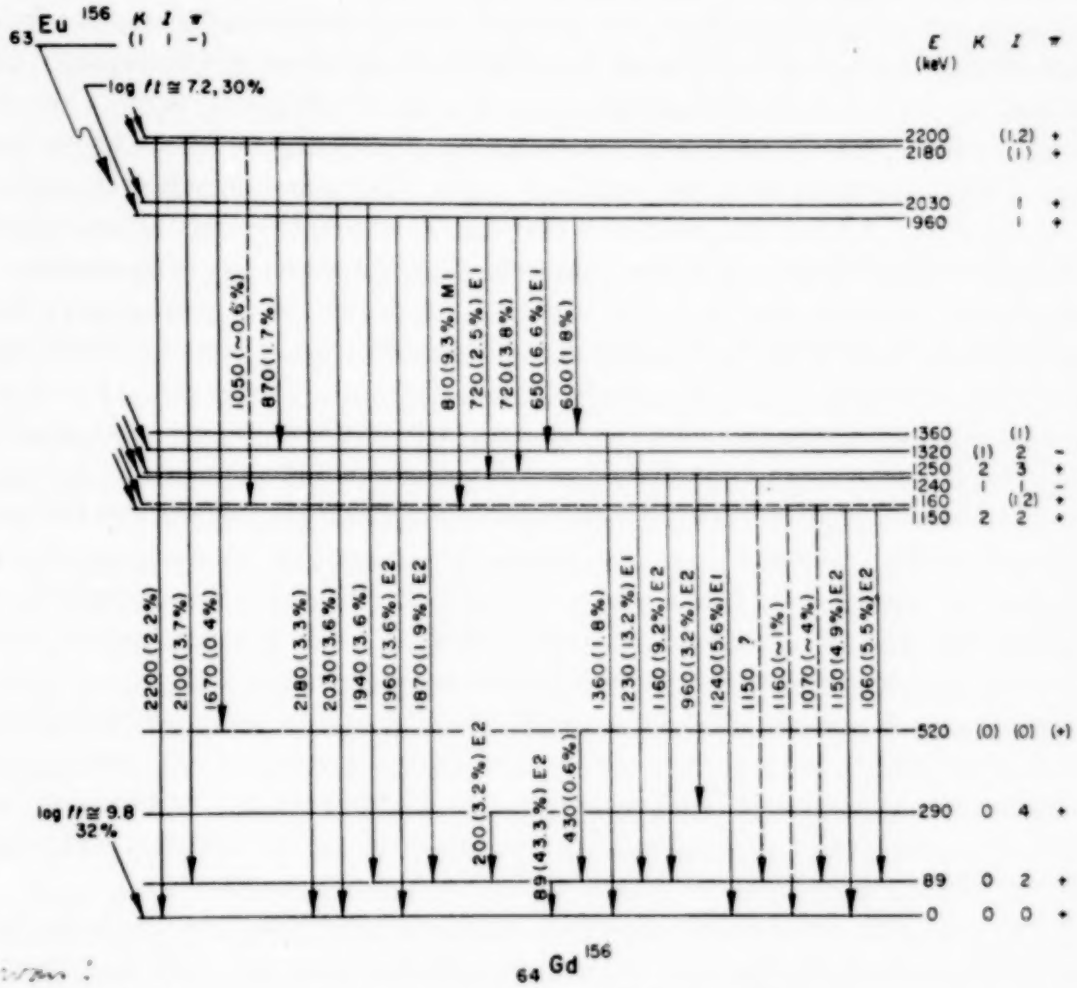

Ewan:
E_β 2450 keV

Fig. 4. Decay scheme of $Eu^{156} \rightarrow Gd^{156}$.

levels. Wherever possible, assignments of the value of K have also been made on the basis of collective structure and gamma-ray intensity arguments. The levels at 89, 290, 1150 and 1250 keV are known from the data on the decay of Tb^{156} to have values for K, I and π of (0,2+), (0,4+), (2,2+) and (2,3+), respectively. A level was tentatively assigned at 520 keV on the basis of a 1670—430 keV coincidence relationship. This level may actually occur at 1760 keV since the gamma rays involved are of nearly equal intensity. A 520 keV transition may also be present in coincidence with the 1670-keV gamma

ray. Data on the 520 keV transition are inconclusive since a large fraction of the spectrum at 1670 keV is due to a single-photon escape peak from the 2180-keV gamma ray, which would give rise to 1670—511 keV coincidences. The probable spin assignment for this level would be either 0, 1 or 2. From the collective model, the level could be the lowest level of the beta vibrational band with values of K, I or π of (0,0+), although the energy is rather low for such a level.

Intensity ratios for the gamma rays from the states at 1150 and 1250 keV are well known. Therefore, the coincidence measurements allow assignments of absolute intensities for these transitions. The remainder of the 1060-keV radiation and a small fraction of the 1160-keV radiation are interpreted as transitions from a level at 1160 keV. The 5 % of the 1050-keV gamma ray in apparent coincidence with itself (shown in table 2) was assigned to a transition from a level at 2200-keV to the 1160-keV state. The probable spin of this level is either 1 or 2. A level was placed at 1240 keV to account for the fraction of the 1240-keV transition not coincident with the 89 keV gamma ray. The measured internal conversion coefficients of the 1230- and 1240-keV gamma rays are consistent with those of E1 transitions [11]). Therefore, the level at 1240 keV has spin 1, negative parity and a probable value of K of 1. The level at 1320 keV, also decaying by a 1240-keV E1 transition to a lower level, satisfies the coincidence relationships observed between the unresolved 1240-keV peak and the 89- and 650-keV gamma rays. The probable spin and parity assignment for this level is 2−. The 1360-keV level was established to account for the coincidence relationship between the 1360- and a 600-keV gamma ray originating from a higher level. The spin of this level is most likely 1. Since the two gamma rays involved in transitions to and from this level have approximately equal intensities, this level may actually occur at 600 keV although it becomes difficult to account for such a level at this energy. The energy levels at 1960, 2030, 2180 and 2200 keV all exhibit ground state transitions and in all cases but that of the decay from the 2180 keV level exhibit transitions to the 89 keV (2+) state as well. Therefore, only spins of 1 or 2 are allowed for these states.

Gamma-gamma directional correlation measurements have been made on the 810—1060, 810—1150, and the 650—1230 cascades from the 1960 keV state,

TABLE 4

Experimental coefficients of $P_2(\cos\theta)$ terms in $\gamma-\gamma$ angular correlation measurements, and spin sequence assignments

Level sequence and transition energies	Coefficient of P_2 term	Spin sequence of levels
1960(810)1150(1060)89	$-(0.011\pm0.010)$	consistent with 1(1)2(1)2 with mixing
1960(810)1150(1150)0	$-(0.145\pm0.023)$	1(1)2(2)0 with mixing
1960(650)1320(1230)89	$-(0.137\pm0.015)$	1(1)2(1)2 with no mixing (all E1 radiation)
2200(2100)89(89)0	$+(0.128\pm0.020)$	either 1(1)2(2)0 or 2(1)2(2)0
2030(1940)89(89)0	$-(0.135\pm0.029)$	1(1)2(2)0 with mixing

the 1940—89 cascade from the 2030 keV level, and the 2100—89 cascade from the 2200 keV level. These data could be fitted with a correlation function containing no Legendre polynomials of order higher than two, since in all cases, the coefficient of the P_4 (cos θ) term was not statistically significant. Table 4 lists the coefficients obtained from these measurements as well as the spin sequences determined for these levels.

The 810—1060 and 810—1150 cascades from the state at 1960 keV involved gamma rays of known multipolarity[11]) which proceeded through an intermediate state of known spin to final states of known spins. The only unknown remaining for these cascades was the spin of the initial state. In the 650—1230 keV cascade, although the multipolarities were known, the spin of the intermediate state had not been definitely established. These three measurements served to determine uniquely the spin of the levels at 1960 and 1320 keV as 1 and 2, respectively. The parities were previously known.

The measurements on the 2100—89 keV gamma-ray cascade failed to determine uniquely the spin of the level at 2200 keV, since the measured correlation function was consistent with either a 1(1)2(2)0 or a 2(1)2(2)0 spin sequence, each requiring a different mixing ratio for the 2100-keV transition. A more precise measurement of the correlation function would be necessary in order to distinguish between the two possibilities. Due to the low coincidence counting rate in this experiment, such a precise measurement could not be made. Since mixing is required to fit the correlation function in either case, the parity of the level at 2200 keV must be positive.

The correlation function for the 1940—89-keV gamma-ray cascade from the level at 2030 keV may be fitted uniquely with a 1(1)2(2)0 spin sequence. The values of the spins assigned on the basis of these measurements are shown in fig. 4.

3.2. DISCUSSION

It is of interest to combine the level scheme of Gd^{156} determined from the decay of Tb^{156} by Gregers Hansen *et al.* [7]) with the scheme determined in this work from the decay of Eu^{156}. The combined decay scheme is shown in fig. 5. The ground state $K = 0$ rotational band is present through the 6+ state, with levels at 0, 89, 290 and 584 keV. The rotational band based on the gamma vibrational state characterized by (2,2+), $n_\beta = 0$, $n_\gamma = 1$ is seen in the levels at 1150 and 1250 keV. The level at 520 keV is possibly the lowest level of the rotational band structure based on the beta vibrational state characterized by (0, 0+), $n_\gamma = 0$ and $n_\beta = 1$. The levels at 1240 and 1320 keV appear to be members of a rotational band based on the state at 1240 keV. Levels at 1507 and 1620 keV appear similarly to be members of a rotational band based on the state at 1507 keV. Such assignments are consistent with the spin assignments, energy spacings, and calculated moments of inertia for these groups of levels.

The same phenomenon occurs again at 1931 and 2042 keV. The remaining tour high energy states appear to be intrinsic states, as do the levels at 1126, 1160 and 1360 keV.

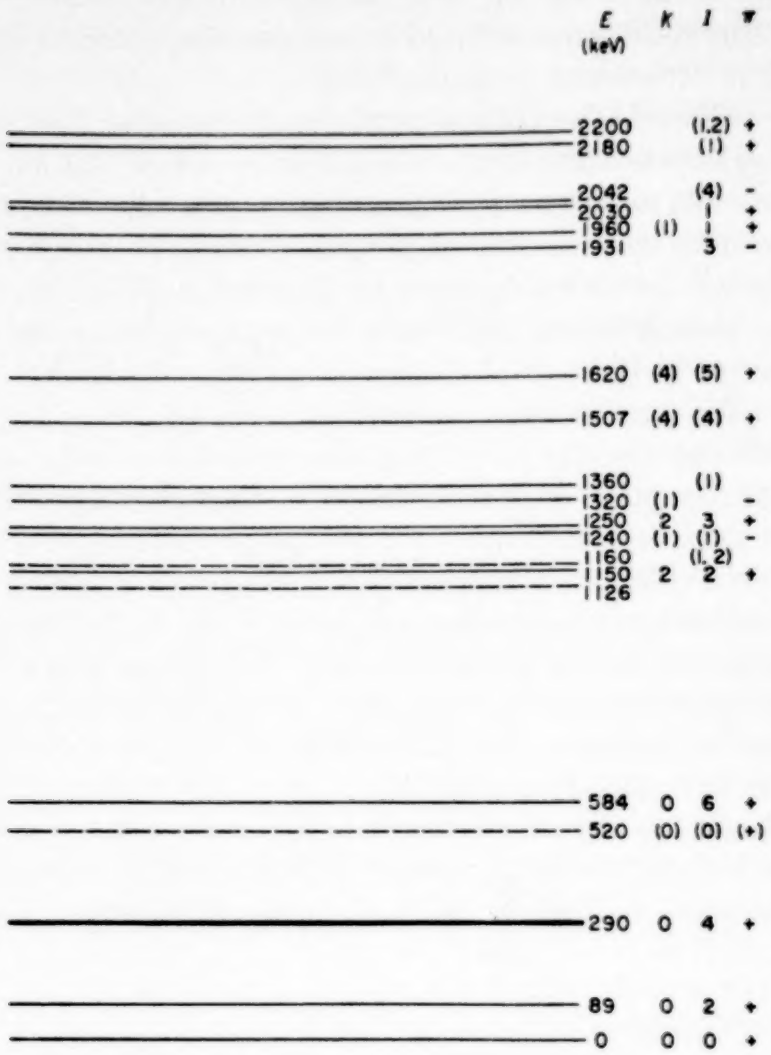

Fig. 5. Composite level scheme for Gd^{156}.

The authors are indebted to the staff of the decay schemes group at this laboratory for many enlightening discussions and in particular to Mr. E. A. C. Yates for assistance in taking some of the data.

References

1) For a rather extensive reference list, see R. K. Sheline, Rev. Mod. Phys. **32** (1960) 1
2) T. H. Hanley and W. S. Lyon, Phys. Rev. **99** (1955) 1415
3) J. W. Mihelich, B. Harmatz and T. H. Hanley, Phys. Rev. **108** (1957) 989
4) L. T. Dillman, R. W. Henry, N. B. Gove and R. A. Beeker, Bull. Am. Phys. Soc. **2** (1957) 341
5) R. W. Henry, L. T. Dillman, N. B. Gove and R. A. Beeker, Bull. Am. Phys. Soc. **2** (1957) 341
6) S. Ofer, Phys. Rev. **115** (1959) 342

7) P. Gregers Hansen, O. B. Nielsen and R. K. Sheline, Nuclear Physics **12** (1959) 389
8) F. Boehm and E. N. Hatch, Bull. Am. Phys. Soc. **1** (1956) 390
9) G. T. Ewan, J. W. Knowles and D. R. MacKenzie, Bull. Am. Phys. Soc. **2** (1957) 259
10) J. E. Cline and R. L. Heath, Bull. Am. Phys. Soc. **5** (1960) 21
11) G. T. Ewan, R. L. Graham and J. S. Geiger, Bull. Am. Phys. Soc. **5** (1960) 21
12) See a description of the method by R. L. Heath, US AEC Report IDO-16408 (unpublished)
13) L. A. Sliv and J. Band, Tables of internal conversion coefficients of gamma rays (Academy of the USSR, Moscow, Leningrad, 1956); report 57ICCK 1, issued by the Physics Department, University of Illinois, Urbana, Illinois (unpublished)

3.B

Nuclear Physics **22** (1961) 610—628 ©*North-Holland Publishing Co., Amsterdam*

Not to be reproduced by photoprint or microfilm without written permission from the publisher

NEGATIVE PARITY LEVELS IN THE EVEN-EVEN NUCLEUS Dy^{160}

G. T. EWAN, R. L. GRAHAM and J. S. GEIGER

Atomic Energy of Canada Limited, Chalk River, Ontario, Canada

Received 3 October 1960

Abstract: The conversion electron spectrum of Tb^{160} has been studied in the Chalk River air-cored $\pi\sqrt{2}\,\beta$-ray spectrometer at resolution settings of 0.04 % to 0.1 %. Gamma-conversion electron coincidence experiments have been made to establish the positions of the levels in Dy^{160}. The level scheme based on the present results is 0(0+), 86.7 (2+), 283.6 (4+), 965.8 (2+), 1048.8 (3+), 1264.4 (2−), 1286.5 (3−), 1358.2 (2−), and 1398.5 keV (3−). This is similar to that of Nathan in the positive parity levels but differs in the negative parity levels. Particular attention has been paid to determining the intensities of weak transitions in the decay scheme. The relative quantum transition probabilities have been deduced from the conversion line measurements using Sliv's theoretical conversion coefficients. The agreement between the observed transition probabilities from the positive parity levels and the theoretical predictions of the Unified Model is greatly improved if a small amount of $K = 0$ band is assumed mixed in the $K = 2$ gamma-vibrational band. The relative transition probabilities from the negative parity levels are not consistent with K being a good quantum number in discussing these levels. The possibility of interaction between the negative parity levels is briefly discussed.

1. Introduction

Negative parity levels can occur in highly distorted even-even nuclei either as a result of octupole vibrations or due to particle excitation. Examples of such levels in the rare earth region have been reported in studies of Sm^{152} [1, 2]) Gd^{152} [1, 2]) and Gd^{156} [3, 4]). Nathan [5]), in his study of the decay of Tb^{160}, reported negative parity levels of spin 2-(1264 keV) and 3-(1358 keV) in Dy^{160} and suggested that these might be members of a band based on an octupole vibration with $K = 2$. Subsequent workers [6]) have reported another level at 1395 keV with spin 3- and a tentative level at 1200 keV with spin 1−. These latter levels and their spin assignments have not been definitely established by coincidence experiments.

The present paper reports the results of a study of the internal conversion electron spectrum of Tb^{160}, using the Chalk River high resolution air-cored β-ray spectrometer. Particular attention has been paid to the resolution of closely-spaced lines, to the measurement of γ-ray energies with sufficient accuracy to locate the transitions unambiguously in the level scheme, and to the determination of the intensities of weak transitions expected from the level scheme. Gamma-conversion electron coincidence measurements have been made to establish the positions of the levels. The level scheme proposed is similar

to that of Nathan for the positive parity levels but differs in the negative parity levels. The relative transition probabilities between levels are compared with the predictions of the Unified Model and those of Davydov and Filippov. The effect of band mixing on the transition probabilities is discussed. A preliminary account of this work was submitted to the International Conference on Nuclear Structure, Kingston, 1960 [7]).

2. Conversion Electron Spectrum

Sources of Tb^{160} were prepared by irradiating Tb_3O_4 in the NRX reactor for periods of one or two months at a flux of 6×10^{13} neutrons per cm^2 per sec. The irradiated material was dissolved in nitric acid and the terbium nitrate sublimed from a boat-shaped tantalum filament through a slot onto a backing of Al foil 800 $\mu g/cm^2$ thick. Two slots were used, one 1.6 mm by 1.25 cm for sources to be studied at 0.1 % resolution and the other 0.8 mm by 1.25 cm for sources to be studied at 0.05 % resolution. For the general survey of the conversion electron spectrum we used a source 1.6 mm by 1.25 cm of initial strength $\approx$ 300 μc and estimated surface density $\approx$ 50 $\mu g/cm^2$.

The conversion electron spectrum was studied in the Chalk River air-cored β-ray spectrometer [8, 9]). The focussed electrons were detected in a continuous flow proportional counter with a 900 $\mu g/cm^2$ Mylar window coated on its inner surface with a conducting film of colloidal graphite (Aquadag) of 100 $\mu g/cm^2$ to prevent charging. This counter, operating at atmospheric pressure, had a plateau from 1900—2500 V with a slope of $\approx$ 0.5 % per 100 V for electrons of energies 30 to 1500 keV. The efficiency of the counter has been assumed to be constant over this range of energies, apart from window absorption corrections for electrons of energy $<$ 90 keV [9]).

A general survey was made of the conversion electron spectrum up to 1500 keV. For this survey the spectrometer was set to give 0.1 % resolution and the current was increased in steps of approximately 0.01 %. In regions where conversion lines were observed or suspected from the survey scan or predicted by the level scheme, the spectrum was studied in greater detail. Short repeated scans were made over these regions to accumulate statistics and to check the reproducibility of the measurements.

During the series of runs the earth's magnetic field was checked periodically. The normal short term fluctuations observed introduce an uncertainty of $\pm$50 gamma in the spectrometer field. This corresponds to an uncertainty in the electron momentum determinations of $\approx$ 1 part in 10^4 for 100 keV electrons and $\approx$ 2 parts in 10^5 for 1 MeV electrons. Other factors affecting the accuracy of momentum determinations are discussed in an earlier paper [9]). In the present experiments the relative accuracy of the electron momenta is estimated to be $\approx$ 1 part in 5000.

The spectrometer was calibrated using a source of Cs^{137}, 1.6 mm wide by 1.25 cm long. The value of the momentum used for the K-661.6 keV line was 3381.08 ± 0.3 gauss · cm [8]. The estimated calibration uncertainty corresponds to a possible error of ≈ 1 part in 5000 in the absolute momentum scale.

The conversion electron spectrum in the energy range 900—970 keV observed in the survey scan is shown in fig. 1. The 962.1 + 965.8 keV doublet suggested by Nathan [5] from his coincidence experiments is clearly resolved. In addition the K conversion line of a transition of 1002.7 keV is seen just below the L_1 962.1

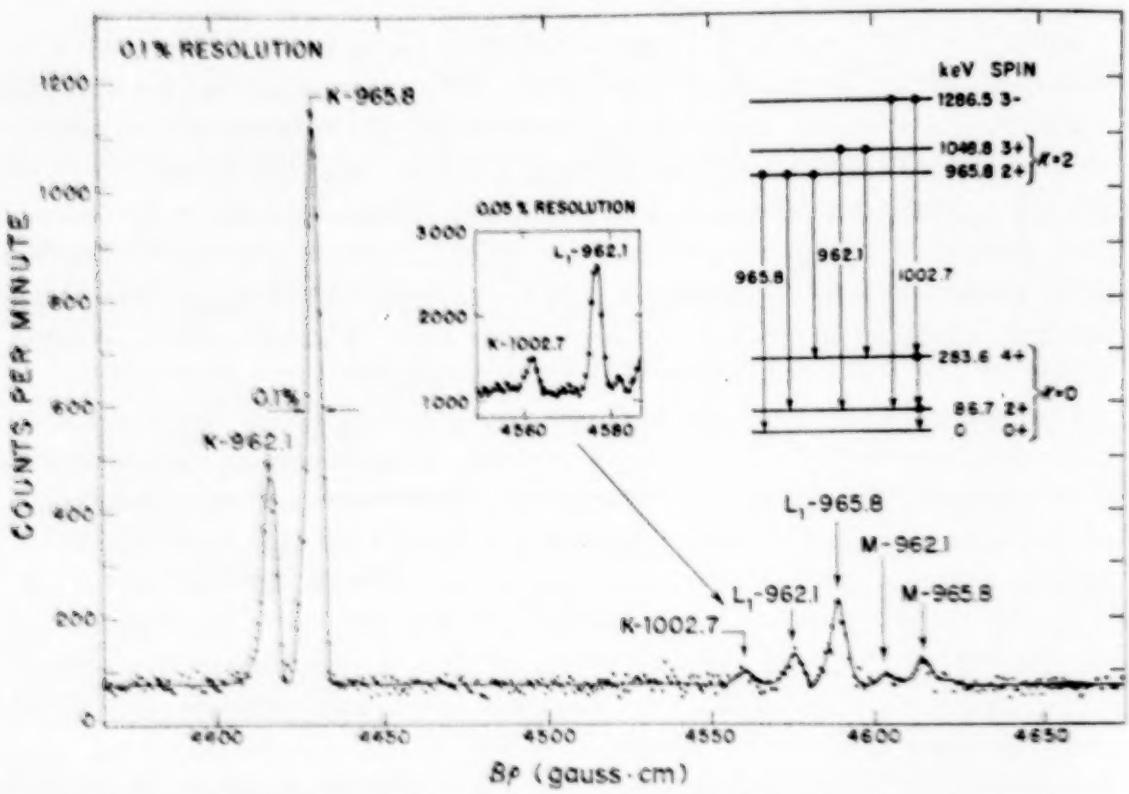

Fig. 1. Conversion electron spectrum of Tb^{160} from 900—970 keV. The 962.1 – 965.8 keV doublet suggested by Nathan is clearly resolved. The K-conversion line of a previously unreported transition of 1002.7 keV is observed. The inset shows a more detailed scan at 0.05 % resolution over the K-1002.7 keV region.

line. The more detailed scan at 0.05 % resolution shown in the inset clearly establishes the existence of this line. This transition has not been reported previously and is confirmed by the results of the coincidence experiments described in section 4.

The results of the study of the conversion electron spectrum are summarized in table 1, giving the energies and intensities of the conversion lines observed. The intensities have been determined from the areas of the lines on an $N/B\rho$ versus $B\rho$ plot and normalized to the total area of the β-ray continuum. The low energy lines have been corrected for the transmission of the 1 mg/cm² Mylar counter window, using the transmission curve given in an earlier paper [9].

TABLE 1

Energies and intensities of Tb^{160} conversion lines

Energy (keV)	Present work		Earlier work					
	Assignment	Intensity [a])	Nathan [b])	Clark		Grigoriev		
32.91	K - 86.7	24 ±3	16.4	20.6	±2	13	±2.4	
40.01	K - 93.8	0.08 ±0.02	0.18					
77.63	L_1 - 86.7	2 ±0.5						
78.09	L_2 - 86.7	15.5 ±0.7	31.2	30.4	±1.5	26	±1.5	
78.88	L_3 - 86.7	15.5 ±0.7						
84.83	M_2 - 86.7	6.5 ±1						
85.38	M_4 - 86.7	0.6 ±0.2						
86.28	N - 86.7	1.5 ±0.2	9.8			7	±0.6	
86.65	O - 86.7	0.4 ±0.15						
91.73	M_1 - 93.8	0.013 ±0.003						
143.18	K - 197.0	0.88 ±0.04	0.90	0.74	±0.04	0.66	±0.03	
161.70	K - 215.5	0.14 ±0.007	0.14	0.14	±0.007	0.11	±0.01	
187.93	L_1 - 197.0	0.095 ±0.01						
188.35	L_2 - 197.0	0.145 ±0.01	0.37	0.32	±0.02	0.18	±0.015	
189.16	L_3 - 197.0	0.11 ±0.01						
195.06	M - 197.0	0.07 ±0.015	0.09					
196.51	N - 197.0	0.018 ±0.004						
206.5	L_1 - 215.5	0.017 ±0.004		0.014	±0.003			
244.7	K - 298.6	0.39 ±0.02	0.42	0.35	±0.02	0.29	±0.015	
255.6	K - 309.4	0.012± 0.0015						
289.5	L_1 - 298.6	0.04 ±0.004						
289.8	L_2 - 298.6	0.008 ±0.002	0.054	0.06	±0.02	0.044	±0.012	
296.4	M - 298.6	0.012 ±0.002						
338.5	K - 392.3	0.011 ±0.0015		≈0.022				
628.4	K - 682.2	0.005 ±0.0015						
711.3	K - 765.3	0.0125±0.001	≈0.011					
825.4	K - 879.2	0.103 ±0.005	0.11	0.094± 0.005		0.09	±0.002	
870.1	L_1 - 879.2	0.016 ±0.001	0.016			0.015	±0.002	
877.2	M - 879.2	0.004 ±0.001				0.003	±0.0006	
908.3	K - 962.1	0.029 ±0.002	0.10	0.091	±0.005	0.079	±0.002	0.025
912.0	K - 965.8	0.072 ±0.004						0.054
948.9	K -1002.7	0.0008±0.00015						
953.1	L_1 - 962.1	0.004 ±0.0004						
956.8	L_1 - 965.8	0.0108±0.001	0.013			0.016	±0.0012	
960.0	M - 962.1	≈0.0012						
963.7	M - 965.8	0.0027±0.0007						
1061.2	K -1115.0	0.0016±0.0001				0.002	±0.0006	
1123.9	K -1177.7	0.012 ±0.0006	0.012	0.0103±0.0008		0.0094	±0.0009	
1146.0	K -1199.8	0.0018±0.0002		0.0012±0.0004		0.0016	±0.0002	
1168.7	L_1 -1177.7	0.0018±0.0004				0.0016	±0.0002	
1217.7	K -1271.5	0.0049±0.0003	≈0.004	0.0052±0.0005		0.0038	±0.0003	
1258.0	K -1311.8	0.0019±0.0001		0.0013±0.0004		0.0021	±0.0003	0.0016
1262.4	L_1 -1271.5	≈0.0008						0.0005

[a]) Intensities are quoted in % per disintegration and were measured relative to the total area of the β-spectrum. The estimated error in the absolute scale is ±10 %.

[b]) Accuracy ≈ 10 %

The conversion electron measurements of Nathan [5]), Clark [6]), and Grigoriev *et al.* [8]) are also given in table 1 for comparison. The higher resolution used in this work, in addition to resolving closely spaced lines, also results in a larger ratio for the conversion line to β-ray continuum counting rates, permitting very weak lines to be observed.

Detailed searches were made for the K-conversion lines of transitions between energy levels in the level scheme of Dy^{160} given in section 6. Upper limits have been placed on the possible intensities of such conversion lines. These upper limits are given in table 2.

TABLE 2

Limits on intensities of K-conversion lines of transitions not observed in present work

From level at	To level at	Transition energy (keV)	Limit on intensity of K-line [a])
1398.5 keV 3−	965.8 keV 2+	432.7	<0.001
	1048.8 keV 3−	349.7	<0.002
	1264.4 keV 2+	134.1	<0.008
	1286.5 keV 3−	112.0	<0.005
1338.2 keV 2+	283.6 keV 4+	1074.6	<0.0005
	1286.5 keV 3−	71.7	<0.005 [b]) (L)
1286.5 keV 3−	0 keV 0+	1286.5	<0.0005
	965.8 keV 2+	320.7	<0.001
	1048.8 keV 3−	237.7	<0.005
1264.4 keV 2+	283.6 keV 4+	980.8	<0.0005
1048.8 keV 3−	965.8 keV 2+	83.0	<0.003
		158.4	<0.005
		1113.2	<0.0002

[a]) In % per disintegration.
[b]) Limit on L—71.7.

3. Gamma-Ray Spectrum

The relative intensities of the gamma-rays were measured in a calibrated 10.2 cm × 10.2 cm NaI(Tl) scintillation spectrometer. The observed γ-ray spectrum is shown in fig. 2. The relative intensities of the gamma-rays were deduced from this spectrum using the known energies of the transitions and the known variation with energy of the pulse height spectrum shape of monoenergetic gamma-rays observed in this NaI spectrometer. The values for the prominent gamma-rays deduced in this manner are listed in table 3, normalized to the value of the intensity of the 879 keV γ-ray given by Nathan. The estimated accuracy of the relative intensity measurements is $\approx \pm 25$ %.

Our values are compared in table 3 with the values given by Clark, Nathan, Grigoriev and Backström [8]). It is seen that for the intense gamma-rays there is good agreement, within the experimental errors, between the different sets of

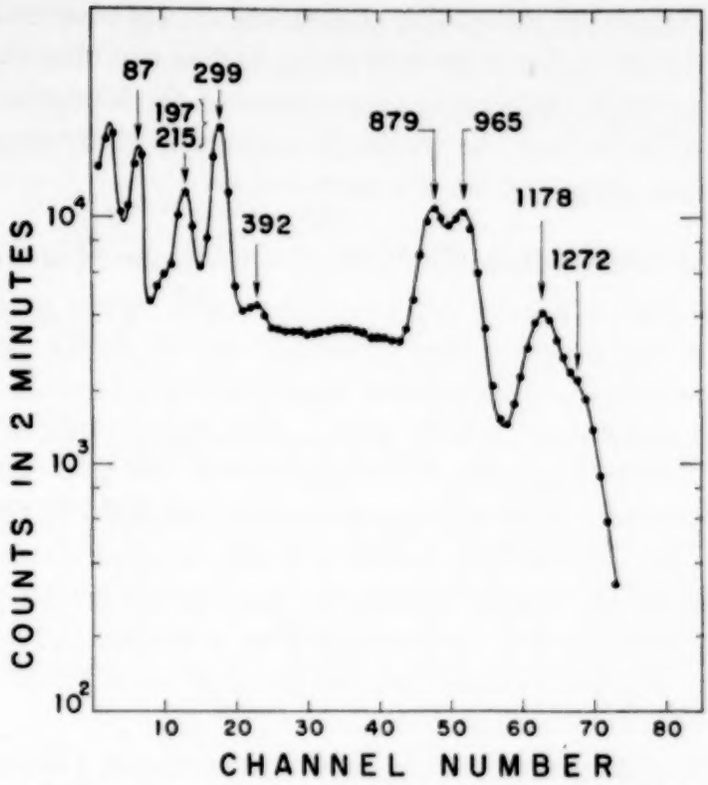

Fig. 2. γ-ray scintillation spectrum of Tb^{160} observed in a 10.2 cm × 10.2 cm NaI(Tl) crystal spectrometer.

TABLE 3
Gamma-ray intensities

γ-ray energy (keV)	Present measurements	Nathan [a])	Clark [b])	Grigoriev [c])	Backström [d])
86.7	15	10.3	13.7		
197.0	8.3	8.1	4.5	4.7	
215.5			3.5	4.0	
298.6	30	30	27	27	
392.3	1.6	2.6	≈1		
682.2					
765.3	≈2		≲2.2		
879.2	33	33	30.6	≡33	33
962.1	36	35	35.8	43	10
965.8					23
1002.7					
1115.0				2.3	1.9
1177.7	17	16	15.6	19	16
1199.8			2.6	2.7	2.9
1271.5	8	7.7	8.5	10.3	
1311.8	2.8		3.4	3.2	2.3

[a]) Estimated accuracy ≈ 30 %.
[b]) Estimated accuracy ≈ 15 %.
[c]) Values normalized to value given by Nathan for γ-879
[d]) Values for γ-962 and γ-966 measured relative to γ-879. Values for the higher energy γ-transitions measured relative to γ-1178.

measurements. Several of the weaker transitions are not observed in the direct NaI spectrum. Some of these have been studied in radiator experiments by Clark, Grigoriev and Backström. We have deduced the intensities of several of the weaker transitions from the results of conversion-electron gamma coincidence experiments described in the next section.

4. Gamma-Conversion Electron Coincidence Measurements

The design of the $\pi\sqrt{2}$ β-ray spectrometer is such that it is easy to place a NaI scintillation spectrometer directly behind the source for electron-gamma coincidence experiments. In the present experiments a 5.1 cm $\times$ 5.1 cm NaI (Tl) crystal optically coupled to an RCA 6342 photomultiplier tube was used as the gamma spectrometer. The tube was magnetically shielded with mu-metal. This slightly distorts the field of the spectrometer but at 0.1 % resolution has a negligible effect on the resolving power and only a small effect ($\approx$ 1 part in 800) on the calibration. The beta-detector used for the coincidence measurements was a stilbene crystal, also mounted on a magnetically shielded 6342 photomultiplier. The pulses from the two counters were fed into a fast-slow coincidence circuit of resolving time $\approx 3\times10^{-8}$ sec.

The source strength used in these experiments was $\approx$ 100 μc. In order to reduce the counting rate in the gamma counter, 1.15 cm of lead were placed in front of the crystal to absorb the low energy gamma-rays. The spectrometer was automatically cycled on and off a conversion line and the coincident gamma-ray spectrum in the energy range 500 to 1400 keV was recorded on a 100-channel pulse height analyzer. The cycling procedure was used to determine the gamma-ray spectrum coincident with the β-ray continuum under the conversion line. The observed coincidence spectrum was corrected for this contribution and for random coincidences.

The net γ-ray spectra coincident with the L_2-86.7, K-197, K-216, and K-299 keV conversion lines are shown in fig. 3, together with the direct γ-ray spectrum. The resolution in the direct spectrum is not as good as that observed in the carefully collimated arrangement used to determine the γ-ray intensities. The variation with energy of the pulse height spectrum due to monoenergetic γ-rays in this arrangement was determined by replacing the Tb^{160} source with sources of Cs^{137} and Na^{22} of approximately the same strength as the Tb^{160} source. Standard peak shapes were deduced from these results for analysis of the coincidence γ-ray spectra.

The γ-ray spectrum coincident with the L_2-86.7 keV conversion line is shown in fig. 3(b). Coincidences are observed with the gamma transitions of 1271, 1178, 962, and 879 keV. A detailed analysis of the coincidence γ-ray spectrum using the standard shapes also shows that there are coincidences with the 1312 and 765 keV transitions. The relative intensities of the transitions deduced from this spectrum are given in column 2, table 4. The values are normalized

to the intensity of the 879 keV transitions observed in the direct spectrum. The values are corrected for absorption in the 1.15 cm of lead in front of the crystal. They are not corrected for possible conversion-electron-gamma-ray angular correlation effects which are discussed below.

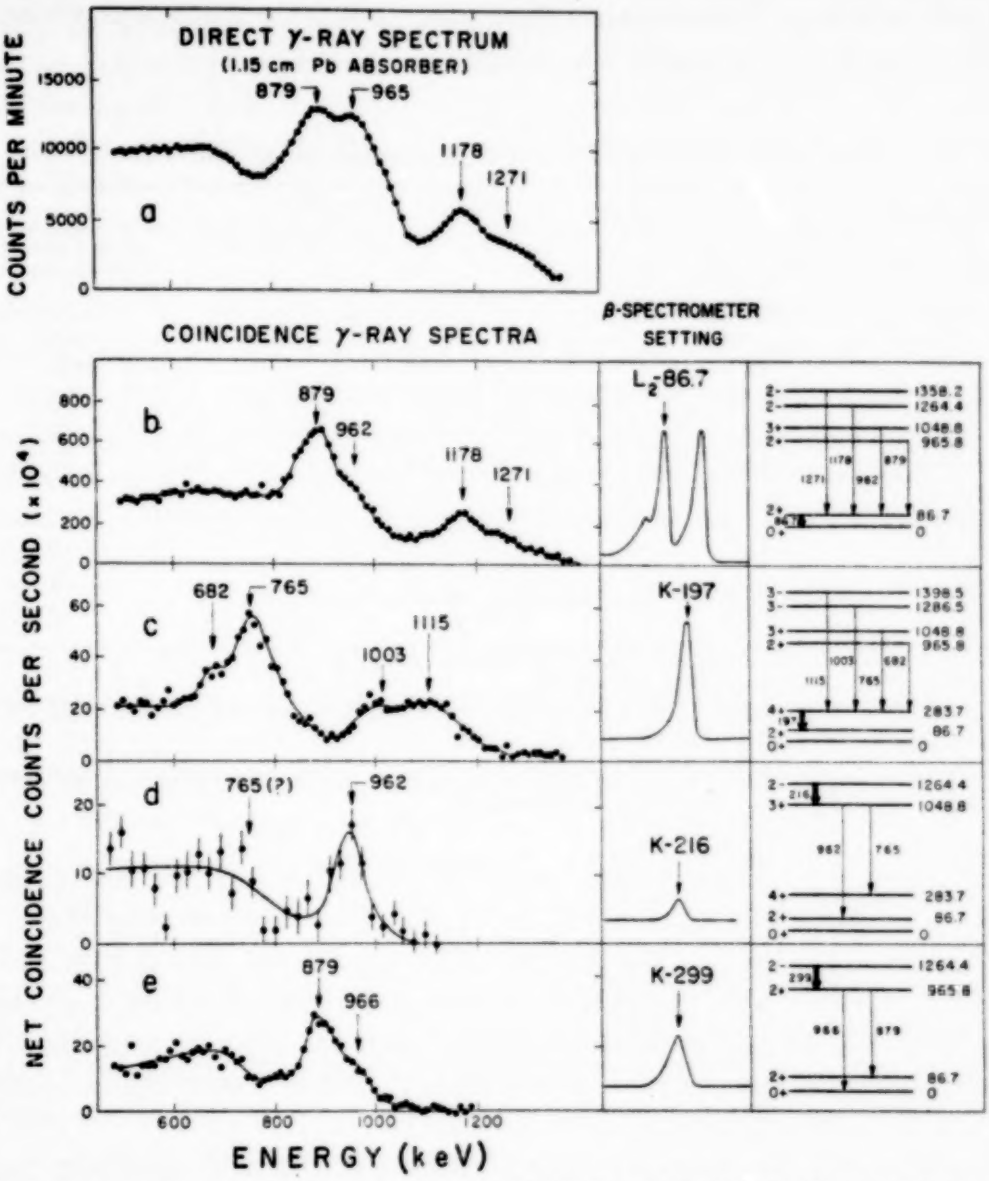

Fig. 3. γ-ray spectra in coincidence with each of the $L_2-86.7$, K-197, K-216, and the K-299 conversion lines. The spectra are the difference between those observed with the spectrometer set on the peak of the line and off the high energy edge of the line. The portion of the conversion line spectrum used is shown to the right of each coincidence spectrum. The interpretation of each spectrum is indicated at the extreme right.

The gamma-ray spectrum coincident with the K-197 keV conversion line is shown in fig. 3(c). The broad peak in the 1000—1100 keV region has been fitted by two gamma-rays of energies 1115 keV and 1003 keV with an intensity ratio of 3 : 2. These are the only transitions in this region which were observed in our study of the conversion electron spectrum. There is also a strong coinci-

dence peak at 765 keV and a weaker poorly resolved peak at 682 keV. The relative intensities of these transitions deduced from the coincidence spectrum are also listed in column 2, table 4, normalized to the value of the intensity of the 879 keV transition observed in the coincidence spectrum with the L_2-86.7 keV conversion line. This normalization can be made as the source was not moved during these two coincidence experiments.

TABLE 4

Gamma-ray intensities deduced from coincidence measurements

γ-transition (keV)	Relative intensities		
	Observed	Corrected for angular correlation [a])	Direct spectrum
682.2	≈0.9	≈0.8	
765.3	2.5	2.5	≈2
879.2	33	33	≡33
962.1	13 8 [b])	7 [c])	11
965.8	16	23	25
1002.7	≈1	≈1	
1115.0	1.5	1.7	
1177.7	16		17
1271.5	7		8
1311.8	≈2.5		2.8

[a]) See text for discussion of this correction.

[b]) Value of 13 deduced from γ-L_2-86.7 coincidence experiment. Value of 8 deduced from γ-K-216 coincidence experiment.

[c]) Value deduced assuming γ-962. 1 is pure E2. If ≈ 10 % M1 admixture is assumed, agreement is obtained with the direct spectrum measurement.

The gamma-ray spectrum coincident with the K-216 keV conversion line is shown in fig. 3(d). The spectrum is not statistically very accurate due to the low intensity of the line and the large contribution of β—γ coincidences. Coincidences are observed with the 962 keV transition. From the level scheme proposed in section 6, we also expect coincidences with the 765 keV transition. The predicted intensity is ≈ 25 % the intensity of the 962 keV coincidence counting rate. Our present experiment does not rule out such a peak.

The gamma-ray spectrum coincident with the K-299 keV conversion line is shown in fig. 3(e). Coincidences are observed with the transitions of 879 keV and 966 keV. The relative intensities of these peaks are also given in column 2, table 4, normalized to the intensity of the 879 keV transition.

The intensities of the gamma-rays deduced from these coincidence experiments are affected by angular correlation between the conversion electron and the gamma-ray. We have estimated these effects in the following manner. Biedenharn and Rose [12]) list correction factors to be applied when the angular correlation is with a K-conversion line instead of the gamma-ray. Using this correction factor, and the solid angle of the counters, we have deduced the

predicted correlation effects in our experiments from the observed gamma-gamma correlations by other workers [10, 11]). In cases where gamma-gamma measurements had not been done the correction has been made assuming that the gamma-transitions involved have pure multipolarities. As no correction factors are available for the L_2 conversion process we have been unable to correct the values of intensities deduced from the gamma-ray spectrum coincident with the L_2-86.7 keV conversion line. The relative intensities when corrected for angular correlation effects are given in column 3, table 4. With the exception of the K-299-γ-966 angular correlation the corrections are not large compared to the estimated experimental accuracy of $\approx \pm 20$ %. The values of the gamma-ray intensities deduced from the direct spectrum are given in column 4 for comparison. Within the experimental accuracy the agreement is good with the possible exception of the intensity of the 962 keV transition. The value given in column 3 was obtained assuming the transition was pure E2 in character. If $\approx$ 10 % M1 admixture is assumed in deducing the effect of angular correlation good agreement is obtained with the direct spectrum measurement. As the transition is from a 3+ level to a 2+ level such an admixture is quite possible.

5. Properties of Gamma-Transitions

The properties of the gamma-transitions are summarized in table 5. The conversion electron intensities given previously in table 1 are listed in columns 2—5. The gamma-ray quantum intensities are listed in column 6. The K-conversion coefficients are compared with the theoretical values [13]) for E1, E2 and M1 in columns 7—10 and the multipolarities assigned to the transitions are given in column 11. For transitions above 300 keV, the multipolarity assignments are based on the observed conversion coefficients. Below 300 keV the L sub-shell conversion line ratio was used in addition to the conversion coefficient to distinguish between M1 and E2 radiations. The multipolarity assignments given in column 11 are the dominant multipolarities. The limits of error in the experimental K conversion coefficients admit the possibility of some M1 admixture in the E2 transitions, and very small amounts (less than 5 %) of M2 admixture in the E1 transitions.

6. Level Scheme of Dy^{160}

The level scheme of Dy^{160} deduced from the results of the present experiments is shown in fig. 4. This scheme is based primarily on energy sum and intensity considerations. The validity of conclusions reached by energy sum considerations is greatly increased by the high precision of the energy measurements, but even so, accidental numerical coincidences can occur. The energy sum method is very powerful however in eliminating alternatives in the placing of gamma-transitions. To establish the level scheme, conclusions reached by this

TABLE 5

Properties of transitions observed in Tb^{199} [a])

γ-ray (keV)	K	L_1	L_2	L_3	I_γ [b])	α_K (Expt.)	α_K (Theoretical) [c])			Assigned [d]) multipolarity
							E1	E2	M1	
86.7	24	2	15.5	15.5	15	1.6(−0)	3.7(−1)	1.6(−0)	2.9(−0)	E2
93.8	0.08		ΣL = 0.05 [e])							M1+E2
197.0	0.88	0.095	0.145	0.11	4.7	1.9(−1)	4.3(−2)	1.8(−1)	2.9(−1)	E2
215.5	0.14	0.017			3.7	3.8(−2)	3.4(−2)	1.4(−1)	2.4(−1)	E1
298.6	0.39	0.040	0.008		30	1.3(−2)	1.5(−2)	4.9(−2)	9.4(−2)	E1
309.4	0.012						1.3(−2)	4.4(−2)	8.5(−2)	
392.3	0.011				1.6	6.9(−3)	7.5(−3)	2.3(−2)	4.4(−2)	E1
682.2	0.005				≈0.8	≈6 (−3)	2.2(−3)	5.9(−3)	1.2(−2)	E2
765.3	0.0125				2.5	5.0(−3)	1.8(−3)	4.5(−3)	8.6(−3)	E2
879.2	0.103	0.016			33	3.1(−3)	1.3(−3)	3.3(−3)	6.2(−3)	E2
962.1	0.029	0.004			36 {11	2.6(−3)	1.1(−3)	2.7(−3)	4.9(−3)	E2
965.8	0.072	0.0108			36 {25	2.9(−3)	1.1(−3)	2.7(−3)	4.9(−3)	E2
1002.7	0.0008				≈1	≈8 (−4)	1.0(−3)	2.5(−3)	4.6(−3)	E1
1115.0	0.0016				1.7	9.4(−4)	8.6(−4)	2.0(−3)	3.4(−3)	E1
1177.7	0.012	0.0018			17	7.1(−4)	7.8(−4)	1.8(−3)	3.0(−3)	E1
1199.8	0.0018				2.5	7.2(−4)	7.6(−4)	1.7(−3)	2.8(−3)	E1
1271.5	0.0049	≈0.0008			8	6.1(−4)	6.8(−4)	1.6(−3)	2.5(−3)	E1
1311.8	0.0019				2.8	6.8(−4)	6.5(−4)	1.5(−3)	2.3(−3)	E1

[a]) All intensities given in % per disintegration.
[b]) Estimated accruacy ≈25 %.
[c]) Values interpolated from tables of Sliv and Band.
[d]) Dominant multipolarities are given.
[e]) Deduced from M-93.8 intensities assuming L/M ≈4.

technique should be tested by gamma-gamma and/or gamma-conversion electron coincidence experiments. The gamma-conversion electron coincidence experiments discussed in section 3 confirm the proposed scheme. It is also consistent with gamma-gamma coincidence experiments reported by other workers [5, 10]).

The positive parity levels at 0(0+), 86.7(2+), 283.6(4+), 965.8(2+) and 1048.8(3+) keV based on the present work correspond to levels proposed by

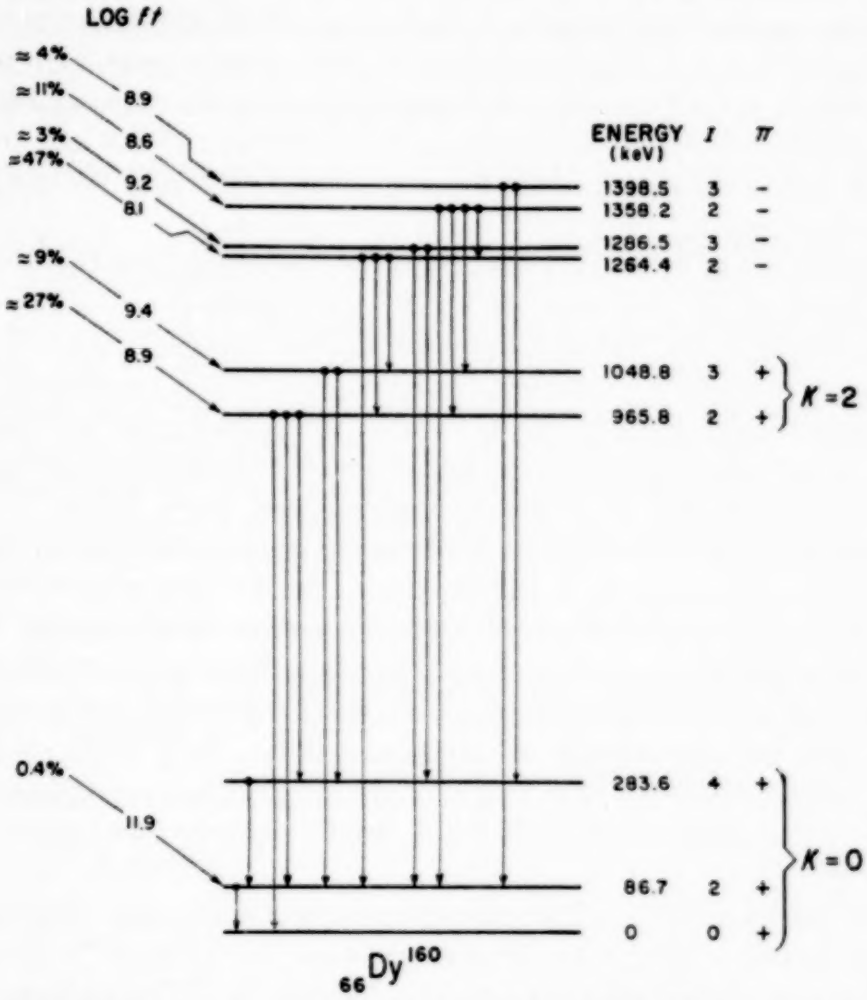

Fig. 4. Level scheme of Dy^{160} observed in study of the β-decay of Tb^{160}. The approximate feeds and log *ft* values for the high energy levels are deduced from the transition intensities. The feed to the 86.7 keV level is that given by Nathan [5]).

earlier workers. We shall consider in more detail the negative parity levels, some of which are different in our scheme from those proposed by Nathan [5]), Backström [6]) and Grigoriev [6]).

Level at 1264.4 keV, 2−: E1 transitions are observed from this level to the 965.8 keV level (2+) and 1048.8 keV level (3+). This establishes the spin as either 2− or 3−. Angular correlation measurements by other workers [10, 11]) indicate a spin of 2−.

Level at 1286.5 keV, 3−: This level is based on the observation of E1 transitions of 1002.7 keV and 1199.8 keV. The conversion electron-gamma coincidence experiments show that the 1002.7 keV transition feeds the 4+ level at 283.6 keV. The 1199.8 keV transition is interpreted as coming from the 1286.5 keV level to the 2+ level at 86.7 keV. The energy difference between these two transitions 197.1±0.3 keV is in good agreement with the observed gamma transition of 197.0±0.1 keV between the 4+ and 2+ levels.

This level has not been suggested previously. The 1199.8 keV transition was interpreted as from a 1− level at 1200 keV to the ground state, with the 1115.0 keV transition going from this proposed level to the 2+ state at 86.7 keV [6]). Our observed energy difference between the 1199.8 and 1115.0 keV transitions is 84.8±0.3 keV: the energy of the 2+ state is 86.7±0.1 keV. We can therefore rule out this interpretation for these two transitions.

Level at 1358.2 keV, 2−: E1 transitions are observed from this level to the two 2+ levels at 86.7 keV and 965.8 keV. A transition is also observed to the 3+ level at 1048.8 keV. As this competes with the E1 transitions it will probably be E1 rather than M2 in character. The spin of the level is therefore 2− or 3−. No transition is observed to the 4+ state. This favours the 2− assignment. This 2− assignment was suggested by Shirley [14]) to explain the angular distribution of gamma-rays he observed from aligned Tb^{160} nuclei.

The earlier assignment of 3− to this level was based on the angular correlation measurements of a γ-ray of $\approx$ 1080 keV with the 197 keV γ-ray [5, 10, 11]) which indicated a spin sequence 3—4—2. Our new results show that the 1080 keV peak in the scintillation spectrum is not a single peak but is a doublet containing both the 1003 and 1115 keV quanta. Both these transitions are in coincidence with the 197 keV gamma-ray on our level scheme. They originate from 3− levels at 1286.5 keV and 1398.5 keV. Thus the angular correlation measurements do not pertain to the 1358.2 keV level assignment and there is no inconsistency.

Level at 1398.5 keV, 3−: The coincidence experiments show that the 1115.0 keV E1 transition feeds the 4+ level at 283.6 eV. The 1311.8 keV E1 transition is now interpreted as feeding the 2+ level at 86.7 keV. This conclusion is in good agreement with the observed energy difference of 196.8±0.3 keV (4+ → 2+ energy separation is 197.0±0.1 keV).

7. Discussion of Relative Transition Probabilities

In this section we compare the relative quantum transition probabilities between levels in Dy^{160} with the theoretical predictions of the Unified Model and of the Davydov and Filippov [15]) model. These comparisons involve several of the weaker transitions whose qantum intensities could not be estimated accurately from the coincidence gamma-ray spectra. For the purposes of this

section, we have, instead, used quantum intensities † deduced from the conversion electron measurements using Sliv's theoretical K-conversion coefficients[13]). It was assumed that all transitions have a pure multipolarity as indicated in table 5. The quantum intensities obtained in this way are believed to be more reliable than those estimated from the coincidence gamma-ray spectra. For consistency the same procedure has also been used for the more intense transitions. Although these values are more precise than those from the gamma-ray quantum measurements, it should be borne in mind that the transition multipolarities may not be pure. The possibility of admixtures would, in some cases, affect the deduced transition probabilities significantly.

7.1. TRANSITIONS FROM POSITIVE PARITY LEVELS AT 965.8 keV (2+) AND 1048.8 keV (3+)

The 965.8 keV 2+ level decays by E2 transitions to the 0+, 2+, and 4+ members of the ground state ($K = 0$) band, and the 1048.8 keV 3+ level to the 2+ and 4+ members of the ground state band. The transition between the 1048.8 keV and 965.8 keV levels was not observed in our experiments.

The reduced E2 transition probability ratios for transitions from these levels are given in column 2, of table 6. Nathan interpreted the levels as members of a gamma-vibrational band with $K = 2$. The theoretical ratios for this interpretation are given in column 3 of table 6. These are only in qualitative agreement

TABLE 6

Reduced E2 transition probabilities from positive parity levels

Reduced E2 transition probabilities	Experimental	Unified model		Asymmetric rotor theory	
		Pure $K = 2$	$K = 2$ with $K = 0$ admixture ($Z = 0.055$) [a])	$\gamma = 11.2°$ [a])	$\gamma = 11.9°$ [b])
$\frac{2+ \to 0+}{2+ \to 2+}$	0.53±0.05	0.7	0.51	0.51	0.48
$\frac{2+ \to 2+}{2+ \to 4+}$	10.5 ±3	20	11.1	11.2	10
$\frac{3+ \to 4+}{3+ \to 2+}$	0.81±0.08	0.4	0.79	0.80	0.9
$\frac{3+ \to 2+ (K = 2)}{3+ \to 2+ (K = 0)}$	<30			28	25

[a]) Parameters chosen to give best fit.
[b]) The value $\gamma = 11.9°$ is deduced from the energy spacing $E'_2/E_2 = 11.1$.

with the experimental ratios. Quantitative agreement can be obtained by considering the effect of interaction between the dominantly $K = 2$ gamma-

† These intensities result from a detailed analysis of the experimental data and in some instances differ slightly from those given in the preliminary report [7]).

vibrational band and the ground state $K = 0$ band. The effect of such an interaction on the properties of levels in Gd^{156} was recently discussed in a paper by Gregers Hansen *et al.* [3]). The calculated effect of such a band mixing on the E2 transition probabilities is summarized in their paper in the form of a table due to Mottelson. We are indebted to Dr. M. A. Preston for independently deriving the modified $B(E2)$ expression from the rotation-vibration interaction of the form originally given by Bohr and Mottelson [16]). The band mixing effect is expressed in terms of a parameter

$$Z = A\left[\frac{B(E2; K = 0, I = 2 \rightarrow K = 0, I = 0)}{B(E2; K = 2, I = 2 \rightarrow K = 0, I = 0)}\right]^{\frac{1}{2}},$$

where A is the amplitude of the admixture between the two 2+ levels. In column 4 of table 6, the theoretical E2 ratios are given for an assumed band mixing parameter $Z = 0.055$. This value of Z gives good agreement with the three experimental Tb^{160} ratios and is close to that of 0.04 used to describe the mixing in Gd^{156}.

The predictions of the asymmetric rotor theory of Davydov and Fillippov are given in columns 5 and 6 of table 6. The value of the asymmetry parameter γ which gives the best fit to the three experimentally observed ratios is $\gamma = 11.2°$. The value $\gamma = 11.9°$, deduced from the energy spacing $E'_2/E_2 = 11.1$, results in predicted ratios which are also consistent with the experimental ratios within the quoted errors. It is interesting to note that the predictions of the Unified Model with band mixing are very similar to those of the asymmetric rotor theory. For each value of γ up to 16° there is a corresponding value of the band mixing parameter Z, which gives essentially the same E2 transition probability ratios from the 2+ and 3+ levels to the 0+, 2+, and 4+ members of the ground state band.

7.2. TRANSITION PROBABILITIES FROM THE NEGATIVE PARITY LEVELS

7.2.1. 2− *Levels at* 1264.4 keV *and* 1358.2 keV.

The 1264.4 keV level (2−) decays by E1 transitions to the 2+ member of the ground state band and the 2+ and 3+ levels of the $K = 2$ band. The level at 1358.2 keV (2−) also decays by E1 transitions to the 2+ member of the ground state band and to the 2+ and 3+ levels of the $K = 2$ band. The reduced relative E1 transition probability ratios to the 2+ and 3+ members of the $K = 2$ band from these two levels are listed in table 7. The E1 transition from the 1264.4 keV level to the 2+ member of the ground state band is hindered by a factor of ≈ 100 relative to the transition to the 2+ member of the $K = 2$ band. For the transition from the 1358.2 keV level the corresponding hindrance factor for the ground state band transition is ≈ 7.

The experimental transition probability ratios are compared in table 7 with the theoretical values for a $K_1 = 1$ or $K_1 = 2$ assignment to these levels. A

$K_1 = 2$ assignment for the 1264.4 keV level seems preferable to the alternative $K_1 = 1$ but the agreement is not very good. The strong hindrance of the E1 transition from this level to the $K_f = 0$ ground state band also favours a $K_1 = 2$ assignment. For the 1358.2 keV level the agreement is again not very good. However, a $K_1 = 1$ assignment is favoured both by the experimental ratio given in table 7 and by the fact that the transition to the ground state is only slightly hindered.

TABLE 7
Reduced E1 transition probabilities from 2-levels

Reduced E1 transition probabilites	Experimental		Theoretical	
	1264.4 keV level	1358.2 keV level	$K_1 = 1$	$K_1 = 2$
$\frac{2- \to 2+(K=2)}{2- \to 3+(K=2)}$	2.4±0.2	0.8±0.15	0.5	2.0

Since the two 2− levels are close to one another in energy one might expect appreciable interaction between them which could influence the relative E1 transition probabilities. We shall now consider the effect of such an interaction on the theoretical transition probability ratios. Let us designate the two interacting 2− states by a and b, and their wave-functions by ψ_a and ψ_b. If state a is dominantly $K_1 = 2$ and state b is dominantly $K_1 = 1$, then for an amplitude admixture A the wave-functions have the form

$$\psi_a = \psi_2 + A\psi_1, \tag{1a}$$

$$\psi_b = -A\psi_2 + \psi_1. \tag{1b}$$

The change in sign of A is required to make the wave-functions orthogonal.

The E1 transition amplitude from level a to a final state f, with spin I_f and $K_f = 2$ will be

$$D_{fa} = \frac{1}{\sqrt{1+A^2}} [\langle 2120|I_f 2\rangle D_{22} + A\langle 2111|I_f 2\rangle D_{21}],$$

where the Clebsch-Gordan coefficients are numerical factors taking account of changes in spin and K, and D_{22} and D_{21} represent the intrinsic E1 matrix elements for transitions from the $K_1 = 2$ level and from the $K_1 = 1$ level to a $K_f = 2$ level respectively. In our experiments we measure the ratio of the reduced E1 transition probabilities from the 1264 keV 2− level of form (1a) to levels in the $K = 2$ band with $I_f = 2$ and $I_f = 3$. In this analysis we assume levels in the $K = 2$ band are pure. The small admixture of $K = 0$ does not significantly affect this discussion. The theoretical ratio is given by

$$\frac{[B(\mathrm{E1}; 2- \to 2+(K=2))]}{[B(\mathrm{E1}; 2- \to 3+(K=2))]} = \frac{(D_{fa})^2}{(D_{fa})^2} = \left[\frac{\langle 2120|22\rangle D_{22} + A\langle 2111|22\rangle D_{21}}{\langle 2120|32\rangle D_{22} + A\langle 2111|32\rangle D_{21}}\right]^2.$$

For the 1358 keV 2− level of form (1b) the corresponding ratio is

$$\frac{[B(\mathrm{E1};2- \to 2+(K=2))]}{[B(\mathrm{E1};2- \to 3+(K=2))]} = \frac{(D_{\mathrm{fb}})^2}{(D_{\mathrm{fb}})^2} = \left[\frac{-A\langle 2120|22\rangle D_{22} + \langle 2111|22\rangle D_{21}}{-A\langle 2120|32\rangle D_{22} + \langle 2111|32\rangle D_{21}}\right]^2.$$

As only two ratios are measured and there are two independent parameters A and D_{21}/D_{22}, the experimental values can be fitted exactly. From the measured values and the errors quoted in table 7, we deduce that A has a magnitude in the range 0.2—0.6 with D_{21}/D_{22} in the range 0.2—0.06.

In addition to the transitions to the members of the $K = 2$ band, transitions are observed from the 2− levels to the 2+ level of the ground state $K = 0$ band. The transition from the 1264 keV level is hindered by a factor of 105 and that from the 1358 keV level by a factor of 7 relative to the corresponding transitions to the 2+ ($K = 2$) levels. Assuming that the ratio D_{21}/D_{22} has a value in the range deduced above these hindrance factors are also consistent with a value of A in the range 0.4 to 0.5.

7.2.2. 3− *Levels at* 1286.5 keV *and* 1398.5 keV

The 3− level at 1286.5 keV decays by E1 transitions to the 2+ and 4+ levels of the ground state $K = 0$ band. The 320.7 keV transition to the 2+, $K = 2$ level at 965.8 keV was not observed. The upper limit on the intensity of the K conversion line of this transition is given in table 2.

The 3− level at 1398.5 keV also decays by E1 transitions to the 2+ and 4+ levels of the ground state $K = 0$ band. The 432.7 keV transition to the 2+, $K = 2$ level at 965.8 keV was not observed and the upper limit of the intensity of its K conversion line is also given in table 2.

The reduced E1 transition probability ratios to the 2+ and 4+ levels of the ground state band from each of the 3− levels are compared in table 8 with the

TABLE 8

Reduced E1 transition probabilities from 3-levels

Reduced E1 transition probabilities	Experimental		Theoretical	
	1286.5 keV level	1398.5 keV level	$K_1 = 0$	$K_1 = 1$
$\frac{3- \to 2+ (K=0)}{3- \to 4+ (K=0)}$	1.7 ± 0.35	0.96 ± 0.1	0.75	1.33

theoretical ratios for a $K_1 = 0$ or a $K_1 = 1$ assignment to these levels. The experimental ratio for the 1398.5 keV level does not agree well with the theoretical value for either a $K_1 = 0$ or a $K_1 = 1$ assignment. The experimental value for the 1286.5 keV level is not statistically very accurate. It differs by only one standard deviation from the theoretical value for $K_1 = 1$.

A similar type of analysis to that discussed for the 2− levels has been carried out assuming there is interaction between the two 3− levels. We have assumed that the 1286.5 keV level is predominantly $K_1 = 1$ in character while the other is predominantly $K_1 = 0$. As before, since only two parameters are required to describe the interaction and only two ratios have been measured, one can obtain exact agreement. The errors on the experimental ratios given in table 8 allow a large range of values of A and D_{00}/D_{01}. A can lie in the range 0.2—1.2 with $D_{00}/D_{01} \approx 0.03$—0.06.

Throughout this section we have used relative E1 quantum intensities which have been deduced from the conversion line intensities assuming pure E1 multipolarity. The measured E1 conversion coefficients indicate that these transitions have less than 5 % M2 quantum admixture. If we had used the ratios deduced from the less precisely measured quantum intensities, the agreement with the theoretical predictions would not have been appreciably changed.

8. Summary

The conversion electron spectrum of Tb^{160} has been studied in the Chalk River air-cored $\pi\sqrt{2}$ β-ray spectrometer at resolution settings of 0.04 % to 0.1 %. Gamma-conversion electron coincidence experiments have established the positions of the levels in Dy^{160}. The multipolarities of the transitions from these levels have been inferred from a comparison of the experimental K conversion coefficients with the theoretical values calculated by Sliv. Spins and parities are assigned to the levels in Dy^{160} from the multipolarities and branching ratios of the transitions from the levels, together with the angular correlation results of other workers. The proposed level scheme is similar to that of Nathan in the positive parity levels but differs in the negative parity levels.

The relative quantum transition probabilities have been deduced from the conversion line measurements using Sliv's theoretical conversion coefficients. The quantum transition probabilities are compared with the theoretical predictions of the Unified Model. Only qualitative agreement is obtained with the relative E2 transition probabilities from the 2+ and 3+ "gamma-vibrational" levels to the 0+, 2+ and 4+ members of the ground state $K = 0$ band. The agreement is greatly improved if a small amount of $K = 0$ band is assumed mixed in the $K = 2$ gamma-vibrational band. These relative transition probabilities are also in good agreement with the predictions of the asymmetric rotor theory of Davydov and Filippov.

Negative parity levels have been observed at 1264.4 keV (2−), 1286.5 keV (3−), 1358.2 keV (2−), and 1398.5 keV (3−). The E1 transition probability ratios from these levels are not in good agreement with a simple interpretation in which a unique value of the quantum number K is assigned to each level. It has been shown that one can account for the experimental quantum-

intensity ratios by assuming that there is interaction between nearby levels of the same spin and parity, i.e., there is an admixture of the two corresponding K values. The experimental quantum ratios require that the amplitude admixtures in the wave functions of the interacting levels be large ($\approx 20\,\%$ to $50\,\%$). Because of the close energy spacing between levels of the same spin and parity such large admixtures might well be expected. A detailed test of the validity of this interpretation requires more experimental information than is presently available.

It is a pleasure to thank Mrs. J. Merritt and Mr. W. Perry for their assistance in source preparation, and Mr. R. B. Walker for his assistance in spectrometer operation.

We wish to thank Drs. T. D. Newton and M. HcManus for many helpful discussions on theoretical aspects of this work and Dr. M. A. Preston for his detailed examination of the rotation-vibration interaction between the $K = 0$ and $K = 2$ positive parity bands. We are also indebted to Dr. A. Bohr for helpful discussions on the similarities between the predictions of the Unified Model with band mixing and the Davydov-Fillipov asymmetric-rotor model.

We are grateful to Dr. L. G. Elliott for his interest in this work and his review of this manuscript.

References

1) O. Nathan and M. A. Waggoner, Nuclear Physics **2** (1957) 548
2) O. Nathan and S. Hultberg, Nuclear Physics **10** (1959) 118
3) P. Gregers Hansen, O. B. Nielsen and R. K. Sheline, Nuclear Physics **12** (1959) 413
4) G. T. Ewan, R. L. Graham and J. S. Geiger, Bull. Am. Phys. Soc. **4** (1960) 21
5) O. Nathan, Nuclear Physics **4** (1957) 125
6) M. A. Clark, Can. Jour. Phys. **38** (1960) 262
Backström, Lindskog, Bergman, Bashandy and Backlin, Ark. Fysik **15** (1959) 121
E. P. Grigoriev, A. V. Zolotavin and B. Kratsik, Izvest. Akad. Nauk SSSR, Ser. Fiz. **23** (1959) 191
7) G. T. Ewan, R. L. Graham and J. S. Geiger, Proceedings of International Conference on Nuclear Structure, Kingston, 1960 (University of Toronto Press)
8) R. L. Graham, G. T. Ewan and J. S. Geiger, Nuclear Instruments (1960);
Ewan, Graham, Geiger and MacKenzie, Phys. Rev. **116** (1959) 930;
Ewan, Graham, Geiger and MacKenzie, Can. Jour. Phys. **37** (1959) 174
9) J. S. Geiger, R. L. Graham and G. T. Ewan, Nuclear Physics **16** (1960) 1
10) S. Ohr, Nuclear Physics **8** (1958) 331
11) R. C. Arns, R. E. Sund and M. L. Wiedenbeck, Nuclear Physics **11** (1959) 411
12) L. C. Biedenharn and M. E. Rose, Rev. Mod. Phys. **28** (1953) 729
13) L. A. Sliv and I. M. Band, Tables of Internal Conversion Coefficients (Academy of Sciences U.S.S.R. Press, Moscow 1956)
14) D. A. Shirley, University of California Radiation Laboratory Report UCRL-9267 (1960), unpublished
15) A. S. Davydov and G. F. Filippov, Nuclear Physics **8** (1958) 237;
A. S. Davydov and V. S. Rostovsky, Nuclear Physics **12** (1959) 58
16) A. Bohr and B. R. Mottelson, Mat. Fys. Medd. Dan. Vid. Selsk. **27**, No. 16 (1953)

7.A

Nuclear Physics **22** (1961) 629—639; © *North-Holland Publishing Co., Amsterdam*
Not to be reproduced by photoprint or microfilm without written permission from the publisher

ON THE ASYMPTOTIC BEHAVIOUR OF CROSS SECTIONS AT HIGH ENERGIES

V. B. BERESTETSKY and I. Ya. POMERANCHUK

Theoretical and Experimental Physics Institute, Academy of Sciences of the USSR, Moscow, USSR

Received 25 June 1960

Abstract: Processes of transformation of two particles into three or four particles in the high energy region are examined in the pole approximation. In the energy range in which the total elastic scattering cross section is independent of energy, the cross section for transformation of two particles into three does not decrease with increasing energy. The cross section for transformation of two particles into four exhibits a logarithmic growth with the energy. This result leads to the assumption that at very high energies the elastic scattering cross section tends to zero.

1. Introduction

Data available at present on collisions of high energy particles make plausible the assumption that with growing energy the total effective cross section approaches a constant limit. Along with the total cross section the diffraction elastic scattering cross section also approaches a constant limit. As far as various inelastic processes are concerned (production of showers with a given number of particles) it seems natural to assume that the cross section for each of them should approach zero with growing energy since the possible number of produced particles should increase infinitely with increasing energy and the constant total cross section should be divided among an ever growing amount of competing processes.

It may be, however, that this simple picture is not correct. We shall give some approximate calculations of the effective cross sections for inelastic processes. These calculations lead to a very different asymptotic behaviour of the inelastic cross sections. The approximations we make cannot be motivated rigorously and hence the results may not be fully convincing. Nevertheless, they show that at high energies a much more complex situation may exist.

2. The Emission of One Particle

Consider the transformation of two particles into three, $p_1+q_1 \to p_2+q_2+k_2$, the formation of a π-meson (k_2) in the collision between some particle and

nucleon p_2. The amplitude for this process A can be written in the following form:

$$A = g\bar{u}(p_2)\gamma_5 u(p_1)\frac{1}{t-\mu^2}A_1 + A', \quad t = (p_1-p_2)^2. \tag{1}$$

Here the first term is a pole term corresponding to the diagram in fig. 1, A' is the remaining part of the amplitude, g is the nucleon-meson coupling constant

Fig. 1. Diagram of one-particle production.

and A_1 is the scattering amplitude of the π meson by particle q_1 (or a π meson or nucleon).

We shall calculate the cross section for the process under consideration in the case of small momentum transfers (of the order of μ) and retain only the pole term [1]). It seems natural to assume that since A' is determined by the singularities at $t > 4\mu^2$ the neglected terms cannot fully compensate for the contribution of the pole term to the cross section. Thus at small values of t the contribution of the pole term should yield a correct order of magnitude of the cross section. A more strict approach to this problem could consist in investigating the amplitude of the process at large values of the orbital angular momentum $l > p/\mu$ (where p is the momentum of the incident particles in the c.m.s.). In such cases the dominating interaction would seem to be associated with exchange of one meson (which corresponds to the pole term). In other words partial cross sections with large values of l will be determined only by the pole diagram considered by us [2]). It should be stressed that the partial cross sections thus obtained can be expressed in terms of the real elastic scattering cross sections determined by amplitude A_1 and are essentially positive quantities. If one takes the sum of the partial cross sections from $l \approx p/\mu$ to $l = \infty$, one finds that the part of the cross section thus obtained is the same in order of magnitude as that one obtains by calculating the cross section with only the pole term of the amplitude and integrating over t up to $\approx -\mu^2$. It may be noted that our analysis is not identical with the Chew and Low "pole" approach [1]). The pole analysis literally yields a negative value for the cross section and is connected with extrapolation of the cross section to the non-physical region $t = \mu^2$. On the other hand, we do not leave the physical region $t < 0$. However, since we depart from the mass shell of the virtual meson by distance $< 2\mu^2$ and the mass

singularities in the meson Green's function are located at values exceeding $9\mu^2$ it appears that the neglected terms will not affect the order of magnitude of the effect.

Retaining only the first term in (1), we arrive at the following expression for the differential cross section

$$d\sigma = \frac{f^2}{\pi}\,\frac{2M^2}{\mu^2}\,\frac{[s_1^2-2(m^2+\mu^2)s_1+(m^2-\mu^2)^2]^{\frac{1}{2}}}{s^2-2(M^2+m^2)s+(M^2-m^2)^2}\,\sigma_1(s_1)ds_1, \tag{2}$$

where $s=(p_1+q_1)^2$, $s_1=(q_2+k_2)^2$, $t=(p_1-p_2)^2$, $f^2=(g^2/4\pi)(\mu/2M)^2\approx 0.08$, M is the nucleon mass, μ the π-meson mass and σ_1 the cross section for elastic scattering of the meson by particle $q_1(q_1^2=m^2)$.

Small momentum transfer $|t|\lesssim\mu^2$ is possible at high colliding particle energies ($s\gg M^2$) if s_1 lies in the interval

$$M^2<s_1<s\frac{\mu}{M}. \tag{3}$$

Indeed, t can be expressed through s, s_1 and the angle ϑ between p_1 and p_2 in the c.m.s.

$$t=m^2+s_1-(s+s_1-M^2)(s+m^2-M^2)/2s$$
$$+2\cos\vartheta\left[\tfrac{1}{4}s-\tfrac{1}{2}(s_1+M^2)+\frac{1}{4s}(s_1-M^2)^2\right]^{\frac{1}{2}}\left[\tfrac{1}{4}s-\tfrac{1}{2}(M^2+m^2)+\frac{1}{4s}(M^2-m^2)^2\right]^{\frac{1}{2}}. \tag{4}$$

For $s\gg M^2$ the condition of smallness of t ($|t|\leqq\mu^2$) can be fulfilled only for $s_1\ll s$. If, moreover, $s_1\gg M^2$, the foregoing expression for t assumes after expansion into a series the following form:

$$t=-M^2\frac{s_1^2}{s^2}-\tfrac{1}{4}s\vartheta^2, \tag{5}$$

from which (3) can be obtained. Formula (3) defines the region in which our pole approximation can be assumed valid.

If $s_1\gg M^2$ the differential cross section (2) can be written in the form

$$d\sigma=\frac{f^2}{\pi}\frac{2M^2}{\mu^2}\,\sigma_1(s_1)\,\frac{s_1ds_1}{s^2}. \tag{6}$$

Assuming σ_1 constant and integrating over the region defined by inequality (3) we obtain for the cross section of the process under consideration

$$\sigma=\frac{f^2}{\pi}\,\sigma_1. \tag{7}$$

The formula (7) is valid both for the process with π^0-meson and π^+ meson emission.

A similar result was obtained by Chew and Low but their coefficient was larger than that in (5) by the factor M^2/μ^2 (see also ref.[4])). This is due to the fact that they integrated over s_1 to values $\approx s$ which corresponds to momentum transfers $|t| \approx M^2$. In our opinion this extension of the region is in need of additional support since the rejected (nonpolar) terms in the amplitude may play a big role.

We thus see that the cross section for shower production is of the value of order 1 mb; it does not diminish with growth of the energy and comprises a finite fraction of the elastic scattering cross section.

We shall now consider the energy spectrum of the produced π-mesons and their angular distribution. To do this we note that the process of π-meson generation has been reduced by us to elastic π meson scattering. A characteristic feature of elastic scattering at high energies is that most of the events involve small scattering angles to which there correspond momentum transfers $t' = (q_1-q_2)^2$ of the order of or smaller than μ^2:

$$|t'| = |(q_1-q_2)^2| \lesssim \mu^2.$$

On the other hand when (2) is integrated over s_1, large values of s_1 are especially important.

We shall now ascertain the consequences to which the conditions

$$|(q_1-q_2)^2| \lesssim \mu^2, \quad s_1 = (q_2+k_2)^2 \gg m^2 \tag{8}$$

lead. In the laboratory system in which $\mathbf{p}_1 = 0$ we have

$$t' = 2m^2-2q_1q_2 = 2m^2-2(E_1E_2-q_1q_2) \approx -\frac{m^2}{E_1E_2}(E_1-E_2)^2-\theta_{12}^2E_1E_2. \tag{9}$$

In deducing this relation the angle θ_{12} between $\mathbf{q}_1$ and $\mathbf{q}_2$ was considered small; otherwise the condition of smallness of t' would be violated.

From (8) and (9) it follows that

$$\theta_{12}^2E_1E_2 \lesssim \mu^2, \quad \frac{m^2(E_1-E_2)^2}{E_1E_2} \lesssim \mu^2. \tag{10}$$

Due to the smallness of the recoil nucleon energy ($|t| \approx \mu^2$), E_1-E_2 is practically equal to the energy of the produced π meson (ω_2).

The second inequality in (10) therefore goes over to the following:

$$\frac{m^2\omega_2^2}{E_1(E_1-\omega_2)} \lesssim \mu^2. \tag{11}$$

In effect this means that ω_2 is restricted by the following upper limit:

$$\omega_2 < \frac{\mu}{m} E_1.$$

Let us consider now the second condition in (8),

$$s_1 = m^2+\mu^2+2(E_2\omega_2-q_2k_2) \gg m^2. \tag{12}$$

In view of the inequality $|t| = |(p_1-p_2)^2| \lesssim \mu^2$ one finds that in the laboratory system $|\mathbf{p}_2| \lesssim \mu$ (since $(p_{10}-p_{20})^2 \lesssim (\mu^2/2M)^2 \ll \mu^2$). This is the momentum of the intermediate meson. Thus the transverse momentum of the "incident" intermediate meson is of the order or less than μ. In virtue of the properties of elastic scattering the transverse momentum k_2 of the "scattered", that is, produced meson, should be of the same order of magnitude (for details see below). Thus the k_2-meson moves practically in the direction of $\mathbf{q}_1$ if its energy is great compared with μ. Taking this into account we get

$$s_1 = \mu^2+m^2+2[E_2\omega_2-\sqrt{E_2^2-m^2}\,\sqrt{\omega_2^2-\mu^2}(1-\tfrac{1}{2}\theta^2_{k_2q_2})] \approx m^2+\mu^2\frac{E_1}{\omega_1}+E_2\omega_2\theta^2_{k_2q_2}.$$

Here $\theta_{k_2q_2}$ is the angle between $\mathbf{k}_2$ and $\mathbf{q}_2$. Introducing the two-dimensional angles $\theta_{q_1k_2}$ and θ_{12}

$$\mathbf{q}_1\cdot\mathbf{q}_2 = |\mathbf{q}_1||\mathbf{q}_2|(1-\tfrac{1}{2}\theta^2_{12}), \quad \mathbf{k}_2\cdot\mathbf{q}_1 = |\mathbf{k}_2||\mathbf{q}_1|(1-\tfrac{1}{2}\theta^2_{k_2q_1}),$$

we see that due to the first inequality in (10) $\theta_{12} \leqq \mu/\sqrt{E_1E_2} \approx \mu/E_1$, whereas $\theta_{k_2q_1}|\mathbf{k}_2|$ being the transverse momentum of the produced meson satisfies the condition $|\mathbf{k}_2|\theta_{k_2q_2} \lesssim \mu$. The two-dimensional angle-vector $\boldsymbol{\theta}_{k_2q_2}$ can be determined through these angles in the usual fashion

$$\boldsymbol{\theta}_{k_2q_2} = \boldsymbol{\theta}_{k_2q_1}+\boldsymbol{\theta}_{12}.$$

Returning to (10), we rewrite it as follows

$$\begin{gathered} s_1 \approx m^2+\mu^2\frac{E_1}{\omega_2}+E_1\omega_2(\theta^2_{k_2q_1}+\theta^2_{12}+2\boldsymbol{\theta}_{k_2q_1}\boldsymbol{\theta}_{12}), \\ \theta_{k_2q_1} \lesssim \frac{\mu}{\omega_2}, \quad \theta_{12} \lesssim \frac{\mu}{E_1}, \quad \omega_2 < \frac{\mu}{m}E_1. \end{gathered} \tag{12a}$$

The only possibility for s_1 to be large is that $\omega_2 \ll E_1$ since the largest contribution from terms containing the angles is made by $E_1\omega_2\theta^2_{k_2q_1} \lesssim \mu^2E_1/\omega_2$, which in order of magnitude is the same as the term μ^2E_1/ω_2. Thus $s_1 \approx \mu^2E_1/\omega_2$. From here and also from formula (4) we obtain the energy distribution of the produced mesons in the region of a constant cross section ($\sigma(s_1) = \text{const.}$)

$$s_1\,ds_1 \approx \frac{d\omega_2}{\omega_2^3}. \tag{13}$$

Summing up, we arrive at the following conclusions concerning the part of the process under consideration:

1. The transverse momenta of all particles at the end of the process are of the order of μ.

2. The energy of the produced π-meson is small compared with that of the incident particle. The energy distribution is given by formula (13).

It will be noted that if the particle q is a fermion (N, Y) parallel with the graph of fig. 1, one should consider a graph differing from the latter by the exchange of the fermion lines ($q_{1,2} \leftrightarrow p_{1,2}$). Hence there arise two groups of π-mesons with small ($\omega_2 \approx \mu$) and large ($\omega_2 = (\mu/M)E_2$) energies.

A principally possible way for an experimental investigation of the foregoing processes would consist in singling out those cases in which the energy and angular distribution of the produced particles correspond to elastic scattering of the incident particle by a particle possessing a mass of the order of the π-meson mass.

3. The Emission of Two Particles

Consider now the transformation of two particles into four: $p_1+q_1 \to p_2+q_2+k_1+k_2$. Under the same assumptions as those made above in our analysis of the transformation of two particles into three, we can single out a certain part of the cross section which is determined by the pole term of the amplitude. There are two types of "pole" processes. First, there is the "single-jet" process depicted in the diagram in fig. 2. The upper block in this diagram is determined

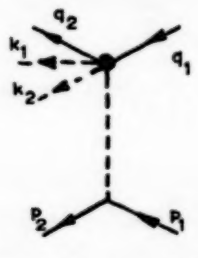

Fig. 2. Diagram of two-particle production ("single-jet").

Fig. 3. Diagram of two-particle production ("two-jet").

by the amplitude for inelastic transformation of two particles into three. Secondly, there is the "two-jet" process represented by the diagram in fig. 3. In the pole approximation the amplitude of the two-jet process has the following form

$$A = \frac{A_1 A_2}{t-\mu^2}, \tag{14}$$

where A_1 and A_2 are the amplitudes for the corresponding elastic scattering

processes. If $t = (p_1-p_2-k_2)^2$ is small ($|t| < \mu^2$) we may consider, as above, that the cross section is defined by amplitude (14). We thus obtain the following expression for the differential cross section of the process

$$d\sigma = \frac{1}{16\pi^3} \frac{[s_1^2-2(m^2+\mu^2)s_1+(m^2-\mu^2)^2]^{\frac{1}{2}}[s_2^2-2(M^2+\mu^2)s_2+(M^2-\mu^2)^2]^{\frac{1}{2}}}{s^2-2(M^2+m^2)s+(M^2-m^2)^2} \times \sigma_1(s_1)\sigma_2(s_2)ds_1 ds_2 \int \frac{dt}{(t-\mu^2)^2}, \tag{15}$$

where $s_1 = (q_2+k_1)^2$ and $s_2 = (p_2+k_2)^2$. As before, we may extend the integration over t to the region $|t| < \mu^2$. In this case the values of s_1 and s_2 must be restricted to the region

$$s_1 s_2 < \mu^2 s. \tag{16}$$

Formula (16) can also easily be deduced in the same way as (3) was. To do this it is sufficient in calculating t to replace p_2 by p_2+k_2, that is, to replace $s_1 \pm M^2$ by $s_1 \pm s_2$ in formula (4). For $s_1 \gg m^2$ and $s_2 \gg M^2$ expression (15) assumes the form

$$d\sigma = \frac{1}{16\pi^3\mu^2} \sigma_1(s_1)\sigma_2(s_2) \frac{s_1 s_2 ds_1 ds_2}{s^2}. \tag{17}$$

Consider now the angular and energy distribution of the produced particles. We shall characterize our process by the following invariants

$$t_1 = (q_1-q_2)^2, \quad s_1 = (k_1+q_2)^2,$$
$$t_2 = (p_1-p_2)^2, \quad s_2 = (k_2+p_2)^2, \quad t = (q_1-q_2-k_1)^2.$$

Due to the properties of the matrix elements A_1 and A_2 we have

$$|t_1| \lesssim \mu^2, \quad |t_2| \lesssim \mu^2.$$

The condition $|t_2| \lesssim \mu^2$ yields (in the coordinate system in which $p_1 = 0$)

$$|t_2| = 2p_1p_2-2M^2 = 2M(\sqrt{M^2+p_2^2}-M) \approx p_2^2 \lesssim \mu^2, |\mathbf{p}_2| \gtrsim \mu. \tag{18}$$

For t_1 we obtain an expression similar to (9)

$$|t_1| \approx m^2 \frac{(E_1-E_2)^2}{E_1E_2} + E_1E_2\theta_{q_1q_2}^2 \lesssim \mu^2, \; E_1E_2\theta_{q_1q_2}^2 \lesssim \mu^2,$$
$$\frac{(E_1-E_2)^2}{E_1E_2} m^2 \approx \frac{(\omega_1+\omega_2)^2m^2}{E_1(E_1-\omega_1-\omega_2)} \lesssim \mu^2, \; \omega_1+\omega_2 < \frac{\mu}{m} E_1. \tag{19}$$

We see that E_2 is close to E_1 and therefore (18) gives for the transverse momentum $\mathbf{q}_{2\perp}$ ($\mathbf{q}_{2\perp}$ is perpendicular to $\mathbf{q}_1$) the following estimate

$$q_{2\perp} \approx E_1\theta_{q_1q_2} \lesssim \mu. \tag{20}$$

The pole approximation we are using imposes the following restriction on t

$$|t| \lesssim \mu^2.$$

Introducing the vector $R = k_1 + q_2$, $R^2 = s_1$ we obtain

$$t = (p_1 - R)^2 = m^2 + s_1 - 2E_1 R_0 + 2\mathbf{q}_1 \mathbf{R}$$
$$= -A^2 - (\sqrt{E_1^2 - m^2} - \sqrt{E_1^2 - s_1})^2 - [\Phi(E_1, E_1) - \Phi(E_1, R_0)], \qquad (21)$$

where

$$A^2 = \sqrt{E_1^2 - m^2}\left[\sqrt{R_0^2 - s_1} - \sqrt{R_0^2 - s_1 - R_\perp^2}\right] > 0,$$
$$\Phi(E_1, R_0) = \sqrt{E_1^2 - m^2}\sqrt{R_0^2 - s_1} - E_1 R_0.$$

The derivative of Φ with respect to R_0 is

$$\frac{\partial \Phi}{\partial R_0} = \frac{R_0}{\sqrt{R_0^2 - s_1}}\sqrt{E_1^2 - m^2} - E_1 = E_1\left[\frac{\sqrt{1 - m^2/E_1^2}}{\sqrt{1 - s_1/R_0^2}} - 1\right] > 0,$$

since $s_1 > m$ and $R_0 < E_1$.

Thus for $R_0 < \Phi$, $\Phi(E_1, E_1)$ is greater than $\Phi(E_1, R_0)$. The signs of all three terms in (21) are therefore the same. From the condition $t \lesssim \mu^2$ we can then determine the restriction on A^2 and therefore also on $R_\perp$:

$$A^2 \lesssim \mu^2, \quad R_\perp^2 \lesssim \mu^2, \quad |\mathbf{k}_{1\perp} + \mathbf{q}_{2\perp}| \lesssim \mu. \qquad (22)$$

Together with (19) this gives

$$|\mathbf{k}_{1\perp}| \approx \omega_1 \theta_{k_1 q_1} \lesssim \mu. \qquad (23)$$

The virtual meson thus possesses a transverse momentum of the order of μ. Finally, it follows from here (on the basis of (18) and (22)) that the transverse momentum of the k_2-meson is also of the order of μ:

$$k_{2\perp} = \omega_2 \theta_{k_2 q_1} \lesssim \mu. \qquad (24)$$

Formulas (20), (23) and (24) give the effective angular region in which the particles are emitted. The transverse momentum of *each* particle is of the order of μ. All particles (except the recoil nucleon p_2) move at small angles with respect to the incident particle. The energy distribution of the produced k_1 and q_2 mesons integrated over their angles is determined by the distribution in s_1 and s_2 (ω_1 and ω_2 being constant)

$$s_1 s_2 ds_1 ds_2. \qquad (25)$$

The relation between s_2 and the frequency ω_2 is

$$s_2 = (p_2 + k_2)^2 = M^2 + \mu^2 + 2\omega_2 \omega_{k_2} - 2\mathbf{p}_2 \mathbf{k}_2.$$

Since according to (18) $|\mathbf{p}_2| \lesssim \mu \ll \mathscr{E}_2 \approx m$ this reduces to the simple form

$$s_2 \approx 2M\omega_2$$

(providing $s_2 \gg M^2$).

In analogy with (12a) $s_1 = (k_1+q_1)^2$ can be expressed as

$$s_1 \approx \mu^2 E_1/\omega_1 \approx \mu^2 s/2m\omega_1.$$

The condition $s_1 s_2 < \mu^2 s$ yields

$$\omega_2 < \omega_1.$$

On the basis of (25) we obtain the energy distribution of the produced mesons

$$\omega_2 \mathrm{d}\omega_2 \frac{\mathrm{d}\omega_1}{\omega_1^3} \quad \left(\mu < \omega_2 < \omega_1, \quad \mu < \omega_1 < \frac{\mu}{m} E_1\right)$$

(the latter condition is a consequence of (16)).

In calculating (17) we did not take into account the exchange diagram (with respect to fig. 3) in which the places of meson lines k_1 and k_2 are changed. The results obtained above show that one may neglect the interference terms which are due to the presence of pole terms corresponding to the diagram in fig. 3 or to the diagram which is an exchange one with respect to it.

Indeed, the quantities s_1 and s_2 which are of the order of $\mu^2 E_1/\omega_1$ and $2m\omega_2$ enter amplitude A which corresponds to the diagram in fig. 3. Correspondingly, s'_1 and s'_2 equal to $\mu^2 E_1/\omega_2$ and $2m\omega_1$ enter the amplitude $A^{(c)}$ corresponding to the exchange diagram. At high energies each elastic scattering matrix element entering A and $A^{(c)}$ is proportional to its parameter s_1 (the amplitude for elastic scattering of π-mesons on nucleons has the form $s_1 f(t_1)$ and $s_2 f(t_2)$, respectively, in the most important diffraction region with $\sigma = \text{const}$). Therefore A is proportional to $s_1 s_2 \approx \omega_2/\omega_1$ and $A^{(c)}$ is proportional to $s'_1 s'_2 \approx \omega_1/\omega_2$. Since $\omega_1 \neq \omega_2$ neglect of the interference terms cannot change the order of magnitude of the cross section.

Let us integrate (17) in the region (16) assuming σ_1 and σ_2 to be constant. This yields, taking into account the exchange diagram and the isotopic states of the outgoing π-mesons, the cross section

$$\sigma = \frac{3}{8} \frac{\mu^2}{\pi^3} \sigma_1 \sigma_2 \ln \frac{s}{M^2}. \tag{26}$$

Formula (26) illustrates the internal inconsistency of the conception that at high energies the total and elastic cross sections are constant. The assumption of a constant elastic scattering cross section and constant total cross section led to a logarithmic growth of the cross section for production of two mesons. The conclusion that the assumption regarding the constancy of the elastic scattering cross section is untenable has independently been drawn by V. N. Gribov [3]) in a different manner.

4. Multiple Particle Production

In a similar way a rough treatment can be made of arbitrary multiple production of particles. The amplitudes of such processes contain pole diagrams of the type shown in fig. 4 in which an arbitrary number of particles are projected

Fig. 4. Diagram of multiple-particle production.

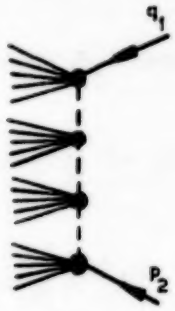

Fig. 5. Diagram of "multi-jet" processes.

from each vertex †. The amplitude

$$A = A_1 A_2/(t-\mu^2),$$

in which A_1 and A_2 are the amplitudes for inelastic processes occurring in the collision between the intermediate meson and particles q_1 and p_1, corresponds to the diagram in fig. 4. Summing the cross sections corresponding to various inelastic processes we obtain the expression

$$d\sigma(s) \approx \sigma(s_1)\sigma(s_2)s_1 s_2 ds_1 ds_2/s^2, \tag{27}$$

where σ is the total cross section. The same internal contradiction as that in (17) is inherent in formula (27). Integration performed under the assumption that the cross section is constant leads to proportionality of the cross section to $\ln s$. It should be noted, however, that formula (27) cannot be regarded as being as definitely established as (17) since, besides the diagrams in fig. 4, a large number of exchange diagrams must be taken into account and it is difficult to assess the corresponding interference terms and calculate the coefficient in formula (27). An analysis of "multi-jet" processes of the type depicted in fig. 5 leads to similar inconsistencies:

$$\sigma \approx (\ln s)^N,$$

where N is the number of "jets".

If one rejects the assumption that the cross section is constant, one can regard (17) and (27) as integral equations which the cross sections $\sigma(s)$ must obey. They are satisfied if the cross section decreases with increasing energy. A very slow decrease (only somewhat faster than $(\ln s)^{-1}$) should be sufficient.

† Such a process at energy 9 GeV was examined by Dremin and Chernavsky [8]).

V. N. Gribov arrived at the same conclusion [3]). It may be mentioned that the showers which arise under these conditions possess a specific distribution in s_1 and s_2, viz. most of them have a mass ($\sqrt{s_1}$ or $\sqrt{s_2}$) which is always small and independent of s whereas the other mass is of the order of s. This type of distribution is very different from that predicted by the Fermi-Landau statistical-thermodynamic theory in which each mass is (on the average) proportional to $s^{\frac{1}{4}}$.

5. Conclusions

It is not exactly clear just what conclusions should be drawn from the results presented above. Possibly they merely signify that the approximation made by us is not valid, i.e. we have been wrong in retaining the pole term and neglecting the others. However, at present we do not see any reasons for believing this to be true. On the other hand if our approximation is reasonable and it may be considered that nuclear interactions at distances exceeding $1/\mu$ decrease exponentially at high energies as well, we are forced to accept the conclusion that the total and elastic cross sections tend to zero with infinite growth of the energy.

Experimental data available at present seem to indicate that the cross sections are constant within a broad energy interval. This result, however, does not contradict the conclusion that the cross sections decrease asymptotically. The point here is that the expressions for the cross section (7) obtained by us contain a small numerical factor. Therefore it may be possible that the effects connected with the processes considered above become noticeable only at ultra-high energies. As mentioned above we were unable to determine the coefficient in (27). The authors must admit that they are surprised at the fact that purely numerical coefficients can lead to the appearance of new asymptotic regions. In order to understand the physics of the drop of the cross sections at high energies it would be extremely desirable to visualize (e.g. by diagrams) the mechanism responsible for this phenomenon, providing, of course, that it exists in reality.

In conclusion we wish to express our appreciation to V. N. Gribov, L. D. Landau, V. N. Melnikov, L. B. Okun and I. M. Shmushkevich for interesting discussions connected with this work.

References

1) G. F. Chew and F. E. Low, Phys. Rev. **113** (1959) 1640
2) L. B. Okun and I. Ya. Pomeranchuk, JETP **36** (1959) 300
3) V. N. Gribov, Nuclear Physics **22** (1961) 249
4) B. Bonsignori and F. Selleri, Nuovo Cim. **15** (1960) 464
5) I. M. Dremin and D. S. Chernavsky, JETP **38** (1960) 229

2.A.1:
2.E

Nuclear Physics **22** (1961) 640—662; © *North-Holland Publishing Co., Amsterdam*
Not to be reproduced by photoprint or microfilm without written permission from the publisher

NEUTRON TOTAL CROSS-SECTIONS IN THE ENERGY RANGE 15 TO 120 MeV

P. H. BOWEN, J. P. SCANLON, G. H. STAFFORD †, J. J. THRESHER †
Atomic Energy Research Establishment, Harwell, Didcot, Berks.
and
P. E. HODGSON
The Clarendon Laboratory, Oxford

Received 3 October 1960

Abstract: A neutron time-of-flight spectrometer has been used to measure the neutron total cross-sections of hydrogen, carbon, aluminium, copper, cadmium, lead and uranium at 64 energies in the range 15 to 120 MeV. The results are compared with previous work in this energy range and are analysed in terms of the optical model of the nucleus.

1. Introduction

The neutron time-of-flight spectrometer which is used in conjunction with the Harwell cyclotron provides a convenient means of doing neutron experiments in the energy range from 15 to 120 MeV. In the experiment to be described here it has been used to make a series of good geometry transmission measurements determining the neutron total cross-sections of hydrogen, carbon, aluminium, copper, cadmium, lead and uranium. Results in 64 overlapping energy bands have been obtained and these have been analysed in terms of the optical model of the nucleus.

A number of measurements have been made by other methods in this energy range, mainly at energies below 20 MeV and above 70 MeV [1]). The only work using a time-of-flight technique is that by Linlor and Ragent at Berkeley [2]) who measured the total cross-sections of carbon and a number of heavy elements between 40 and 200 MeV.

2. Apparatus

The neutron time-of-flight spectrometer has been discussed in detail elsewhere [3]), only a brief description will be given here. The internal proton beam of the Harwell cyclotron is deflected vertically onto a thick aluminium target to produce bursts of neutrons which are separated by 5ms. Each burst has a total duration of 16 ns and a full width at half height of 9 ns. The resolution

† Now at the National Institute for Research in Nuclear Science, Harwell, Didcot, Berks.

available at the end of the 27 m flight-path is thus 0.33 ns/m corresponding to energy resolutions which vary from $3\frac{1}{2}$ % at 15 MeV to $12\frac{1}{2}$ % at 130 MeV. The spectrum of neutrons produced is continuous and extends up to a maximum energy of about 135 MeV.

Fig. 1 illustrates the general arrangement of apparatus used in the experiment. Neutrons from the target in the cyclotron were collimated to provide two beams which diverged at an angle of 1°. The main beam passed through collimators A_1 to A_5 in the concrete shielding walls and entered the counter at the end of the flight-path. This beam was used for the transmission measurements. It was defined by the counter itself which was 4 cm in diameter, and by collimator A_1 which was 1.25 cm². The remaining collimators had dimensions sufficient to clear the beam so defined.

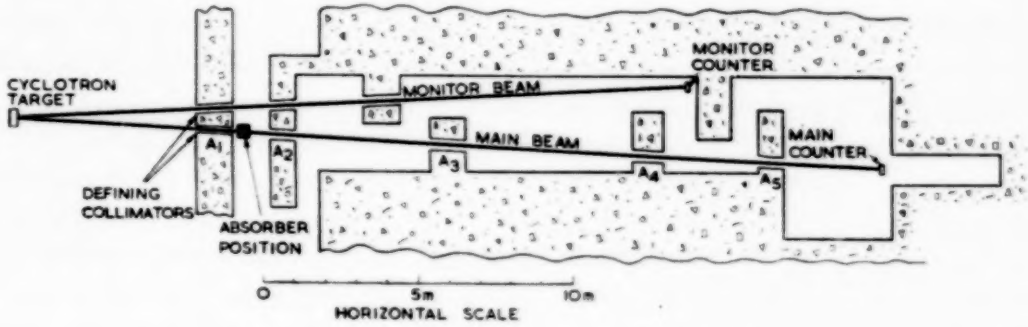

Fig. 1. General arrangement of the apparatus.

The second beam, which was used for monitoring, originated in the same part of the target as the main beam and was defined in much the same way.

Absorbers consisting of carefully machined cylindrical rods of polyethylene, carbon, aluminium, copper, cadmium, lead and uranium were placed immediately behind the first concrete shielding wall and could be moved in and out of the main beam by remote control. They were checked both by ultrasonic methods and by X-ray photography to ensure the absence of blow-holes and other internal flaws, and the length and density of each were measured to better than 0.1 %. The polyethylene absorber was used in a carbon-polyethylene difference measurement to obtain the hydrogen cross-sections and had the same surface density of carbon as the carbon absorber. The other six absorbers all had transmissions of about 0.1 at an energy of 50 MeV.

Fast organic scintillators, 4 cm in diameter and 2 cm thick, viewed by RCA 6342 photomultipliers, were used for both the main and the monitor beam counters. The same arrangement of electronics was used for each counter, so only the details of the main beam electronics, which are shown schematically in fig. 2, will be discussed.

Pulses produced at the collector of the photomultiplier had a rise time of 4 ns

and were of 20 ns duration. They were fed via a 300 MHz distributed amplifier to a pulse height limiter and then to the timesorter input.

The function of the timesorter was to measure the interval between the arrival of a marker pulse related to the time when a neutron burst was produced at the target, and the arrival of a pulse from the counter, produced when a neutron in the burst was detected. This measured time interval was converted into a proportional voltage pulse which was fed into a 100 channel kicksorter. The timesorter sensitivity, which was adjustable, was set to be about 20 ns/volt corresponding to about 5 ns/kicksorter channel. It was calibrated by simulating the marker and counter pulses with test pulses from a pulse generator and then measuring the change in the output pulse height of the timesorter when delays known to better than 0.5 ns were introduced in the line to the distributed amplifier. This calibration procedure was repeated at regular intervals during the experiment to check stability.

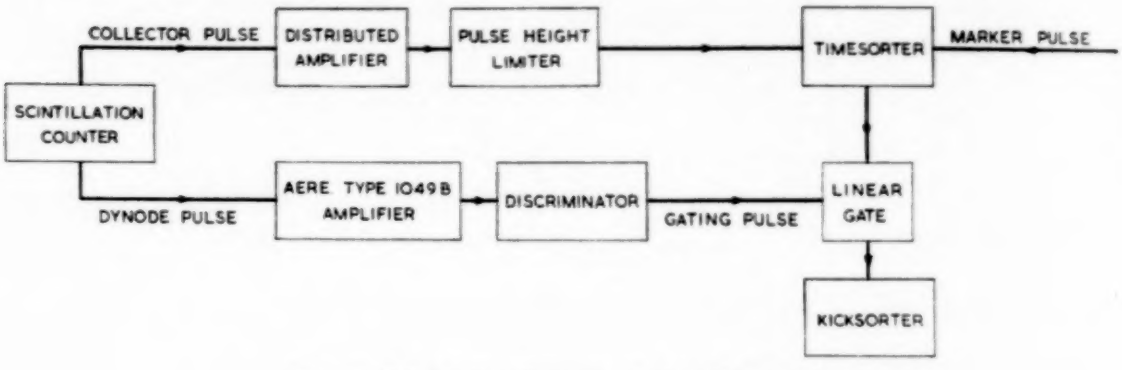

Fig. 2. Schematic diagram of the electronics.

All the pulses analysed had first to fire a trigger circuit [4]) at the timesorter input. It was found that the switching time of this circuit increased appreciably as the amplitude of the input pulse was reduced and for a pulse which just exceeded the triggering threshold it was greater than 30 ns and very badly defined. As a result, timing errors were introduced which depended on the magnitudes of the input pulses. In practice only relative timing errors between pulses were serious, and these were avoided in most cases by using the pulse height limiter to standardise the pulses before they reached the timesorter. There was, nevertheless, an appreciable number of small pulses which could not be standardised in this way and as the triggering threshold had to be set at a level significantly lower than the limited pulse height, many of these pulses fired the trigger circuit and were analysed. Such events contained large timing errors and a linear gating circuit was used at the kicksorter input to reject them. Pulses taken from the last dynode of the photomultiplier were amplified by an A.E.R.E. Type 1049B amplifier and fed into a discriminator whose output was used to open the gate. The bias level of the discriminator was set so that all

pulses which fired it came from events in which the corresponding pulses from the collector of the photomultiplier were fully limited when they reached the timesorter. Thus, the timesorter output was allowed through to the kicksorter only when the errors due to the firing time of the trigger circuit were negligible.

It should be noted that only one event per burst could be analysed by the timesorter, the event being the first to produce a counter pulse large enough to fire the input trigger circuit. Counting losses were therefore introduced and these depended on the ungated counting rate. Accordingly an arrangement was incorporated enabling the gating circuit to be by-passed so that the ungated spectrum could be measured.

3. Experimental Procedure

Only the transmissions of the carbon absorber were measured absolutely, all other transmissions being measured relative to carbon. Thus, apart from the carbon-polyethylene transmission ratios, which represented the transmissions of the hydrogen contained in the polyethylene and so could be used directly to calculate the hydrogen cross-sections, the results of the relative measurements had first to be combined with the measured transmissions of the carbon absorber before any cross-sections could be calculated.

The method of measuring the carbon transmissions was simply to measure, as a function of time-of-flight, the number of neutrons detected per unit monitor count both with the absorber in the beam and with the absorber out of the beam. The measurements covered the whole energy range from 15 to 130 MeV and the transmissions in 64 overlapping energy bands, corresponding to the 64 kicksorter channels covered by the neutron time-of-flight spectrum, were calculated from the results.

Fig. 3 shows the incident and transmitted spectra obtained in this way. The peaks to the left of the neutron spectra are due to γ-rays which were produced in the target at the same time as the neutrons and which were also detected by the counter and analysed. As the time-of-flight of the γ-rays was accurately known, the position of each peak provided a very convenient calibration point on the kicksorter and, knowing the timesorter sensitivity, the time-of-flight corresponding to any chosen pulse height could be obtained. Furthermore, any drifts in the zero of the time scale which occurred during the course of the measurements were indicated immediately by a shift in the position of the peak and corrections for these could be made when necessary.

Errors due to long term drifts in the gains of the main and monitor electronics were minimised by dividing the measurements into a series of 60 short runs made alternately with and without the absorber in the beam, and systematic errors in monitoring were avoided by keeping the operating conditions of the cyclotron and the spectrometer, as far as possible, constant for all the runs. In

order to ensure that the corrections for counting losses could be made reliably, measurements of the ungated spectra were made at frequent intervals and as a further precaution the overall counting rate was limited to a maximum of 25 per sec so that the corrections themselves were small. This meant that the beam

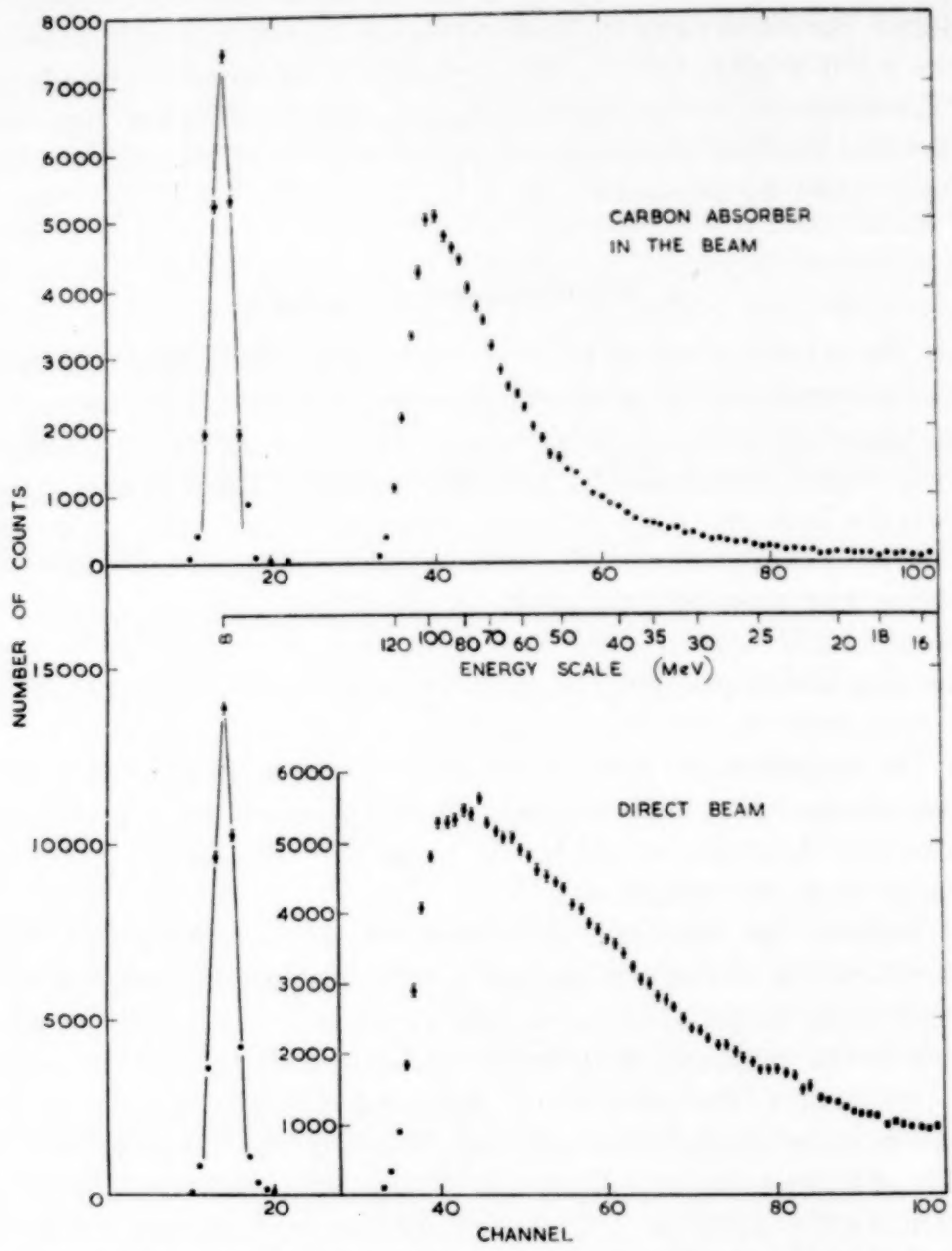

Fig. 3. Incident and transmitted spectra obtained in the measurement of the carbon transmissions.

intensity had to be limited to a level which gave this counting rate for measurements in the direct beam. The counting rate in the transmitted beam was therefore less than 3 per s.

Because of the large difference between the counting rates in the direct and transmitted beams any systematic variations in the performance of the

apparatus with counting rate could have introduced errors into the results. Tests on the timesorter sensitivity and on the gain of the photomultiplier and its associated electronics did not however indicate that any such effects occurred. Furthermore a subsidiary measurement of the carbon transmissions made at three times the normal beam level gave results in excellent agreement with those made at the lower counting rate.

In the carbon-polyethylene comparison there was no need for measurements to be made in the direct beam and although the general procedure was basically the same as that for the measurements on carbon the beam intensity could be increased until the counting rate with the carbon in the beam reached 25 per s. The corresponding counting rate when the polyethylene was in the beam was 15 per s.

The other relative measurements were also made with the beam at this level for it was again unnecessary to measure the direct beam intensity. All counting rates were now in the region of 25 per s and information on each transmitted spectrum was therefore obtained more rapidly than in the case of an absolute measurement. The cross-sections of aluminium, copper, cadmium, lead and uranium which were obtained by combining the results of these relative measurements with the carbon transmissions have statistical errors which are generally somewhat larger than those on the carbon cross-sections since they include the errors on the carbon transmissions, but the results were obtained in about one third of the time needed to obtain the same statistical accuracy directly by absolute transmission measurements.

4. Calculation of the Cross-Sections

The total cross-sections of carbon, aluminium, copper, cadmium, lead and uranium were obtained by calculating the transmissions of the absorbers from the experimental data and then using the relation

$$\sigma = \frac{1}{N} \ln \frac{1}{T},$$

where σ is the total cross-section of the element concerned, N the number of nuclei/cm^2 in the corresponding absorber and T the transmission of the absorber.

The cross-sections of hydrogen were obtained from the ratios of the carbon and polyethylene transmissions by means of the relation

$$2\sigma_H = \frac{1}{N_P}\left[\ln \frac{T_C}{T_P} + \sigma_C(N_C - N_P)\right],$$

where N_C and N_P are the numbers of carbon nuclei/cm^2 in the carbon and polyethylene absorbers respectively. The quantity $(N_C - N_P)/N_P$ was 0 ± 0.001 so that

the second term in the square bracket could be neglected without introducing an appreciable error. The ratio of hydrogen to carbon atoms in the polyethylene was $(2\pm0.002) : 1$.

In calculating the transmissions a number of corrections were made to the data. The most important of these were the corrections for counting losses. They had to be applied to each measured spectrum and were calculated from the relation

$$G'_n = G_n \left(1 - \sum_{k=1}^{n} U_k\right)^{-M/m},$$

where G'_n and G_n are respectively the average corrected and the average observed numbers of counts/burst obtained in channel n of the kicksorter during a gated run, while U_k is the average observed number of counts/burst obtained in channel k during the associated ungated run. M and m represent the average number of monitor counts/burst for the gated and ungated runs respectively. Strictly they should have been corrected for counting losses, but the ratio M/m was sufficiently close to unity for the corrections to be neglected.

Corrections for the effects of pulse pile-up had also to be made. These effects were negligible at the input to the timesorter because of the short duration of the pulses involved but were significant at the input of the discriminator which operated the linear gate. The pulses arriving at this point were about 1 μs long and pile-up was almost certain to occur when the counter produced more than one pulse/burst. This affected the results of the gated runs, for there was a chance that events which should have been rejected by the linear gate had passed through to the kicksorter because the gate discriminator had been fired by a combination of two or more small pulses.

Further corrections of about the same magnitude as those for pile-up were necessary to allow for cases in which a pulse which fired the timesorter but not the gate discriminator was followed in the same burst by one large enough to fire the discriminator. Here the first event was analysed by the timesorter, the output of which, instead of being rejected, was allowed through to the kicksorter by the second event. In practice, this effect and the pile-up effect were treated together. The combined corrections which depended on the difference between the gated and ungated counting rates were always less than 2 % and could be made with negligible error.

The only other corrections that were made to the data were for backgrounds. They were found by measuring the counting rate when 1.25 m of steel was placed immediately in front of collimator A_4 and were significant only in the measurement of the hydrogen cross-sections. In all cases the corrections for plural scattering and for impurities in the absorbers were less than 0.2 % of the final results and were neglected.

The final step in the calculations was to determine the effective energies of

the transmissions measured in each kicksorter channel. Since the spread in flight-times of the neutrons recorded in each channel represented a comparatively small spread in energies, the transmissions within the channel could be taken as varying linearly with energy and the average energy $\bar{E}$ of the neutrons detected in the unattenuated beam gave the energy required.

For any channel in the range of flight-times from about 215 to 525 ns corresponding to neutron energies between 100 and 15 MeV, $\bar{E}$ was with negligible error the nominal value E_n of the channel energy, where E_n for a given channel is defined as the energy of a neutron whose time-of-flight is that represented by the centre of the channel. It was calculated from a knowledge of the timesorter and kicksorter calibrations and the length of the flight-path, using the relativistic relation between the energy and velocity of the neutron.

For channels representing flight-times of less than 215 ns, that is in the region of the initial rise of the neutron time-of-flight spectrum where, as may be seen in fig. 3, the counting rate varied very rapidly from channel to channel, the average energies were significantly lower than the nominal values. This was almost entirely due to the finite time resolution of the spectrometer which caused the distribution of the neutrons counted in these channels to be weighted in favour of long flight-times.

Using the approximation, adequate for this purpose, that the time resolution could be represented by a gaussian curve and the observed initial rise by an integrated gaussian, the true shape of the rise could be obtained analytically. It was then possible to calculate the time distribution, and hence the average energy, of the neutrons counted in each of the relevant channels. The difference between the nominal and average channel energies varied from 2 MeV at 117.5 MeV to 1 MeV at 100 MeV.

5. The Experimental Results

The results of this experiment are presented in table 1 and illustrated in figs. 4 and 5. The errors indicated are the statistical errors in counting only, for other random errors were found to be negligible from the self-consistency of the data in each set of measurements. Systematic errors in the hydrogen cross-sections are believed to be less than ± 2 % and in the other cross-sections, less than ± 1 %.

The energies have been quoted together with limits which specify the full width at half maximum of the corresponding energy distributions which are approximately gaussian in shape. In general the uncertainties in estimating the energies are about ± 2 % and are the result of uncertainties in calibrating the timesorter. In addition, errors may have been introduced in calculating the effects of the time resolution on the initial rise of each of the time-of-flight

TABLE 1

The neutron total cross-sections of hydrogen, carbon, aluminium, copper, cadmium, lead and uranium. The energies are given together with limits which specify the width at half maximum of the corresponding energy distributions

Energy (MeV)	Hydrogen (millibarns)	Carbon (barns)	Aluminium (barns)	Copper (barns)	Cadmium (barns)	Lead (barns)	Uranium (barns)
15.80±0.33	537 ±30	1.46 ±0.032	1.84 ±0.069	2.63±0.115	4.10±0.18	5.81±0.18	5.83±0.24
16.13±0.33	634 ±34	1.48 ±0.032	1.75 ±0.068	2.72±0.110	4.54±0.18	5.50±0.18	6.30±0.23
16.46±0.34	580 ±33	1.45 ±0.032	1.77 ±0.068	2.73±0.080	3.48±0.18	5.89±0.17	6.24±0.24
16.80±0.35	597 ±32	1.45 ±0.031	1.80 ±0.067	2.73±0.078	4.55±0.17	5.77±0.17	6.24±0.23
17.15±0.36	561 ±29	1.47 ±0.031	1.66 ±0.067	2.56±0.075	4.22±0.17	5.76±0.17	6.49±0.24
17.52±0.37	544 ±28	1.39 ±0.031	1.76 ±0.065	2.56±0.075	3.65±0.17	5.75±0.17	5.84±0.22
17.90±0.39	533 ±27	1.52 ±0.030	1.89 ±0.063	2.54±0.074	3.99±0.17	6.11±0.17	6.54±0.25
18.29±0.40	517 ±27	1.47 ±0.030	1.87 ±0.062	2.60±0.072	3.88±0.16	5.96±0.17	6.03±0.22
18.69±0.42	523 ±28	1.48 ±0.030	1.80 ±0.061	2.50±0.072	3.88±0.16	5.72±0.16	6.44±0.22
19.11±0.43	498 ±40	1.45 ±0.029	1.69 ±0.061	2.40±0.071	3.68±0.16	5.77±0.16	6.14±0.22
19.55±0.44	522 ±26	1.48 ±0.045	1.65 ±0.075	2.36±0.100	3.66±0.15	5.68±0.16	6.37±0.26
20.00±0.46	479 ±24	1.45 ±0.028	1.80 ±0.060	2.47±0.068	3.53±0.15	5.81±0.16	6.33±0.22
20.46±0.47	479 ±22	1.50 ±0.028	1.85 ±0.060	2.53±0.068	4.01±0.14	5.87±0.16	6.59±0.21
20.93±0.48	449 ±21	1.46 ±0.027	1.84 ±0.054	2.51±0.067	3.85±0.14	5.74±0.15	6.41±0.20
21.41±0.50	447 ±20	1.41 ±0.025	1.85 ±0.054	2.49±0.066	3.58±0.13	5.76±0.14	6.22±0.19
21.91±0.51	420 ±20	1.42 ±0.025	1.83 ±0.053	2.48±0.064	3.84±0.13	5.84±0.14	6.48±0.18
22.43±0.52	408 ±20	1.396±0.023	1.77 ±0.052	2.42±0.062	3.61±0.13	5.63±0.13	6.37±0.18
22.96±0.54	433 ±19	1.439±0.022	1.84 ±0.051	2.45±0.059	3.46±0.12	5.79±0.13	6.57±0.17
23.51±0.57	397.7±16	1.367±0.022	1.82 ±0.050	2.35±0.056	3.24±0.12	5.69±0.13	6.11±0.17
24.09±0.59	393.0±15	1.375±0.021	1.74 ±0.048	2.47±0.056	3.36±0.12	5.56±0.12	5.83±0.17
24.69±0.61	393.5±14	1.393±0.021	1.88 ±0.048	2.47±0.055	3.50±0.11	5.54±0.12	6.32±0.16
25.31±0.63	362.9±13.5	1.340±0.020	1.78 ±0.047	2.42±0.054	3.25±0.11	5.38±0.12	5.90±0.16
25.94±0.65	377.6±12.7	1.335±0.020	1.82 ±0.044	2.42±0.052	3.25±0.103	5.40±0.11	5.99±0.15
26.60±0.68	345.7±12.3	1.349±0.019	1.87 ±0.043	2.40±0.050	3.38±0.100	5.46±0.11	5.97±0.15
27.29±0.72	335.4±11.5	1.315±0.018	1.84 ±0.043	2.42±0.049	3.21±0.097	5.23±0.11	5.79±0.15
28.03±0.76	321.5±11.0	1.298±0.018	1.88 ±0.042	2.44±0.048	3.22±0.93	5.19±0.103	5.71±0.14
28.80±0.78	312.2±10.5	1.291±0.017	1.88 ±0.042	2.45±0.046	3.23±0.091	5.08±0.099	5.96±0.14
29.59±0.80	309.1±9.5	1.258±0.016	1.79 ±0.039	2.39±0.043	3.05±0.079	4.92±0.092	5.88±0.13
30.40±0.83	281.7±8.8	1.250±0.016	1.82 ±0.039	2.40±0.043	3.08±0.080	4.92±0.092	5.88±0.13

28.03±0.76	321.5±11.0	1.298±0.018	1.88 ±0.042	2.44±0.048	3.22±0.93	5.19±0.103	5.71±0.14
28.80±0.78	312.2±10.5	1.291±0.017	1.88 ±0.042	2.45±0.046	3.23±0.091	5.08±0.099	5.96±0.14
29.59±0.80	309.1± 9.5	1.258±0.016	1.79 ±0.039	2.39±0.043	3.08±0.086	4.92±0.092	5.86±0.13
30.40±0.83	281.7± 8.8	1.250±0.016	1.82 ±0.039	2.40±0.043	3.08±0.086	4.92±0.092	5.86±0.13
31.24±0.86	286.4± 8.3	1.237±0.015	1.90 ±0.038	2.53±0.043	3.17±0.083	4.82±0.087	5.71±0.12
32.12±0.90	288.7± 7.4	1.220±0.015	1.81 ±0.037	2.44±0.043	3.08±0.080	4.78±0.085	5.46±0.12
33.05±0.96	276.0± 6.8	1.231±0.014	1.79 ±0.034	2.46±0.040	2.98±0.077	4.70±0.083	5.51±0.12
34.03±1.01	260.1± 7.2	1.203±0.020	1.80 ±0.040	2.45±0.056	3.11±0.095	4.63±0.110	5.48±0.13
35.08±1.07	245.8± 6.7	1.180±0.014	1.82 ±0.033	2.55±0.038	3.07±0.073	4.61±0.077	5.20±0.11
36.20±1.12	220.0± 9.9	1.191±0.013	1.88 ±0.032	2.58±0.037	3.19±0.071	4.71±0.075	5.26±0.104
37.32±1.15	226.8± 6.3	1.143±0.013	1.80 ±0.031	2.60±0.036	3.18±0.070	4.49±0.073	5.10±0.101
38.48±1.21	223.5± 6.0	1.123±0.012	1.83 ±0.030	2.52±0.036	3.10±0.068	4.40±0.068	4.88±0.096
39.75±1.29	219.1± 5.7	1.096±0.012	1.79 ±0.029	2.64±0.036	3.35±0.065	4.34±0.065	4.90±0.090
41.10±1.38	204.6± 5.4	1.081±0.011	1.81 ±0.027	2.66±0.035	3.19±0.062	4.36±0.062	5.01±0.088
42.53±1.45	196.0± 5.2	1.068±0.011	1.78 ±0.026	2.65±0.035	3.23±0.060	4.34±0.060	4.84±0.083
44.00±1.50	189.1± 4.9	1.052±0.011	1.77 ±0.026	2.69±0.035	3.42±0.058	4.29±0.058	4.82±0.082
45.50±1.60	187.3± 4.6	1.012±0.010	1.77 ±0.025	2.73±0.035	3.36±0.057	4.36±0.056	4.79±0.079
47.10±1.70	170.3± 4.0	0.967±0.009	1.69 ±0.025	2.64±0.035	3.30±0.054	4.13±0.054	4.65±0.074
48.80±1.80	166.8± 4.1	0.969±0.009	1.69 ±0.024	2.68±0.035	3.37±0.053	4.29±0.052	4.76±0.073
50.60±1.90	152.0± 3.8	0.930±0.009	1.68 ±0.023	2.77±0.033	3.40±0.051	4.29±0.050	4.82±0.069
52.5 ±2.0	152.0± 3.6	0.912±0.009	1.63 ±0.021	2.74±0.031	3.39±0.049	4.30±0.050	4.68±0.068
54.5 ±2.1	144.8± 3.3	0.878±0.009	1.62 ±0.019	2.72±0.031	3.45±0.048	4.41±0.048	4.78±0.065
56.6 ±2.2	141.5± 3.1	0.844±0.008	1.53 ±0.019	2.69±0.030	3.44±0.047	4.39±0.046	4.68±0.063
58.8 ±2.3	135.8± 2.9	0.808±0.008	1.50 ±0.018	2.62±0.028	3.50±0.045	4.43±0.045	4.69±0.061
61.1 ±2.4	124.3± 2.8	0.782±0.007	1.51 ±0.018	2.63±0.028	3.50±0.044	4.46±0.044	4.80±0.059
63.5 ±2.5	116.8± 2.6	0.775±0.007	1.453±0.017	2.63±0.027	3.54±0.043	4.64±0.043	4.86±0.057
66.1 ±2.7	114.9± 2.5	0.740±0.007	1.406±0.016	2.54±0.026	3.53±0.042	4.61±0.042	5.04±0.056
68.9 ±3.0	109.6± 2.3	0.698±0.009	1.343±0.019	2.52±0.036	3.58±0.049	4.62±0.055	5.03±0.064
72.0 ±3.2	100.1± 2.3	0.666±0.006	1.319±0.015	2.49±0.024	3.52±0.039	4.69±0.040	5.10±0.053
75.3 ±3.5	100.3± 3.6	0.654±0.006	1.272±0.015	2.41±0.022	3.54±0.038	4.76±0.039	5.12±0.051
78.9 ±3.8	94.7± 2.1	0.617±0.006	1.254±0.015	2.37±0.021	3.53±0.038	4.79±0.038	5.07±0.051
82.8 ±4.0	85.3± 1.9	0.582±0.006	1.184±0.014	2.25±0.020	3.40±0.035	4.78±0.037	5.22±0.050
86.9 ±4.3	82.1± 1.9	0.555±0.006	1.103±0.013	2.22±0.019	3.32±0.035	4.75±0.036	5.19±0.049
91.3 ±4.6	77.7± 1.7	0.535±0.006	1.062±0.013	2.13±0.019	3.24±0.035	4.69±0.036	5.19±0.049
96.0 ±4.8	72.1± 1.6	0.509±0.006	1.032±0.013	2.05±0.019	3.17±0.034	4.69±0.035	5.20±0.049
101.0 ±5.0	71.5± 1.7	0.472±0.006	0.955±0.012	1.97±0.017	3.02±0.035	4.56±0.035	5.08±0.049
106.0 ±5.3	69.4± 1.6	0.456±0.005	0.910±0.012	1.86±0.017	2.93±0.035	4.45±0.034	4.92±0.051
111.5 ±5.7	68.3± 2.1	0.435±0.007	0.889±0.012	1.79±0.017	2.82±0.035	4.40±0.034	4.84±0.054
117.5 ±6.0		0.405±0.012	0.818±0.012	1.68±0.017	2.66±0.033	4.21±0.034	4.61±0.066

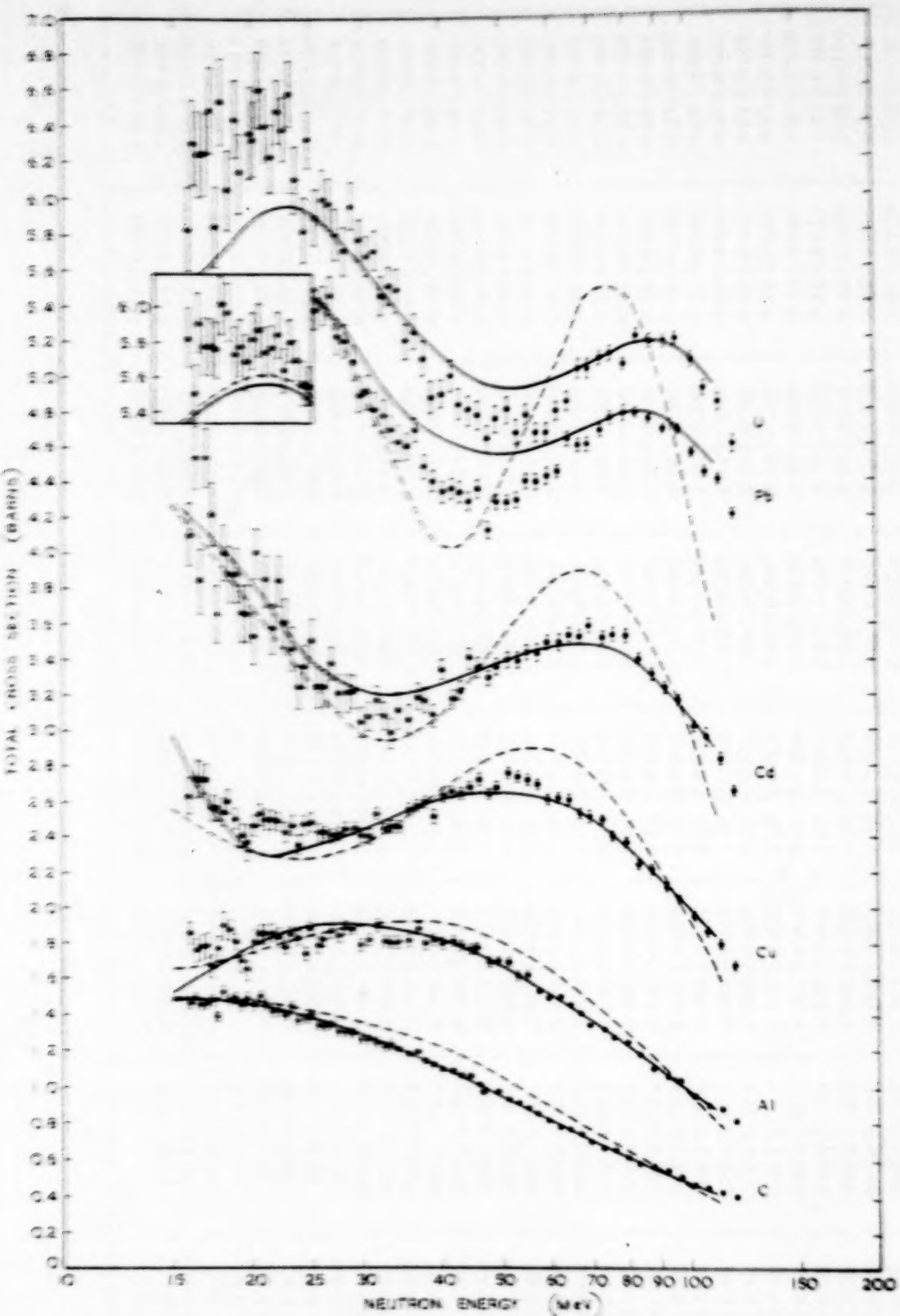

Fig. 4. The neutron total cross-sections of carbon, aluminium, copper, cadmium, lead and uranium measured in the present experiment. The solid and broken curves are the results of optical model calculations and are discussed in the text.

spectra, but it was possible to place upper limits on these which varied from ± 0.2 % at 100 MeV to ± 0.5 % at 117.5 MeV.

In figs. 6 and 7 the present results, which are represented by the smooth

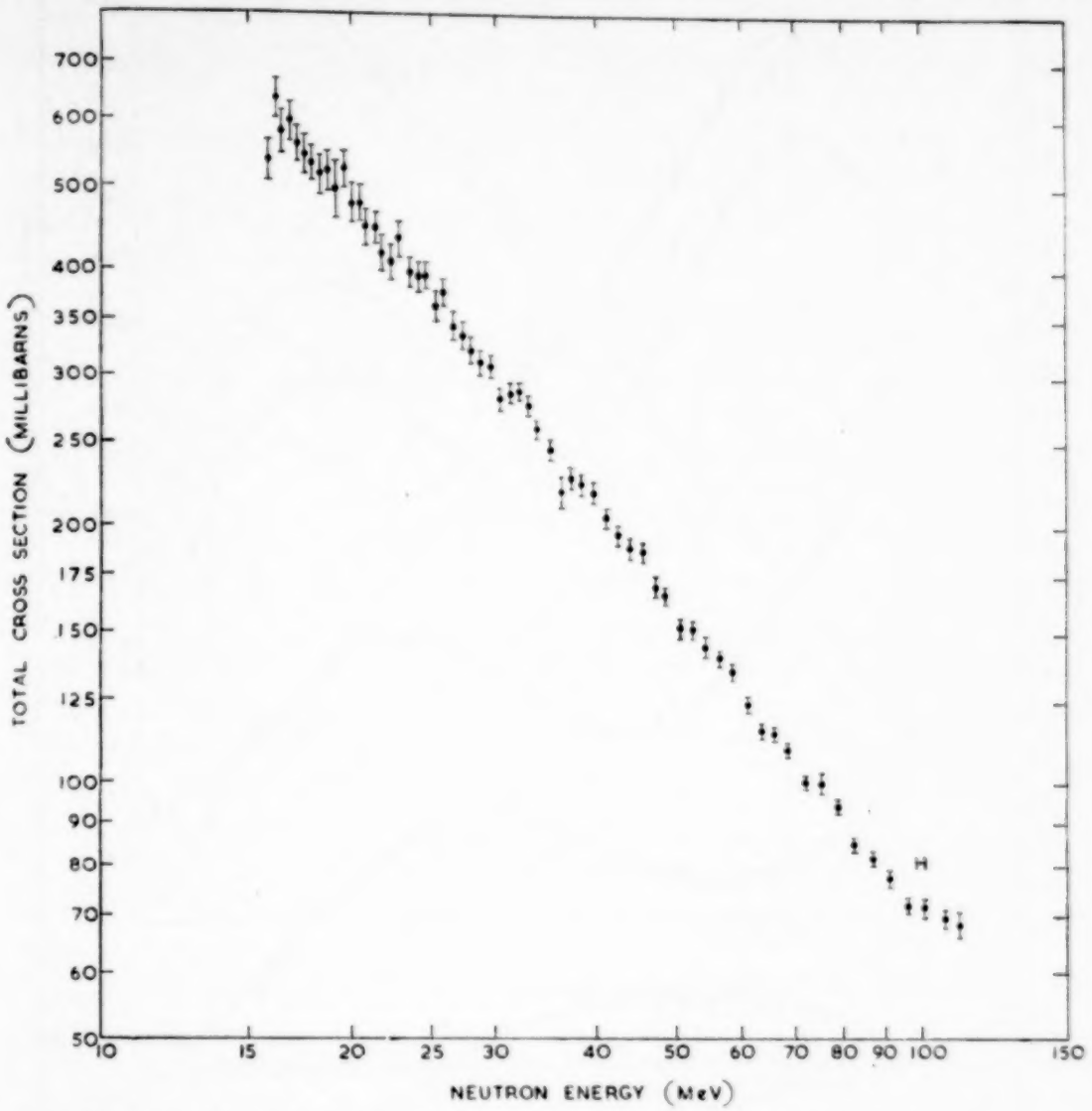

Fig. 5. The neutron total cross-sections of hydrogen measured in the present experiment.

curves, are compared with other available results. The agreement is generally very good, although, between 15 and 30 MeV, there is a tendency for the present results to lie below those of other workers, notably in the case of hydrogen. It is seen that the present work provides considerably more information on the energy dependence of the cross-sections than has been available hitherto.

6. Analysis

The results have been analysed in terms of the optical model of the nucleus. According to this model the individual nucleon-nucleon interactions may be

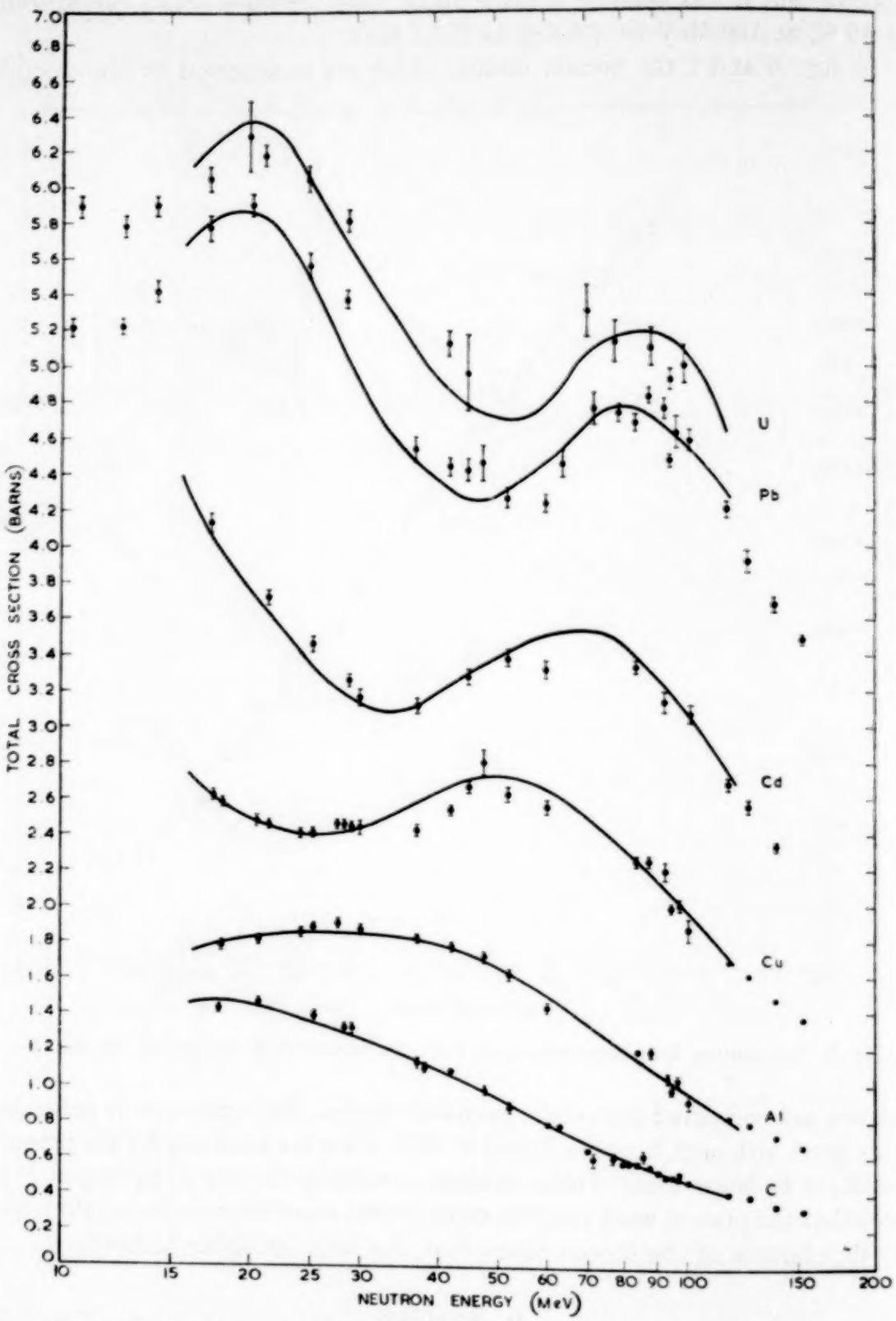

Fig. 6. The neutron total cross-sections of carbon, aluminium, copper, cadmium, lead and uranium. The results of previous work are compared with the present results which are represented by the solid curves.

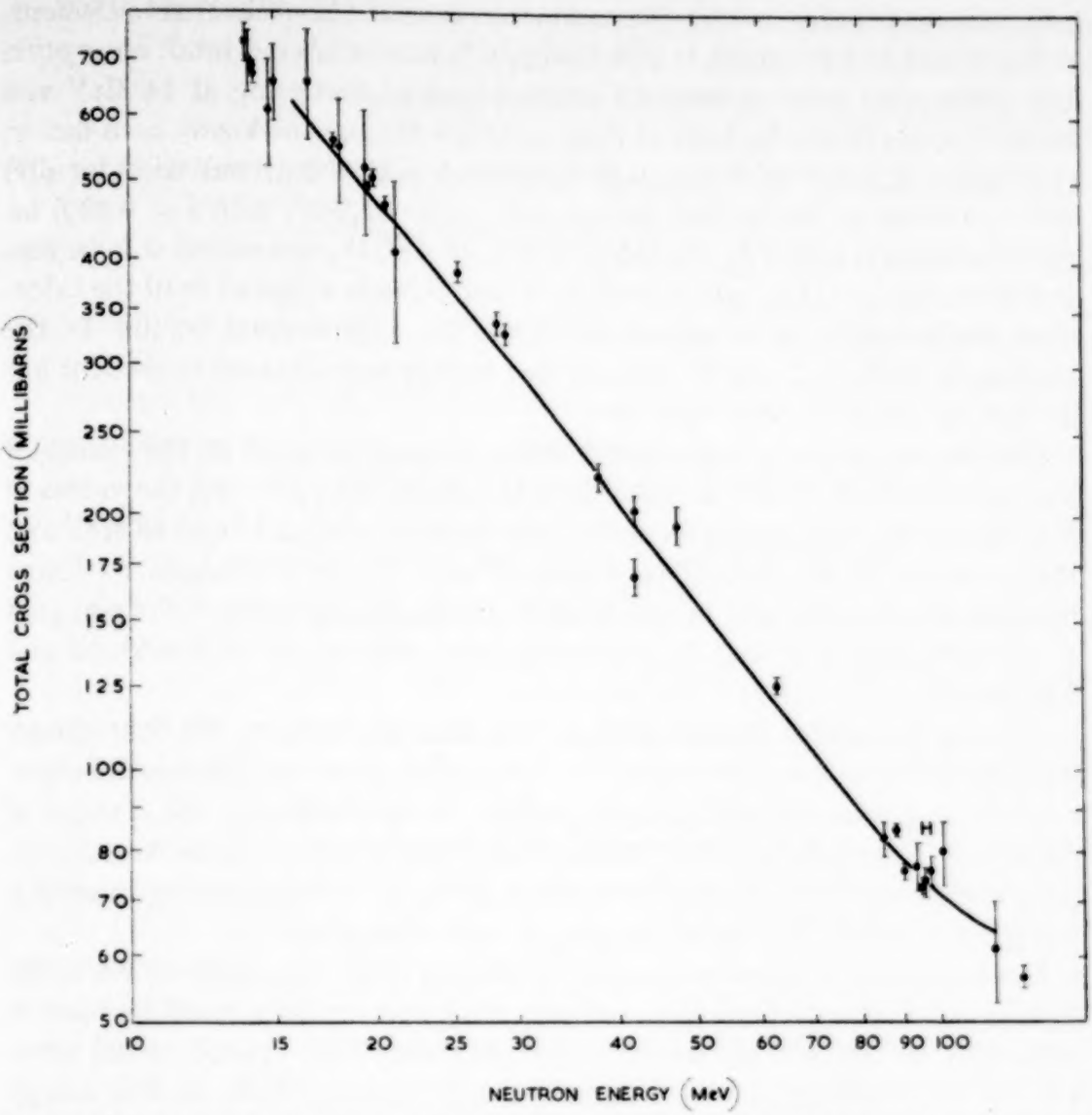

Fig. 7. The neutron total cross-sections of hydrogen. The results of previous work are compared with the present results which are represented by the solid curve.

replaced by a two-body potential of the form [5])

$$V = U\rho(r) + iWg(r) + \left(\frac{\hbar}{mc}\right)^2 (U_s + iW_s)\,\frac{1}{r}\,\frac{\mathrm{d}\rho(r)}{\mathrm{d}r}\,\boldsymbol{\sigma}\cdot\mathbf{l},$$

where U and W are the strengths of the real and imaginary parts of a central potential, U_s and W_s are the corresponding strengths of a spin-orbit potential, $(\hbar/mc)$ is the Compton wave-length of the pion, $\rho(r)$ and $g(r)$ are the radial form factors for the potentials concerned and $\boldsymbol{\sigma}\cdot\mathbf{l}$ gives the spin-orbit coupling.

In its simplest form such an interaction has seven adjustable parameters which, in principle, may depend on the neutron energy and the target nucleus. It is conventional however to vary only the four potential strengths with energy

and, as far as possible, to keep the parameters constant from element to element.

Bjorklund and Fernbach [5]) and Hodgson [6]) have analysed total, absorption and differential cross-sections for neutron-nucleus scattering at 14 MeV and 96 MeV respectively. In both of these analyses the Saxon-Woods form factor, $[1+\exp(r-R_0)/a]^{-1}$ with $a = 0.65f$ (where $f = 10^{-13}$ cm) was used for $\rho(r)$ and a gaussian at the nuclear surface, $\exp[-(r-R_0)^2/b^2]$ with $b = 0.98f$, for $g(r)$. The nuclear radius R_0 was taken to be $1.25A^{\frac{1}{3}}f$, W_s was assumed to be zero and the remaining three parameters U, W and U_s were adjusted until the calculated cross-sections gave reasonable fits to the experimental results. In the analysis at 96 MeV, U and W were allowed to vary from element to element but in that at 14 MeV they were not.

The present analysis was started using parameters based on the results of this previous work. Thus the radial form factors $\rho(r)$ and $g(r)$ and the values of a, b, R_0 and W_s were chosen to be the same as those used at 14 and 96 MeV and the strengths of the central potentials, U and W, were obtained by linear interpolation between the 14 and 96 MeV values. The strength of the real part of the spin-orbit potential U_s was taken from other work by Bjorklund and Fernbach [7]).

Using the optical model potential with these parameters, the Schrödinger wave equation was solved to give the total, absorption and differential cross-sections and polarizations for each nucleus, except hydrogen, for a range of energies †. The resulting total cross-sections, represented by the broken curves, are compared with the experimental values in fig. 4. Although the agreement is not good in detail, the overall trends are well reproduced.

In attempting to improve on these results an effort was made to see if the details of the energy dependence of the total cross-sections could be used in some way to provide additional information about the optical model parameters. The maxima and minima in the cross-sections which, in this energy range, are clearly in evidence for copper, cadmium, lead and uranium, have been ascribed to a nuclear type of Ramsauer effect in which the part of the neutron wave passing through the nucleus interferes with that going round it, producing a maximum in the cross-section when the phase difference is an odd multiple of π and a minimum when it is an even multiple of π. This idea was first suggested by Lawson [8]) to explain the maxima in the cross-sections found by Taylor and Wood [9]), and in an approximate and very simple calculation, he showed that maxima corresponding to a phase difference of π were predicted at approximately the energies indicated by their measurements.

For a given nucleus the phase difference depends on k_1, the change which occurs in the neutron wave number when the neutron enters the nucleus. This

† The numerical work was done using both a Ferranti Mercury Computer and an I.B.M. 704 Computer. The details of the programme for the Mercury Computer will be published elsewhere [6]). The programme for the I.B.M. 704 Computer is that used by Bjorklund and Fernbach [5]).

is given approximately by

$$k_1 = \left(\frac{2M}{\hbar^2}\right)^{\frac{1}{2}} [(E+U)^{\frac{1}{2}} - E^{\frac{1}{2}}],$$

where E is the neutron energy and M its mass.

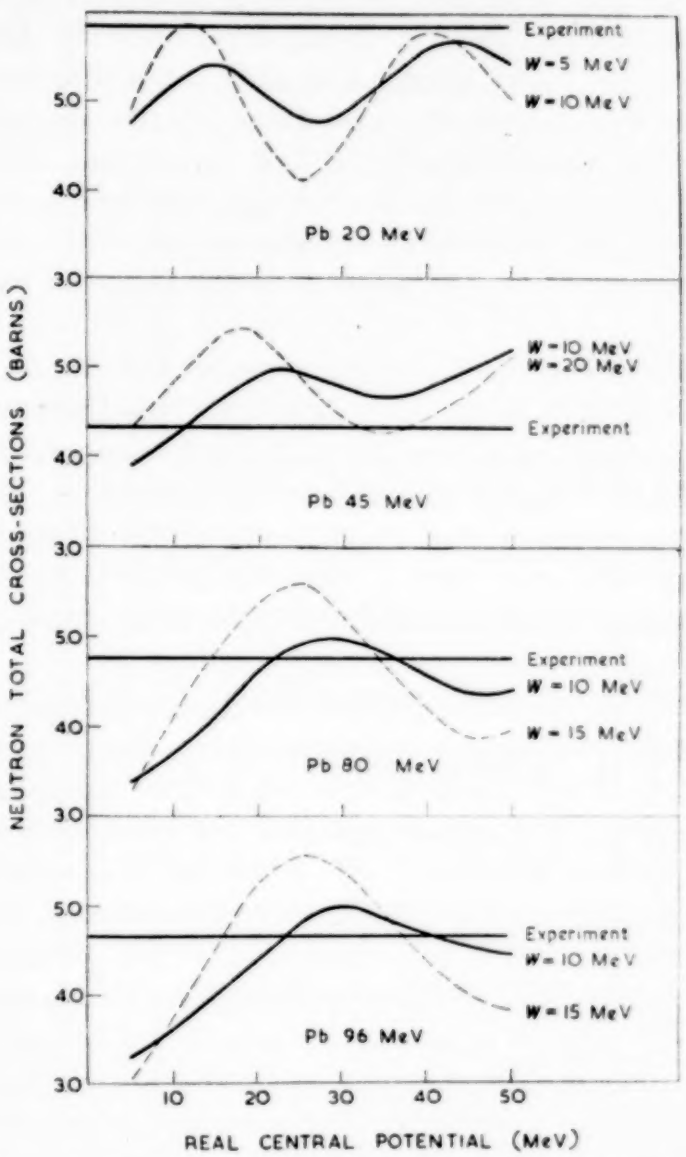

Fig. 8. Calculated values of the neutron total cross-sections of lead at 96, 80, 45 and 20 MeV, plotted as a function of U. The solid curves were calculated using $\rho(r) = g(r) = [1+\exp(r-R_0)/a]^{-1}$ with $R_0 = 1.25\,A^{\frac{1}{3}}f$ and $a = 0.65\,f$. The broken curves were calculated using $\rho(r) = [1+\exp(r-R_0)/a]^{-1}$ and $g(r) = \exp[-(r-R_0)^2/b^2]$ with $R_0 = 1.25\,A^{\frac{1}{3}}f$, $a = 0.65f$ and $b = 0.98f$.

Clearly, if changes in E cause the phase difference to change, so also will changes in U, and the cross-sections when plotted as a function of U should also exhibit maxima and minima. In fig. 8 the calculated values of the lead cross-sections at 96, 80, 45 and 20 MeV are plotted as a function of U for two

different choices of $g(r)$. The values of W shown have been chosen to give absorption cross-sections in reasonable agreement with those obtained by interpolating between the experimental results of Voss and Wilson [10]) and others [1]). The maxima and minima exhibited in the curves shown in fig. 8 correspond to phase differences of π, 2π and 3π. The actual energies at which these phase differences occur may, of course, be obtained from the positions of the various maxima and minima in the experimentally determined cross-sections. Thus at each such energy a method is available for determining U which simply involves choosing the value which gives the appropriate maximum or minimum in the calculated value of the cross-section. The value of U so chosen will not, however, give the correct magnitude for the total cross-section unless the radial parameters have suitable values. This criterion therefore restricts the choice of radial parameters as well as fixing the value of U within close limits.

As an example consider the high energy maximum in the lead cross-sections which occurs at 80 MeV. Here the values of the radial parameters should be varied until the calculated cross-section at the first maximum in a plot of total cross section against U agrees with the experimental result. The value of U is then fixed automatically at that which produces this maximum. Clearly the two sets of radial parameters used to obtain the curves in fig. 8 are not acceptable at 80 MeV since in each case the value of the total cross-section at the first maximum lies well above the experimental value.

It appears that the value of U fixed in this manner is reasonably insensitive to variations in the other optical model parameters. This is particularly true of variations in a, b, W and U_s. Thus, even when these parameters are not well chosen and the calculated cross-section does not agree with experiment it is possible to determine a value for U that should not be in error by more than a few MeV. This is illustrated in table 2 where the values of U obtained at 80 MeV for lead are shown for various choices of the other parameters. The calculated values of the total and absorption cross-sections are also given so that they may be compared with the experimental results. It will be seen that changes in R_0 cause U to change approximately as $1/R_0^2$ and changing $g(r)$ from the Saxon Woods form to a Gaussian at the nuclear surface causes U to change by about 15 %. However, at 45 and 20 MeV where the lead cross-sections pass through the first minimum and second maximum respectively U appears to be less sensitive to changes in R_0 than at 80 MeV, and the effect of the change in $g(r)$ is less than 3 %. At all three energies changes in U_s have little effect on either U or the total cross-section.

In addition to providing information about the dependence of U on the choice of the other optical model parameters, this analysis has also made it possible to place some limits on the values of the radial parameters that may be used to fit the lead cross-sections at 80, 45 and 20 MeV.

TABLE 2

A comparison of the values of U which give the first maximum in the calculated cross-sections of lead at 80 MeV for various choices of the other optical model parameters. The calculated and measured values of the total and absorption cross-sections are also shown.

$\rho(r)$	$[1+\exp(r-R_0/a]^{-1}$		$[1+\exp(r-R_0)/a]^{-1}$						
$g(r)$	$\exp[-(r-R_0)^2/b^2]$		$[1+\exp(r-R_0)/a]^{-1}$						
U (MeV)	23.5	24.0	26.5	26.5	31.5	28.5	29.0	29.2	27.5
W (MeV)	30	15	8.5	12.0	14	10	15	10	10
R_0 (f)	$1.25A^{\frac{1}{3}}$	$1.25A^{\frac{1}{3}}$	1.30	1.30	1.20	1.25	1.25	1.25	1.25
a (f)	0.65	0.65	0.20	0.65	0.65	0.65	0.65	0.65	0.65
b (f)	0.65	0.98							
U_s (MeV)	3.6	3.6	3.6	3.6	3.6	3.6	3.6	0	7.2
σ_t (calc) (barns)	5.26	5.55	4.76	5.36	4.48	4.93	4.76	4.93	4.97
σ_a (calc) (barns)	2.02	2.00	2.02	2.08	2.09	2.05	2.28	2.05	2.03
σ_t (expt) $= 4.75 \pm 0.04$ barns			σ_a (expt) $= 2.00 \pm 0.06$ barns						

Using the Saxon-Woods form factor for $\rho(r)$ and a Gaussian at the nuclear surface for $g(r)$ it was found that at 80 MeV the nuclear radius R_0 had to be less than $1.20\ A^{\frac{1}{3}}f$ if the other radial parameters were not to be improbably small. At 45 and 20 MeV, however, a range of values of R_0 extending up to $1.30\ A^{\frac{1}{3}}f$ could be used without difficulty. This is illustrated in table 3 where a few typical sets of parameters are shown.

TABLE 3

Values of R_0, a and b required to fit the total and absorption cross-sections of lead at 80, 45 and 20 MeV. The values of U and W associated with each set of radial parameters are also given.

$\rho(r) = [1+\exp(r-R_0)/a]^{-1}$; $g(r) = \exp[-(r-R_0)^2/b^2]$									
E (MeV)	80			45			20		
R_0 (f)	$1.20A^{\frac{1}{3}}$	$1.25A^{\frac{1}{3}}$	$1.30A^{\frac{1}{3}}$	$1.20A^{\frac{1}{3}}$	$1.25A^{\frac{1}{3}}$	$1.30A^{\frac{1}{3}}$	$1.20A^{\frac{1}{3}}$	$1.25A^{\frac{1}{3}}$	$1.30A^{\frac{1}{3}}$
a (f)	0.40			0.90	0.70	0.60	0.82	0.65	0.60
b (f)	0.80			1.2	1.2	1.0	1.2	1.2	1.00
U (MeV)	24.0			36.5	35.0	34.5	43.0	40.3	38.5
W (MeV)	30.0			13.5	11.5	14.0	10.2	10.5	13.0
$\rho(r) = g(r) = [1+\exp(r-R_0)/a]^{-1}$									
E (MeV)	80			45			20		
R_0 (f)	$1.20A^{\frac{1}{3}}$	$1.25A^{\frac{1}{3}}$	$1.30A^{\frac{1}{3}}$	$1.20A^{\frac{1}{3}}$	$1.25A^{\frac{1}{3}}$	$1.30A^{\frac{1}{3}}$	$1.20A^{\frac{1}{3}}$	$1.25A^{\frac{1}{3}}$	$1.30A^{\frac{1}{3}}$
a (f)	0.75	0.56	0.20	0.55	0.40		0.78	0.70	0.55
U (MeV)	31.5	28.2	26.5	33.7	36.5		42.0	42.8	40.0
W (MeV)	11.0	11.0	12.0	20.0	17.0		4.7	4.5	4.3

When both $\rho(r)$ and $g(r)$ were chosen to have the Saxon-Woods form with a common radius R_0 and a common surface thickness parameter a a range of values of R_0 could again be used provided that a varied with R_0 in a suitable way. However, there seemed to be no combination of R_0 and a that was acceptable at more than one of the three energies. The values of a required for three choices of R_0 are also given in table 3 to illustrate this.

If it is assumed that the optical model parameters do not change from nucleus to nucleus — an assumption which should be reasonable for the heavier elements at least — then the acceptable sets of parameters obtained from the analysis of the lead cross-sections should be suitable for predicting the cross-sections of other elements. Furthermore it should be possible to extend the analysis to include the measured cross-sections of other elements to obtain parameters at other energies.

To test this assumption the sets of parameters determined at 80, 45 and 20 MeV were used to calculate the cross-sections of copper and carbon and the results were compared with the experimental values. For copper it was found

that the sets involving the Saxon-Woods form factor for $g(r)$ gave results which were within 5 % of the measured cross-sections at 80 MeV but which were generally more than 10 % out at 45 and 20 MeV. On the other hand the sets in which a Gaussian at the nuclear surface had been used for $g(r)$ gave good agreement with the measured cross-sections at 45 and 20 MeV but not at 80 MeV. At all three energies the agreement was better for $R_0 = 1.25\ A^{\frac{1}{3}}f$ than for $R_0 = 1.20\ A^{\frac{1}{3}}$ or $1.30\ A^{\frac{1}{3}}f$. For carbon the situation was very similar though in general the agreement was not as good as it had been for copper. Only the sets of parameters with $R_0 = 1.25\ A^{\frac{1}{3}}f$ gave results which were within 5 % of the experimental results.

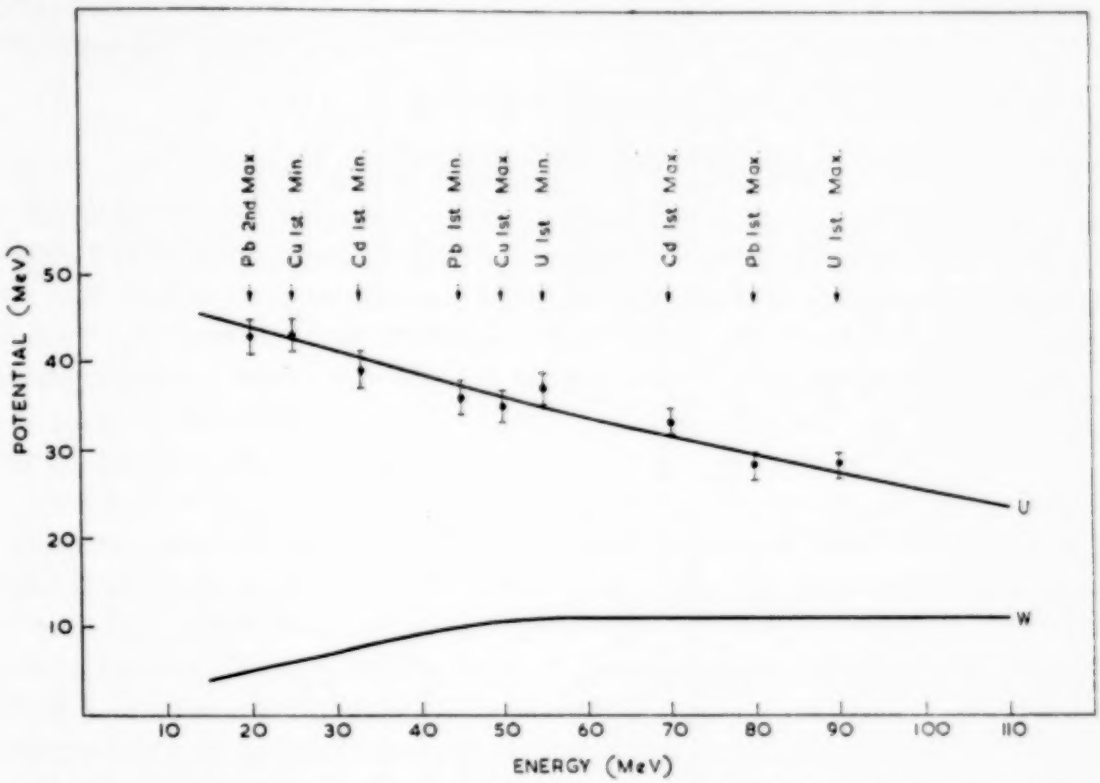

Fig. 9. Values of U and W derived from the analysis of total and absorption cross-sections of copper, cadmium, lead and uranium as discussed in the text.

It was therefore decided to put R_0 equal to $1.25\ A^{\frac{1}{3}}f$ and to analyse the cross-sections of copper, cadmium and uranium at the energies where they too exhibit maxima and minima so as to determine U at six further energies. These energies as well as those for the lead cross-sections are given in table 4 together with the values of U derived from the analysis. The results are also plotted as a function of energy in fig. 9.

Relativistic corrections have not been applied to these results. At the higher energies they would tend to reduce the values of U by a few per cent. The errors of ± 5 % which have been assigned allow for uncertainties in estimating the energies at which the maxima and minima occur and for possible variations

TABLE 4

The values of U determined at energies where the cross-sections of U, Pb, Cd and Cu exhibit maxima or minima. The Saxon-Woods form factor $[1-\exp(r-R_0)/a]^{-1}$ with $R = 1.25\,A^{\frac{1}{3}}f$ and $a = 0.6f$ was used for both the real and imaginary parts of the central potential.

Element	U 1st Max	Pb 1st Max	Cd 1st Max	U 1st Min	Cu 1st Max	Pb 1st Min	Cd 1st Min	Cu 1st Min	Pb 2nd Max
Energy (MeV)	90	80	70	55	50	45	33	25	20
U (MeV)	28.3	28.2	33.4	37.0	35.0	36.0	39.1	43.0	42.5

in the choice of radial parameters. For any one set of radial parameters however, U can probably be determined to better than $\pm 2\,\%$. The set used to obtain the results in table 4 was $\rho(r) = g(r) = [1+\exp(r-R_0)/a]^{-1}$, $R_0 = 1.25\,A^{\frac{1}{3}}f$ and $a = 0.60f$. The cross-sections calculated with these radial parameters and with the values of U and W indicated by the smooth curves in fig. 9, are shown by the solid curves in fig. 4. At energies above 50 MeV the results are in good agreement with the measured cross-sections, even for aluminium and carbon, but the agreement is not maintained at lower energies. However, if a Gaussian at the nuclear surface is used in place of the Saxon-Woods form for $g(r)$ with values of R_0, a and b similar to those given for 45 or 20 MeV in table 3, the cross-sections calculated at energies below 50 MeV agree very well with the experimental results.

7. Summary and Conclusions

In analysing the total cross-sections measured in the present experiment a method of obtaining U at energies where the total cross-sections exhibit maxima and minima has been adopted which is virtually independent of the magnitudes of the cross-sections at these energies. Thus, by using absorption cross-sections derived from other work to fix W, it has been possible to make use of the magnitudes of the total cross-sections to place limits to the choice of the radial parameters.

No set of radial parameters has been found that can be used unchanged over the energy range from 90 to 20 MeV and there is strong evidence to support the view that the form factor for the absorptive part of the potential changes from one giving predominantly volume absorption at energies near 80 MeV and above to one giving a strong surface absorption at energies below about 50 MeV. On the other hand it seems likely that at any one energy a single set of parameters may be used satisfactorily for all heavy and medium weight nuclei.

Finally an attempt has been made to establish the energy dependence of U by analysing the cross-sections of copper, cadmium, lead and uranium to determine values of U at the energies where the respective cross-sections exhibit maxima or minima. Since U appears to be insensitive to variations in the other optical model parameters it is believed that the values so determined (see fig. 9) should not be in error by more than $\pm 5\,\%$ over the energy range from 90 to 20 MeV.

The authors offer their sincere thanks to the cyclotron crew for their cooperation and to their colleagues Mr. G. C. Cox, Mr. A. Langsford and Mr. G. B. Huxtable for their invaluable help in the latter stages of this work. They have had many interesting discussions with Drs. C. J. Batty and K. Parker, also with Mr. B. Rose and other members of the Harwell cyclotron group. Finally

they would like to thank Professors F. Bjorklund and S. Fernbach for permission to use their Optical Model Programme.

References

1) D. J. Hughes and R. B. Schwartz, Neutron Cross-Sections, Sec. Ed., July 1958 BNL 325 (U. S. Govt. Printing Office, Washington D.C.)
2) W. I. Linlor, UCRL **2303**, unpublished;
B. Ragent, UCRL **2337**, unpublished
3) J. P. Scanlon, G. H. Stafford, J. J. Thresher and P. H. Bowen, Rev. Sci. Inst. **28** (1957) 749
4) W. F. Moody, G. J. R. Maclusky and M. O. Deighton, Electronic Engineering **24** (1952) 214
5) F. Bjorklund and S. Fernbach, Phys. Rev. **109** (1958) 1295
6) P. E. Hodgson, to be published
7) F. Bjorklund and S. Fernbach, in Proc. Sec. Intern. Conf. Peaceful Uses of Atom. En. (1958)
8) J. D. Lawson, Phil. Mag. **44** (1953) 102
9) A. E. Taylor and E. Wood, Phil. Mag. **44** (1953)
10) R. G. P. Voss and R. Wilson, Proc. Roy. Soc. A **236** (1956) 41

8.B

Nuclear Physics **22** (1961) 663—676; © *North-Holland Publishing Co., Amsterdam*

Not to be reproduced by photoprint or microfilm without written permission from the publisher

APPROXIMATE EQUATIONS FOR PARTIAL π—K SCATTERING AMPLITUDES

P. S. ISAEV and M. SEWERYNSKI

Joint Institute for Nuclear Research, Dubna, USSR †

Received 1 July 1960

Abstract: Approximate integral equations for partial π—K scattering amplitudes are obtained with the help of the double Mandelstam representation in the low energy range.

1. Introduction

Investigation of the π—K-interaction is of interest not only from the purely theoretical point of view, but also from the "applied" point of view. In fact, π—K-interection is inseparable from the study of elastic and inelastic processes of K-meson-hyperon interaction, and, in particular, of K-meson-nucleon scattering.

There are two types of interaction considered in perturbation theory. Firstly, the

$$\overline{\mathrm{K}}\pi\mathrm{K}\text{-interaction} \qquad (1)$$

which is shown in fig. 1. It was introduced by Schwinger [1]) and discussed in

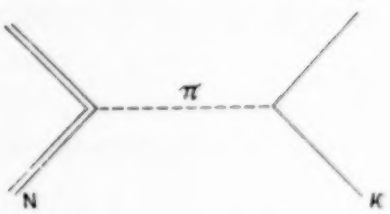

Fig. 1

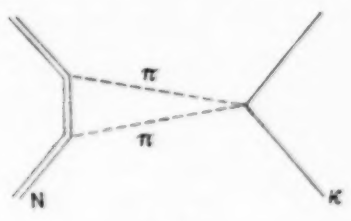

Fig. 2

detail by Minami [2]) and Pais [3]). And secondly, the

$$\overline{\mathrm{K}}\mathrm{K}\pi\pi\text{-interaction} \qquad (2)$$

shown in fig. 2 and discussed in detail by Barshay [4]).

It is not clear at present which of the above types of interactions is to be preferred. One may adduce the following consideration in favour of the second

† Reported at the All-Union Interuniversity Conference on the Quantum Field and Elementary Particle Theory (Uzhgorod, May 12—18, 1960).

type: if the interaction of K-mesons and baryons is assumed to have the form $\overline{Y}KY$, then to render the theory renormalizable it is necessary to introduce the term $g_{K\pi}\overline{K}K\pi^2$ into the Hamiltonian of the interaction (in a way similar to that of introducing the term λq^4 in mesodynamics or the term $\varepsilon A_\mu A_\mu \pi^2$ in meso-electrodynamics).

The analysis of experimental data on K—N-scattering [3–5]) has shown that there is good agreement between experiment and theory in the low energy range (up to 200 MeV) if one uses interaction (2) and assumes that the coupling constant of π—K-interaction equals approximately 1—5.

Mention should also be made of Chou Kuang Chao's results [6]) about the possible symmetry of the π—K-system. Proceeding from the Hamiltonian in the form

$$H = H_\pi + H_K + g_{K\pi}\pi_\alpha \pi_\alpha \overline{K}_\lambda K_\lambda, \tag{3}$$

where H_π is the Hamiltonian describing the π—π-interaction, H_K is the Hamiltonian describing the K-meson interaction, and assuming Hamiltonian (3) to be invariant with respect to rotations in isobaric π-mesonvector and K-meson isospinor spaces, he obtained that all the amplitudes of π—K-scattering without charge exchange are equal, that all the amplitudes of charge-exchange scattering equal zero, and that the annihilation process $K+\overline{K} \to n\pi$ occurs only through the isoscalar state.

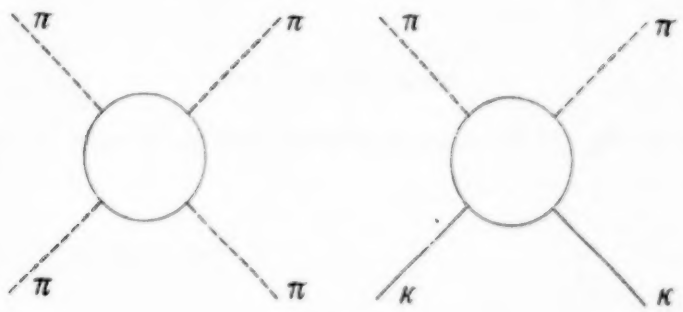

Fig. 3

The present paper attempts to study the π—K interaction by the method of Mandelstam's double representations. At the first stage of the investigation we have derived approximated integral equations for partial π—K-scattering amplitudes in the low energy range. Investigation of π—K-interaction by the method of double dispersion relation was stimulated, first, by the importance of this interaction for the study of K—N-scattering, and, secondly, by the work of Efremov, Meshcheryakov and Shirkov [7]) who successfully avoided kinematics singularities by considering the corresponding symmetrical and anti-symmetrical expressions.

The logical sequence of processes for strong interacting particles in studying π—K scattering is plotted in fig. 3. A detailed study of π—π-scattering was

made by Chew and Mandelstam [8]) and by Chew, Mandelstam and Noyes [9]). In our equations for π—K scattering the π—π-scattering phase-shifts are assumed to be given.

The π—K-scattering amplitude is considered in the complex plane of variable $\mathbf{q}^2$ ($\mathbf{q}^2$ is the momentum in the centre-of-mass system of the $\pi+\mathrm{K} \to \pi'+\mathrm{K}'$ reaction). A kinematic cut along $\mathbf{q}^2$ in the interval $-M^2 \leqq q^2 \leqq -\mu^2$, where M and μ are K-meson and π-meson masses, respectively, is eliminated by the method proposed in ref. [7]). The analyticity region of the imaginary part of the π—K-scattering amplitude is determined from the Mandelstam representation and perturbation theory under the assumption of the interaction (2).

A non-physical cut from $\pi+\pi \to \mathrm{K}+\bar{\mathrm{K}}$ reaction is eliminated by Muskhelishvili-Omnes method [10]). Employing further the unitarity condition we obtained a closed set of approximate integral equations for π—K-scattering amplitudes which involved π—π-scattering phase-shifts. The approximation consisted in taking into account only nearest singularities while deriving the set of integral equations. This, naturally, led to a reasonable restriction on π—K scattering by the lowest partial waves, s and p. Their set of integral equations was obtained by two methods: 1) for partial amplitudes averaged over all scattering angles and 2) for partial amplitudes taken at the backward scattering angle.

2. π—K Scattering Amplitude and its Isobaric Structure

Matrix elements of the scattering process

$$\text{(I)} \quad \pi + \mathrm{K} \to \pi' + \mathrm{K}',$$
$$\text{(II)} \quad \pi' + \mathrm{K} \to \pi + \mathrm{K}',$$

and pair production of K-mesons

$$\text{(III)} \quad \pi + \pi' \to \mathrm{K}' + \bar{\mathrm{K}},$$

can be represented in the form

$$\langle \mathrm{f}|S|\mathrm{i}\rangle = \langle \mathrm{f}|1+iT|\mathrm{i}\rangle = \delta_{\mathrm{if}} + \delta(\textstyle\sum p_i)\, \dfrac{i}{(2\pi)^2} \left(\dfrac{1}{16 p_{10} p_{20} q_{10} q_{20}}\right)^{\frac{1}{2}} T, \qquad (4)$$

where $\sum p_i$ is the sum of four momenta of all particles, p_{10} and p_{20} is the K-meson energy, q_{10} and q_{20} is π-meson energy, T is the Green's function.

For the scattering process (I) the differential cross section is expressed by the formula

$$\frac{\mathrm{d}\sigma}{\mathrm{d}\Omega} = \frac{1}{(2\pi)^2} \frac{|\mathbf{q}_2|}{|\mathbf{q}_1|} \frac{1}{16 p_{10} p_{20}} |T|^2. \qquad (5)$$

In the centre-of-mass system $|\mathbf{q}_2| = |\mathbf{q}_1|$, $p_{20} = p_{10} = E_{\mathrm{K}}$ and relation (5) assumes the form of $\mathrm{d}\sigma/\mathrm{d}\Omega = |T/8\pi E_{\mathrm{K}}|^2$. The isobaric structure of the π—K-

scattering amplitude has the form

$$T_{\alpha\beta} = A\delta_{\alpha\beta} + \tfrac{1}{2}[\tau_\alpha, \tau_\beta]B, \tag{6}$$

where A and B are scalar functions dependent on the scalar product of the four momenta p_1, p_2, q_1, q_2.

The connection of A and B with isobaric states of the π—K-system is given by

$$A = \tfrac{2}{3}T^{\frac{3}{2}} + \tfrac{1}{3}T^{\frac{1}{2}}, \quad B = -\tfrac{1}{3}T^{\frac{3}{2}} + \tfrac{1}{3}T^{\frac{1}{2}},$$

where $T^{\frac{3}{2}}$ and $T^{\frac{1}{2}}$ are states of isobaric spin $\frac{3}{2}$ and $\frac{1}{2}$ respectively.

The isobaric structure of process (III) coincides with that of processes (I) and (II), while the connection of T^0 and T^1 (states of isobaric spins 0 and 1, respectively) with A and B is quite simple:

$$T^0 = A\sqrt{6}, \quad T^1 = 2B. \tag{7}$$

3. Kinematics of Reactions

We shall consider the A and B factors as functions of invariant variables S_1, S_2 and S_3 determined by the usual method:

$$S_1 = -(p_1+q_1)^2; \quad S_2 = -(p_1+p_2)^2; \quad S_3 = -(p_1+p_2)^2.$$

In the centre-of-mass system of reaction (I) these invariant variables take the form

$$\begin{aligned} S_1 &= M^2+\mu^2+2\mathbf{q}_1^2+2\sqrt{(\mathbf{q}_1^2+\mu^2)(\mathbf{q}_1^2+M^2)}, \\ S_2 &= M^2+\mu^2-2\mathbf{q}_1^2\cos\theta_1-2\sqrt{(\mathbf{q}_1^2+\mu^2)(\mathbf{q}_1^2+M^2)}, \\ S_3 &= -2\mathbf{q}_1^2(1-\cos\theta_1), \end{aligned} \tag{8}$$

where θ_1 is the scattering angle of the incident meson. It follows from relations (6) and (7) that the substitution of $\alpha \rightleftarrows \beta$ corresponds to the substitution of $S_1 \rightleftarrows S_2$ and in this case

$$A(S_1, S_2, S_3) = A(S_2, S_1, S_3), \quad B(S_1, S_2, S_3) = -B(S_2, S_1, S_3). \tag{9}$$

Hence, it appears that in expanding the A and B factors into partial waves of the third reaction only even waves will appear in the case of the A expansion and only odd waves in case of the B expansion.

4. Analytic Properties of the π—K-Scattering Amplitude in the Centre-of-Mass System of the First Reaction

In what follows we assume that the Mandelstam representation holds for the functions $A(S_1, S_2, S_3)$ and $B(S_1, S_2, S_3)$. If we consider functions A and B in the complex variable plane $\mathbf{q}_1^2$ at a fixed scattering angle $\cos\theta_1 = z_1 = \text{const}$.

it is possible to obtain from the Mandelstam representation all the cuts over $\mathbf{q}_1^2$: from reaction (I) the cut is in the interval $[0, +\infty]$, from reaction (II) in the interval $[-M^2, -\infty]$ for $z_1 \geqq \mu/M$ angles and in the interval $[-\tau_{z_1} - M^2]$ for $z_1 \leqq \mu/M$ angles, from reaction (III) it is in the interval $[-2\mu^2/1-z_1, -\infty]$.

Apart from these cuts there is one more, a kinematic one, which lies in the interval $-M^2 \leqq \mathbf{q}_1^2 \leqq -\mu^2$. The latter cut is eliminated by the method proposed in ref. [7]). For this purpose, alongside with the variables S_1 and S_2 (see ref. [8])), we shall introduce new variables

$$\dot{S}_1 = M^2+\mu^2+2\mathbf{q}_1^2-2\sqrt{(\mathbf{q}_1^2+\mu^2)(\mathbf{q}_1^2+M^2)},$$

$$\dot{S}_2 = M^2+\mu^2-2\mathbf{q}_1^2 z_1+2\sqrt{(\mathbf{q}_1^2+\mu^2)(\mathbf{q}_1^2+M^2)}. \tag{10}$$

If we now require that (in variables of reaction (II))

$$\dot{S}_1 = S_1, \quad \dot{S}_2 = S_2, \tag{11}$$

we shall obtain that $A(\dot{S}_1, \dot{S}_2, S_3)$ is an amplitude of reaction (II) in its physical region. Fig. 4 represents the connection between the variables of the first and second reactions as expressed by relations (10) and (11).

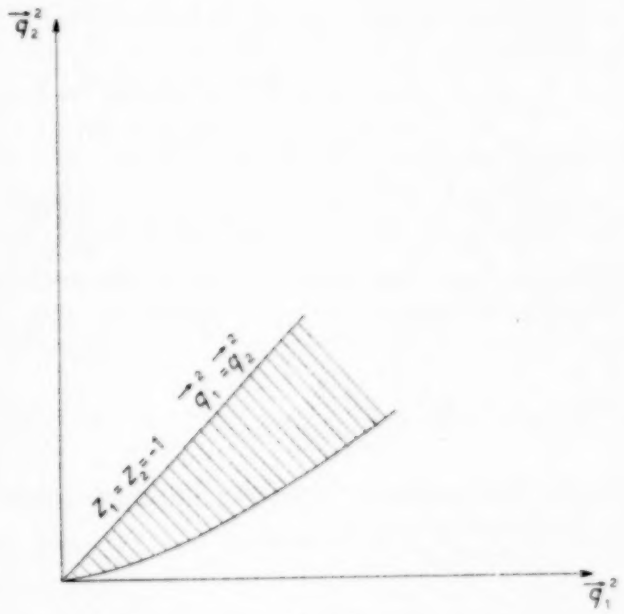

Fig. 4

Thus, side by side with functions $A(S_1, S_2, S_3)$ and $B(S_1, S_2, S_3)$ we shall consider functions $A(\dot{S}_1, \dot{S}_2, S_3)$ and $B(\dot{S}_1, \dot{S}_2, S_3)$. Symmetrical and asymmetrical combinations of these functions will not depend irrationally on the root $K(\mathbf{q}_1^2) = \sqrt{(\mathbf{q}_1^2+\mu^2)(\mathbf{q}_1^2+M^2)}$. Thus, functions

$$\Phi_s = \frac{\Phi(\mathbf{q}_1^2, z_1, +K(\mathbf{q}_1^2)) + \Phi(\mathbf{q}_1^2, z_1, -K)}{2},$$

and

$$\Phi_a = \frac{\Phi(\mathbf{q}_1^2, z_1, +K) - \Phi(\mathbf{q}_1^2, z_1, -K)}{2K},$$

where Φ denotes either function (A or B), will not contain a kinematic cut.

The cuts of the $\Phi(\mathbf{q}_1^2, z_1, -K)$ function from reaction (II) are in the $[0, +\infty]$ and $[-M^2, -\tau_z]$ intervals for $z_1 \geqq \mu/M$; from reaction (III) they are in the interval $[-2\mu^2/1-z_1, -\infty]$. There is no cut from reaction (I). If we now write the usual Cauchy theorem in the complex plane $\mathbf{q}_1^2$ for functions Φ_s and Φ_a and return again to functions Φ we obtain

$$\Phi(\mathbf{q}_1^2, \pm K) = \frac{1}{\pi}\left\{\int_0^\infty \frac{\operatorname{Im}\Phi(\mathbf{q}_1'^2, +K)\chi(\pm) + \operatorname{Im}\Phi(\mathbf{q}_1'^2, -K)\chi(\mp)}{\mathbf{q}_1'^2 - \mathbf{q}_1^2}\, d\mathbf{q}_1'^2\right.$$

$$+ \int_{-\infty}^{q_1^2(z_1)} \frac{\operatorname{Im}\Phi(\mathbf{q}_1'^2, +K)}{\mathbf{q}_1'^2 - \mathbf{q}_1^2}\chi(\pm)d\mathbf{q}_1'^2 + \vartheta\left(z_1 - \frac{\mu}{M}\right)\int_{-\tau_{z_1}}^{-M^2} \frac{\operatorname{Im}\Phi(\mathbf{q}_1'^2, -K)}{\mathbf{q}_1'^2 - \mathbf{q}_1^2}\chi(\mp)d\mathbf{q}_1'^2$$

$$\left. + \int_{-\infty}^{-\frac{2\mu^2}{1-z_1}} \frac{\operatorname{Im}\Phi(\mathbf{q}_1'^2, +K)\chi(\pm) + \operatorname{Im}\Phi(\mathbf{q}_1'^2, -K)\chi(\mp)}{\mathbf{q}_1'^2 - \mathbf{q}_1^2}\, d\mathbf{q}_1'^2,\right. \tag{12}$$

where

$$q_1^2(z_1) = \begin{cases} -M^2, & \text{for } z_1 \geqq \mu/M, \\ -\tau_{z_1}, & \text{for } z_1 \leqq \mu/M, \end{cases}$$

$$\tau_{z_1} = \frac{M^2 + \mu^2 - 2M\mu z_1}{1 - z_1^2}, \quad \chi(\pm) = 1 \pm \frac{K(\mathbf{q}_1^2)}{K(\mathbf{q}_1'^2)}.$$

Fig. 5 shows the domains of integration over $\mathbf{q}_1'^2$ in eq. (12) depending on z_1.

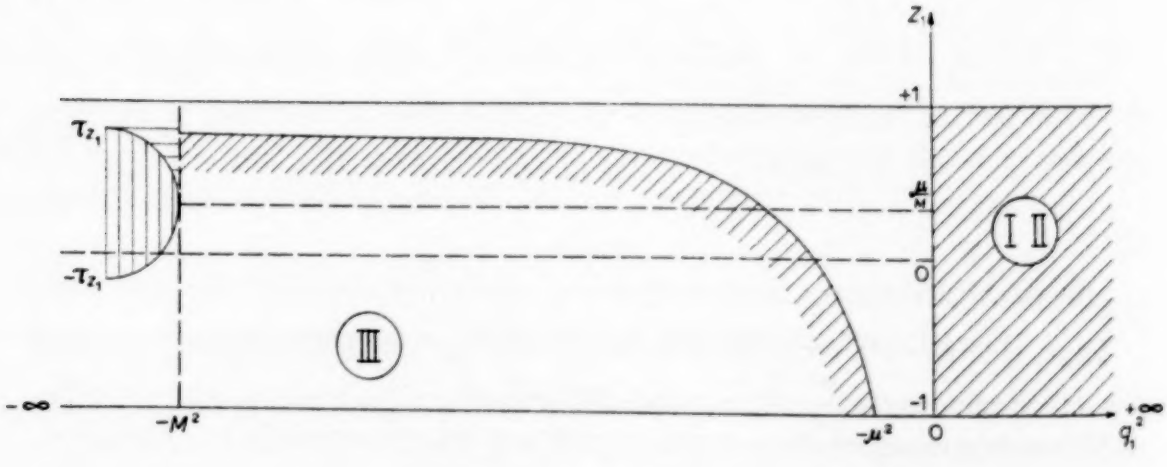

Fig. 5

It can be seen from fig. 5 that at $z_1 = 1$ the only non-zero integration domains will be $\mathbf{q}_1'^2 \geqq 0$. This corresponds to the transition to the usual dispersion relations for the forward scattering case.

At $z_1 = -1$ a contribution from the negative $\mathbf{q}_1'^2$ is made only by the cut from reaction (III).

Eq. (12) was derived from the Mandelstam representation without using any approximation. Restricting ourselves to only nearest singularities, namely, taking into account only part of the cut from reaction (III) we shall further on consider such an equation

$$\Phi(\mathbf{q}_1^2, \pm K) = \frac{1}{\pi}\int_0^\infty \frac{\operatorname{Im}\Phi(\mathbf{q}_1'^2, +K)\chi(\pm) + \operatorname{Im}\Phi(\mathbf{q}_1'^2, -K)\chi(\mp)}{\mathbf{q}_1'^2 - \mathbf{q}_1^2}\,\mathrm{d}\mathbf{q}_1'^2$$

$$+ \frac{1}{\pi}\int_{-\frac{8\mu^2}{1-z_1}}^{-\frac{2\mu^2}{1-z_1}} \frac{\operatorname{Im}\Phi(\mathbf{q}_1'^2, +K)\chi(\pm) + \operatorname{Im}\Phi(\mathbf{q}_1'^2, -K)\chi(\mp)}{\mathbf{q}_1'^2 - \mathbf{q}_1^2}\,\mathrm{d}\mathbf{q}_1'^2. \quad (13)$$

4. Elimination of Non-Physical Cut from Reaction (III)

In eq. (13) imaginary parts $\operatorname{Im}\Phi(\mathbf{q}_1'^2, +K)$ and $\operatorname{Im}\Phi(\mathbf{q}_1'^2, -K)$ in the interval $[-2\mu^2/1-z_1, -8\mu^2/1-z_1]$ will be considered as analytic continuations of the corresponding functions from the region $S_3 \geqq 4M^2$.

Let us expand the amplitude $\Phi(S_1, S_2, S_3)$ into partial waves of reaction (III) in the region of physical values of $\mathbf{q}_3^2$ and $\cos\theta_3$:

$$\Phi(S_1, S_2, S_3) = 2p_3 q_3 \sum_l (2l+1)\phi_{\mathrm{III}}^l(\mathbf{q}_3^2)p_l(\cos\theta_3). \quad (14)$$

As follows from eq. (9) summation over even l is taken in relation (14) for $\Phi = A$ and summation over odd l is taken for $\Phi = B$. Let us also write unitarity relation for reaction (III):

$$\operatorname{Im}\Phi(S_1, S_2, S_3) = \frac{1}{32\pi^2}\frac{|\mathbf{q}_3|}{W(\mathbf{q}_3^2)}\int \mathrm{d}\Omega'\,\Phi_{\mathrm{III}}(\Omega')\Pi^*(\Omega''). \quad (15)$$

Here Π^* denotes hermitian conjugate amplitude of the reaction $\pi+\pi \to \pi+\pi$ †.

It follows from eqs. (7) and (15) that

$$\operatorname{Im} A = \frac{1}{32\pi^2}\frac{|\mathbf{q}_3|}{W_3}\int \mathrm{d}\Omega'\,A(\Omega')\dot{\Pi}^0(\Omega''), \quad \operatorname{Im} B = \frac{1}{32\pi^2}\frac{|\mathbf{q}_3|}{W_3}\int \mathrm{d}\Omega'\,B(\Omega')\dot{\Pi}^1(\Omega'').$$

† Isobaric structure of the relation $\pi+\pi \to \pi+\pi$ has the form (see, for instance, ref. [8])):

$$\Pi^{\alpha\beta,\gamma\varepsilon} = \Pi_1\delta_{\alpha\beta}\delta_{\gamma\varepsilon} + \Pi_2\delta_{\alpha\varepsilon}\delta_{\beta\gamma} + \Pi_3\delta_{\alpha\gamma}\delta_{\varepsilon\beta},$$

while the isobaric states of spin 0 (Π^0) and of sin 1 (Π^1) are related to the coefficients Π_1, Π_2, Π_3 in the following way:

$$\Pi^0 = 3\Pi_1 + \Pi_2 + \Pi_3, \quad \Pi^1 = \Pi_2 - \Pi_3.$$

If in expanding Π^0 and Π^1 into partial waves we restrict ourselves to only s and p-waves, respectively, we obtain

$$\begin{aligned} \text{Im } A_{\text{III}}(\mathbf{q}_3^2) &= \frac{1}{8\pi}\frac{|\mathbf{q}_3|}{W_3} A^0_{\text{III}}(\mathbf{q}_3^2) e^{i\delta_0} \sin\delta_0, \\ \text{Im } B_{\text{III}}(\mathbf{q}_3^2) &= \frac{1}{8\pi}\frac{|\mathbf{q}_3|}{W_3} B^1_{\text{III}}(\mathbf{q}_3^2) e^{i\delta_1} \sin\delta_1 \cos\theta_3. \end{aligned} \tag{16}$$

It is evident that the expansion of (16) over $z_3 = \cos\theta_3$ in the reaction $\pi+\pi' \to \text{K}'+\bar{\text{K}}$ can be analytically continued up to the first singularity at which the imaginary part of reaction (III) amplitude is discontinuous. The boundary of the first discontinuity is found in a way similar to that of ref. [11]).

The boundary curves for the spectral functions have the form

$$\begin{aligned} &[S_3-16\mu^2][S_1-(M+\mu)^2][S_1-(M-\mu)^2]-64S_1\mu^4 = 0 \\ &\text{(asymptotes } S_1 = (M+\mu)^2 \text{ and } S_3 = 16\mu^2) \end{aligned} \tag{17}$$

and

$$\begin{aligned} &[S_3-4\mu^2][S_1-(M+3\mu)^2]-32\mu^3(M+\mu) = 0 \\ &\text{(asymptotes } S_1 = (M+3\mu)^2 \text{ and } S_3 = 4\mu^2). \end{aligned} \tag{18}$$

It follows from eqs. (17) and (18) that the imaginary part of the amplitude of the reaction (III) can be analytically continued over variable $\mathbf{q}_1^2$ (at physical z_1) up to $-21.3\mu^2$.

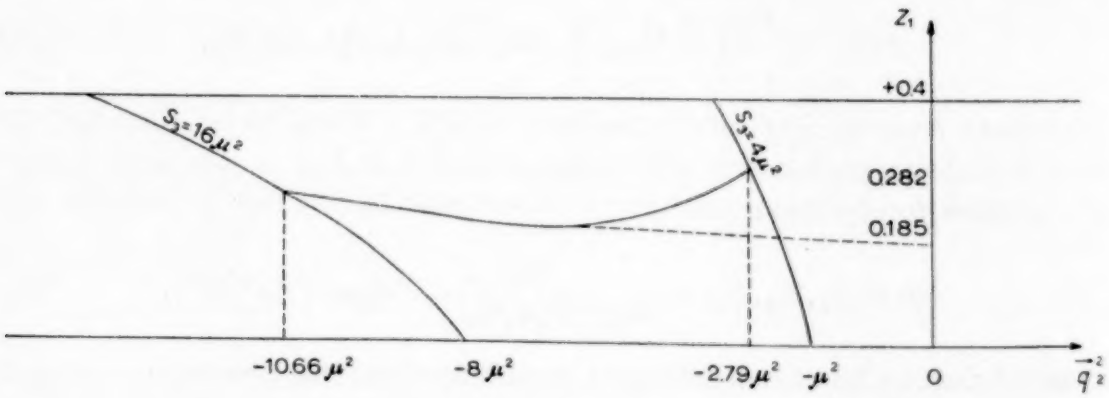

Fig. 6.

The analyticity of the real part of the reaction (III) amplitude is determined from the Mandelstam representation with the help of Hein's theorem [12]).

The boundary in the variables $\mathbf{q}_1^2$ and z_1 of the analytic continuation of the third reaction amplitude is plotted in fig. 6.

Applying now the Mushkhelishvili-Omnes method [10]) to the function

$$\Phi_s e^{-u(\mathbf{q}_1^2, z_1)},$$

where

$$u(\mathbf{q}_1^2, z_1) = \frac{1}{\pi}\int_{-2.79\mu^2}^{-\frac{2\mu^2}{1-z_1}} \frac{\delta_0\left(-\frac{1}{2}\mathbf{q}_1^2(1-z_1)-\mu^2\right)}{\mathbf{q}_1'^2-\mathbf{q}_1^2}\,\mathrm{d}\mathbf{q}_1'^2,$$

and δ_0 is the s phase-shift of the π-π scattering, and again returning to the function Φ, we obtain the following set of equations for A:

$$A(\mathbf{q}_1^2, z_1, \pm) = \frac{1}{\pi}\int_0^\infty \mathrm{d}\mathbf{q}_1'^2 \eta_\pm \frac{\operatorname{Im} A_{\mathrm{I}}(\mathbf{q}_1'^2, z_1)}{\mathbf{q}_1'^2-\mathbf{q}_1^2} + \frac{1}{\pi}\int_0^\infty \frac{\operatorname{Im} A_{\mathrm{II}}(\mathbf{q}_1'^2, z_1)}{\mathbf{q}_1'^2-q_1^2}\eta_\mp \mathrm{d}\mathbf{q}_1'^2, \quad (19)$$

where

$$\eta_\pm(u, \mathbf{q}_1'^2, \mathbf{q}_1^2) = \tfrac{1}{2}\left[\mathrm{e}^{u(\mathbf{q}_1^2, z_1)-u(\mathbf{q}_1'^2, z_1)} \pm \frac{K(\mathbf{q}_1^2)}{K(\mathbf{q}_1'^2)}\right].$$

To eliminate the non-physical cut in the equations for the B function, consider the functions $\tilde{B} = B/S_1-S_2$ and $\Phi_{sB}\mathrm{e}^{-\beta}/S_1-S_2$, where

$$\beta = \frac{1}{\pi}\int_{-2.79\mu^2}^{-\frac{2\mu^2}{1-z_1}} \frac{\delta_1\left(-\frac{1}{2}\mathbf{q}_1'^2(1-z_1)-\mu^2\right)}{\mathbf{q}_1'^2-\mathbf{q}_1^2}\,\mathrm{d}\mathbf{q}_1'^2,$$

and δ_1 is the p phase-shift of the π-π scatterring.

The function $\Phi_{sB}\mathrm{e}^{-\beta}/S_1-S_2$ does not contain new singularities and the same Mandelstam representation will hold for it as it did for Φ_{sB}.

In a way analogous to that for the function $A(\pm\mathrm{K})$ we obtain the following system for the $\tilde{B}$ function:

$$\tilde{B}(\mathbf{q}_1^2, z_1, \pm K) = \frac{1}{\pi}\int_0^\infty \frac{\operatorname{Im}\tilde{B}(\mathbf{q}_1'^2, z_1, +K)\xi_\pm}{\mathbf{q}_1'^2-\mathbf{q}_1^2}\,\mathrm{d}\mathbf{q}_1'^2 + \frac{1}{\pi}\int_0^\infty \frac{\operatorname{Im}\tilde{B}(\mathbf{q}_1'^2, z_1, -K)\xi_\mp}{\mathbf{q}_1'^2-\mathbf{q}_1^2}\,\mathrm{d}\mathbf{q}_1'^2, \quad (20)$$

where

$$\xi_\pm = \tfrac{1}{2}\left[\mathrm{e}^{\beta(\mathbf{q}_1^2, z_1)-\beta(\mathbf{q}_1'^2, z_1)} \pm \frac{K(\mathbf{q}_1^2)}{K(\mathbf{q}_1'^2)}\right].$$

5. Integral Equations for Partial Scattering Amplitudes

In order to pass from eqs. (19) and (20) to partial amplitude equations, we shall use expansion of $T^{\frac{1}{2}}$ and $T^{\frac{3}{2}}$ into Legendre polynomial series and the unitarity condition

$$\begin{aligned} T^I(\mathbf{q}_1^2, z_1) &= \sum (2l+1)T_l^I(\mathbf{q}_1^2)p_l(z_1), \\ T^I(\mathbf{q}_2^2, z_2) &= \sum (2l+1)T_l^I(\mathbf{q}_2^2)p_l(z_2), \end{aligned} \quad (21)$$

$$\begin{aligned} \operatorname{Im} T_l^I(\mathbf{q}_1^2) &= \frac{1}{8\pi}\frac{|\mathbf{q}_1|}{W(\mathbf{q}_1^2)}|T_l^I(\mathbf{q}_1^2)|^2, \\ \operatorname{Im} T_l^I(\mathbf{q}_2^2) &= \frac{1}{8\pi}\frac{|\mathbf{q}_2|}{W(\mathbf{q}_2^2)}|T_l^I(\mathbf{q}_2^2)|^2. \end{aligned} \tag{22}$$

Here, $I = \frac{1}{2}, \frac{3}{2}$.

Restricting ourselves to s- and p-waves we obtain from eqs. (19)—(20) and from the orthogonality condition of Legendre polynomials

$$\begin{aligned} 2T_l^{\frac{3}{2}}(\mathbf{q}^2)+T_l^{\frac{1}{2}}(\mathbf{q}^2) = \frac{1}{16\pi^2}\int_0^\infty d\mathbf{q}'^2\frac{|\mathbf{q}'|}{W(\mathbf{q}'^2)}\{n_l(\mathbf{q}'^2,q^2)[2|T_0^{\frac{3}{2}}(\mathbf{q}'^2)|^2+|T_0^{\frac{1}{2}}(\mathbf{q}'^2)|^2] \\ +3\varphi_l(\mathbf{q}'^2,\mathbf{q}^2)[2|T_1^{\frac{3}{2}}(\mathbf{q}'^2)|^2+|T_1^{\frac{1}{2}}(\mathbf{q}'^2)|^2]\}, \end{aligned} \tag{23}$$

$$\begin{aligned} T_l^{\frac{1}{2}}(\mathbf{q}^2)-T_l^{\frac{3}{2}}(\mathbf{q}^2) = \frac{1}{16\pi^2}\int_0^\infty d\mathbf{q}'^2\frac{|\mathbf{q}'|}{W(\mathbf{q}'^2)}\{\varepsilon_l(\mathbf{q}'^2,\mathbf{q}^2)[|T_0^{\frac{1}{2}}(\mathbf{q}'^2)|^2-|T_0^{\frac{3}{2}}(\mathbf{q}'^2)|^2] \\ +3\omega_l(\mathbf{q}'^2,\mathbf{q}^2)[|T_1^{\frac{1}{2}}(\mathbf{q}'^2)|^2-|T_1^{\frac{3}{2}}(\mathbf{q}'^2)|^2]\}. \end{aligned} \tag{24}$$

In eqs. (23), (24) the following notations are introduced:

$$W(\mathbf{q}^2)=\sqrt{M^2+\mu^2+2\mathbf{q}^2+2\sqrt{(\mathbf{q}^2+\mu^2)(\mathbf{q}^2+M^2)}},$$

$$f(\mathbf{q}^2,z_1)=\frac{r+2z_1(\mathbf{q}^2+K)-M^2-\mu^2}{2(1-z_1^2)},$$

$$z_2(\mathbf{q}^2,z_1)=1-\frac{f(\mathbf{q}^2,z_1)}{\mathbf{q}^2}(1-z_1),$$

$$\mathscr{D}(\mathbf{q}^2,z_1)=\frac{2K+2\mathbf{q}^2+\mu^2}{2K}\,\frac{rz_1-z_1(M^2+\mu^2)+2(\mathbf{q}^2+K)}{r(1-z_1^2)},$$

$$r=\sqrt{(M^2-\mu^2)^2-4z_1(M^2+\mu^2)(\mathbf{q}^2+K)+4z_1^2M^2\mu^2+4(\mathbf{q}^2+K)^2},$$

$$\tilde{\eta}_-=\eta_-[u(f(\mathbf{q}'^2,z_1),z_1),\mathbf{q}^2,f(\mathbf{q}'^2,z_1)],$$

$$\tilde{\xi}_-=\xi_-[\beta(f(\mathbf{q}'^2,z_1),z_1),\mathbf{q}^2,f(\mathbf{q}'^2,z_1)],$$

$$\alpha_\pm(\mathbf{q}'^2,\mathbf{q}^2,z_1)=\xi_\pm\frac{s_1(\mathbf{q}^2)-s_2(\mathbf{q}^2)}{s_1(\mathbf{q}'^2)-s_2(\mathbf{q}'^2)},$$

$$\tilde{\alpha}_\pm=\tilde{\xi}_\pm\frac{s_1(\mathbf{q}^2)-s_2(\mathbf{q}^2)}{s_1[f(\mathbf{q}'^2,z_1)]-s_2[f(\mathbf{q}'^2,z_1)]},$$

$$n_l(\mathbf{q}'^2,\mathbf{q}^2)=\int_{-1}^{+1}dz_1p_l(z_1)\left[\frac{\eta_+}{\mathbf{q}'^2-\mathbf{q}^2}+\frac{\tilde{\eta}_-\mathscr{D}(\mathbf{q}'^2,z_1)}{f(\mathbf{q}'^2,z_1)-\mathbf{q}^2}\right],$$

$$\varphi_l(\mathbf{q}'^2,\mathbf{q}^2)=\vartheta\left(z_1-\frac{\mu}{M}\right)\int_{-1}^{+1}dz_1p_l(z_1)\left[\frac{\eta_+z_1}{\mathbf{q}'^2-\mathbf{q}^2}+\frac{\tilde{\eta}_-z_2(\mathbf{q}'^2,z_1)\mathscr{D}(\mathbf{q}'^2,z_1)}{f(\mathbf{q}'^2,z_1)-\mathbf{q}^2}\right],$$

$$\varepsilon_l(\mathbf{q}'^2;\mathbf{q}^2)=\int_{-1}^{+1}\mathrm{d}z_1 p_l(z_1)\left[\frac{\alpha_+}{\mathbf{q}'^2-\mathbf{q}^2}+\frac{\tilde{\alpha}_-\mathscr{D}(\mathbf{q}'^2,z_1)}{f(\mathbf{q}'^2,z_1)-\mathbf{q}^2}\right],$$

$$\omega_l(\mathbf{q}'^2,\mathbf{q}^2)=\int_{-1}^{+1}\mathrm{d}z_1 p_l(z_1)\left[\frac{\alpha_+ z_1}{\mathbf{q}'^2-\mathbf{q}^2}+\frac{\tilde{\alpha}_- z_2(\mathbf{q}'^2,z_1)\mathscr{D}(\mathbf{q}'^2,z_1)}{f(\mathbf{q}'^2,z_1)-\mathbf{q}^2}\right].$$

We shall further on proceed from the assumption that in eqs. (23) and (24) it is sufficient to perform one subtraction. In the case under consideration there does not exist a convenient symmetrical point for subtraction as there is in the case of $\pi-\pi$-scattering, since the K-méson and π-meson masses are different. We shall, therefore, agree upon subtracting at the point $\mathbf{q}_1^2=0$. In this case, the s-phase-shifts will be related to scattering lengths $a^{\frac{1}{2}}$ and $a^{\frac{3}{2}}$ by the corresponding isobaric states $T_0^{\frac{1}{2}}$ and $T_0^{\frac{3}{2}}$ which will appear in equations as parameters. As a result of simple calculations, we obtain the following equations

$$\begin{aligned}
&\mathrm{Re}\,[2T_l^{\frac{3}{2}}(\mathbf{q}^2)+T_l^{\frac{1}{2}}(\mathbf{q}^2)]=\mathrm{Re}[2T_l^{\frac{3}{2}}(0)+T_l^{\frac{1}{2}}(0)]\\
&+\frac{1}{16\pi^2}\mathrm{P}\int_0^\infty \mathrm{d}\mathbf{q}'^2\frac{|\mathbf{q}'|}{W(\mathbf{q}'^2)}\{[n_l(\mathbf{q}'^2,\mathbf{q}^2)-n_l(\mathbf{q}'^2,0)][2|T_0^{\frac{3}{2}}(\mathbf{q}'^2)|^2+|T_0^{\frac{1}{2}}(\mathbf{q}'^2)|^2]\\
&+3[\varphi_l(\mathbf{q}'^2,\mathbf{q}^2)-\varphi_l(\mathbf{q}'^2,0)][2|T_1^{\frac{3}{2}}(\mathbf{q}'^2)|^2+|T_1^{\frac{1}{2}}(\mathbf{q}'^2)|^2]\},
\end{aligned}\tag{25}$$

$$\begin{aligned}
&\mathrm{Re}\,[T_l^{\frac{1}{2}}(\mathbf{q}^2)-T_l^{\frac{3}{2}}(\mathbf{q}^2)]=\mathrm{Re}\,[T_l^{\frac{1}{2}}(0)-T_l^{\frac{3}{2}}(0)]\\
&+\frac{1}{16\pi^2}\mathrm{P}\int_0^\infty \mathrm{d}\mathbf{q}'^2\frac{|\mathbf{q}'|}{W(\mathbf{q}'^2)}\{[\varepsilon_l(\mathbf{q}'^2,\mathbf{q}^2)-\varepsilon_l(\mathbf{q}'^2,0)][|T_0^{\frac{1}{2}}(\mathbf{q}'^2)|^2-|T_0^{\frac{3}{2}}(\mathbf{q}'^2)|^2]\\
&+3[\omega_l(\mathbf{q}'^2,\mathbf{q}^2)-\omega_l(\mathbf{q}'^2,0)][|T_1^{\frac{1}{2}}(\mathbf{q}'^2)|^2-|T_1^{\frac{3}{2}}(\mathbf{q}'^2)|^2]\},
\end{aligned}\tag{26}$$

$$\mathrm{Re}\,T_1^{\frac{1}{2}}(0)=\mathrm{Re}\,T_1^{\frac{3}{2}}(0)=0.$$

We shall now obtain a set of equations for partial amplitudes in the system of reaction I for backward scattering. In this case $\mathbf{q}_1^2=\mathbf{q}_2^2$ and $z_1=z_2=-1$. To derive the set of equations we shall proceed from eqs. (19) and (20). The validity of the expansion at the point $z_1=-1$ follows from the analyticity properties of functions A and B at this point.

Thus, we have

$$\begin{aligned}
T^I(\mathbf{q}_1^2,z_1)&=T^I(\mathbf{q}_1^2,-1)+(1+z_1)\partial_{z_1}T^I(\mathbf{q}_1^2,z_1)|_{z_1=-1}+\ldots\\
T^I(\mathbf{q}_2^2,z_2)&=T^I(\mathbf{q}_2^2,-1)+(1+z_2)\partial_{z_2}T^I(\mathbf{q}_1^2,z_2)|_{z_2=-1}+\ldots.
\end{aligned}\tag{27}$$

$$\begin{aligned}
\mathrm{Im}\,T^I(\mathbf{q}_1^2,z_1)&=\frac{|\mathbf{q}_1|}{8\pi W(\mathbf{q}_1^2)}(|T_0{}^I(\mathbf{q}_1^2)|^2+3z_1|T_1{}^I(\mathbf{q}_1^2)|^2+\ldots),\\
\mathrm{Im}\,T^I(\mathbf{q}_2^2,z_2)&=\frac{|\mathbf{q}_2|}{8\pi W(\mathbf{q}_2^2)}(|T_0{}^I(\mathbf{q}_2^2)|^2+3z_2|T_1{}^I(\mathbf{q}_2^2)|^2+\ldots),
\end{aligned}\tag{28}$$

$$T^I(\mathbf{q}_1^2,-1)=T_0{}^I(\mathbf{q}_1^2)-3T_1{}^I(\mathbf{q}_1^2),\qquad \partial_z T^I(\mathbf{q}^2,z)|_{z_1=-1}=3T_1{}^I(\mathbf{q}^2).\tag{29}$$

Employing expressions (27)—(29), expanding integrands in eqs. (19), (20) into Taylor series, equating coefficients of identical powers z_1 and performing one subtraction at the point $\mathbf{q}_1^2 = 0$ we shall obtain a different set of equations for partial amplitudes (in all the equations argument -1 denotes that the function is taken at the point $z_1 = z_2 = -1$):

$$\begin{aligned}
&\mathrm{Re}\,[2T_0^{\frac{3}{2}}(\mathbf{q}^2)+T_0^{\frac{1}{2}}(\mathbf{q}^2)] = \mathrm{Re}[2T_0^{\frac{3}{2}}(0)+T_0^{\frac{1}{2}}(0)] \\
&+\frac{\mathrm{P}}{8\pi^2}\int_0^\infty \mathrm{d}\mathbf{q}'^2\,\frac{|\mathbf{q}'|}{W(\mathbf{q}'^2)}\left\{\frac{2|T_0^{\frac{3}{2}}(\mathbf{q}'^2)|^2+|T_0^{\frac{1}{2}}(\mathbf{q}'^2)|^2}{\mathbf{q}'^2(\mathbf{q}'^2-\mathbf{q}^2)}\times[\mathbf{q}'^2(V(\mathbf{q}'^2,\mathbf{q}^2)-V(\mathbf{q}'^2,0))+\mathbf{q}^2V(\mathbf{q}'^2,0)]\right. \\
&\left.+3\,\frac{2|T_1^{\frac{3}{2}}(\mathbf{q}'^2)|^2+|T_1^{\frac{1}{2}}(\mathbf{q}'^2)|^2}{\mathbf{q}'^2(\mathbf{q}'^2-\mathbf{q}^2)}\,[\mathbf{q}'^2(L(\mathbf{q}'^2,\mathbf{q}^2)-L(\mathbf{q}'^2,0))+\mathbf{q}^2L(\mathbf{q}'^2,0)]\right\}, \qquad (30)
\end{aligned}$$

$$\begin{aligned}
&\mathrm{Re}\,[2T_1^{\frac{3}{2}}(\mathbf{q}^2)+T_1^{\frac{1}{2}}(\mathbf{q}^2)] \\
&=\frac{\mathrm{P}}{8\pi^2}\int_0^\infty \mathrm{d}\mathbf{q}'^2\,\frac{|\mathbf{q}'|}{W(\mathbf{q}'^2)}\left\{\frac{2|T_0^{\frac{3}{2}}(\mathbf{q}'^2)|^2+|T_0^{\frac{1}{2}}(\mathbf{q}'^2)|^2}{\mathbf{q}'^2(\mathbf{q}'^2-\mathbf{q}^2)}\,[\mathbf{q}'^2(C(\mathbf{q}'^2,\mathbf{q}^2)-C(\mathbf{q}'^2,0))+\mathbf{q}^2C(\mathbf{q}'^2,0)]\right. \\
&\left.+3\,\frac{2|T_1^{\frac{3}{2}}(\mathbf{q}'^2)|^2+|T_1^{\frac{1}{2}}(\mathbf{q}'^2)|^2}{\mathbf{q}'^2(\mathbf{q}'^2-\mathbf{q}^2)}\,[\mathbf{q}'^2(Q(\mathbf{q}'^2,\mathbf{q}^2)-Q(\mathbf{q}'^2,0))+\mathbf{q}^2Q(\mathbf{q}'^2,0)]\right\}, \qquad (31)
\end{aligned}$$

$$\begin{aligned}
&\mathrm{Re}\,[T_0^{\frac{1}{2}}(\mathbf{q}^2)-T_0^{\frac{3}{2}}(\mathbf{q}^2)] = \mathrm{Re}\,[T_0^{\frac{1}{2}}(0)-T_0^{\frac{3}{2}}(0)] \\
&+\frac{\mathrm{P}}{8\pi^2}\int_0^\infty \mathrm{d}\mathbf{q}'^2\,\frac{|\mathbf{q}'|}{W(\mathbf{q}'^2)}\left\{\frac{|T_0^{\frac{1}{2}}(\mathbf{q}'^2)|^2-|T_0^{\frac{3}{2}}(\mathbf{q}'^2)|^2}{\mathbf{q}'^2(\mathbf{q}'^2-\mathbf{q}^2)}\,[\mathbf{q}'^2(E(\mathbf{q}'^2,\mathbf{q}^2)-E(\mathbf{q}'^2,0))+\mathbf{q}^2E(\mathbf{q}^2,0)]\right. \\
&\left.+3\,\frac{|T_1^{\frac{1}{2}}(\mathbf{q}'^2)|^2-|T_1^{\frac{3}{2}}(\mathbf{q}'^2)|^2}{\mathbf{q}'^2(\mathbf{q}'^2-\mathbf{q}^2)}\,[\mathbf{q}'^2(F(\mathbf{q}'^2,\mathbf{q}^2)-F(\mathbf{q}'^2,0))+\mathbf{q}^2F(\mathbf{q}'^2,0)]\right\}, \qquad (32)
\end{aligned}$$

$$\begin{aligned}
&\mathrm{Re}\,[T_1^{\frac{1}{2}}(\mathbf{q}^2)-T_1^{\frac{3}{2}}(\mathbf{q}^2)] \\
&=\frac{\mathrm{P}}{8\pi^2}\int_0^\infty \mathrm{d}\mathbf{q}'^2\,\frac{|\mathbf{q}'|}{W(\mathbf{q}'^2)}\left\{\frac{|T_0^{\frac{1}{2}}(\mathbf{q}'^2)|^2-|T_0^{\frac{3}{2}}(\mathbf{q}'^2)|^2}{\mathbf{q}'^2(\mathbf{q}'^2-\mathbf{q}^2)}\,[\mathbf{q}'^2(G(\mathbf{q}'^2,\mathbf{q}^2)-G(\mathbf{q}'^2,0))+\mathbf{q}^2G(\mathbf{q}'^2,0)]\right. \\
&\left.+3\,\frac{|T_1^{\frac{1}{2}}(\mathbf{q}'^2)|^2-|T_1^{\frac{3}{2}}(\mathbf{q}'^2)|^2}{\mathbf{q}'^2(\mathbf{q}'^2-\mathbf{q}^2)}\,[\mathbf{q}'^2(H(\mathbf{q}'^2,\mathbf{q}^2)-H(\mathbf{q}'^2,0))+\mathbf{q}^2H(\mathbf{q}'^2,0)]\right\}, \qquad (33)
\end{aligned}$$

where

$$V(\mathbf{q}'^2,\mathbf{q}^2) = \eta_+(-1)+\partial_{z_1}\eta_+ +\tilde{\eta}_-(-1)\mathscr{D}(\mathbf{q}'^2,-1)+(\mathbf{q}'^2-\mathbf{q}^2)\partial_{z_1}\left[\tilde{\eta}_-\frac{\mathscr{D}(\mathbf{q}'^2,z_1)}{f(\mathbf{q}'^2,z_1)-\mathbf{q}^2}\right]_{z_1=-1},$$

$$L(\mathbf{q}'^2,\mathbf{q}^2) = -\partial_{z_1}\eta_+ -\tilde{\eta}_-(-1)\mathscr{D}(\mathbf{q}'^2,-1)+(\mathbf{q}'^2-\mathbf{q}^2)\partial_{z_1}\left[\tilde{\eta}_-\frac{\mathscr{D}(\mathbf{q}'^2,z_1)z_2(\mathbf{q}'^2,z_1)}{f(\mathbf{q}'^2,z_1)-\mathbf{q}^2}\right]_{z_1=-1},$$

$$C(\mathbf{q}'^2,\mathbf{q}^2) = \partial_{z_1}\eta_+ +(\mathbf{q}'^2-\mathbf{q}^2)\partial_{z_1}\left[\tilde{\eta}_-\frac{\mathscr{D}(\mathbf{q}'^2,z_1)}{f(\mathbf{q}'^2,z_1)-\mathbf{q}^2}\right]_{z_1=-1},$$

$$Q(\mathbf{q}'^2, \mathbf{q}^2) = \eta_+(-1) - \partial_{z_1}\eta_+ + (\mathbf{q}'^2 - \mathbf{q}^2)\partial_{z_1}\left[\tilde{\eta}_- \frac{\mathscr{D}(\mathbf{q}'^2, z_1) z_2(\mathbf{q}'^2, z_1)}{f(\mathbf{q}'^2, z_1) - \mathbf{q}^2}\right]_{z_1=-1},$$

$$E(\mathbf{q}'^2, \mathbf{q}^2) = \alpha_+(-1) + \partial_{z_1}\alpha_+ + \tilde{\alpha}_-(-1)\mathscr{D}(\mathbf{q}'^2, -1) + (\mathbf{q}'^2 - \mathbf{q}^2)\partial_{z_1}\left[\alpha_- \frac{\mathscr{D}(\mathbf{q}'^2, z_1)}{f(\mathbf{q}'^2, z_1) - \mathbf{q}^2}\right]_{z_1=-1},$$

$$F(\mathbf{q}'^2, \mathbf{q}^2) = -\partial_z\alpha_+ - \tilde{\alpha}_-(-1)\mathscr{D}(\mathbf{q}'^2, -1) + (\mathbf{q}'^2 - \mathbf{q}^2)\partial_{z_1}\left[\tilde{\alpha}_- \frac{\mathscr{D}(\mathbf{q}'^2, z_1) z_2(\mathbf{q}'^2, z_1)}{f(\mathbf{q}'^2, z_1) - \mathbf{q}^2}\right]_{z_1=-1},$$

$$G(\mathbf{q}'^2, \mathbf{q}^2) = \partial_z\alpha_+ + (\mathbf{q}'^2 - \mathbf{q}^2)\partial_{z_1}\left[\tilde{\alpha}_- \frac{\mathscr{D}(\mathbf{q}'^2, z_1)}{f(\mathbf{q}'^2, z_1) - \mathbf{q}^2}\right]_{z_1=-1},$$

$$H(\mathbf{q}'^2, \mathbf{q}^2) = -\partial_{z_1}\alpha_+ + \alpha_+(-1) + (\mathbf{q}'^2 - \mathbf{q}^2)\partial_{z_1}\left[\tilde{\alpha}_- \frac{\mathscr{D}(\mathbf{q}'^2, z_1) z_2(\mathbf{q}'^2, z_1)}{f(\mathbf{q}'^2, z_1) - \mathbf{q}^2}\right]_{z_1=-1}.$$

It is observed that in eqs. (25), (26) integration in u and β was performed from $-2.79\mu^2$ to $-2\mu^2/1-z_1$, while in eqs. (30)—(33) from $-4\mu^2$ to $-\mu^2$.

6. Conclusion

It can be seen from eqs. (26), (32)—(33) that we have derived systems of approximate non-linear integral equations which may have several solutions.

One of the possible solutions of these equations is the $T^{\frac{1}{2}} = T^{\frac{3}{2}}$ solution, which coincides with the results obtained in refs. [6, 13]). However, this solution is to be considered approximate, since the subtraction terms $\mathrm{Re}\, T^{\frac{1}{2}}(0)$ and $\mathrm{Re}\, T^{\frac{3}{2}}(0)$ must not, generally speaking, be equal to each other, and, besides, the cross-section of the charge-exchange K—N scattering is known to be non-zero.

Inequality of the subtraction terms can be naturally connected with a different effect exercised by higher-energy baryon states on isobaric spin states $T^{\frac{1}{2}}$ and $T^{\frac{3}{2}}$ of the $\pi-K$ scattering amplitudes.

It is possible that due to the non-linearity of eqs. (26) and (32)—(33) other solutions than the $T^{\frac{1}{2}} = T^{\frac{3}{2}}$ solution may exist even in the case when $\mathrm{Re}\, T^{\frac{1}{2}}(0) = \mathrm{Re}\, T^{\frac{3}{2}}(0)$.

If one takes into account hyperon states in relations (22) and (28), then eqs. (26) and (32)—(33) will involve additional terms which will change even more the $T^{\frac{1}{2}} = T^{\frac{3}{2}}$-solution. However, due to the high energy threshold of hyperon states their role in contributing to eqs. (26), (32)—(33) remains unclear so far.

The authors express their gratitude to D. V. Shirkov, A. V. Efremov and V. A. Meshcheryakov for making available the results of their work [7]) prior to publication, as well as for helpful advice and discussions. We are also indebted to A. A. Anseln and V. M. Schekhter for the discussion of the charge-exchange problem in $\pi-K$-scattering.

References

1) J. Schwinger, Phys. Rev. **104** (1956) 1164
2) S. Minami, Progr. Theor. Phys. **17** (1957) 508
3) A. Pais, Phys. Rev. **112** (1959) 624
4) S. Barshay, Phys. Rev. **109** (1958) 2160; **110** (1958) 743
5) W. Krolikowski, Bull. Acad. Pol. Sc. **8** (1960) 63
6) Chou Kuang-Chao, JETP **38** (1960) 1015
7) A. V. Efremov, V. A. Meshcheryakov and D. V. Shirkov, preprint Joint Institute for Nuclear Research, D-503; JETP **39** (1960) 438
8) C. F. Chew and S. Mandelstam UCRL-8728, preprint
9) G. F. Chew, S. Mandelstam and H. P. Noyes, UCRL-9001, peprint
10) N. N. Muskhelishvili, Singular integral equations (Moscow, 1946);
R. Omnes, Nuovo Cim. **8** (1958) 316
11) S. Mandelstam, Phys. Rev. **115** (1959) 1752
12) E. Gobbson, Theory of spherical and ellipsoidal functions (Moscow, 1952) chapter II
13) S. Okubo, preprint NYO-2627, 1959

1.E.3 *Nuclear Physics* **22** (1961) 677—688; © *North-Holland Publishing Co., Amsterdam*
Not to be reproduced by photoprint or microfilm without written permission from the publisher

EFFECTIVE MOMENTS IN K^{39} AND K^{40}

A. DE-SHALIT †

Institute of Theoretical Physics, Department of Physics, Stanford University, Stanford, California ††

Received 27 October 1960

Abstract: It is pointed out that by comparing magnetic moments of levels belonging to the same nucleon configuration in an odd-odd nucleus, or M1 transitions between such levels, an important information on the effective moments of found nucleons can be obtained. This analysis is carried out for K^{40} and the results agree very well with the magnetic moment of K^{39}. An atempt is made to include the effects of configuration mixing in K^{40}, induced by the residual proton-neutron interaction. A δ-type interaction which reproduces the spectrum of Cl^{38} is assumed. The resulting agreement is considerably deteriorated, indicating that such an admixture of configurations is probably negligible in K^{40}. Further experiments are suggested to check the validity of the concept of an effective moment.

1. Introduction

Nuclear models generally involve a number of simultaneous assumptions. The comparison of a model with experimental results is therefore not always meaningful, since a big enough number of parameters can always be made to fit a limited number of data. One has therefore tried in the past few years to look for experimental evidence which would either support or clearly contradict selected hypotheses in a given model. Bohr and Mottelson's classical analysis of the rotational bands in nuclei, and the observed branching ratios for transitions from any state to the various members of a rotational band, are some of the most outstanding successes of such an approach [1]). It strongly supports the description of nuclear kinematics in terms of collective adiabatic rotations superimposed on an intrinsic structure with higher characteristic frequencies. No further details of the model are involved in explaining the above features. Only if one wants to understand, say, the actual values of the moments of inertia, or of the observed transition rates, does one need to invoke further assumptions of the model.

A similar, though for the time being less spectacular, success has been achieved by Talmi and others in analyzing non-deformed nuclei in terms of the Shell Model [2]). Here again, by using essentially the method of Goudsmit and Bacher [3]), augmented by the techniques of the powerful Racah-Algebra, one is able to

† On leave from the Weizmann Institute of Science, Rehovoth, Israel.

†† Work supported in part by the U.S. Air Force through the Air Force Office of Scientific Research.

test a very few basic features of the Shell Model without invoking other more detailed assumptions. Thus it was possible, in a number of cases, to test successfully the validity of the *jj*-coupling central field approximation with a weak residual effective two-body interaction without making any assumption on the shape of the central field or the detailed properties of the residual interaction. Such tests are made by noting that the above approximation implies certain *relations* between spectra of different nuclei. The violation of such relations would have undermined the very foundations of the Shell Model. Their establishment in an increasing number of cases therefore gives strong support to the Shell Model.

Such general tests have, however, some weakness. It is not clear, usually, whether these relations, predicted on general grounds, would not follow also from other, very different, models. The purpose of this paper is to study further this question. We concentrate, for the sake of this study, on two nuclei, Cl^{38} and K^{40}, the analysis of which has been so successful using the *jj*-coupling shell model[4,5]). We shall first show that the *jj*-coupling wave functions for these nuclei describe also the electromagnetic properties of some of the states. Then, using the neutron-proton interaction as deduced from the level structure of Cl^{38}, we shall try to estimate the contribution of configuration mixing to the electromagnetic properties of these nuclei. The coherence of the picture is thereby considerably deteriorated, indicating that the straightforward use of configuration mixing is perhaps not justified. An analysis of the meaning of the proton-neutron interaction deduced from the levels of Cl^{38} will then show that, under some conditions, this interaction already contains the effects of configuration mixing.

2. The Experimental Data

The experimental information available on Cl^{38} and K^{40}, which is relevant for our discussion, is summarized[6]) in fig. 1. The first four levels of Cl^{38} are believed to be the four states of the configuration $(d_{\frac{3}{2}}, f_{\frac{1}{2}})$, i.e., a proton in $d_{\frac{3}{2}}$ and a neutron

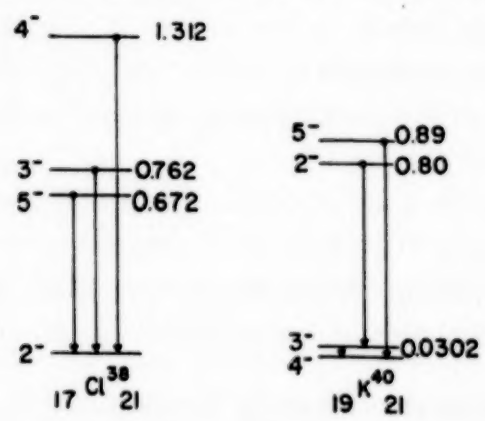

Fig. 1. The energy levels of Cl^{38} and K^{40}.

in $f_{\frac{7}{2}}$. The levels of K^{40} are believed to be those of the configuration $(d_{\frac{3}{2}}^3, f_{\frac{7}{2}})$, which again has four states with $J = 2, 3, 4$, and 5 since the three protons in $d_{\frac{3}{2}}^3$ can give rise only to one state with $J_p = \frac{3}{2}$.

The general relation between the energy levels of the particle-particle configuration (j_1, j_2) and the corresponding hole-particle configuration (j_1^{-1}, j_2) is[5]

$$E(j_1^{-1}, j_2 J) - E_{av}(j_1^{-1}, j_2) = \sum (2J'+1) \begin{Bmatrix} j_1 j_2 J' \\ j_2 j_1 J \end{Bmatrix} [E(j_1 j_2 J') - E_{av}(j_1 j_2)]. \quad (1)$$

Here E_{av} is the average energy in the configuration

$$E_{av}(j_1^{\pm 1}, j_2) = [\sum (2J+1) E(j_1^{\pm 1}, j_2 J)]/(2j_1+1)(2j_2+1),$$

and serves just as a convenient normalization of the energy scale. The symbol in the curly brackets is a 6-j symbol related to the Racah coefficient by

$$\begin{Bmatrix} j_1 j_2 j_3 \\ l_1 l_2 l_3 \end{Bmatrix} = (-1)^{j_1+j_2+l_1+l_2} W(j_1 j_2 l_2 l_1; j_3 l_3).$$

Using eq. 1, the energy levels of Cl^{38}, calculated from those of K^{40}, turn out to be at 0.70, 0.75 and 1.32 MeV in very good agreement with experiment, justifying the configuration and spin assignments of the various levels in Cl^{38} and K^{40}.

Assuming that the states in Cl^{38} and K^{40} are well represented by the configurations (j_1, j_2) and (j_1^3, j_2) respectively $(j_1 \equiv d_{\frac{3}{2}}, j_2 \equiv f_{\frac{7}{2}})$, we can use the resulting wave functions to calculate moments and transition probabilities in these nuclei. Using some simple relations of tensor algebra [7]), we obtain for the magnetic moment in the state $|j_1^p(J_p) j_2^n(J_n); J_f\rangle$ the following expression:

$$\langle J_f \| \mu \| J_f \rangle = (-1)^{J_p + J_n + J_f + 1} (2J_f+1) \times \left[\begin{Bmatrix} J_p J_f J_n \\ J_f J_p 1 \end{Bmatrix} \langle j_1^p J_p \| \mu_p \| j_1^p J_p \rangle + \begin{Bmatrix} J_n J_f J_p \\ J_f J_n 1 \end{Bmatrix} \langle j_2^n J_n \| \mu_n \| j_2^n J_n \rangle \right]. \quad (2)$$

Here, J_p and J_n are the total angular momenta of the p protons in j_1 and the n neutrons in j_2 respectively. The reduced matrix element of the magnetic moment is related to the measured magnetic moment μ by

$$\langle J \| \mu \| J \rangle = \sqrt{\frac{(2J+1)(2J+2)}{2J}}\, \mu. \quad (3)$$

The probability of emission of an M1 radiation in a transition between two states of the *same* configuration is similarly given by

$$T_{i \to f} = \alpha^2 (2J_f+1) \times \left[\begin{Bmatrix} J_p J_f J_n \\ J_f J_p 1 \end{Bmatrix} \langle j_1^p J_p \| \mu_p \| j_1^p J_p \rangle + (-1)^{J_i - J_f} \begin{Bmatrix} J_n J_f J_p \\ J_f J_n 1 \end{Bmatrix} \langle j_2^n J_n \| \mu_n \| j_2^n J_n \rangle \right]^2. \quad (4)$$

Here, J_i and J_f are the spins of the initial state $|j_1^p(J_p), j_2^n(J_n); J_i\rangle$ and the final state $|j_1^p(J_p), j_2^n(J_n); J_f\rangle$ respectively. α^2 is given by

$$\alpha^2 = \tfrac{1}{3}\frac{e^2}{\hbar c}\frac{Mc^2}{\hbar}\left(\frac{E}{Mc^2}\right)^3 = 4.20\times 10^{12}[E(\mathrm{MeV})]^3\ \mathrm{sec}^{-1}, \tag{5}$$

where M is the proton's mass and E is the energy of the transition considered. It is to be noted that, given J_p and J_n, the magnetic moments and M1 transition probabilities are all expressed in terms of the two parameters $\langle j_1^p J_p \| \mu_p \| j_1^p J_p\rangle$ and $\langle j_2^n J_n \| \mu_n \| j_2^n J_n\rangle$. In Cl^{38}, for instance, these two parameters should yield the four magnetic moments of the four states with $J = 2, 3, 4$ and 5 as well as the rate of the three M1 transitions $4^- \to 3^-$, $4^- \to 5^-$, and $3^- \to 2^-$. None of these quantities is presently known; however in K^{40} two similar quantities are known. The measured magnetic moment of the ground state is [8])

$$\mu(K^{40}, 4^-) = -1.298\ \text{n.m.},$$

and the transition probability from 3^- to 4^-, corrected for internal conversion is [9])

$$T_{3^-\to 1^-} = (1.39\pm 0.14)10^8\ \mathrm{sec}^{-1}.$$

Inserting these values into (2) and (4) with $p = 3$, $n = 1$, $J_p = j_1 = \frac{3}{2}$, $J_n = j_2 = \frac{7}{2}$, and using (3), we obtain for the effective magnetic moments of the proton and the neutron in K^{40}

$$\mu_p^{(\mathrm{eff})} = (0.40\pm 0.05)\text{n.m.}, \quad \mu_n^{(\mathrm{eff})} = (-1.65\pm 0.03)\ \text{n.m.} \tag{6}$$

We cannot at this stage check the validity of the model which underlies these two numbers, since they were derived from only two independent measurements. Magnetic moments of other states in K^{40} or other M1 transition rates in this nucleus should be determined before these numbers could be taken more seriously. It is however instructive to compare these values with magnetic moments of other K isotopes, listed in table 1.

TABLE 1

Magnetic moments of the K isotopes

Isotopes	K^{39}	K^{40}	K^{41}	K^{42}	K^{43}	K^{40} M1 transition problem
Experimental	0.391	−1.2982	0.21453	−1.137	±0.163	$(1.39\pm 0.14)\times 10^8\ \mathrm{sec}^{-1}$
Present values	0.40±0.05	−1.298	0.272	−1.273	0.203	$1.39\times 10^8\ \mathrm{sec}^{-1}$
Talmi's values	0.335	−1.256	0.208	−1.199	0.187	$1.11\times 10^8\ \mathrm{sec}^{-1}$

We note first that the effective moment found for the proton in K^{40} is practically identical with the observed moment of K^{39}. The very close fit is

probably accidental in view of the rather large errors in the lifetime of the 3^- state in K^{40} and in the internal conversion coefficient for the M1 transitions; both these quantities were used in deriving $\mu_p^{(eff)}$. However, even with the relatively large error on the calculated value of $\mu_p^{(eff)}$, the fact that it does come out so close to the moment of K^{39} is reassuring, and, as we shall see, of some significance. It is also gratifying that the effective moment of the neutron does come out to have a "reasonable" value, deviating from the Schmidt value (−1.91) in the direction observed for all odd-neutron nuclei.

We also wish to compare the present values of the effective moments with those derived earlier by Talmi [2]). Writing the wave function of the ground state of the K^{39+n} isotope as

$$\psi(K^{39+n} J) = \sum_{J'} a_{J'}^{(n, J)} \psi(d_{\frac{3}{2}}^3, (f_{\frac{7}{2}}^n)_{J'}; J), \tag{7}$$

the coefficients $a_{J'}^{(n, J)}$ can be derived from the observed spectra of some nuclei [10]). Using these coefficients Talmi was able to fit the moments of all the K isotopes by choosing $\mu_p^{(eff)} = 0.335$ and $\mu_n^{(eff)} = -1.56$. His results were included in table

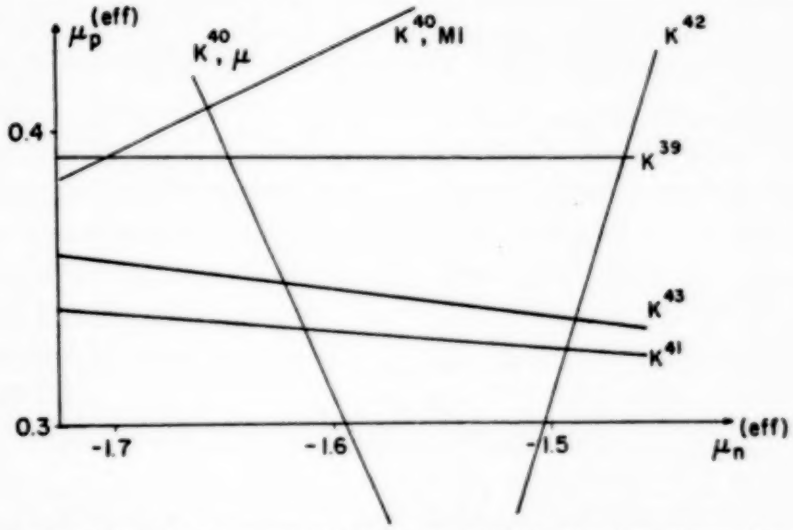

Fig. 2. For each of the isotopes of K we have plotted the line given by the equation $\mu_{exp} = a\mu_p^{(eff)} + b\mu_n^{(eff)}$, where a and b are determined from the configuration assignment as discussed in the text. For the M1 transition in K^{40} we have plotted the line $[T_{(exp)}]^{\frac{1}{2}} = a'\mu_p^{(eff)} + b'\mu_n^{(eff)}$.

1 for comparison; we have added also the M1 transition probability evaluated with his effective moments. We have calculated the magnetic moments of K^{41}, K^{42} and K^{43}, using the same coefficients $a_{J'}^{(n, J)}$, but with the effective moments (6) deduced from K^{40}. The results are included in table 1 in order to demonstrate the sensitivity of the calculated moments to variations in the effective moments. This is illustrated also in fig. 2 which gives, for each isotope, the location of the points $[\mu_p^{(eff)}, \mu_n^{(eff)}]$ which will reproduce the observed moment or transition rates using eq. (7). In an ideal situation all these lines should have intersected

in one point giving a value for $\mu_p^{(eff)}$ and $\mu_n^{(eff)}$ which would reproduce all the data. As seen from fig. 2 we could improve the agreement between the calculated moment and the observed moment for K^{42} by using, for this nucleus, a smaller value of $\mu_n^{(eff)}$ keeping $\mu_p^{(eff)}$ unchanged. This is not unreasonable in view of the fact that K^{42} has three neutrons in the $f_{\frac{7}{2}}$ orbit, and the magnetic moment of Ca^{43} shows that for such a configuration $\mu_n^{(eff)} = -1.315$. We shall come back to this point when we shall discuss possible mechanisms for producing effective moments. Here it is only worthwhile to note that the magnetic moments of K^{42} and K^{43} are not sensitive to the value of $\mu_n^{(eff)}$ (see fig. 2).

3. Interpretation of the Data

The effective moments $\mu_p^{(eff)}$ and $\mu_n^{(eff)}$ are notably different from the Schmidt values. This clearly indicates that the simple single particle wave functions used to describe the various states of K^{40} cannot be the correct wave functions, or that at most they are "model wave functions" whose use is only justified with modified magnetic moment operators.

There were many interesting attempts to explain the deviations of magnetic moments from the Schmidt lines. The most successful one was that suggested by Blin-Stoyle [11]) and Noya, Arima and Horie [12]): Considering a single nucleon in the state $j = l \pm \frac{1}{2}$ they concentrated on admixed states which involved the orbit $j' = l \mp \frac{1}{2}$. Such admixtures give contributions to the magnetic moment which are *linear* in the mixing amplitude, and could therefore lead to appreciable changes in the moments with relatively small changes in the energies. For a nucleus like ${}_{17}Cl^{37}_{20}$ whose shell model wave function in the ground state is given by the proton configuration $(d_{\frac{3}{2}}^6, d_{\frac{3}{2}})_{J=\frac{3}{2}}$ (the neutrons are in a closed shell), a small admixture of the proton configuration $[d_{\frac{3}{2}}^5, (d_{\frac{3}{2}}^2)_2]_{J=\frac{3}{2}}$ would lead to an appreciable change in the magnetic moment. In fact the measured moment is $\mu(Cl^{37}) = 0.684$ n.m. as compared with a Schmidt value of $\mu_{Sch} = 0.124$ n.m. For ${}_{19}K^{39}_{20}$, with 19 protons, the Shell Model configuration in the ground state is $(d_{\frac{3}{2}}^6, d_{\frac{3}{2}}^3)_{J=\frac{3}{2}}$. Here a similar admixture is not possible, since the promotion of a $d_{\frac{3}{2}}$ proton to the $d_{\frac{3}{2}}$ orbit would lead to a closed $d_{\frac{3}{2}}$-shell and the angular momentum of the state will be $\frac{5}{2}$ instead of the required $\frac{3}{2}$. This situation is born out by the observed moment of K^{39}, $\mu(K^{39}) = 0.391$ n.m., which is indeed considerably closer to the Schmidt value than that of Cl^{37}.

If we proceed, however, to K^{40}, its ground state configuration is $(d_{\frac{3}{2}}^6, d_{\frac{3}{2}}^3; f_{\frac{7}{2}})_{J=4}$, and now there is no reason why there should be no admixture of the configuration $(d_{\frac{3}{2}}^5, d_{\frac{3}{2}}^4; f_{\frac{7}{2}})_{J=4}$. Thus, the mechanism which supposedly was operative in causing the deviation of $\mu(Cl^{37})$ from the Schmidt line, and could not operate in K^{39}, is free to operate again in K^{40}. However, we saw in the previous section that the proton effective moment in K^{40} was practically identical with that of K^{39} and was very far from that of Cl^{37}! For some reason,

therefore the above mechanism does not show up in K^{40} although it does in Cl^{37}.

Before we look into the possible reasons for such a behaviour let us try to estimate the expected effects on the magnetic moments of K^{40} due to configuration mixture. For that purpose let us write the wave function for the ground state of K^{40} in the form

$$|J_t\rangle = |J_p, J_n; J_t\rangle + a_p^t |J'_p, J_n; J_t\rangle + a_n^t |J_p, J'_n; J_t\rangle. \tag{8}$$

Here J_p stands for the ground state configuration as well as for its total angular momentum, i. e., "J_p" $= (d_{\frac{3}{2}}^6, d_{\frac{3}{2}}^3)_{J=\frac{1}{2}=J_p}$; similarly J'_p stands for "J'_p" $\equiv (d_{\frac{3}{2}}^5, d_{\frac{3}{2}}^4)_{J=\frac{1}{2}=J'_p}$. For the neutron configuration "J_n" $\equiv f_{\frac{7}{2}}$ and "J'_n" $\equiv f_{\frac{5}{2}}$. The a's are the appropriate admixture coefficients to be discussed later. We also need the corrected wave function for the first excited state in K^{40}, which we shall write as

$$|J_1\rangle = |J_p, J_n; J_1\rangle + a_p^1 |J'_p, J_n; J_1\rangle + a_n^1 |J_p, J'_n; J_1\rangle. \tag{9}$$

Keeping only terms linear in the admixture coefficients a, it is then easy to see that the magnetic moment and the M1 transition rate are given by expressions similar to (2) and (4) with the reduced matrix elements being replaced by the following expressions:

$$\langle J_p \| \mu_p \| J_n \rangle \to \langle J_p \| \mu_p \| J_p \rangle \times \left[1 + \frac{\langle J_p \| \mu_p \| J'_p \rangle}{\langle J_p \| \mu_p \| J_p \rangle} \times \begin{cases} 2a_p^t \dfrac{\begin{Bmatrix} J'_p & J_t & J_n \\ J_t & J_p & 1 \end{Bmatrix}}{\begin{Bmatrix} J_p & J_t & J_n \\ J_t & J_p & 1 \end{Bmatrix}} & \text{(for } \mu\text{)} \\ \dfrac{a_p^t \begin{Bmatrix} J'_p & J_t & J_n \\ J_1 & J_p & 1 \end{Bmatrix} + a_p^1 \begin{Bmatrix} J_p & J_t & J_n \\ J_1 & J'_p & 1 \end{Bmatrix}}{\begin{Bmatrix} J_p & J_t & J_n \\ J_1 & J_p & 1 \end{Bmatrix}} & \text{(for M1)} \end{cases} \right],$$

$$\langle J_n \| \mu_n \| J \rangle \to \langle J_n \| \mu_n \| J_n \rangle \times \left[1 + \frac{\langle J'_n \| \mu_n \| J_n \rangle}{\langle J_n \| \mu_n \| J_n \rangle} \times \begin{cases} 2a_n^t \dfrac{\begin{Bmatrix} J'_n & J_t & J_p \\ J_t & J_n & 1 \end{Bmatrix}}{\begin{Bmatrix} J_n & J_t & J_p \\ J_t & J_n & 1 \end{Bmatrix}} & \text{(for } \mu\text{)} \\ \dfrac{a_n^t \begin{Bmatrix} J'_n & J_t & J_p \\ J_1 & J_n & 1 \end{Bmatrix} + a_n^1 \begin{Bmatrix} J_n & J_t & J_p \\ J_1 & J'_n & 1 \end{Bmatrix}}{\begin{Bmatrix} J_n & J_t & J_p \\ J_1 & J_n & 1 \end{Bmatrix}} & \text{(for M1)} \end{cases} \right]. \tag{10}$$

We see from these expressions that if configuration-mixture is taken into account one no longer expects to be able to express the magnetic moments and transition rates within a given configuration of an odd nucleus with the help of just two effective moments. Unfortunately we do not yet have more than two experimental values of such quantities for a single odd-odd nucleus so that we can have no direct check on the importance of configuration mixing. It is nevertheless interesting to see what configuration mixing would do to the effective moments of K^{40}, since we have found that without such mixing the proton effective moment was so close to that of K^{39}.

Taking for the magnetic moment operator the expression $\boldsymbol{\mu} = g_l \mathbf{l} + g_s \mathbf{s}$, and noting that $\langle d_{\frac{3}{2}}^6 d_{\frac{3}{2}}^3 \tfrac{3}{2} \| \sum \mu_i \| d_{\frac{3}{2}}^5 d_{\frac{3}{2}}^4 \tfrac{5}{2} \rangle = -\langle d_{\frac{3}{2}} \| \mu \| d_{\frac{3}{2}} \rangle$, we obtain

$$\frac{\langle J_p \| \mu_p \| J'_p \rangle}{\langle J_p \| \mu_p \| J_p \rangle} = -\frac{2}{5} \frac{g_s - g_l}{g_l - \frac{1}{5}(g_s - g_l)} \approx -5.5, \quad \frac{\langle J'_n \| \mu_n \| J_n \rangle}{\langle J_n \| \mu_n \| J_n \rangle} = -\sqrt{\tfrac{4}{3}},$$

where for $g_s^{(p)}$ we took the value obtained from the magnetic moment of K^{39}. If we take the free-nucleon value of $g_s^{(p)}$, $|\langle J_p \| \mu_p \| J'_p \rangle / \langle J_p \| \mu_p \| J_p \rangle|$ will be even bigger. Using these values we find that the effective moments in (2) and (4) have to be replaced roughly by

$$\begin{aligned} \langle J_p \| \mu_p \| J_p \rangle &\to \langle J_p \| \mu_p \| J_p \rangle \times \begin{cases} [1 - 13.7 a_p^{\,t}] & \text{for } \mu, \\ [1 + 4.6 a_p^{\,t} - 2.4 a_p^{\,1}] & \text{for M1}, \end{cases} \\ \langle J_n \| \mu_n \| J_n \rangle &\to \langle J_n \| \mu_n \| J_n \rangle \times \begin{cases} [1 + 0.8 a_n^{\,t}] & \text{for } \mu, \\ [1 + 0.2 a_n^{\,t} - 3.4 a_n^{\,1}] & \text{for M1}. \end{cases} \end{aligned} \tag{11}$$

The admixture amplitudes a_p and a_n are given, in first order, by

$$a_p^{\,t} = -\frac{\langle J'_p, J_n; J_t | V_{pn} | J_p, J_n; J_t \rangle}{|E(J'_p) - E(J_p)|}, \quad \text{etc.}, \tag{12}$$

where $|E(J'_p) - E(J_p)|$ is the magnitude of the excitation energy from J_p to J'_p. Only V_{pn} contributes to these amplitudes, the contributions of V_{pp} and V_{nn} vanishing on account of $J_p \neq J'_p$. We have, of course, no direct knowledge of V_{pn}, but *if it is the same interaction* between all protons and neutrons in K^{40} we can estimate it in the following way: The splitting of the energy levels in Cl^{38} is presumably due to the interaction between a $d_{\frac{3}{2}}$ proton and an $f_{\frac{7}{2}}$ neutron. If we assume for this interaction the form

$$V_{pn} = [g_0 + g_1 \boldsymbol{\sigma}_p \cdot \boldsymbol{\sigma}_n] \delta(\mathbf{r}_p - \mathbf{r}_n), \tag{13}$$

we find that

$$g_0 F_0 = -0.930 \text{ MeV}, \qquad g_1 F_0 = -0.089 \text{ MeV}, \tag{14}$$

reproduces quite well the level-spacings (F_0 is a Slater integral). Indeed, using

the results derived elsewhere [13]) we find then for these spacings the following values (in MeV):

	$E(J=5)-E(J=2)$	$E(J=3)-E(J=2)$	$E(J=4)-E(J=2)$
Calc	0.606	0.731	1.360
Exp	0.672	0.762	1.312

The values (14) for the strength of the δ-force between protons and neutrons are also in qualitative agreement with other estimates [12]). We therefore feel that, provided V_{pn} does not depend strongly on the configurations considered, we can use (13) and (14) to estimate the coefficients a_p^f, etc. This turns out to be very convenient since these coefficients then involve the same Slater integral F_0, and its explicit evaluation can be avoided. For the energy denominator in (12) we take $|E(d_{\frac{5}{2}})-E(d_{\frac{3}{2}})| \approx 6$ MeV and $|E(f_{\frac{7}{2}})-E(f_{\frac{5}{2}})| \approx 8$ MeV. These values may be somewhat on the high side, but as we shall see, even they lead to very big configuration-mixing effects. We obtain then, for the mixing amplitudes, the following values:

$$a_p^f = -0.07, \quad a_p^i = +0.08, \quad a_n^f = 0.02, \quad a_n^i = +0.04. \tag{15}$$

Thus, with the above configuration mixing the magnetic moment of, and the M1 transition to, the ground state of K^{40} are given by

$$\mu = \tfrac{8}{15}\mu_p^{(eff)}(1+0.96)+\tfrac{32}{35}\mu_n^{(eff)}(1-0.02),$$
$$T_{i\to f} = \tfrac{20}{21}\alpha^2[\mu_p^{(eff)}(1-0.5)-\tfrac{3}{7}\mu_n^{(eff)}(1-0.14)]^2.$$

These equations, when taken with the experimental values, lead to the solution $\mu_n^{(eff)} = -2.26$ and $\mu_p^{(eff)} = 0.70$. Thus we see that even a "conservative" estimate of configuration mixing, when applied consistently to K^{40} does not give very reasonable values for the effective, "unperturbed," values of the magnetic moments. We must conclude from these results that although a proton-neutron interaction is seemingly effective in producing the splittings of the levels in Cl^{38} and K^{40}, this interaction does not admix the $d_{\frac{3}{2}}^6$, $d_{\frac{3}{2}}^1$ states with those of $d_{\frac{3}{2}}^5$, $d_{\frac{3}{2}}^4$.

4. Discussion

The conclusion that Cl^{38} and K^{40} are described well by *jj*-coupling [4, 5]) was reached on the basis of the very nice agreement between experiment and the predictions of eq. (1). It must, however, be remembered that whereas the *jj*-coupling shell model implies, to first order in $\sum V_{pn}$, the relation (1) between the spectra of Cl^{38} and K^{40}, the reverse statement is not necessarily true. One

can think of more general conditions under which a relation identical with eq. (1) will continue to hold. Let us consider, for example, some second order contributions to the energies of Cl^{38} and K^{40}, induced by the proton-neutron interaction. If we excite a neutron from j_2 to j'_2 we obtain in Cl^{38}

$$E(j_1 j_2 J) = \langle j_1 j_2 J | V_{\rm pn} | j_1 j_2 J \rangle + \sum_{j'_2} \frac{|\langle j_1 j_2 J | V_{\rm pn} | j_1 j'_2 J \rangle|^2}{\Delta E}.$$

The same excitation in K^{40} will lead to

$$E(j_1^{-1} j_2 J) = \langle j_1^{-1} j_2 J | \sum V_{\rm pn} | j_1^{-1} j_2 J \rangle + \sum_{j'_2} \frac{|\langle j_1^{-1} j_2 J | \sum V_{\rm pn} | j_1^{-1} j'_2 J \rangle|^2}{\Delta E}.$$

Assume for a moment that $V_{\rm pn}$ is a pure interaction between two multipoles of order k, $V_{\rm pn} = \mathbf{T}^{(k)}(\mathrm{p}) \cdot \mathbf{T}^{(k)}(\mathrm{n})$. In this case it is easy to see that

$$\langle j_1^{-1} j_2 J | \sum_{\rm p} \mathbf{T}^{(k)}_{(\rm p)} \cdot \mathbf{T}^{(k)}_{(\rm n)} | j_1^{-1} j'_2 J \rangle = (-1)^{k+1} \langle j_1 j_2 J | \mathbf{T}^{(k)}_{(\rm p)} \cdot \mathbf{T}^{(k)}_{(\rm n)} | j_1 j'_2 J \rangle.$$

Hence, if k is odd, then we have for such an interaction

$$E(j_1 j_2 J) = E(j_1^{-1} j_2 J),$$

and this relation holds both in first order as well as if we include the special second order contributions described above. The same remains valid also if $V_{\rm pn}$ is a *sum* of interactions between multipoles of odd orders. However, if $V_{\rm pn}$ is an interaction between multipoles of *even* orders only, we find that

$$E(j_1^{-1} j_2 J) = \langle j_1^{-1} j_2 J | \sum V^{\rm even}_{\rm pn} | j_1^{-1} j_2 J \rangle + \sum \frac{|\langle j_1^{-1} j_2 J | \sum V^{\rm even}_{\rm pn} | j_1^{-1} j'_2 J \rangle|^2}{\Delta E}$$

$$= -\langle j_1 j_2 J | V^{\rm even}_{\rm pn} | j_1 j_2 J \rangle + \sum \frac{|\langle j_1 j_2 J | V^{\rm even}_{\rm pn} | j_1 j'_2 J \rangle|^2}{\Delta E}.$$

Therefore, to first order in perturbation theory, we have

$$E(j_1 j_2 J) = -E(j_1^{-1} j_2 J),$$

but this relation is no longer satisfied when we include contributions of second order.

Although this example is especially simple, it already shows that a relation like eq. (1) can well be satisfied even if parts of the interaction are included to higher than first order. One may be tempted to equate all such contribution to an expectation value of an "effective interaction," thereby actually defining this effective interaction. This, however, is generally not very meaningful, since higher order corrections which do not alter the relation between $E(j_1 j_2 J)$ and $E(j_1^{-1} j_2 J)$, may, generally, affect the relation between $E(j_1 j_2 J)$ and, say, $E(j_1^2 j_2 J)$. We can only speak of an "effective interaction" if its matrix elements

can repoduce the spectra of the configurations $j_1^p j_2^n$ with arbitrary values of p and n.

The admixture of excited configurations given by (15) affects the energies of the levels in K^{40} and Cl^{38} very little — by a few keV at most. It would therefore be hard to eliminate them or to confirm their existence on the basis of measured energies. The moments and transition probabilities, which may involve these coefficients linearly, are more sensitive tests, as we have seen. It seems from our results that even these small admixtures are not there in K^{40}, and that one gets a better description of the levels of K^{40} by using pure shell model wave functions with effective moments. The necessity of using effective moments of course means that the shell model wave functions we are using are functions of "quasi-particles" (not necessarily identical with those of BCS) rather than functions of the simple real particles. In this sense they may involve even a big admixture of real particle states. However, the interesting thing is that the mechanism which produces these single quasi-particle wave functions does it for each particle separately without being influenced by the presence of the other particles. This is, at least, what is indicated by the close fit of the effective moment of the protons in K^{40} and in K^{39}. A simple configuration mixing has not got this feature; there the admixture, and therefore also the resulting "effective moment", does depend on the state of the other nucleons and cannot, generally, be done for each nucleon separately.

These conclusions are highly speculative since they are based on the detailed analysis of only one case. There are, however, some indications that they may have a more general validity. We mentioned already that the moment of ${}_{17}Cl^{37}_{20}$, when compared with that of ${}_{19}K^{39}_{20}$, does show an effect which may be interpreted by admixing the proton configuration $d_{\frac{3}{2}}^5$, $d_{\frac{3}{2}}^2$. This admixture can take place via the proton-proton interaction and could therefore exist despite the apparent absence of the similar admixture induced by the proton-neutron interaction. Similarly we can expect that in ${}_{19}K^{42}_{23}$, for instance, the effective moment of the $f_{\frac{7}{2}}^3$ neutron configuration will be different from that of the single $f_{\frac{7}{2}}$ neutron configuration. Indeed, through the neutron-neutron interaction, we can admix the configuration $f_{\frac{7}{2}}^2$, $f_{\frac{3}{2}}$, thereby reducing the magnitude of the effective moment. A similar admixture in the $f_{\frac{7}{2}}^1$ configuration could proceed only via the proton-neutron interaction. The magnetic moment of Ca^{43}, presumably that of the $f_{\frac{7}{2}}^3$ configuration, is found to be $\mu = -1.315$ as compared with $\mu = -1.65$ we have found for the effective moment of the single $f_{\frac{7}{2}}$ neutron in K^{40}. We see from fig. 2 that for K^{42} we do indeed obtain a better agreement with the experimental moment if we reduce the magnitude of $\mu_n^{(eff)}$.

The usefulness of the concept of an effective moment can be put to a very direct experimental test. Already for K^{40} we see that our analysis will predict a magnetic moment $\mu = -1.65$ n.m. for Ca^{41}. It was often claimed that Ca^{41}, being a closed LS-coupling nucleus plus one particle, should have just the

Schmidt value for its magnetic moment, like the well-known case of O^{17}. However, the same argument holds for K^{39} whose moment, though close to the Schmidt value, does deviate from it significantly. Drell and Walecka [13]) have recently re-evaluated the contribution of the Pauli principle to the quenching of the magnetic moment. They point out that it is of the same order of magnitude as a number of other small effects which change the magnetic moment of a bound nucleon. It could then be that the agreement of the moment of O^{17} with the Schmidt value is, in a sense, accidental.

Other tests, still in K^{40} or Cl^{38}, would involve measurements of M1 transition probabilities between the states of the configuration $d_{\frac{3}{2}}^{-1}$, $f_{\frac{7}{2}}$ or those of $d_{\frac{3}{2}}$, $f_{\frac{7}{2}}$, as well as magnetic moments of the unstable states in these configurations. If the effective moment approximation is valid, one would expect these quantities to be given by (2) and (4) with the values (6) for the effective moments in K^{40}, and with $\mu_p^{(\mathrm{eff})} = \mu(Cl^{37}) = 0.68$ n.m. $\mu_n^{(\mathrm{eff})} = -1.65$ n.m. for the levels in Cl^{38}. Experiments could be carried out also in other nuclei, the most promising ones being, perhaps, the odd isotopes of Tl.

Similar analysis can be undertaken for the study of effective charges by measuring quadrupole moments and E2 transition probabilities in odd nuclei.

This study was inspired by Talmi's interpretation of the magnetic moments of the ground states of the K isotopes. I should like to thank him for making his results available to me before their publication.

It is also a pleasure to thank Professor L. I. Schiff and the staff of the Department of Physics at Stanford University for their wonderful hospitality, and many stimulating discussions.

References

1) See, for instance, the review article by A. Kerman in Nuclear Reactions, edited by P. M. Endt and M. Demeur (North-Holland Publishing Co., Amsterdam 1959)
2) A survey of the methods employed in this analysis, and many of the results thus obtained, is given in I. Talmi and I. Unna, Ann. Rev. Nuclear Sci. **10** (1960) (to be published)
3) S. Goudsmit and R. F. Bacher, Phys. Rev. **46** (1934) 948
4) S. Goldstein and I. Talmi, Phys. Rev. **102** (1956) 589
5) S. P. Pandya, Phys. Rev. **103** (1956) 956
6) The data in eq. 1 is taken from Nuclear Data Sheets and ref. [4])
7) For a compilation of such relations, see M. Rottenberg, R. Bivins, N. Metropolis and J. K. Wooten, The 3-*j* and 6-*j* symbols (Technology Press, Massachusetts Institute of Technology, 1959)
8) Nuclear Data Sheets
9) L. J. Lynch and R. E. Holland, Phys. Rev. **114** (1959) 825
10) B. Oquidam and B. Jancovici, Nuovo Cim. **11** (1959) 578
11) R. J. Blin-Stoyle, Rev. Mod. Phys. **28** (1956) 75, and references quoted there
12) For an extensive list of references see H. Noya, A. Arima and H. Horie, Suppl. Progr. Theoret. Phys. **8** (1958) **33**
13) A. de-Shalit, Phys. Rev. **91** (1953) 1479
14) S. Drell and J. D. Walecka, Phys. Rev. (to be published)

3.B

Nuclear Physics **22** (1961) 689—691; ©*North-Holland Publishing Co., Amsterdam*

Not to be reproduced by photoprint or microfilm without written permission from the publisher

CONCERNING THE DECAY OF Se^{75}

E. P. GRIGORIEV and A. V. ZOLOTAVIN

Leningrad State University, Leningrad, USSR

Received 20 August 1960

Abstract: No lines corresponding to the 188 keV and 203 keV have been detected in the internal and external conversion spectrum of Se^{75}.

In 1959 and 1960 there have appeared several papers concerned with the radiation of Se^{75} [1–5]). The investigations performed by De Croës and Bäkström [5]) reveal 188 and 203 keV transitions (fig. 1) which were not observed in other investigations. Basing themselves on their results, the authors complemented the scheme of As^{75} levels with a new, 76 keV level lying below the first excited 199 keV of As^{75} hitherto known.

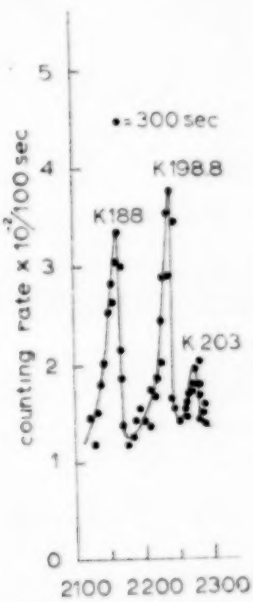

Fig. 1. A portion of the spectrum of internal conversion electrons of Se^{75} according to ref. [5]). R is a conventional unit of current in the magnet coil.

The results we have obtained in investigating the decay of Se^{75} warrant the conclusion that the conversion lines found in ref. [5]) do not belong to the radiation of Se^{75} but are caused by radioactive contaminations or instrument effects. Fig. 2 represents the same portion of conversion spectrum as fig. 1. We have obtained this spectrum while using the preparation of Se enriched by the isotope

of Se^{74} up to ≈ 40 % for making Se^{75}. As is clear from fig. 2, the 188 and 203 keV lines (fig. 1) would be well perceptible if they belonged to the decay of Se^{75}. Besides, no lines with close intensities are observed near the K lines of the

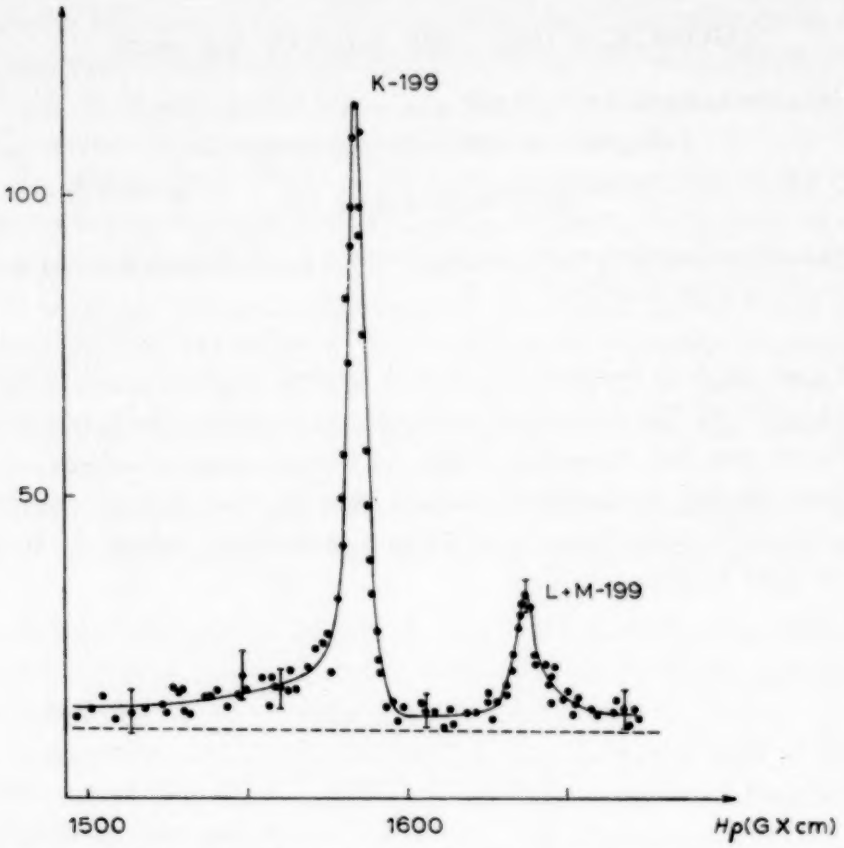

Fig. 2. A portion of the spectrum of internal conversion electrons of Se^{75} according to ref. [2]). A dot-and-dash line represents the background of the counter.

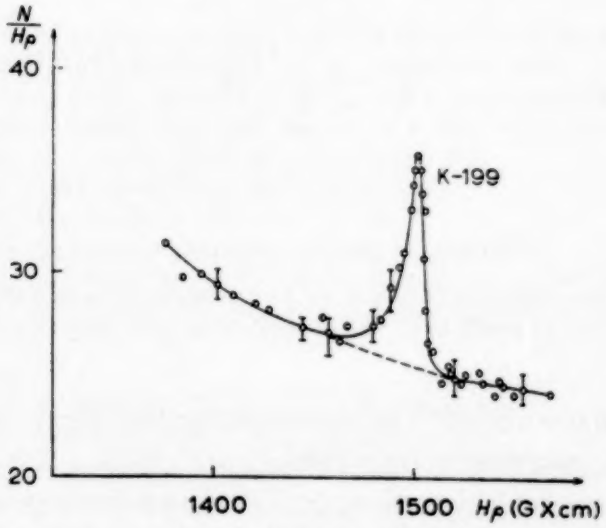

Fig. 3. A portion of the spectrum of photoelectrons in the region of 199 keV transition with a target of Ag (0.25 mg/cm²).

199 keV transition (fig. 3) in investigating the spectrum of photoelectrons [2]).

From the above it follows that there are as yet no grounds for introducing the 76 keV excited level of As^{75} [5]).

References

1) A. A. Bashilov and V. V. Ilyin, Izv. Akad. Nauk SSSR (Ser.-Fiz.) **23** (1959) 154
2) E. P. Grigoriev, A. V. Zolotavin, V. N. Klementyev and P. V. Sinitzyn, Izv. Akad. Nauk SSSR (Ser.-Fiz.) **23** (1959) 159;
E. P. Grigoriev and A. V. Zolotavin, Nuclear Physics **14** (1959/60) 443
3) W. F. Edwards, C. J. Galagher, Jr., and J. W. Dumond, Bull. Am. Phys. Soc. **4** (1959) 279
4) F. R. Metzger and W. B. Todd, Nuclear Physics **10** (1959) 220
5) M. de Croës and G. Bäkström, Arkiv f. Fys. **16** (1960) 567

2.G

Nuclear Physics **22** (1961) 692—697; ©*North-Holland Publishing Co., Amsterdam*

Not to be reproduced by photoprint or microfilm without written permission from the publisher

ANGULAR DISTRIBUTION OF THE $V^{51}(n, d)Ti^{50}$ GROUND STATE DEUTERONS

I. ŠLAUS, P. TOMAŠ and N. STIPČIĆ

Institute "Rudjer Bošković", Zagreb, Yugoslavia

Received 24 October 1960

Abstract: The angular distribution of deuterons from the reaction $V^{51}(n, d)Ti^{50}_{gs}$ has been measured at the incident neutron energy of 14.4 MeV by means of a thin scintillator method. The data show a pronounced maximum at 40° indicating the predominance of the direct interaction process. A reasonable fit has been obtained with a Butler $L_p = 3$ curve using $r_0 = 6.15 \times 10^{-13}$ cm. The reduced width has been found to be 0.03.

1. Introduction

It is well known that the study of (d, p), (d, n), (n, d) and (p, d) reaction may yield valuable information concerning both the properties of the nuclear states involved and the reaction mechanism [1, 2]). Several measurements of the angular distributions of deuterons from (n, d) reactions on elements up to $A = 35$ have been performed [3]) and it was found that the data could be successfully analyzed in terms of a direct interaction theory. Recently a systematic study of (n, d) reactions has been initiated at the CISE laboratory [4]). However, the experimental material for (n, d) reactions on heavier nuclei is still rather scarce. The study of the angular distribution of deuterons from the $V^{51}(n, d)Ti^{50}$ reaction has been undertaken with the aim to contribute to the investigation of (n, d) reactions in the region of medium heavy nuclei.

2. Experimental

Monoenergetic neutrons were produced by means of the $T(d, n)He^4$ reaction using the deuteron beam from a 200 keV Cockcroft-Walton accelerator at the Institute "Rudjer Bošković" [5]). The source provided 14.4 MeV neutrons of approximately 0.3 MeV width at the laboratory angle (60° to the incident deuterons) employed in the experiment.

The neutron flux was measured in three independent ways. First, by measuring neutrons either with an anthracene scintillation counter or with a Hornyak scintillator (NE 451). Second, by a BF_3 counter. Third, by detecting alpha particles from the $T(d, n)He^4$ reaction. The background was reduced by using as a detector a thin crystal scintillator counter. A CsI(Tl) crystal was polished down to a thickness of 10 mg/cm². The pulses from the scintillation counter,

after passing through standard electronic equipment, were analyzed in the multichannel pulse height analyzer. A typical spectrum is shown on fig. 1.

The agreement among the monitors was usually better than 5 %. During the measurement the neutron yield was kept constant and equal to 10^9 neutrons/sec.

The measurement of the angular distribution of deuterons from the $V^{51}(n, d)Ti^{50}$ reaction was performed in a small scattering chamber equipped with a scintillation counter. Deuterons were detected by a CsI(Tl) crystal

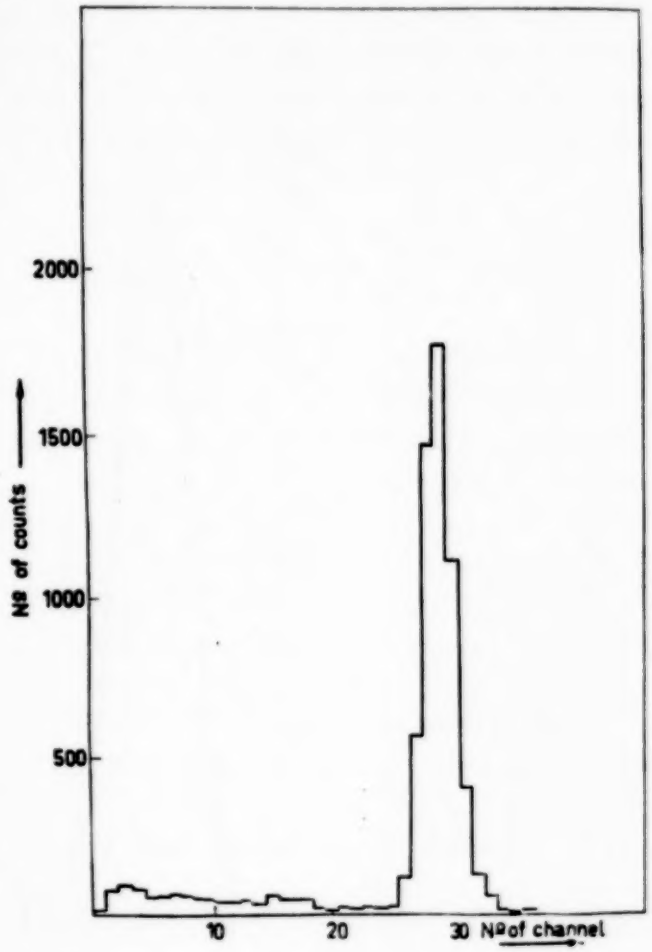

Fig. 1. Spectrum of alpha particles from the $T(d, n)He^4$ reaction.

polished down to a thickness of 100 ± 6 mg/cm². The area of the crystal was 120 mm². In order to have the crystal thickness always sufficient to just stop deuterons, of energy varying from 7.5 MeV to 8.7 MeV in laboratory system, the effective thickness of the crystal was changed from angle to angle by changing its orientation relative to the target. In front of the detector was a gold collimator and the target was put at the end of it. In such an arrangement the resolution of the scintillation counter for Po^{210} alpha particles was 6 %. Pulses from the detector, after passing through the standard electronic equipment, were analyzed by a 256-channel pulse-height analyzer.

The energy scale was determined by means of 14 MeV recoil protons and alpha particles from standard sources (Po^{210} 5.3 MeV, ThC 6.05 MeV and ThC′ 8.78 MeV).

The measurements were performed in a poor geometry arrangement. The distance between the neutron source and the target was usually 12 cm, and the distance between the target and the detector 9 cm. This results in an average angular resolution of $\pm 10°$.

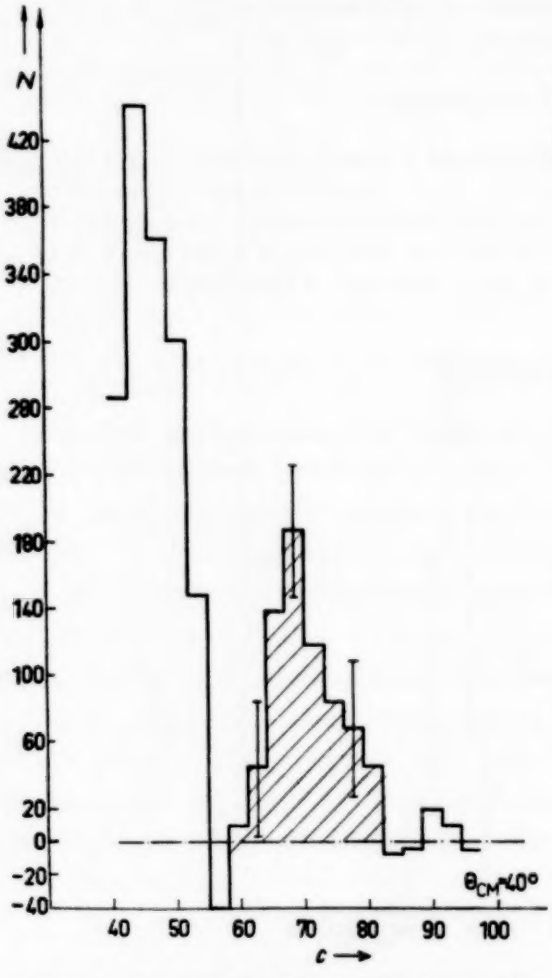

Fig. 2. The pulse height distribution obtained by neutron bombardment of vanadium after the background has been subtracted. The measurement was done at the laboratory angle of 38°.

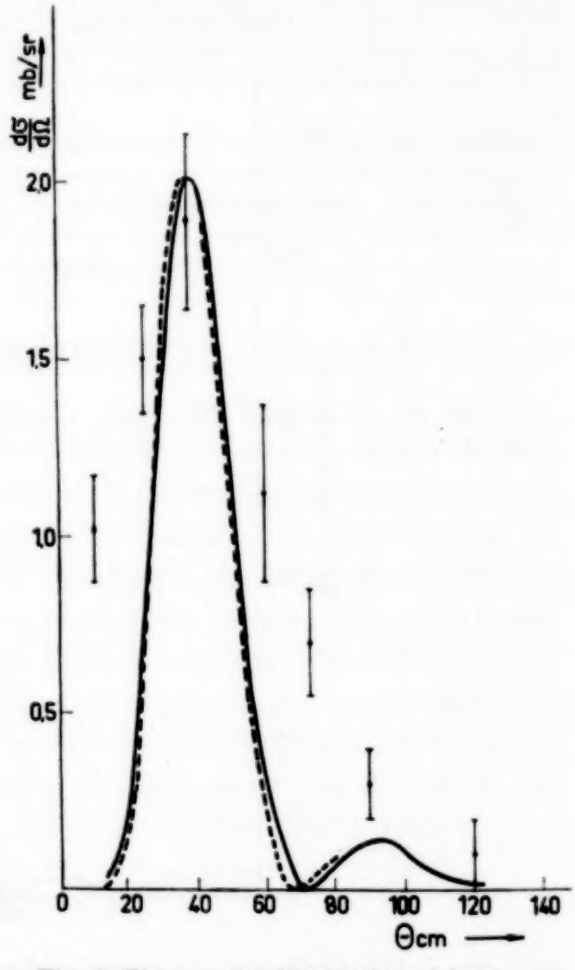

Fig. 3. The angular distribution of deuterons from the $V^{51}(n, d)Ti^{50}$ reaction. The vertical bars represent the statistical error. The solid curve is a pick up $L_p = 3$ curve with $r_0 = 6.15 \times 10^{-13}$ cm. The dotted curve is calculated by taking into account the Coulomb effects on the transferred nucleon.

The target was a commercial vanadium foil, 9.5 ± 0.5 mg/cm² thick. A 9 mg/cm² gold absorber was placed in front of the detector to increase the relative separation between the ground state and first excited states deuterons and also to separate alpha particles from deuterons.

A pulse height distribution obtained by neutron bombardment of vanadium

with the detector set at the laboratory angle of 38°, after the background has been subtracted, is shown on fig. 2. The shaded area represents the ground state deuteron group.

3. Results

The experimental values of the absolute differential cross section for the reaction $V^{51}(n, d)Ti^{50}_{gs}$ are plotted versus the centre of mass angle on fig. 3. The vertical bars represent the statistical error.

In a poor geometry experiment the observed cross section σ_{obs} can significantly differ from the value $\sigma(\theta_0)$ at the nominal angle θ_0, especially if the cross section varies rapidly with the angle. Effects due to the finite geometry have been eliminated using the following expression [6]):

$$\sigma_{obs} = \sigma(\theta_0)\left[1+a+b\frac{\sigma'(\theta_0)}{\sigma(\theta_0)}+c\frac{\sigma''(\theta_0)}{\sigma(\theta_0)}\right],$$

where a, b and c are constants depending on the size of the target, its orientation, the aperture of the detector and the distance between the target and the detector. The derivatives are with respect to the angle.

The finite geometry correction never exceeded 10 % and we estimated that the uncertainty in it was less than 2 %.

While the relative accuracy of the data within the angular distribution is well represented by the statistical errors, the total error in the measurement of the absolute cross section can be as much as 100 %. The main source of error comes from the large background which decreases steeply with the pulse height. The peak of ground state deuterons after subtracting the background was superimposed on a tail of the pulse height distribution of other particles. The uncertainty in subtracting this type of background is estimated to amount to 10 %. The absolute measurement of the neutron flux was done with an accuracy of 15 %.

In the measurement a target of natural vanadium was employed. The natural vanadium is composed of 99.76 % of V^{51} and 0.24 % of V^{50} and as there is no reason why the cross sections for the (n, d) reactions on these two isotopes should considerably differ we neglected the contribution from the $V^{50}(n, d)Ti^{49}$ reaction.

4. Discussion

The angular distribution shows a pronounced maximum at 40° indicating the predominance of the direct interaction process. The spin and the parity of the ground state of V^{51} have been directly determined to be $\frac{7}{2}-$ (ref. [7])) and it is expected that the ground state configuration is $(f_{\frac{7}{2}})^3_{\frac{7}{2}}-$ for protons with a complete $f_{\frac{7}{2}}$ shell of neutrons. Since the ground state of Ti^{50} is 0+ with the proton

configuration $(f_{\frac{7}{2}})^2_{0+}$, one expects that the angular distribution could be fitted with a pick up $L_p = 3$ curve. The solid curve on fig. 3 is a pick up $L_p = 3$ curve calculated from Lubitz's tables [8]) by using $r_0 = 6.15 \times 10^{-13}$ cm. The value of r_0 is close to the Gamow-Critchfield value $(1.22\ A^{\frac{1}{3}} + 1.7) \times 10^{-13}$ cm, and is also in agreement with the analysis of (d, p) reaction on calcium, chromium and vanadium [9]).

A similar structure of the ground states of Ti^{50} and V^{51} implies a large reduced width. Assuming that the reaction proceeds entirely through a pick up process and that Coulomb and nuclear interactions between the nuclei and particles involved in the reaction can be neglected, the reduced width θ^2 has been extracted following the procedure of MacFarlane and French [10]) and it was found to be 0.03. This value is for a factor of 3—4 larger than the one obtained from stripping reactions at a similar energy, involving nuclear states represented by a complete proton shell and an $(f_{\frac{7}{2}})^3_{\frac{7}{2}-}$ neutron configuration.

In view of the scarcity of data and rather large error a distorted wave Born approximation analysis has not been attempted. However, in $[A+1, Z+1]+n \leftrightarrow [A, Z]+d$ reactions the corrections due to the Coulomb interaction between the nucleus and the transferred proton can easily be taken into account following the technique due to Butler [2]). The wave number k corresponding to the binding energy of the transferred nucleon should be replaced by k^* determined from the equation

$$k^{*2} = k^2 + \frac{2m_c}{\hbar^2} \frac{Ze^2}{r_0},$$

where m_c is the reduced mass of the nucleus $[A]$ and the transferred nucleon.

The cross section $\sigma^L_{tab}(x, k^* r_0)$ given in Lubitz's tables should be replaced by

$$\sigma^{*L}_{tab}(x, k^* r_0) = \left(\frac{x^2 + k^{*2} r_0^2}{x^2 + k^2 r_0^2}\right)^2 \sigma^L_{tab}(x, k^* r_0).$$

The dotted curve on fig. 3 is the curve calculated according to this procedure. It was found that in order to fit the experimental points one should use $r_0 = 6.45 \times 10^{-13}$ cm. The related reduced width has been found to be 0.026.

It is evident that at this bombarding energy and for a reaction with a not too negative Q value ($Q = -5.82$ MeV) the shape of the Butler pick up curve does not change appreciably by taking into account the Coulomb effect on the transferred nucleon. The broader experimental maximum can be due to Coulomb effects on the outgoing deuterons and to the nuclear interactions.

References

1) S. T. Butler, Proc. Roy. Soc. A **208** (1950) 559
2) S. T. Butler, O. M. Hittmair, Nuclear stripping reactions (John Wiley, New York 1957)

3) F. L. Ribe, Phys. Rev. **87** (1952) 205;
R. R. Carlson, Phys. Rev. **107** (1957) 1094;
Glenn M. Frye, Jr., Phys. Rev. **93** (1954) 1086;
G. E. Veljukov, A. N. Prokofjev and S. V. Starobudcev, Doklady AN SSSR **127** (1959) 781;
G. E. Veljukov, A. N. Prokofjev and S. V. Starobudcev, JETP **39** (1960) 563
4) L. Colli, F. Cvelbar, S. Micheletti and M. Pignanelli, Nuovo Cim. **14** (1959) 1220;
L. Colli, F. Cvelbar, S. Micheletti and M. Pignanelli, Nuovo Cim. **14** (1959) 81;
L. Colli private communication
5) M. Paić, K. Prelec, P. Tomaš, M. Varićak and B. Vošicki, Glasnik mat.-fiz. i astr. **12** (1957) 269;
B. Antolković, M. Paić, K. Prelec and P. Tomaš, Glasnik mat.-fiz. i astr. **15** (1960) 61
6) I. E. Dayton, G. Schrank, Phys. Rev. **101** (1956) 1358
7) B. Bleany, D. J. E. Ingram and H. E. D. Scovil, Proc. Phys. Soc. A **64** (1951) 601
8) C. R. Lubitz, Numerical table of Butler-Born approximation stripping cross sections, University of Michigan Report (1957)
9) C. K. Bockelman, C. M. Braams, C. P. Browne, W. W. Buechner, R. R. Sharp and A. Sperduto, Phys. Rev. **107** (1957) 176;
C. K. Bockelman, W. W. Buechner, Phys. Rev. **107** (1957) 1366;
F. A. El-Bedewi, S. Tadros, Nuclear Physics **8** (1958) 71;
A. J. Elwyn, F. B. Shull, Phys. Rev. **111** (1958) 925;
I. Šlaus, Nuclear Physics **10** (1959) 457
10) M. H. MacFarlane, J. B. French, Stripping reactions and the structure of light and intermediate nuclei, NYO **2846** (1959)

10.A

Nuclear Physics **22** (1961) 698; © *North-Holland Publishing Co., Amsterdam*

NEWS ITEM

PROFESSOR V. F. WEISSKOPF AT CERN

A Directorate is being appointed to assist the Director-General of CERN in his increasingly ardous duties. The Directorate will consist of five members, namely the Director-General who is head of the Organization, two Members for research, one Member for administration and a Member for applied physics.

Prof. Victor F. Weisskopf recently accepted an appointment as one of the research members of the Directorate. Prof. Weisskopf was born in Vienna on 19 September 1908. He obtained his doctorate in physics 23 years later at the University of Göttingen where he studied under Max Born and James Franck. In 1931 he became assistant to Heisenberg at Leipzig and one year later joined Schrödinger in Berlin. After a period of some months at Kharkov in USSR, Prof. Weisskopf moved first to Zürich and then to Copenhagen before taking up an appointment as Professor at the University of Rochester in the United States. He remained at Rochester until 1943, spent about two years at Los Alamos, and then went to Massachusetts Institute of Technology in October 1945 to teach physics.

Prof. Weisskopf was recently granted a leave of absence from M. I. T. and he took up his appointment at CERN on 12 September 1960.

He is a corresponding member of the French Academy of Sciences, a member of the National Academy of Sciences in the United States and, until the end of this year, he is the President of the American Society of Physics. He was awarded the Planck medal by the German Society of Physics in 1960 in recognition of his work.

10.B

REPORT

KINGSTON CONFERENCE ON NUCLEAR STRUCTURE

(Kingston, Ontario, August 29—September 3, 1960)

The main conference on low-energy nuclear physics since the Paris conference of 1958 was distinguished by the large amount of information that the rapporteurs managed to give in their talks. This vast amount of material has been made almost immediately available to the physics public by the herculean efforts of editors D. A. Bromley and E. W. Vogt through the Proceedings, available only some weeks after the close of the conference. The Proceedings are impressively well organized and handy for reference. They contain 1004 pages, and many research reports not given at the conference. Without a doubt, they are the "Handbook for 1960 Nuclear Physics".

The conference was thoroughly and efficiently planned by the secretary, L. G. Elliott, and the organizing committee. While the standard of rapporteur talks was high, one felt that in some cases much of the material, included more for completeness than for interest, could have been left out of the oral presentation and simply committed to the Proceedings, especially since they appeared so rapidly after the end of the conference. This would have given more time for short reports of immediate interest. These latter suffered. For example, B. L. Cohen had only a few minutes to explain his side of the controversy about the excitation of collective versus single-particle states, Blair's work on diffraction inelastic scattering was confined to ten minutes, and Jacob's report on p—2p reactions to even less time.

The high point of the conference was the summary by V. F. Weisskopf, which was well worth forcing him to attend all the meetings.

G. E. Brown

10.E *Nuclear Physics* **22** (1961) 699; © *North-Holland Publishing Co., Amsterdam*

ERRATUM

Z. Grabowski, S. Gustafsson, I. Marklund and I. Häller, Angular Correlation Measurements in Ba^{136}, Nuclear Physics **20** (1960) 159.

4.4. 270 keV—1065 keV CORRELATION

In this subsection, the coincidence contribution from the 830 keV—1065 keV cascade has incorrectly not been taken into account earlier. This will change the correlation coefficients to $A_2 = -0.126 \pm 0.010$, $A_4 = -0.007 \pm 0.020$, and the possible spin values for the 2170 keV level will be $3(\delta \leqq 3 \times 10^{-2})$ and $5(6 \times 10^{-2} \leqq \delta \leqq 10^{-1})$.

The error made does not introduce any further changes in the article.

AUTHOR INDEX

AGUILAR, J., *see* HODGSON

ANDERSEN, S. L., O. DØRUM, E. GAUTVIK and T. HOLTEBEKK, Resonance energies and half-widths for proton capture in sodium and phosphorus 245

ARBMAN, E., and I. B. HÄLLER, On the decay of barium 129 . . . 341

AUSTIN, S. M., S. E. DARDEN, A. OKAZAKI and Z. WILHELMI, The polarization of neutrons from the $Li^7(p, n)Be^7$ reaction (II) 451

BAGLIN, J. E. E., M. N. THOMPSON and B. M. SPICER, Photodisintegration of Al^{27}. (I) Photoneutron cross section 207

BAGLIN, J. E. E., M. N. THOMPSON and B. M. SPICER, Photodisintegration of Al^{27}. (II) Theoretical 216

BARANGER, ELIZABETH and CHONG WAN LEE, Spurious states arising from the centre-of-mass motion of a nucleus 157

BARASHENKOV, V. S., Inelastic interactions of π-mesons with nucleons at 6.8 GeV 71

BEINER, M. and K. BLEULER, Geometrical representation of nuclear properties 589

BERESTETSKY, V. B. and I. YA. POMERANCHUK, On the asymptotic behaviour of cross sections at high energies. 629

BERGQVIST, I. and N. STARFELT, Gamma-ray spectra from capture of fast neutrons 513

BLOKHINTSEV, D. I. and WANG YUNG, $\pi\pi$ Interactions in πN-collisions at high pion energies 410

BLEULER, K., *see* BEINER

BODENSTEDT, E., H. J. KÖRNER, C. GÜNTHER and J. RADELOFF, The gyromagnetic ratio of the 80 keV rotational state of Erbium 166 . . . 145

BOWEN, P. H., J. P. SCANLON, G. H. STAFFORD, J. J. THRESHER and P. E. HODGSON, Neutron total cross-sections in the energy range 15 to 120 MeV. 640

BREMOND, B., On the effective interaction in finite nuclei. 434

BRENE, N., L. EGARDT and B. QVIST, On the $K_{\mu 3}$ and K_{e3} decay modes . 553

BRENIG, W., Long range correlations and photo effect in nuclei 14

BROWN, G. E., L. CASTILLEJO and J. A. EVANS, The dipole state in nuclei 1

BUDAGOV, YU. A., S. WIKTOR, V. P. DZHELEPOV, P. F. YERMOLOV and V. I. MOSKALEV, Elastic scattering of negative pions by protons at 128 and 162 MeV. 226

CASTILLEJO, L., *see* BROWN

CHONG WAN LEE, *see* BARANGER
CHRISTY, ROBERT F., Corrections to nuclear Q values resulting from atomic binding and excitation 301
CINDRO, N., I. ŠLAUS, P. TOMAŠ and B. EMAN, The $O^{16}(n, \alpha)C^{13}$ reaction by the thin crystal method 96
CLASS, C. M., *see* REST ER
CLINE, J. E. and R. L. HEATH, Levels in Gd^{156} fed by the decay of 15-day Eu^{156} 598
COHEN, L., Matrix elements for the alpha-particle 492
CONNOR, D. W., *see* WAPSTRA
CROW, T. T. and W. G. HOLLADAY, A contribution to the anomalous magnetic moments of the baryons 164
DĄBROWSKI, J. and J. SAWICKI, The high energy optical model and nuclear forces. 318
DARDEN, S. E., T. R. DONOGHUE and C. A. KELSEY, The polarization of neutrons from the $Li^7(p, n)Be^7$ reaction (I). 439
DARDEN, S. E., *see* AUSTIN
DE-SHALIT, A. and J. D. WALECKA, Spectra of odd nuclei 184
DE-SHALIT, A., Effective moments in K^{39} and K^{40}. 677
DONOGHUE, T. R., *see* DARDEN
DØRUM, O., *see* ANDERSEN
DURHAM, F. E., *see* REST ER
DZHELEPOV, Y. P., *see* BUDAGOV
EFREMOV, A. V., V. A. MESHCHERYAKOV, D. V. SHIRKOV and H. Y. TZU, On deriving equations from the Mandelstam representation 202
EGARDT, L., *see* BRENE
EKSPONG, A. G., Å. FRISK, S. NILSSON and B. E. RONNE, Antiproton annihilations in complex nuclei. 353
ELBEK, B., *see* SKURNIK
EMAN, B., *see* CINDRO
ENGLAND, J. B. A., *see* HODGSON
EVANS, J. A., *see* BROWN
EWAN, G. T., R. L. GRAHAM and J. S. GEIGER, Negative parity levels in the even-even nucleus Dy^{160} 610
FRISK, Å., *see* EKSPONG
GALE, N. H., J. B. GARG and K. RAMAVATARAM, Neutron angular distributions for the reaction $^{16}O(^3He, n)^{18}Ne$ 500
GARCÍA, A., *see* HODGSON
GARG, J. B., *see* GALE
GAUTVIK, F., *see* ANDERSEN
GEIGER, J. S., *see* EWAN
GLASHOW, S. L., Partial-symmetries of weak interactions 579

GOLDEMBERG, J., *see* NASCIMENTO
GRAHAM, R. L., *see* EWAN
GRIBOV, V. N., Asymptotic behaviour of the scattering amplitude at high energies 249
GRIGORIEV, E. P., and A. V. ZOLOTAVIN, Concerning the decay of Se^{75} . 689
GÜNTHER, C., *see* BODENSTEDT
HÄLLER, I. B., *see* ARBMAN
HAMILTON, JOSEPH H., *see* HULTBERG
HAMILTON, J. H., *see* PETTERSSON
HEATH, R. L., *see* CLINE
HODGSON, P. E., J. AGUILAR, A. GARCÍA and J. B. A. ENGLAND, The elastic scattering of 19.5 MeV deuterons by krypton 138
HODGSON, P. E., *see* BOWEN
HOLLADAY, W. G., *see* CROW
HOLTEBEKK, T., *see* ANDERSEN
HULTBERG, SÖLVE, TOM O'CONNOR and JOSEPH H. HAMILTON, Angular distributions of photoelectrons ejected from uranium by 1.118 MeV gamma rays 306
ISAEV, P. S. and M. SEWERYNSKI, Approximate equations for partial π—K scattering amplitudes 663
JOHANSSON, SVEN A. E., Nuclear octupole deformation and the mechanism of fission 529
KELSEY, C. A., *see* DARDEN
KOMAR, A., "Minimal property" of electromagnetic interaction for spin $\frac{3}{2}$ particles 101
KÖRNER, H. J., *see* BODENSTEDT
KÜMMEL, H., Compound pair states in imperfect Fermi gases 177
MARGOLIS, B., Neutron polarization by Coulomb scattering 498
MESHCHERYAKOV, V. A., *see* EFREMOV
METZGER, F. R., *see* ROTHEM
MOORE, M. S., *see* RESTER
MOSCATI, G., *see* NASCIMENTO
MOSKALEV, V. I., *see* BUDAGOV
NAKAMURA, HIROSHI and TOSHIYUKI TOYODA, Connection of spinor fields 524
NASCIMENTO, I. C., G. MOSCATI and J. GOLDEMBERG, Systematics of $(\gamma, 2n)$ reactions 484
NIELSEN, O. B., *see* TOTH
NILSSON, S., *see* EKSPONG
O'CONNOR, TOM, *see* HULTBERG
OLESEN, M. C., *see* SKURNIK
OKAZAKI, A., *see* AUSTIN

PAPPAS, ALEXIS C., *see* RUDSTAM
PETTERSSON, B. G., J. H. HAMILTON and J. E. THUN, Higher-order effects in an allowed positon decay in Co^{56}. 131
PILKUHN, H., Isospin for $N+\bar{N} \rightarrow K+\bar{K}+k\pi$ and similar reactions . . 168
POMERANCHUK, I. YA., *see* BERESTETSKY
PRANGE, RICHARD E., The moment of inertia of large superfluid fermion systems 283
QVIST, B., *see* BRENE
RADELOFF, J., *see* BODENSTEDT
RAMAVATARAM, K., *see* GALE
RESTER, D. H., M. S. MOORE, F. E. DURHAM and C. M. CLASS, Internal conversion electrons from Coulomb excitation of heavy elements . . 104
ROBSON, D., Polarization in (d, p) reactions 34
ROBSON, D., Spin-orbit effects in the stripping reaction involving polarized particles 47
RONNE, B. E., *see* EKSPONG
ROTHEM, T., F. R. METZGER and C. P. SWANN, Lifetimes of the 668-keV and 961-keV excited states in Cu^{63} 505
RUDSTAM, GÖSTA and ALEXIS C. PAPPAS, Mass and charge distribution in high energy induced fission 468
SAWICKI, J., *see* DĄBROWSKI
SCANLON, J. P., *see* BOWEN
SEWERYNSKI, M., *see* ISAEV
SHIRKOV, D. V., *see* EFREMOV
SKURNIK, E. Z., B. ELBEK and M. C. OLESEN, Inelastic scattering from Th^{232} and U^{238} 316
ŠLAUS, I., *see* CINDRO
ŠLAUS, I., P. TOMAŠ and N. STIPČIČ, Angular distribution of the V^{51}(n, d)Ti^{50} ground state deuterons 692
SPICER, B. M., *see* BAGLIN
STAFFORD, G. H., *see* BOWEN
STARFELT, N., *see* BERGQVIST
STIPČIČ, N., *see* ŠLAUS
SWANN, C. P., *see* ROTHEM
THOMPSON, M. N., *see* BAGLIN
THOULESS, D. J., Vibrational states of nuclei in the random phase approximation 78
THRESHER, J. J., *see* BOWEN
THUN, J. E., *see* PETTERSSON
TOMAŠ, P., *see* CINDRO
TOMAŠ, P., *see* ŠLAUS
TOTH, K. S. and O. B. NIELSEN, Dy^{155} and Dy^{157} decay schemes 57

TOYODA, TOSHIYUKI, *see* NAKAMURA
TRUE, W. W. and E. K. WARBURTON, On the 5.16 MeV and 7.56 MeV states of B^{10} 426
TZU, H. Y., *see* EFREMOV
UMEZAWA, H. and A. VISCONTI, A new Majorana field theory 262
VISCONTI, A., *see* UMEZAWA
WALECKA, J. D., *see* DE-SHALIT
WAPSTRA, A. H. and D. W. CONNOR, The persistence of nuclear polarization produced by the capture of polarized thermal neutrons 336
WARBURTON, E. K., *see* TRUE
WIKTOR, S., *see* BUDAGOV
WILHELMI, Z., *see* AUSTIN
YERMOLOV, P. F., *see* BUDAGOV
YUNG, WANG, *see* BLOKHINTSEV
ZOLOTAVIN, A. V., *see* GRIGORIEV

SUBJECT INDEX

1. Nuclear Structure

1.C *Many-particle systems*

Compound pair states in imperfect Fermi gases, H. Kümmel 177
The moment of inertia of large supperfluid fermion systems, Richard E. Prange 283
The high energy optical model and nuclear forces, J. Dąbrowski and J. Sawicki 318

1.D *Nuclear models*

1.D.1 *Shell model*

The dipole state in nuclei, G. E. Brown, L. Castillejo and J. A. Evans . 1
Spurious states arising from the centre-of-mass motion of a nucleus, Elizabeth Baranger and Chong Wan Lee 157
Spectra of odd nuclei, A. De-Shalit and J. D. Walecka 184
On the 5.16 MeV and 7.56 MeV states of B^{10}, W. W. True and E. K. Warburton 426
On the effective interaction in finite nuclei, B. Bremond 434

1.D.2 *Collective model*

The dipole state in nuclei, G. E. Brown, L. Castillejo and J. A. Evans 1

1.D.4 *Relationship between different models*

Vibrational states of nuclei in the random phase approximation, D. J. Thouless. 78

1.E *Properties of nuclei*

1.E.1 *Energy levels*

Spectra of odd nuclei, A. De-Shalit and J. D. Walecka 184
Geometrical representation of nuclear properties, M. Beiner and K. Bleuler 589
Levels in Gd^{156} fed by the decay of 15-day Eu^{156}, J. E. Cline and R. L. Heath. 598

1.E.2 *Binding energies; Masses*

Corrections to nuclear Q values resulting from atomic binding and excitation, Robert F. Christy. 301

1.E.3 *Electric and magnetic moments*

Effective moments in K^{39} and K^{40}, A. De-Shalit 677

1.E.4 *Transition probabilities; Cross sections*

Matrix elements for the alpha-particle, L. Cohen 492

1.E.6 *Nuclear moments of inertia*

The moment of inertia of large superfluid fermion systems, Richard E. Prange 283

2. Nuclear Reactions

2.A *General properties*

2.A.1 *Cross-sections, energy relations*

Neutron total cross-sections in the energy range 15 to 120 MeV, P. H. Bowen, J. P. Scanlon, G. H. Stafford, J. J. Thresher and P. E. Hodgson 640

2.B *Angular distributions; correlations polarization*

The $O^{16}(n, \alpha)C^{13}$ reaction by the thin crystal method, N. Cindro, I. Šlaus, P. Tomaš and B. Eman 96
The persistence of nuclear polarization produced by the capture of polarized thermal neutrons, A. H. Wapstra and D. W. Connor 336
The polarization of neutrons from the $Li^7(p, n)Be^7$ reaction (I), S. E. Darden, T. R. Donoghue and C. A. Kelsey 439
The polarization of neutrons from the $Li^7(p, n)Be^7$ reaction (II), S. M. Austin, S. E. Darden, A. Okazaki and Z. Wilhelmi 451
Neutron polarization by Coulomb scattering, B. Margolis 498
Neutron angular distributions for the reaction $^{16}O(^3He, n)^{18}Ne$, N. H. Gale, J. B. Garg and K. Ramavataram 500

2.C *Resonance reactions; R-matrix theory*

Resonance energies and half-widths for proton capture in sodium and phosphorus, S. L. Andersen, O. Dørum, E. Gautvik and T. Holtebekk 245

2.E *Optical model*

The elastic scattering of 19.5 MeV deuterons by krypton, P. E. Hodgson, J. Aguilar, A. García and J. B. A. England 138
The high energy optical model and nuclear forces, J. Dąbrowski and J. Sawicki 318
Neutron total cross-sections in the energy range 15 to 120 MeV, P. H. Bowen, J. P. Scanlon, G. H. Stafford, J. J. Thresher and P. E. Hodgson 640

2.G *Stripping and pick up*

Polarization in (d, p) reactions, D. Robson 34
Spin-orbit effects in the stripping reaction involving polarized particles, D. Robson 47
Neutron angular distributions for the reaction $^{16}O(^3He, n)^{18}Ne$, N. H. Gale, J. B. Garg and K. Ramavataram 500
Angular distribution of the $V^{51}(n, d)Ti^{50}$ ground state deuterons, I. Šlaus, P. Tomaš and N. Stipčič 692

2.H *Coulomb excitation*

Internal conversion electrons from Coulomb excitation of heavy elements, D. H. Rester, M. S. Moore, F. E. Durham and C. M. Class 104
Inelastic scattering from Th^{232} and U^{238}, E. Z. Skurnik, B. Elbek and M. C. Olesen 316

2.I *Photonuclear processes*

Long range correlations and photo effect in nuclei, W. Brenig 14
Photodisintegration of Al^{27}. (I) Photoneutron cross section, J. E. E. Baglin, M. N. Thompson and B. M. Spicer 207

Photodisintegration of Al^{27}. (II) Theoretical, J. E. E. Baglin, M. N. Thompson and B. M. Spicer 216
Systematics of (γ, 2n) reactions, I. C. Nascimento, G. Moscati and J. Goldemberg 484

2.J *Fission and spallation*

Mass and charge distribution in high energy induced fission, Gösta Rudstam and Alexis C. Pappas 468
Nuclear octupole deformation and the mechanism of fission, Sven A. E. Johansson 529

3. Electromagnetic Radiation

3.A *Gamma radiation*

Dy^{155} and Dy^{157} decay schemes, K. S. Toth and O. B. Nielsen 57
Higher-order effects in an allowed positon decay in Co^{56}, B. G. Pettersson, J. H. Hamilton and J. E. Thun 131
The gyromagnetic ratio of the 80 keV rotational state of Erbium 166, E. Bodenstedt, H. J. Körner, C. Günther and J. Radeloff 145
Angular distributions of photoelectrons ejected afrom uranium by 1.118 MeV gamma rays, Sölve Hultberg, Tom O'Connor and Joseph H. Hamilton . . . 306
Lifetimes of the 668-keV and 961-keV excited states in Cu^{63}, T. Rothem, F. R. Metzger and C. P. Swann 505
Gamma-ray spectra from capture of fast neutrons, I. Bergqvist and H. Starfelt. 513
Levels in Gd^{156} fed by the decay of 15-day Eu^{156}, J. E. Cline and R. L. Heath . 598

3.B *Internal conversion*

Dy^{155} and Dy^{157} decay schemes, K. S. Toth and O. B. Nielsen 57
Internal conversion electrons from Coulomb excitation of heavy elements, D. H. Rester, M. S. Moore, F. E. Durham and C. M. Class 104
Angular distributions of photoelectrons ejected from uranium by 1.118 MeV gamma rays, Sölve Hultberg, Tom O'Connor and Joseph H. Hamilton . . . 306
On the decay of barium 129, E. Arbman and I. B. Häller 341
Negative parity levels in the even-even nucleus Dy^{160}, G. T. Ewan, R. L. Graham and J. S. Geiger 610
Concerning the decay of Se^{75}, E. P. Grigoriev and A. V. Zolotavin 689

4. Beta Decay; Parity

4.E *Analysis of data*

Higher-order effects in an allowed positon decay in Co^{56}, B. G. Pettersson, J. H. Hamilton and J. E. Thun 131
On the decay of barium 129, E. Arbman and I. B. Häller 341

7. Quantum Field Theory

7.A *General*

Asymptotic behaviour of the scattering amplitude at high energies, V. N. Gribov 249
Connection of spinor fields, Hiroshi Nakamura and Toshiyuki Toyoda. . . . 524
On the asymptotic behaviour of cross sections at high energies, V. B. Berestetsky and I. Ya. Pomeranchuk 629

7.B *Quantum electrodynamics*

"Minimal property" of electromagnetic interaction for spin $\frac{3}{2}$ particles, A. Komar 101

8. Elementary Particles

8.A *Experimental*

Elastic scattering of negative pions by protons at 128 and 162 MeV, Yu. A. Budagov, S. Wiktor, V. P. Dzhelepov, P. F. Yermolov and V. I. Moskalev . 226
Antiproton annihilations in complex nuclei, A. G. Ekspong, Å. Frisk, S. Nilsson and B. E. Ronne 353

8.B *Theory; interactions, transformation properties*

Inelastic interactions of π-mesons with nucleons at 6.8 GeV, V. S. Barashenkov 71
A contribution to the anomalous magnetic moments of the baryons, T. T. Crow and W. G. Holladay 164
Isospin for $N+\bar{N} \to K+\bar{K}+k\pi$ and similar reactions, H. Pilkuhn 168
On deriving equations from the Mandelstam representation, A. V. Efremov, V. A. Meshcheryakov, D. V. Shirkov and H. Y. Tzu 202
A new Majorana field theory, H. Umezawa and A. Visconti 262
$\pi\pi$ Interactions in πN-collisions at high pion energies, D. I. Blokhintsev and Wang Yung 410
On the $K_{\mu 3}$ and K_{e3} decay modes, N. Brene, L. Egardt and B. Qvist 553
Partial-symmetries of weak interactions, S. L. Glashow 579
Approximate equations for partial π—K scattering amplitudes, P. S. Isaev and M. Sewerynski 663

10. News Items

10.A *News items*

News item 699

10.B *Reports on conferences and congresses*

Report Kingston conference 699

10.E *Errata*

G. E. Tauber and T. Y. Wu, Nuclear shell model: Hartree-Fock approximation with Gammel-Thaler two-nucleon potential 339
M. L. Mehta and M. Gaudin, On the density of eigenvalues of a random matrix 340
Z. Grabowski, S. Gustafsson, I. Marklund and I. Häller, Angular correlation measurements in Ba^{136} 699

NORTH-HOLLAND BOOKS

by J. L. SYNGE
Dublin Institute for Advanced Studies

Relativity, The General Theory

Among the topics discussed are frames of reference, Fermi transport, integral conservation, gravitational waves and geometrical optics. There is an extensive bibliography, with references to reviews of the works cited.

6×9" 521 pp. 102 figs. Guilders 55.00 (104s.)

Relativity, The Special Theory

"The book is full of wise saws and modern instances, all eminently quotable if space did but permit. It is cheerful in style, profusely illustrated by diagrams, and beautifully printed".

Nature

6×9" 466 pp.
107 figs.
Guilders 38.00
(76s.)

The Relativistic Gas

"The book can be recommended to those interested in relativity, gas dynamics and statistical mechanics, and to all others who enjoy seeing a well-defined problem treated rigorously".

Proc. Physical Society

6×9" 120 pp.
15 figs.
Guilders 15.00
(30s.)

Send your order to your bookseller or directly to:

NORTH-HOLLAND PUBLISHING COMPANY

P. O. Box 103, Amsterdam - Netherlands

We introduced a

PERSONAL SUBSCRIPTION SCHEME

for

NUCLEAR PHYSICS

8 volumes (1961, vols. 21—28) at the total price of $ 20.00 (£ 7.10.0)

Write for details:

NORTH-HOLLAND PUBLISHING COMPANY

P.O. BOX 103 — AMSTERDAM, HOLLAND